

Myeloid cells' response to infection with  
*Staphylococcus aureus* and *Streptococcus pyogenes*

**Inauguraldissertation**

zur

Erlangung des akademischen Grades eines  
Doktors der Naturwissenschaften (Dr. rer. nat.)

der

Mathematisch-Naturwissenschaftlichen Fakultät

der

Universität Greifswald

Vorgelegt von

Lea Alessandra Tölken

Greifswald, 08.12.2023

Dekan: Prof. Dr. Gerald Kerth

1. Gutachter: Prof. Dr. Nikolai Siemens

2. Gutachter: PD Dr. Sonja Oehmcke-Hecht

Tag der Promotion: 26.02.2024

"The Guide says there is an art to flying", said Ford, "or rather a knack. The knack lies in learning how to throw yourself at the ground and miss."

Douglas Adams, *Life, the Universe and Everything*





---

## TABLE OF CONTENTS

LIST OF SCIENTIFIC PAPERS AND MANUSCRIPTS .....	II
LIST OF FIGURES .....	III
LIST OF ABBREVIATIONS.....	IV
1. SUMMARY .....	1
2. ZUSAMMENFASSUNG .....	3
3. BACKGROUND .....	5
3.1 Innate Immune System .....	5
3.2 <i>Staphylococcus aureus</i> .....	9
3.3 <i>Streptococcus pyogenes</i> .....	10
3.4 Study Objectives .....	16
4. RESEARCH APPROACH.....	17
4.1 Ethics Statement.....	17
4.2 Bacterial Strains .....	17
4.3 Isolation of Human Myeloid Cells and Infection .....	18
4.4 Analysis of Immune Cell Phenotype Post-Infection .....	20
4.5 Cytokine Secretion in Response to GAS Infection.....	21
5. RESULTS & DISCUSSION.....	22
5.1 Cobalt and Chromium Ions Impair Macrophage Response to <i>Staphylococcus aureus</i> Infection.....	22
5.2 Hyper-virulent <i>Streptococcus pyogenes</i> Impairs Interleukin-18 Response in Human Monocytic Cells.....	26
5.3 Neutrophil-derived Reactive Agents Induce a Transient SpeB Negative Phenotype in <i>Streptococcus pyogenes</i> .....	29
6. CONCLUSIONS .....	32
7. REFERENCES .....	35
8. APPENDIX .....	47

## LIST OF SCIENTIFIC PAPERS AND MANUSCRIPTS

The following scientific papers/manuscripts are included in this thesis:

- I. **Lea A. Tölken**, Georgi I. Wassilew, Daniel Grolimund, Timm Weitkamp, Bernhard Hesse, Anastasia Rakow, Nikolai Siemens#, Janosch Schoon#; Cobalt and Chromium Ions Impair Macrophage Response to *Staphylococcus aureus* Infection; accepted for publication in ACS Biomaterials Science & Engineering, 06. December 2023; # equal contribution
- II. **Lea A. Tölken**, Antje D. Paulikat, Lana H. Jachmann, Alexander Reder, Manuela Gesell Salazar, Laura M. Palma Medina, Stephan Michalik, Uwe Völker, Mattias Svensson, Anna Norrby-Teglund, Katharina J. Hoff, Michael Lammers, and Nikolai Siemens; Reduced Interleukin-18 Secretion by Human Monocytic Cells in Response to Infections with Hyper-Virulent *Streptococcus pyogenes*; Submitted to Journal of Biomedical Science, 08. December 2023
- III. Patience Shumba, Thomas Sura, Kirsten Moll, Bhavya Chakrakodi, **Lea A Tölken**, Jörn Hoßmann, Katharina J Hoff, Ole Hyldegaard, Michael Nekludov, Mattias Svensson, Per Arnell, Steinar Skrede; INFECT Study Group; Anna Norrby-Teglund, Nikolai Siemens; Neutrophil-derived Reactive Agents Induce a Transient SpeB Negative Phenotype in *Streptococcus pyogenes*, J Biomed Sci 30, 52 (2023). <https://doi.org/10.1186/s12929-023-00947-x>

## LIST OF FIGURES

Figure 1 Phagocytosis by macrophages .....	6
Figure 2 DC maturation and presentation of antigens to T cells .....	7
Figure 3 GAS virulence mechanisms .....	12
Figure 4 General experimental approach for Paper I and Paper II. ....	18
Figure 5 Gating strategies used to identify human myeloid cells .....	21
Figure 6 Effects of metal exposure on macrophage phenotype.....	23

LIST OF ABBREVIATIONS

---

ALTR	Adverse local tissue reaction
APC	Antigen presenting cell
CA-MRSA	Community acquired MRSA
CD	Cluster of differentiation
cDC	Classical/conventional DC
CLSM	Confocal laser scanning microscopy
CoCrMo	Cobalt Chromium Molybdenum
CovR/S	Control of virulence R/S
CXCL	C–X–C motif chemokine ligand
DAMP	Danger associated molecular pattern
DC	Dendritic cell
FSC	Forward scatter
GAS	Group A streptococcus
GM-CSF	granulocyte-macrophage colony-stimulating factor
GSDMA	Gasdermin A
GSDMD	Gasdermin D
HLA-DR	Human leukocyte antigen
HMGB1	High motility group box 1
IFN	Interferon
IL	Interleukin
IVIG	Intravenous immunoglobulin
MHC	Major histocompatibility complex
moDC	Monocyte-derived DC
MOI	Multiplicity of infection
MPO	Myeloperoxidase
MRSA	Methicillin-resistant <i>Staphylococcus aureus</i>
NET	Neutrophil extracellular trap
NF	Necrotizing fasciitis
NLRP3	NLR family pyrin domain containing 3
NSTI	Necrotizing skin and soft tissue infection
PAMP	Pathogen associated molecular pattern
pDC	Plasmacytoid DC
PVL	Panton Valentin Leukocidin
PRR	Pattern recognition receptor
RopB	Regulator of Protease
ROS	Reactive oxygen species
SCV	Small colony variant
SLO	Streptolysin O
SLS	Streptolysin S
SpeB	Streptococcal pyrogenic exotoxin B
SSC	Sideward scatter
STSS	Streptococcal toxic shock syndrome
TcR	T cell receptor
THY	Todd-Hewitt broth supplemented with 1.5% (w/v) yeast extract
TNF	Tumor necrosis factor
TLR	Toll like receptor

---

## 1. SUMMARY

During infections, innate immune cells are crucial for initiating a pro-inflammatory immune response and clearing the invading pathogen. Delay in pathogen clearance or initiation of an immune response due to impaired functionality of immune cells can result in devastating consequences. The cellular compartment of the innate immune system comprises an array of specialized cell types: Macrophages are tissue-resident professional phagocytes that clear cellular debris, pathogens, and foreign objects. Dendritic cells (DCs) are immune sentinels specialized in antigen uptake and subsequent T cell priming. They are primary sources of cytokines in response to infection. Neutrophils are efficient effector cells that respond rapidly to infection and clear bacteria by different mechanisms. If effector mechanisms of these cells are affected by either bacterial or other factors, infections might not be resolved and can spread throughout the host.

Cobalt-chromium-molybdenum biomaterial is widely used in arthroplasty. Implant-derived wear particles and ions lead to macrophage-driven adverse local tissue reactions: Such reactions have been linked to an increased risk of periprosthetic joint infection after revision arthroplasty. While metal-induced cytotoxicity is well characterized in human macrophages, direct effects on their functionality remain elusive. In Paper I, we show that local peri-implant tissue is exposed to Co and Cr *in situ*. Influx of macrophages is also evident. Exposure of isolated human monocytes/macrophages to Cr<sup>3+</sup> *in vitro* had only minor effects. However, exposure of monocytes/macrophages to pathologic concentrations of Co<sup>2+</sup> significantly impaired both phenotype and functionality. High concentrations of Co<sup>2+</sup> induced loss of surface markers, including CD14 and CD16. Both Co<sup>2+</sup> and Cr<sup>3+</sup> impaired macrophage responses to *Staphylococcus aureus* infection. Co<sup>2+</sup>-exposed macrophages, in particular, showed decreased phagocytic activity. These findings demonstrate the immunosuppressive effects of locally elevated metal ions on the innate immune response.

*Streptococcus pyogenes* (group A streptococcus, GAS) causes a variety of diseases ranging from mild to severe necrotizing soft tissue infections (NSTIs). In the host environment hyper-virulent GAS variants carrying mutations within the genes encoding for control of virulence (Cov)R/S two component system are enriched. This adaptation is associated with loss of SpeB secretion. In Paper II, we show that *in vitro* infections with hyper-virulent GAS variants harboring dysfunctional CovR/S suppress secretion of IL-8 and IL-18 by human monocytic cells. This phenotype was mediated by a caspase-8 dependent mechanism. Knockout of streptococcal SLO in a GAS strain carrying functional CovR/S even increased secretion of IL-1 $\beta$  and IL-18 by moDCs. Of 67 fully sequenced GAS NSTI isolates, 28 contained *covS* or *covR*

mutations that rendered the TCS dysfunctional. However, no differences in systemic IL-8 and IL-18 were detected in these patients.

GAS isolates recovered from patients often display a mixed phenotype, consisting of SpeB positive (SpeB<sup>+</sup>) and SpeB negative (SpeB<sup>-</sup>) clones. Irreversible loss of SpeB expression is often caused by loss of function mutations in regulatory components (CovR/S, RopB). Loss of SpeB is often associated with hyper-virulence. In Paper III, we show that the host environment induces transiently abrogated secretion of SpeB by GAS. Tissue inflammation, neutrophil influx, and degranulation correlated with increased frequencies of SpeB<sup>-</sup> GAS clones. Isolates recovered from tissue expressed but did not secrete SpeB, which was reversible. Neutrophil-derived ROS were identified as the main factor responsible for abrogated SpeB secretion. Hyper-virulent SpeB<sup>-</sup> clones also exhibit better survival within and induce excessive degranulation of neutrophils.

## 2. ZUSAMMENFASSUNG

Während einer Infektion sind die Zellen des innate Immunsystems unabdingbar für die schnelle Initiation einer proinflammatorischen Immunantwort und die Bekämpfung des eindringenden Erregers. Eine verspätete Reaktion oder eine Beeinträchtigung der Funktionalität der Immunzellen kann verheerende Folgen haben. Das innate Immunsystem besteht aus einer Vielzahl spezialisierter Effektorzellen mit spezifischen Aufgaben. Makrophagen sind geweberesidente Zellen, welche Fremdkörper, Zelltrümmer und eindringende Pathogene phagozytieren und abtöten. Dendritische Zellen (DCs) sind spezialisiert auf die Präsentation von Antigenen für T Zellen und deren Aktivierung. Zu diesem Zweck sekretieren DCs auch eine Vielzahl von Zytokinen. Neutrophile sind effiziente Effektorzellen, die schnell auf Infektionen reagieren und Bakterien über verschiedene Wege abtöten. Wenn die Mechanismen dieser Zellen durch bakterielle oder anderweitige Faktoren gestört oder beeinflusst werden, können entstehende Infektionen eventuell nicht rechtzeitig eingedämmt werden und die Erreger breiten sich im Körper aus.

Kobalt-Chrom-Molybdän (CoCrMo) Legierungen sind gängige Endoprothesenmaterialien, welche häufig in der Arthroprothetik zum Einsatz kommen. Durch Abnutzungsvorgänge vom Implantat freigesetzte Partikel und Ionen können zu adversen lokalen Gewebsreaktionen führen. Diese werden häufig durch Makrophagen verursacht und gehen mit einem erhöhten Risiko von periprosthetischen Infektionen einher. Metallinduzierte Zytotoxizität gegenüber humanen Makrophagen ist ein gut charakterisiertes Phänomen. Wohingegen die Auswirkungen von Metallexposition auf Funktion und Phänotyp von Makrophagen noch unbekannt sind. In Paper I wird gezeigt, dass das periprosthetische Gewebe gegenüber Co und Cr exponiert ist. Außerdem wurden Areale mit verstärkter Einwanderung von Makrophagen beobachtet. Exposition gegenüber Cr<sup>3</sup> hatte nur geringe Effekte auf den Phänotyp der Makrophagen, während Exposition gegenüber Co<sup>2+</sup> Phänotyp und Funktion stark beeinträchtigte. Pathologische Konzentrationen von Co<sup>2+</sup> induzierten den Verlust von Oberflächenexpression bestimmter Marker (CD14, CD16). Sowohl Co<sup>2+</sup> als auch Cr<sup>3+</sup> verhinderten Aktivierung von Makrophagen nach Infektion mit *Staphylococcus aureus*. Diese Ergebnisse zeigen, dass lokal erhöhte Konzentrationen von Metallionen immunsuppressive Effekte haben und die Funktion innater Immunzellen beeinträchtigen.

*Streptococcus pyogenes* (GAS, Gruppe A Streptokokken) verursacht eine Vielzahl humaner Erkrankungen. Diese reichen von milden, bis hin zu schweren nekrotisierenden Weichteilinfektionen (NSTI). Innerhalb des Wirtes können hypervirulente GAS-Klone entstehen. Dies geschieht häufig durch Mutationen der für das Zweikomponentensystem

CovR/S kodierenden Gene *covS* und *covR*. Dies geht oft mit Verlust der Sekretion der Protease SpeB einher. In Paper II wird gezeigt, dass hypervirulente GAS Stämme die Sekretion von Interleukin (IL)-8 und IL-18 durch humane monozytäre Zellen supprimieren. Dieser Phänotyp wurde durch die Initiator-Caspase-8 vermittelt. Deletion des Zytolysins SLO in einem Stamm mit funktionalem CovR/S führte außerdem zu erhöhter Sekretion von IL-1 $\beta$  und IL-18 durch infizierte DCs. In 67 sequenzierten GAS Isolaten aus NSTI Patienten konnten 28 potenziell inaktivierende Mutationen von *covS* oder *covR* gefunden werden. Allerdings konnten im Plasma der Patienten keine Unterschiede der systemischen Konzentrationen von IL-8 und IL-18 festgestellt werden.

GAS Patientenisolate zeigen oft einen gemischten Phänotyp, bestehend aus SpeB positiven (SpeB<sup>+</sup>) und SpeB<sup>-</sup> Klonen. Irreversibler Verlust der Sekretion von SpeB wird oft durch Mutationen in regulatorischen Elementen (CovR/S, RopB) verursacht, welche mit Hypervirulenz verbunden sind. In Paper III wird gezeigt, dass die Wirtsumgebung zu einem transienten Verlust der Sekretion von SpeB durch GAS führt. Inflammation des Gewebes, Einwanderung von neutrophilen und neutrophile Degranulation korrelierten mit dem vermehrten auftreten SpeB<sup>-</sup> GAS Klone. Aus Gewebe isolierte GAS exprimierten SpeB, während sie dieses jedoch nicht sekretieren. Von Neutrophilen produzierte reaktive Sauerstoffspezies waren der Hauptfaktor, welcher zum Verlust der SpeB Sekretion durch GAS führte. Außerdem verursachten hypervirulente SpeB<sup>-</sup> Klone exzessive Degranulierung von Neutrophilen und konnten intrazellulär replizieren.



### 3. BACKGROUND

#### 3.1 Innate Immune System

The innate immune system is the first line of defense against invading pathogens. Its primary function is to sense pathogens and rapidly initiate an inflammatory response. It consists of different components that have various functions: epithelial surfaces, e.g., skin or mucosal surfaces, function as barriers to prevent pathogens from entering the host. If such barriers are breached, acellular components like the complement system are in place to detect and kill bacteria. The cellular components of the innate immune system comprise an array of either circulating or tissue-resident specialized cell types. These are equipped to fight invading pathogens and, if necessary, initiate a specific, adaptive immune response (1–3).

##### 3.1.1 Sensing of Pathogens & Inflammasome Activation

In general, innate immune cells sense conserved molecular patterns signaling danger (Pathogen/danger-associated molecular patterns (DAMP/PAMPs)) via specific pattern recognition receptors (PRRs). Recognition of PAMPs by their respective receptors induces activation of intracellular signaling cascades, which ultimately result in initiation of a proinflammatory immune response (4). This includes production of cytokines, chemokines like interleukin (IL)-8, and antimicrobial proteins.

Inflammasomes represent additional mechanisms to sense invading pathogens. This process eventually leads to release of strongly proinflammatory cytokines IL-1 $\beta$  and IL-18. While most cell types can produce both cytokines, myeloid cells, especially macrophages and dendritic cells (DCs), are the primary sources of both cytokines (5,6). In contrast to other eukaryotic cells, cells of monocytic origin do not require a priming step before inflammasome activation. In short, recognition of PAMPs and DAMPs induces assembly of inflammasomes. These are cytosolic multiprotein complexes consisting of adaptor proteins, e.g., ASC, that link caspase-1 with sensor proteins like NLR family pyrin domain containing 3 (NLRP3). Upon activation, these proteins oligomerize, and caspase-1 autocatalytically activates itself. Active caspase-1 processes the precursors of gasdermin D (GSDMD), pro-IL-1 $\beta$ , and pro-IL-18 into their respective mature forms. The N-terminal products of GSDMD form pores in the cell membrane, through which the mature cytokines IL-1 $\beta$  and IL-18 are released (7). IL-1 $\beta$  induces a range of proinflammatory effects, including production of proinflammatory cytokines and activation of macrophage and neutrophil effector functions (5). IL-18, together with IL-12, induces Th1 polarization and secretion of interferon (IFN)- $\gamma$  (7,8). Other caspases were also shown to process and mediate release of mature IL-1 $\beta$  and IL-18, including caspase-4/5 (7) and caspase-8 (9–13).

### 3.2.1 Myeloid Cells

Myeloid cells are a heterogeneous group of different innate immune cells. They can be broadly grouped into monocytes, granulocytes (neutrophils, eosinophils, and mast cells), macrophages, and DCs. All of these cell types are derived from a common progenitor that differentiates into the respective cell types in the bone marrow (14).

#### 3.2.1.1 Macrophages & Monocytes

Macrophages, e.g. alveolar macrophages, Langerhans cells and Kupffer cells, are tissue-resident cells specialized in phagocytosis and clearance of pathogens, cellular debris, and other foreign objects. In their function as sessile immune sentinels, macrophages monitor their immediate surroundings in epithelial and mucosal surfaces (15,16). Phagocytosis is a multi-step process (**Figure 1**), starting with recognition of a pathogen/foreign object via PRRs, followed by engulfment of the particle. Then, the phagosome is formed, which matures and eventually fuses with lysosomes, generating the phagolysosome. Inside the phagolysosome, acidic pH, reactive oxygen species (ROS), and antimicrobial compounds kill pathogens or degrade other foreign objects (17). Macrophages show a high degree of plasticity: they can respond to infection by clearing pathogens and secreting cytokines and chemokines, showing an overall pro-inflammatory phenotype. In addition, macrophages are critically involved in tissue homeostasis and wound healing, where they show a more anti-inflammatory phenotype. Different factors like cytokines determine the phenotype, which can also be changed during an infection (15,16,18). If tissue-resident macrophages are depleted, circulating monocytes are recruited and differentiate into macrophages (15,16).

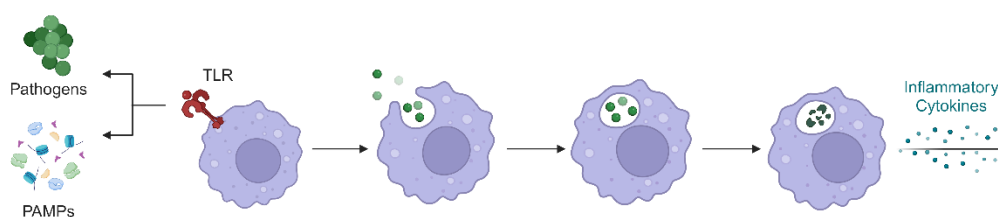


**Figure 1 Phagocytosis by macrophages**

Phagocytosis is a multi-step process. First, the phagocyte recognizes PAMPs or DAMPs via TLRs. The particle/pathogen is engulfed by the phagocyte cell membrane, and the phagosome is formed. After maturation of the phagosome and fusion with the lysosome, acidic pH and antimicrobial peptides/enzymes kill the pathogen or degrade other PAMPs/DAMPs. If a pathogen is detected, the secretion of inflammatory cytokines recruits further immune cells to the site of infection. (Figure created with BioRender)

Monocytes are highly abundant, circulating cells that are recruited to the site of inflammation via chemokine gradients. The existing pro-inflammatory conditions induce differentiation of

monocytes into macrophage- or DC-like cells (15,16). These cell types exhibit further pro-inflammatory phenotypes and produce high levels of cytokines and chemokines (16,19).

### 3.2.1.2 Dendritic Cells

DCs are mobile sentinel leukocytes involved in control of infections and tolerance (7). Their primary function is to initiate and regulate an adaptive immune response upon encountering a pathogen. Recognition and phagocytosis of pathogens induce processing of antigens and activation of DCs. To induce a pathogen-specific adaptive immune response, DCs migrate to secondary lymphoid organs and present the processed antigens to naïve T cells via MHC molecules. This process is visualized in **Figure 2**. Thus, DCs bridge the innate and adaptive arm of the immune system.

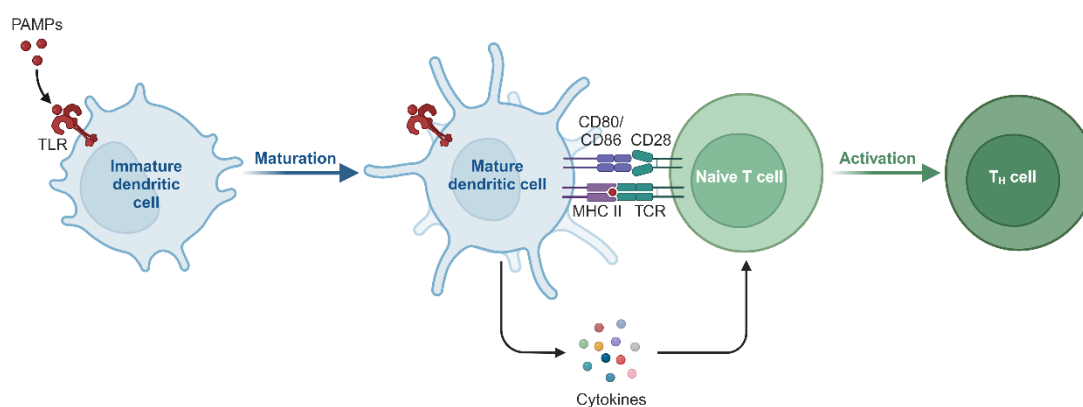


**Figure 2 DC maturation and presentation of antigens to T cells**

Immature DCs recognize PAMPs via e.g. TLRs. Subsequently, they mature and present the processed antigens to T cells via e.g. MHC II molecules. In addition, they increase the surface expression of co-stimulatory molecules, e.g., CD80/CD86, which interact with receptors on T cells, e.g., CD28. By secretion of different cytokines, DCs shape the direction of  $T_H$  cell differentiation. Presentation of antigens, co-stimulation, and cytokines lead to T cell activation. (Figure was created with BioRender)

As the most potent type of APCs, DCs are located throughout the whole body: they are present in blood and lymphoid as well as non-lymphoid tissues (20,21). DCs are a heterogeneous cell population and can be generally divided into two major subgroups: conventional or classical DCs (cDCs) and plasmacytoid DCs (pDCs). cDCs can be further divided into cDC1 and cDC2 subsets (20,21). cDC1 and cDC2 are also functionally distinct: while cDC1s specialize in cross-presentation of antigens to  $CD8^+$  T cells via MHC I, cDC2s mainly present antigens to  $CD4^+$  T cells via MHCII (20–23). pDCs are mainly located in human blood and tonsils. They are specialized in sensing viral pathogens and are characterized by rapid and excessive production of type I and III interferons in response to activating stimuli (23,24). Monocyte-derived DCs (moDCs) are another subgroup of DCs that may arise during inflammatory conditions (25–27). Since circulating DCs are scarce, much of the knowledge about DC function and response to infection was obtained by working with moDCs. They can be

generated *in vitro* by culturing human monocytes with granulocyte-macrophage colony-stimulating factor (GM-CSF) and IL-4 for several days. The obtained cells share certain traits with cDCs, e.g., maturing in response to infections, secretion of proinflammatory cytokines, and limited presentation of antigens (21–23,28).

### 3.2.1.3 Neutrophils

Neutrophils are the most abundant type of circulating leukocytes, making up 50-70% of total blood leukocytes. Due to their short lifespan, they are continuously released from the bone marrow (29). Neutrophils are among the first immune cells recruited to the site of infection. They are recruited via a multi-step process, encompassing binding to endothelial layers and transmigrating to connecting tissues via chemokine gradients (29–31). Once at the site of infection, neutrophils fight the invading pathogen using multiple antimicrobial mechanisms (32). Three main effector mechanisms are in place to fight infections:

- i. Degranulation: Neutrophils possess intracellular granules containing an array of different antimicrobial proteins and proteases. These granules, namely azurophilic, specific, tertiary granules, and secretory vesicles, are ready to use but differ in content. Some components are only present in one type of granule, e.g., myeloperoxidase (MPO) in azurophilic granules, while other components are present in multiple granules, e.g., resistin (33,34). During degranulation, granules fuse with the cell membrane and release their contents into the extracellular milieu. Antimicrobial peptides like LL-37 or defensins directly kill the pathogen, while enzymes like lysozyme attack the bacterial cell wall or proteases degrade key virulence factors and toxins (35). Degranulation is a primary effector mechanism for neutrophils and, therefore, tightly controlled by different signaling pathways. However, excessive neutrophil degranulation is associated with different disease pathologies, including inflammatory conditions like septic shock (36). In addition to antimicrobial compounds, neutrophil granules also contain pre-formed cytokines (37,38).
- ii. Neutrophil extracellular traps (NETs): NET formation is characterized by release of decondensed chromatin and granule proteins into the extracellular space by activated neutrophils. The chromatin traps bacteria, while the granule contents like LL-37 and histones kill the bacteria. Although this process helps to clear pathogens, excessive NET formation was shown to be involved in sepsis (39).
- iii. Phagocytosis and oxidant killing: This pathway includes uptake and killing of bacteria using ROS and reactive nitrogen species. ROS are generated via the NADPH oxidase or the myeloperoxidase-hydrogen peroxide system (40). Hydrogen peroxide (H<sub>2</sub>O<sub>2</sub>) is generated via spontaneous or dismutase-driven conversion of a superoxide

intermediate (41).  $H_2O_2$  can then be further converted to hydroxyl radicals or used as a substrate for generation of hypochlorous acid (HOCl) by MPO (42). These ROS are then used to kill bacteria.

### 3.2 *Staphylococcus aureus*

*Staphylococcus aureus* is a Gram-positive opportunistic pathogen, persistently colonizing the gut, nasopharynx, and skin of up to one-third of human population (43,44). Clinical manifestations of *S. aureus* disease range from mild skin and throat infections to severe, life-threatening diseases like necrotizing skin and soft tissue infections (NSTIs) or necrotizing pneumonia. (45) The increasing prevalence of antibiotic resistant strains, especially methicillin-resistant *S. aureus* (MRSA) strains, represent a significant healthcare concern (46). Since the mid-1990s, an increasing number of non-hospital associated MRSA infections, so-called community-acquired MRSA infections (CA-MRSA), have been registered. In contrast to hospital acquired infections, this type of infection also affects healthy individuals and is associated with more severe outcomes (47,48).

*S. aureus* infection is partially driven by secretion of a wide array of virulence factors (49). Pore-forming toxins like Panton Valentine Leukocidin (PVL), alpha-hemolysin, LukAB, and LukED are known to target innate immune cells via receptor-mediated lysis (50–55). In addition, *S. aureus* is able to internalize and persist in various cell types, including professional phagocytes, epithelial, and endothelial cells (56). The cytoplasmic environment induces a switch to small-colony variants (SCV), which are characterized by slow metabolism and antibiotic tolerance (57). In the form of SCVs, *S. aureus* is able to persist and cause recurrent infections (58,59).

#### 3.2.1 Periprosthetic Joint Infections

Joint replacement surgeries comprise successful orthopedic procedures to treat patients suffering from chronic pain and degenerative joint diseases (60). A projection based on age, gender, socioeconomic status, and year indicates increasing numbers of total joint replacements and corresponding implant revisions until 2030 (61). Tissue inflammation is a common complication of such procedures, often caused by implant-derived wear products. In severe cases, such wear products can induce adverse local tissue reactions (ALTRs). These include tissue necrosis and pseudotumor formation and can lead to implant revision (62,63). ALTRs are mainly driven by the innate immune response, characterized by extensive macrophage infiltration of peri-prosthetic tissue. However, lymphocyte infiltration is also evident. The infiltrating immune cells create a strongly proinflammatory environment, induced

by wear particle- and metal ion-mediated inflammasome activation as well as induction of necrosis (62,64–67). In clinical context, implant-derived metal ions and tissue inflammation are associated with early implant revisions (68–71), which occur in 7 to 15% of total hip or knee replacements (61).

Periprosthetic joint infections (PJIs) are another complication of arthroplasty. *S. aureus* is among the most prevalent causative pathogens (45,72–78). Simultaneous with increasing numbers of joint replacements and revisions, the incidence of PJIs has increased over past decades (79–81). Common symptoms include pain, swelling, and erythema of the affected joint (74). The majority of PJIs occur within 1 year of initial surgery and are considered low-grade infections, meaning a low bacterial load is present within the tissue (74). Exposure of bone marrow and peri-implant tissue to implant-derived wear products is believed to create an environment favorable for PJIs (79,82). Treatment of PJIs includes revision surgery with partial or complete exchange or explantation of the implant (83), debridement of necrotic/infected tissue, and prolonged antibiotic treatment (84–87).

### 3.3 *Streptococcus pyogenes*

*Streptococcus pyogenes* is a  $\beta$ -hemolytic, Gram-positive part of the commensal human microbiome (88). It is also referred to as group A streptococcus (GAS), based on the presence of Lancefield group A polysaccharide in the cell wall (89). However, GAS can also cause a broad spectrum of human diseases, ranging from mild superficial infections like pharyngitis to severe, life-threatening conditions like necrotizing fasciitis (NF) and streptococcal toxic shock syndrome (STSS) (90). In addition, post-streptococcal sequelae like rheumatic fever, rheumatic heart disease, or acute glomerulonephritis can occur following streptococcal infections (91). Host and bacterial factors can contribute to a switch from colonizing to pathogenic phenotype (91,92). GAS has emerged as a significant cause of morbidity and mortality, especially in low-income countries (91). GAS are estimated to cause disease in 18.1 million people and to cause approx. 500,000 deaths annually (91). From an epidemiological standpoint, GAS serotypes are classified based on the expression of different variants of the *emm*-gene, encoding for the highly abundant surface M-protein (93). So far, more than 200 *emm*-types have been identified, which are globally distributed (93). Depending on the geographical location, certain *emm*-types, e.g., *emm1* or *emm3* in industrial countries, are frequently associated with invasive disease (91). Recently, an increase in invasive GAS infections caused by a highly virulent *emm1*-clone, termed M1<sub>UK</sub>, was reported in several countries (94,95). Despite the long history of GAS research, no commercial vaccine is currently available (96).

### 3.3.1 Necrotizing Skin and Soft Tissue Infections

NSTIs are rare, severe, and rapidly progressing diseases. These infections are associated with high morbidity and mortality (97,98). Based on microbial etiology, three types of NSTIs can be distinguished: type I NSTIs are of polymicrobial origin, affecting mainly older individuals with underlying conditions (99,100). Type II NSTIs are monomicrobial infections, primarily affecting young and previously healthy individuals (99,101). GAS are among the most common pathogens, causing monomicrobial NSTIs (98,102), accounting for up to 31% of NSTI cases (98,102). Type III infections account for less than 1% of cases and are caused by *Vibrio* species, typically confined to warm coastal areas (99).

Delayed diagnosis can lead to multiple organ failure, a symptom of STSS, further complicating the treatment of NSTIs. Initial symptoms are non-specific, including fever, nausea, soft tissue edema, erythema, and sudden onset of severe pain (101). Treatment of NSTIs comprises extensive tissue debridement and intravenous antibiotic treatment, often a combination of a  $\beta$ -lactam like penicillin and clindamycin (103–106). Other therapies considered in treatment of NSTIs are admission of intravenous immunoglobulin (IVIG) (103) and hyperbaric oxygen therapy (107).

### 3.3.2 GAS Virulence Mechanisms

The course of human GAS infection is a multifactorial process involving bacterial and human factors. GAS produce a multitude of different virulence factors mediating tissue invasion, immune evasion, and bacterial survival. The composition and amount of virulence factors depend on M-type and environmental factors, meaning not all factors are present under all conditions (108–110). In this section, the most prominent virulence factors and regulation of virulence factor production are summarized. The main virulence mechanisms are visualized in **Figure 3**.

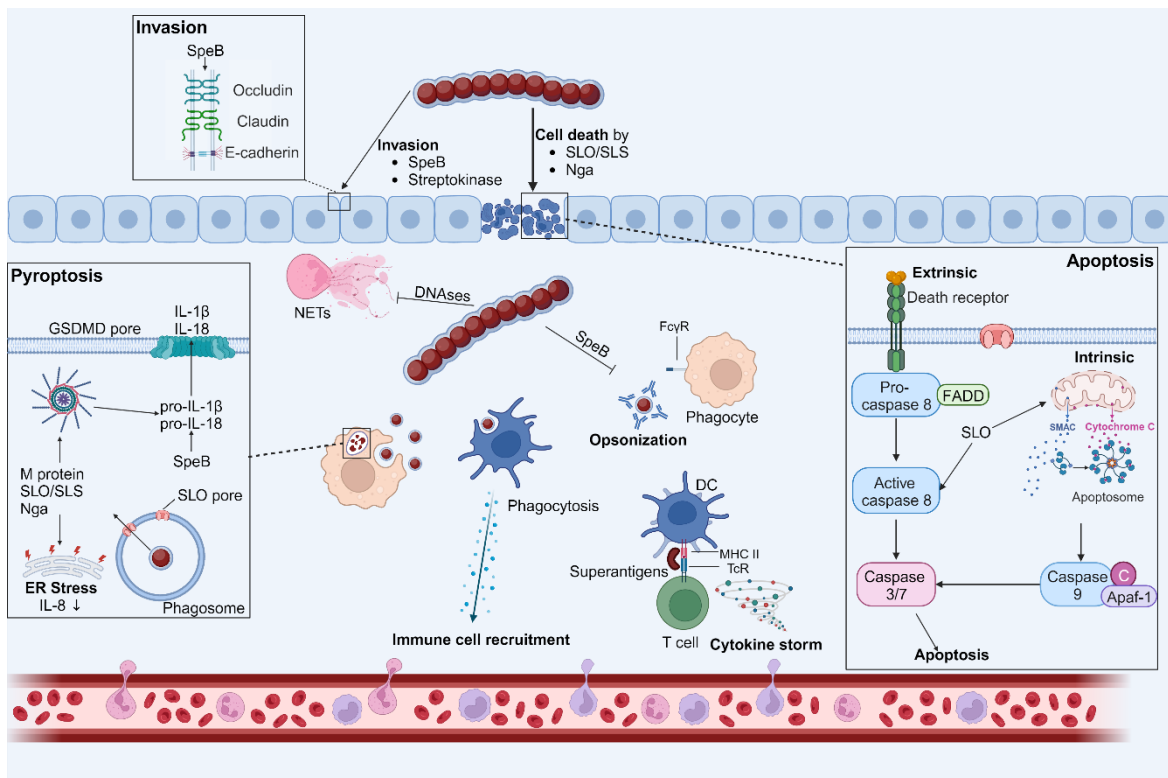


**Figure 3 GAS virulence mechanisms**

GAS possesses a plethora of different virulence factors, which help to invade host tissues/cells and evade the immune system. The cysteine protease SpeB can cleave cell junction proteins, granting the bacteria access to deeper tissue layers. The cytolysins SLO and SLS can induce apoptosis of epithelial cells, which disrupts the barrier function. GAS can escape from NETs by secreting DNases that degrade the DNA backbone. SpeB inhibits opsonization and subsequent phagocytosis by degrading antibodies. Superantigens induce pathological secretion of cytokines (cytokine storm). SLO mediates escape from phagosomes. SLO and Nga can induce ER stress and inflammasome activation, leading to release of IL-1 $\beta$  and IL-18. (Figure was created with BioRender, adapted from (96))

GAS virulence is tightly regulated. One of the main regulators is the two component system (TCS) CovR/S (control of virulence, also known as CsrRS (capsule synthesis regulon)). It consists of the membrane-associated sensor kinase CovS and the DNA-binding response regulator CovR. CovS activates and autophosphorylates upon sensing activating stimuli, e.g., pH acidification, high bacterial cell density, and high salt concentrations (111–113). Phosphorylated CovS then transfers the phosphate to position D53 at bound CovR, which induces dissociation from CovS (112). Phosphorylated CovR binds to DNA and either induces or represses transcription of target genes (114,115). Overall, CovR/S was found to regulate expression of up to 15% of the *S. pyogenes* genome (116). Dysfunctional CovR/S allows GAS to adopt a hyper-virulent phenotype. Such clones are frequently isolated from patients and in mice experiments, indicating a central role for CovR/S in GAS pathogenesis (117–122).

CovR/S controls production of several key virulence factors. It acts as a positive regulator of *speB* transcription. SpeB (streptococcal pyrogenic exotoxin B) is a highly conserved cysteine protease that is involved in many infectious processes. In addition to CovR/S, SpeB expression



is regulated by the global regulator of protease (RopB) (123). Despite its name, SpeB is neither an exotoxin nor pyrogenic (124,125). During *in vitro* culture of GAS, SpeB is produced and secreted as an inactive 42 kDa zymogen that autocatalytically cleaves itself into a 28 kDa active enzyme (126,127). SpeB cleaves host, as well as bacterial proteins. Known target proteins on the host side are extracellular matrix proteins (128), epithelial junction proteins (129), complement components (130), and the antimicrobial peptide LL-37 (131). Streptococcal proteins cleaved by SpeB include the M protein, the DNase Sda1, and streptolysin O (SLO), among others (132–135). This range of targets on both bacterial and host sites enables SpeB to modify the response to infection. SpeB has direct immunomodulatory effects by attenuating autophagy and improving intracellular bacterial survival (136) or impairing recruitment of immune cells by degrading chemokines (137). This protease also displays direct pro-inflammatory effects by cleaving inactive pro-IL-1 $\beta$  into its mature form (138). Moreover, pro-IL-18 and pro-IL-36 $\gamma$ , which are secreted by keratinocytes, are also cleaved to their respective mature forms by SpeB (139,140). In addition, SpeB is known to induce caspase-independent induction of pyroptosis by cleaving GSDMA. (141,142). Although the presence of SpeB at early stages of infection is beneficial for the course of infection, SpeB-negative isolates are frequently isolated from patients (117,143,144). This phenotype is often observed due to dysfunctional CovR/S.

For most virulence factors, CovR/S acts as a transcriptional repressor. It represses production of, e.g., the capsule synthesis operon, M-protein, SLO, and SpyCEP (145). The hyaluronic acid capsule of *S. pyogenes* was shown to confer protection from phagocytes (146,147) and mediate initial adherence to skin and pharynx epithelial cells (148). The chemical composition of the capsule is identical to human hyaluronic acid, enabling GAS to avoid detection by immune cells. However, capsule production does not seem essential for GAS virulence since isolates completely lacking the *hasABC* operon, responsible for capsule synthesis, or harboring inactivating mutations of *hasAB* were reported (149–152). The M-protein was shown to bind host plasminogen/plasmin or fibrinogen (88) and histones, conferring resistance to killing by the innate immune compartment (153). It also mediates adherence to host cells (154–156), and some M-types induce activation of the NLRP3 inflammasome (157,158). Hyper-virulent strains display a mucoid colony morphology and increased surface abundance of the M protein (159).

The clinical significance of the switch to a hyper-virulent phenotype is underscored by the finding that >50% of strains isolated from STSS patients possessed *covR/S* mutations, while only 2% of noninvasive isolates did (160,161). STSS is characterized by rapidly progressing multi-organ failure and is associated with high morbidity and mortality (162). Streptococcal superantigens are potent exotoxins and are involved in the pathogenesis of STSS (163).

Superantigens can crosslink the  $\beta$ -chain of the TcR and the MHC II molecules of APCs without prior antigen processing. This induces uncontrolled, non-antigen-specific activation and proliferation of up to 20% of total T cells (164,165). Excessive release of cytokines was shown to contribute to STSS and scarlet fever (94,164). Superantigens, especially SpeA, were shown to be essential during the initial phase of infection, enhancing bacterial colonization (166,167). In addition, superantigens induce activation and cytokine release of human mucosal-associated invariant T (MAIT) cells, which was shown to contribute to the pathological cytokine storm during STSS (168). Hypervirulent GAS variants often display increased production of superantigens (159,169).

STSS isolates were also found to produce increased levels of SLO (160,170), which is the case in hyper-virulent variants, as functional CovR/S represses transcription of *slo* (122). SLO and streptolysin S (SLS) are pore-forming toxins and are widely distributed in GAS clinical isolates. SLO is a cholesterol-dependent cytolysin that mediates host cell lysis via binding multiple glycan receptors (171). SLS is a small non-immunogenic peptide that accumulates at the bacterial surface and causes eukaryotic membranes to collapse (172,173). Both toxins induce cell death of a wide range of host cells, including innate immune cells (172,174,175). In addition, both toxins were shown to induce activation of the NLRP3 inflammasome in human macrophages (158). *Slo* is co-expressed with *nga*, a NAD glycohydrolase (NADase) (176). The physical interaction of SLO and Nga was shown to co-stabilize the two toxins after secretion (177,178). In addition, Nga facilitates the binding of SLO to the cell membrane, promoting SLO pore formation. Translocation of Nga to the host cell cytosol is dependent on SLO (179). In the cytosol, it depletes energy stores and induces cell death (180,181). The combined action of both toxins contributes to bacterial pathogenesis (182) by mediating escape from phagolysosomal killing (183,184) and disrupting host cell protein synthesis and trafficking (185,186). Moreover, it was recently shown that NADase activity suppresses release of type I IFNs by macrophages, promoting inflammation and severe disease (187). Increased expression of SLO and Nga is associated with increased disease severity and emergence of new, highly virulent strains (109,151,188).

### 3.3.3 Interaction of GAS with Neutrophils and DCs

Severe GAS infections, e.g., NSTIs, are characterized by high bacterial loads and extensive immune cell infiltration, including neutrophils (189,190). Extensive neutrophil degranulation and release of proteolytic enzymes are associated with substantial tissue damage. Several GAS virulence factors were shown to induce neutrophil degranulation, including the M protein (189–191). GAS can escape NETs, mediated by DNases (192). So far, six different DNases have been described, and all sequenced clinical isolates encode for at least one DNase (193).

DNases release trapped bacteria from NETs by degrading the DNA framework (194,195). They also impair recognition of bacteria by immune cells via TLR9 (196,197). In addition, GAS can interfere with neutrophil recruitment by degrading the chemokine IL-8 using the cell envelope serine protease SpyCEP (198–200). SLO was shown to promote bacterial resistance to phagocytic killing by impairing neutrophil oxidative burst (201). SLS was shown to impair neutrophil recruitment and opsonophagocytic killing of bacteria by targeting neurons, causing invasive disease (202).

Little is known about the interaction of GAS and DCs. One study has identified DCs as an essential part of defense against GAS infection in a mouse model (203). In general, DCs were shown to mature and secrete IL-12 in response to GAS infection (204,205). However, both capsule and SLO were shown to interfere with DC maturation and, in the case of SLO, induce significant cell death (206,207).

### 3.4 Study Objectives

The innate immune system, particularly myeloid cells, is crucial for detecting invading pathogens and rapidly initiating a pro-inflammatory response. However, different factors, both host and bacterial, can affect key effector mechanisms. Metal-based implants are widely used in arthroplasty and are well-known factors affecting immune cells' function and phenotype. Both *S. aureus* and GAS are Gram-positive human commensals that can cause severe disease. GAS, in particular, have developed multiple mechanisms to evade and manipulate the human immune system. Delay or even prevention of myeloid cell activation could severely affect the outcome of infection. Understanding the underlying disease mechanisms and contributions of individual virulence factors provides targets to improve existing therapies/materials or develop new ones.

This thesis aims to characterize how implant-derived metal ions and bacterial phenotype switches impact and modulate the innate immune systems' response to infection.

The specific objectives are:

- i. To investigate how exposure of monocytes/macrophages to implant-derived  $\text{Co}^{2+}$  and  $\text{Cr}^{3+}$  ions impacts the cellular response to *S. aureus* infection (Paper I)
- ii. To characterize the cytokine response of moDCs to infections with virulent and hyper-virulent GAS strains (Paper II)
- iii. To identify the mechanism responsible for the SpeB negative phenotype in GAS observed in patient tissue (Paper III)

## 4. RESEARCH APPROACH

The detailed experimental methods are described in the methods section of the corresponding papers. Selected methods are presented below.

### 4.1 Ethics Statement

All studies were conducted in accordance with the Helsinki Declaration. Patient samples were retrieved from the INFECT patient cohort consisting of patients with NSTI (INFECT study; ClinicalTrials.gov, NCT01790698). The patient biopsies and plasma were obtained at surgical interventions, and GAS infections were primarily identified by routine diagnostics. Patient enrolment and sample analyses were approved by the regional Ethical Review Board at the National Committee on Health Research Ethics in Copenhagen (Ref. No. 1211709), the regional ethics committee in Gothenburg (Ref. No. 930-12), the regional ethics committee Vest, Norway (REK, Ref. No. 325786), and the regional Ethics Committee in Stockholm (Ref. No. 2012/2110-31/2).

Peri-implant soft tissue samples were collected during aseptic arthroplasty implant revisions at the University Medicine Greifswald. The ethical research committee at the University Medicine Greifswald approved the study (BB 178/20). All patients gave written informed consent to participate in this study.

Blood samples from healthy volunteers or buffy coats of blood provided by the blood bank at the University Medicine Greifswald were used. The buffy coats were provided anonymously. The ethical research committee at the University Medicine Greifswald approved the study (Ref. No. BB 014/14 and Ref. No. BB 006/18). All experiments were carried out in accordance with the approved guidelines.

### 4.2 Bacterial Strains

The GAS strains (5448, 5626, 8003, and 8157) were isolated from NSTI patients in Canada (208,209). The strains 2002 and 2006 were obtained during the INFECT study (210,211). In addition, two hyper-virulent strains harboring dysfunctional CovR/S, MGAS5005 (159) and 5448AP (118,212) were used. All strains were grown in Todd-Hewitt broth supplemented with 1.5% (w/v) yeast extract (THY) at 37°C and 5% CO<sub>2</sub> for 16-18 h.

*S. aureus* strain 6005 (213) was grown overnight at 37°C in casein hydrolysate and yeast extract medium with agitation (214).

### 4.3 Isolation of Human Myeloid Cells and Infection

Myeloid cells are critical first responders to infection. While macrophages are resident cells, DCs are highly mobile, migrating cells. Both cell types are difficult to obtain from peripheral blood but can be generated from monocytes under inflammatory conditions. *In vitro*, this is achieved by isolating monocytes from peripheral blood and culturing them in presence of cytokines for several days. The obtained macrophages or DCs were shown to respond to infections similar to their tissue-resident counterparts (7,15,16,215). Neutrophils are among the first cells recruited to the site of infection. Since neutrophils have a short lifespan, they were freshly isolated from whole blood of healthy donors and immediately infected with GAS. The general experimental approach of Paper I and Paper II is shown below (**Figure 4**).

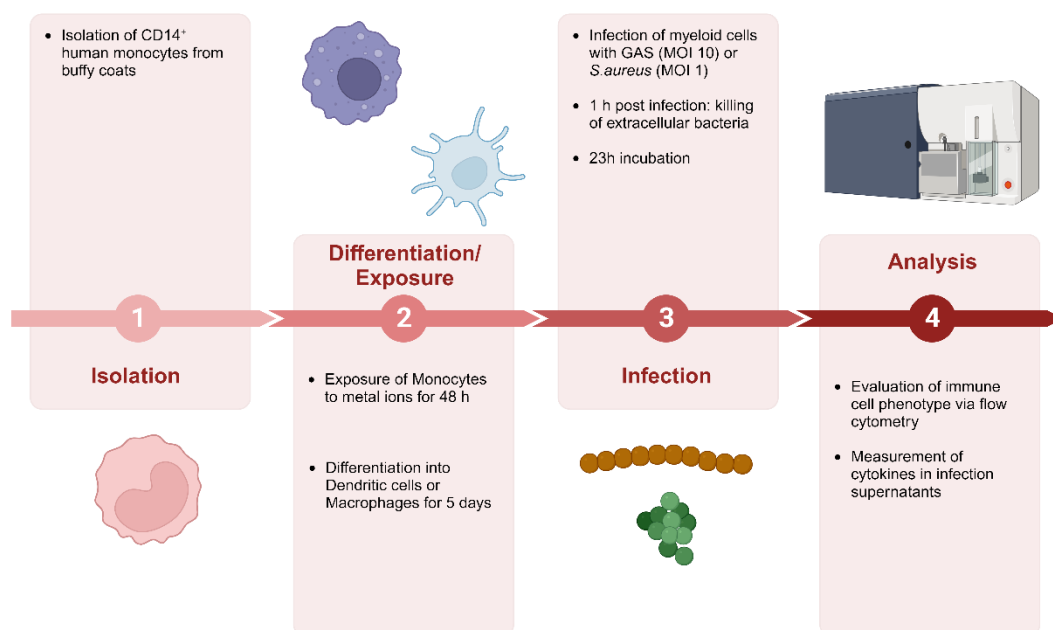


**Figure 4** General experimental approach for Paper I and Paper II.

CD14<sup>+</sup> monocytes were isolated from human buffy coats via positive selection. The obtained monocytes were either exposed to Co<sup>2+</sup> or Cr<sup>3+</sup> ions or a combination of both for 48 h, or they were used to generate moDCs or monocyte-derived macrophages. After 24 h of metal exposure, monocytes/macrophages were infected with *S. aureus* (MOI 1), while moDCs and macrophages were infected with GAS (MOI 10) after 5 d of differentiation. In both cases, extracellular bacteria were killed by addition of antibiotics 1 h post-infection. To ensure full maturation of cells, they were incubated for additional 23 h. To evaluate immune cell phenotype post-infection, the cells were stained for different surface markers and analyzed via flow cytometry. In case of GAS infections, the cytokine response was evaluated using a bead-based, flow cytometric assay. (Figure was created with BioRender)

#### 4.3.1 Isolation of Human Monocytes, Exposure to Metal Ions & Infection with *S. aureus*

Macrophages were shown to contribute to tissue pathology of ALTRs. However, the influence of metal exposure on the cellular phenotype and response to infections is still unclear. Paper I aimed to elucidate the impact of metal exposure on monocyte/macrophage phenotype and their response to infection. To analyze metal ion-mediated effects on human monocytes/macrophages, monocytes were isolated from buffy coats using a bead-based positive selection approach. Cobalt (II) chloride hexahydrate and chromium (III) chloride hexahydrate were dissolved in human AB serum and incubated overnight at 37 °C to mimic *in vivo* formation of biomacromolecule-ion-complexes. Isolated monocytes were exposed to metal salt solutions for 48 h. Metal-stimulated monocytes/macrophages were infected with *S. aureus* 6005 at a multiplicity of infection (MOI) of 1 for 1 h to mimic initial low-grade infections. Extracellular bacteria were killed by addition of antibiotics. For flow cytometry, infected monocytes were incubated for additional 23 h. For assessing intracellular bacterial counts, monocytes were infected as described above. 1 h after addition of antibiotics, cells were washed and lysed, and intracellular bacteria were plated on blood agar plates.

#### 4.3.2 Isolation of Human Monocytes, Generation of moDCs & Infection with GAS

DCs are essential for resolving infections and initiation of an adaptive immune response. However, little is known about interactions of GAS and DCs. Paper II aimed to analyze the impact of hyper-virulent GAS variants on the cytokine response of human monocytic cells. To generate moDCs and monocyte-derived macrophages, human monocytes were isolated from buffy coats using a bead-based positive selection approach. The moDCs were generated by culturing monocytes for 5 d in presence of GM-CSF and IL-4. The monocyte-derived macrophages were generated by culturing monocytes in presence of only GM-CSF for 7 d. Monocytes, monocyte-derived macrophages, or moDCs were infected with GAS strains at a MOI 10 for 1 h. Next, extracellular bacteria were killed by addition antibiotics. To ensure full maturation in response to infection, cells were incubated for additional 23 h. Supernatants were collected from all cell types and the moDCs were directly prepared for flow cytometry. For assessing intracellular bacterial survival kinetics, moDCs were infected as described above. After addition of antibiotics, the cells were washed, lysed, and intracellular bacteria plated on blood agar plates.

#### 4.3.3 Isolation of human neutrophils and infection with GAS

NSTIs are characterized by extensive immune cell infiltration, including neutrophils (189,190). Extensive neutrophil degranulation is associated with increased tissue pathology. Paper III aimed to characterize the impact of SpeB<sup>-</sup> phenotype GAS on the neutrophil response. Human primary neutrophils were isolated from healthy donors using density gradient centrifugation on Polymorphprep. After isolation, neutrophils were immediately infected with GAS at a MOI 10 for 1 h. Extracellular bacteria were killed by addition of antibiotics. At indicated time points (Paper III), neutrophils were washed lysed, and intracellular bacteria were plated on casein agar plates to assess SpeB secretion. Neutrophil degranulation was assessed by secretome analysis of supernatants post-infection with GAS.

#### 4.4 Analysis of Immune Cell Phenotype Post-Infection

Myeloid cells can undergo drastic phenotypic changes upon encountering a pathogen. MoDCs will mature in response to infection, meaning they stop antigen uptake and increase expression of surface markers essential for T cell stimulation (HLA-DR, CD80, CD83, CD86, CD40) (7). Monocytes and macrophages also express a distinct array of surface markers that changes in response to infection (19). To evaluate the cellular response to infection of both metal-exposed and infected monocytes/macrophages and infected moDCs, expression of surface markers was assessed via flow cytometry. First, dead cells were labeled, and unspecific binding of immunoglobulins was blocked by addition of an Fc-blocking agent. Cells were incubated with titrated amounts of monoclonal antibodies directed against different surface and intracellular molecules. Cells were washed between each staining step and fixed. Data were acquired using a FACSAriaIII flow cytometer. The respective gating strategies for monocytes/macrophages (Paper I; Fig. 5A) and moDCs (Paper II; Fig. 5B) are shown in **Figure 5**.



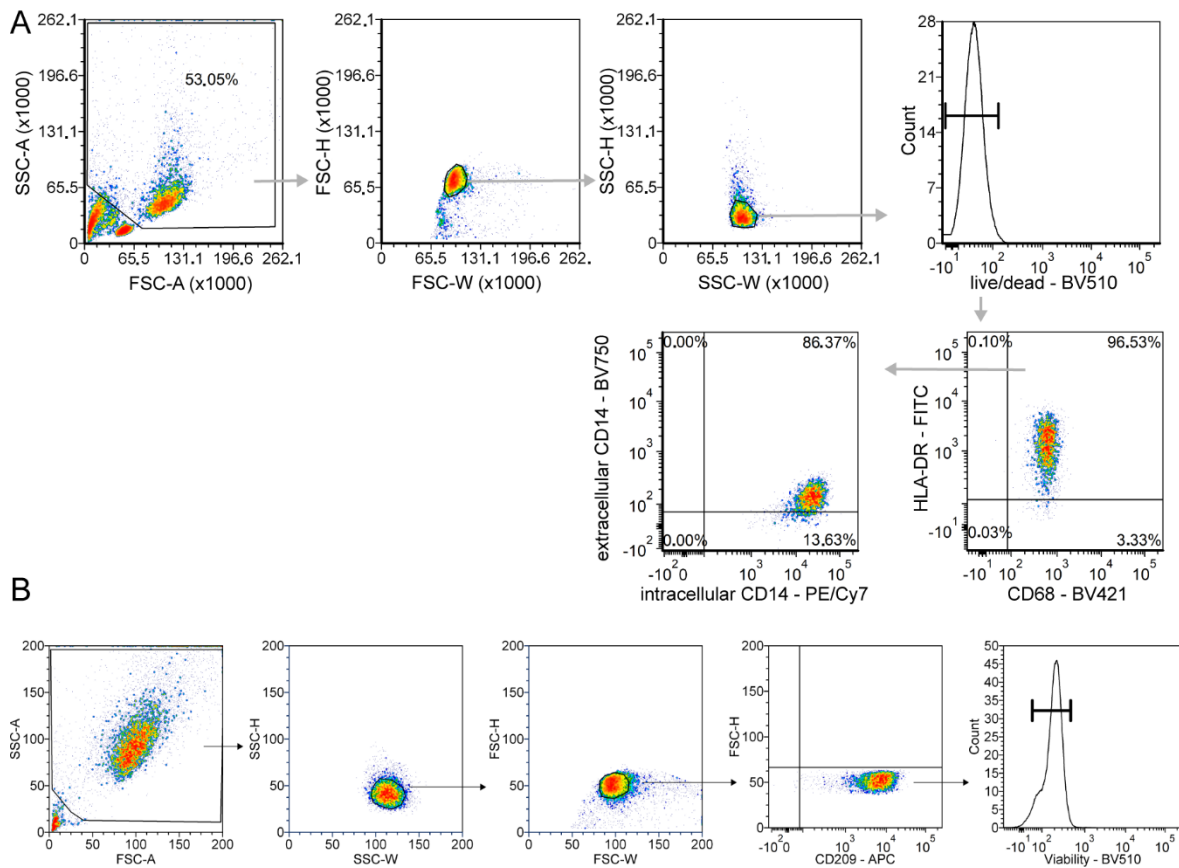


**Figure 5** Gating strategies used to identify human myeloid cells

(A) Monocytes/Macrophages: doublets were excluded by consecutive gating of FSC-H/FSC-W and SSC-H/SSC-W. Dead cells were excluded by using the Zombie Aqua™ Fixable Viability Kit. Monocytes/macrophages were selected based on the expression of HLA-DR and CD68. Macrophage subsets were further distinguished based on expression of intracellular and extracellular CD14. Subsequently, the macrophage subsets were analyzed for positivity and surface expression of CD16, CD38, HLA-DR, and PD-L1. (B) MoDCs: doublets were excluded by consecutive gating of FSC-H/FSC-W and SSC-H/SSC-W. MoDCs were selected based on the expression of the specific moDC marker DC-SIGN (CD209). Dead cells were excluded by using the Zombie Aqua™ Fixable Viability Kit. MoDCs were analyzed for positivity and expression of different costimulatory surface markers, including CD40, CD80, CD83, CD86, and HLA-DR.

#### 4.5 Cytokine Secretion in Response to GAS Infection

In addition to presenting antigens and clearing pathogens, myeloid cells secrete cytokines to shape the T cell response. DCs were shown to be the primary sources of IL-12 (7), while macrophages are potent producers of tumor necrosis factor (TNF), IL-6, and IL-8 (19). Moreover, myeloid cells are the main producers of inflammasome-derived IL-1 $\beta$  and IL-18 (7). Therefore, supernatants of the infected cells were collected, and cytokine concentrations were measured using a bead-based multiplex assay. Data were acquired with a FACSria III flow cytometer.

## 5. RESULTS & DISCUSSION

### 5.1 Cobalt and Chromium Ions Impair Macrophage Response to *Staphylococcus aureus* Infection

CoCrMo alloys are biomaterials widely used in arthroplasty. Development of ALTRs due to implant-derived wear particles and metal ions is associated with an increased risk for revision arthroplasty and PJI. ALTRs are characterized by macrophage infiltration (62). Metallic wear particles and ions, in particular  $\text{Co}^{2+}$  and  $\text{Cr}^{3+}$ , were shown to induce cytotoxicity (216) and interfere with macrophage migration (217) and activation (63). However, little is known about the effects of exposure to  $\text{Co}^{2+}$  and  $\text{Cr}^{3+}$  ions on human primary macrophages and its subsequent influence on the cellular response to bacterial infection.

#### 5.1.1 Local Metal Exposure and Macrophage Infiltration Are Evident in Patient Tissue

Local exposure of peri-implant tissue to  $\text{Co}^{2+}$  and  $\text{Cr}^{3+}$  ions (217) and macrophage infiltration (62) are well-accepted phenomena in arthroplasty. Local exposure to Co and Cr was evident in all biopsies used in this study (Paper I, Figs. 1,2). To evaluate macrophage infiltration, confocal laser scanning microscopy (CLSM) was performed. This revealed highly auto-fluorescent metal particles distributed in the tissue (Paper I, Fig. 3A), as well as dense areas of macrophage infiltration (Paper I, Fig. 3B). These results confirmed local exposure of macrophages to implant-derived metallic wear particles and metal ions.

#### 5.1.2 Exposure to Metal Ions Induces Loss of Surface Markers

To evaluate how exposure to pathological concentrations of  $\text{Co}^{2+}$  and  $\text{Cr}^{3+}$  ions impacts monocyte/macrophage phenotype, primary human monocytes were isolated. Subsequently, cells were exposed to  $\text{Co}^{2+}$  and/or  $\text{Cr}^{3+}$  ions for 48 h, and the cell phenotype was analyzed via flow cytometry. In all conditions, monocytes differentiated into macrophages (Paper I, Fig. S1), and exposure to metal ions did not significantly reduce macrophage viability (Paper I, Fig. 4A). Analysis of macrophage phenotype revealed an almost complete loss of surface CD14 when cells were exposed to high concentrations of  $\text{Co}^{2+}$  (Paper I, Fig. 4B). However, solely CD14<sup>+</sup> macrophages were detected via CLSM (Paper I, Fig. 3B). Since immunostaining of tissue biopsies requires permeabilization steps, distinction between surface-associated and intracellular CD14-staining was not possible via this method. Therefore, *in vitro* metal-exposed monocytes/macrophages were stained for intracellular CD14. In all conditions, the entire population stained positive for intracellular CD14 (Paper I, Fig. 4C and S2). In addition, expression of the FCγRIII receptor CD16 was analyzed, showing an almost complete loss of surface CD16 when cells were exposed to high concentrations of  $\text{Co}^{2+}$  (Paper I, Fig. 4D). Metal

ions, especially  $\text{Co}^{2+}$ , were shown to induce intracellular oxidative stress (218). Loss of surface CD14, paired with detectable intracellular CD14, suggests that high concentrations of  $\text{Co}^{2+}$  induce ER or Golgi stress. Induction of both pathways can lead to disruption of intracellular protein trafficking, which interferes with immune cell functionality (219). Tissue-resident macrophages readily phagocytose implant-derived wear particles. However, due to their inorganic nature, such particles cannot be fully degraded, and the phagolysosomal acidic pH even leads to release of additional ions from those particles (218). The released ions can diffuse to the cytosol and induce oxidative stress and misfolding of proteins, resulting in ER stress induction via the unfolded protein response (218).

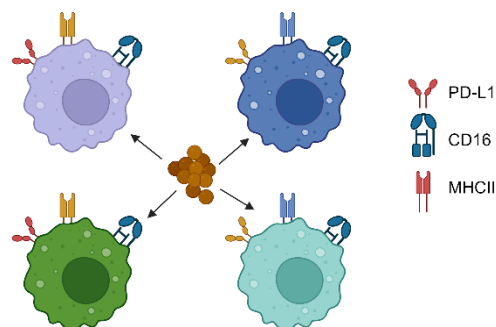


**Figure 6 Effects of metal exposure on macrophage phenotype**

Human primary monocytes were left untreated (purple) or exposed to  $\text{Co}^{2+}$  (blue),  $\text{Cr}^{3+}$  (green) or  $\text{Co}^{2+}/\text{Cr}^{3+}$  (turquoise). In all conditions, monocytes differentiated to macrophages. Macrophage phenotype and response to infection were analyzed. PD-L1, CD16, and MHC II are included in this figure. Blue indicates downregulated, yellow indicates unchanged, and red indicates upregulated expression of surface markers in response to infection. (Figure created with BioRender)

Since previous studies have reported activation of macrophages in response to stimulation with metal ions (220,221), surface expression of activation marker CD38, antigen-presenting HLA-DR, and checkpoint inhibitor PD-L1 were assessed. Exposure to metal ions did not cause macrophage activation on a cellular level, as shown by lack of CD38 expression (Paper I, Fig. 5A) and unchanged expression of PD-L1 (Paper I, Fig. 5C). In addition, a decrease of HLA-DR expression was detected in macrophages exposed to high concentrations of  $\text{Co}^{2+}$  (Paper I, Fig. 5B). In the mentioned studies, macrophage activation was analyzed by expression of cytokine mRNAs (*IL1B*, *CXCL8*) (220) and release of cytokines ( $\text{IL-1}\beta$ , *CXCL8*) (221), both referred to as indicative of macrophage activation. However, we did not detect any signs of macrophage activation on a cellular level, as shown by the lack of upregulation of activation markers (CD38, HLA-DR, PD-L1). Expression of HLA-DR was even downregulated after exposure to high concentrations of  $\text{Co}^{2+}$ , which was also confirmed on transcript level (Paper I, Fig. S4E, **Figure 6**). These results point to metal ion-mediated immuno-suppressive effects but not activation. However, induction of ER stress was shown to induce inflammasome

activation and release of IL-1 $\beta$ , suggesting cytokine release by induction of stress responses rather than activation of macrophages (219).

### 5.1.3 Exposure to Metal Ions Impairs Macrophages' Response to Infection

Next, we assessed the metal-exposed macrophages' response to infection. Since *S. aureus* is a common cause of PJIs, cells were infected with methicillin-susceptible *S. aureus* strain 6005. To mimic peri-implant tissue conditions, the cells were continuously exposed to metal ions. Since exposure of macrophages to high concentrations of Co<sup>2+</sup> led to an almost complete loss of surface CD16 (Paper I, Fig. 6D), we also assessed the phagocytic capacity of metal-exposed cells. Here, macrophages exposed to high concentrations of Co<sup>2+</sup> showed reduced uptake of *S. aureus*, as compared to the other conditions (Paper I, Fig. 6A, **Figure 6**). In all other conditions, macrophages showed reduced expression of surface CD16 post-infection (Paper I, Fig. 6D). CD16 is a Fc $\gamma$ III receptor that facilitates phagocytosis of opsonized bacteria (222). As the experiments were carried out in presence of human serum, opsonization of bacteria is likely to occur in this setting. *S. aureus* is a common colonizer among humans (43,44), and antibodies directed against staphylococcal proteins can readily be detected in sera of healthy people (223). The almost complete loss of surface CD16 provides a probable cause for the reduced phagocytosis. Binding of the antibodies Fc region to CD16 induces activation of several signaling cascades, ultimately leading to engulfment of the receptor-bound antibody and bacteria within a phagosome (224). In addition, Fc $\gamma$  receptors can take a more anti-inflammatory role triggered by binding of free IgG and IVIG. Anti-inflammatory effects include dampening ROS response and reduced influx of immune cells to inflamed tissue (224,225). Although speculative, reduced phagocytosis could delay bacterial clearance in a tissue setting, while loss of anti-inflammatory effector functions could aggravate tissue damage by excessive immune cell activation. If bacteria are not cleared, they could proliferate and spread to surrounding tissue, as well as enter biofilm formation. Cases of biofilm formation have been described in PJI patients (74,226).

In addition, cellular activation of macrophages was analyzed in response to infection. Metal ions completely suppressed activation of infected macrophages, shown by lack of expansion of CD38<sup>+</sup> cells (Paper I, Fig. 7A). In addition, macrophages exposed to high concentrations of Co<sup>2+</sup> showed diminished upregulation of PD-L1 expression in response to infection (Paper I, Fig. 7C, **Figure 6**). PD-L1 is part of the inhibitory immune checkpoint receptor set PD-1/PD-L1. Activation of this pathway inhibits T cell activation and provides a mechanism to prevent excessive, pathologic T cell activation (227). Therapeutics targeting this pathway are used in treatment of several forms of cancer (227). Reduced PD-L1 expression in response to activating stimuli might provide an additional explanation for the pro-inflammatory environment

in ALTRs. Stimulation of T cells by clinical *S. aureus* isolates leads to activation and surface expression of PD-1, the receptor for PD-L1 (228). Interaction of PD-1 and PD-L1 inhibits excessive T cell activation and cytokine secretion. Thus, if inhibition of T cells via the PD-1/PD-L1 axis is reduced, uncontrolled T cell activation and extensive secretion of cytokines are likely to contribute to ALTR pathology.

In conclusion, these findings provide insights into the biological side effects of a widely used biomaterial. Development of ALTRs as a consequence of local and systemic exposure to implant-derived wear particles and metal ions is well-studied. Understanding the detailed mechanisms of the local tissue response and the consequences for the immune response is critical to improving existing biomaterials as well as developing new materials. This study shows that exposure to metal ions significantly interferes with essential effector functions of monocytes/macrophages. These results provide an explanation for the increased risk of PJIs following revision surgeries. In this very active field of study, this study might help to re-assess the use of CoCrMo in considering the possible long-term effects of implant-derived wear products. In the future, analysis of *ex vivo* samples regarding macrophage phenotype and response to infection should be considered.

## 5.2 Hyper-virulent *Streptococcus pyogenes* Impairs Interleukin-18 Response in Human Monocytic Cells

Myeloid cells are primary sources of cytokines and chemokines upon detecting invading pathogens. The composition of cytokines/chemokines determines which immune cells are recruited and shapes the subsequent T cell response needed to clear the infection. However, bacteria, including GAS, have developed several ways to circumvent the host response. In severe infections, GAS were shown to adopt a hyper-virulent phenotype to avoid clearance and influence the immune response.

### 5.2.1 GAS Harboring Dysfunctional CovR/S Suppress IL-8 and IL-18 Secretion in Myeloid Cells

Hyper-virulent GAS strains were shown to induce an excessive pro-inflammatory response, which is often associated with STSS (160). Myeloid cells, especially DCs, are primary sources for the IL-1 family cytokines IL-1 $\beta$  and IL-18 (7). Both cytokines are released via the inflammasome axis and are closely linked to NSTIs and development of STSS (168,229–231). To determine whether virulent and hyper-virulent GAS strains induce differential cytokine responses by moDCs, cells were infected with either four strains harboring functional CovR/S (CovR/S<sup>+</sup>) or four strains harboring dysfunctional CovR/S (CovR/S<sup>-</sup>). While secretion of IL-1 $\beta$  was unaffected by GAS phenotype (Paper II, Fig. 1A), moDCs infected with hyper-virulent strains secreted significantly reduced levels of IL-18 (Paper II, Fig. 1B) and IL-8 (Paper II, Fig. 1C). A similar phenotype was observed in infections of monocytes and monocyte-derived macrophages, showing that it is not restricted to moDCs (Paper II, Fig.2).

In addition to cytokine secretion, DC maturation is characterized by expression of co-stimulatory surface markers to provide activating signals for T cells. Therefore, moDC maturation in response to GAS infection was assessed. MoDCs remained viable (Paper II, Fig. 3B) and readily matured in response to infections, irrespective of GAS phenotype (Paper II, Fig. 3A-G). In addition, analysis of whole proteome of infected moDCs did not reveal significant global differences between CovR/S<sup>+</sup> and CovR/S<sup>-</sup> infection (Paper II, Fig. 3H). This suggests that, although hyper-virulent strains lead to abrogated secretion of IL-8 and IL-18, overall maturation of moDCs is not affected.

### 5.2.2 Caspase-8 Inhibition Restores Secretion of IL-8 and IL-18 by MoDCs in CovR/S<sup>-</sup> Infections

Hyper-virulent strains exhibit increased production of the cell-envelope protease SpyCEP (122), which has been shown to reduce levels of IL-8 in GAS infections (120,198). Thus, we focused on elucidating the mechanism responsible for abrogated IL-18 secretion in moDCs.

Pro-IL-18 contains predicted cleavage sites for caspase-1 and caspase-3 (232). Processing of IL-18 by caspase-3 yields biologically inactive fragments (233). To determine whether inhibition of caspase-3 or its activator caspase-8 would restore secretion of IL-18 by moDCs, cells were pretreated with specific caspase inhibitors and subsequently infected with a hyper-virulent strain. Secretion of IL-1 $\beta$  was not affected by caspase inhibition (Paper II, Fig. 4A-B). Caspase-8 and pan-caspase inhibition restored secretion of IL-18 (Paper II, Fig. 4C) and IL-8 in response to CovR/S<sup>-</sup> infections (Paper II, Fig. 4D). Next, caspase-8 activity was measured in infected moDCs. Infections with a CovR/S<sup>-</sup> strain activated caspase-8 in moDCs, while infections with the CovR/S<sup>+</sup> strain did not (Paper II, Fig. 5C). Caspase-8 is involved in many cellular processes. It was shown to participate in necroptosis as part of the ripoptosome, which ultimately leads to activation of NF- $\kappa$ B and a pro-inflammatory response (234). In addition, caspase-8 can substitute for loss of caspase-1 in pyroptosis, resulting in release of both mature IL-1 $\beta$  and IL-18 (10,12,13). This protease is dysregulated in many cancer cells, emphasizing its central role in cellular signaling (234). Caspase-8 undergoes post-translational modifications depending on cellular function and activating stimulus. Such modifications shape and shift its activity and affinity for different target molecules (234,235). Although speculative, CovR/S<sup>+</sup> and CovR/S<sup>-</sup> strains might induce differential post-translational modification of caspase-8. This could prevent activation in infections with CovR/S<sup>+</sup> strains and induce cleavage of IL-18 in infections with CovR/S<sup>-</sup> strains, potentially yielding inactive IL-18. Alternatively, another protease downstream of caspase-8 could cleave IL-18 in CovR/S<sup>-</sup> infections of moDC.

### 5.2.3 Impact of Dysfunctional CovR/S on Systemic Cytokine Levels in NSTI Patients

Elevated levels of IL-18 were detected in plasma and saliva in pharyngitis human challenge trial participants, suggesting a role for IL-18 in human GAS infections (236). In addition, the IL-12/IL-18 axis (168) is closely linked to NSTIs and STSS. Therefore, the CovR/S phenotype of GAS isolates collected during the INFECT study was determined and correlated to previously measured plasma concentrations of IL-8, IL-1 $\beta$ , and IL-18 (231). Matching of CovR/S phenotype to plasma cytokine concentrations of respective patients revealed equal systemic concentrations of IL-18, irrespective of CovR/S status (Paper II, Fig. 6A-C). In addition, patients were grouped based on clinical presentation, with and without septic shock. No differences in systemic concentrations of IL-18 were detected between patient groups (Paper II, Fig. 6F). The main function of IL-18 is induction of IFN- $\gamma$  secretion by T cells (8). IFN- $\gamma$  is one of the primary driving forces of STSS development (163). In STSS, MAIT cells were the major contributors to IFN- $\gamma$  production in response to GAS (168). Reduced local IL-18 concentrations could impair or delay activation of MAIT cells and corresponding secretion of IFN- $\gamma$ . As IFN- $\gamma$  primes macrophages for phagocytosis and induces an overall more pro-

inflammatory phenotype (237), abrogated secretion could improve bacterial survival. However, hyper-virulent GAS were shown to produce increased amounts of superantigens (228), potentially negating the effects of reduced IL-18.

#### 5.2.4 Secretion of IL-1 $\beta$ and IL-18 by MoDCs Is Increased in Infections with 5448 $\Delta$ *slo*

SLO was previously shown to interfere with maturation of murine DCs (207) and to induce caspase activation (175). As its expression is under CovR/S control, we hypothesized that SLO is involved in suppressing the secretion of IL-18 by moDCs. Since we were not successful in constructing a *slo* mutant in 5448AP genetic background, experiments were performed with 5448 $\Delta$ *slo*. Here, we hypothesized that infections of moDCs with 5448 $\Delta$ *slo* would further increase the IL-18 response compared to wild-type infections. Both strains induced secretion of equal levels of IL-8 (Paper II, Fig. 7F). However, concentrations of IL-1 $\beta$  (Paper II, Fig. 7G) and IL-18 (Paper II, Fig. 7H) were significantly higher in infections of moDCs with 5448 $\Delta$ *slo* as compared to wild-type infections. Our data suggests that SLO is involved in suppression/reduction of cytokine secretion by moDCs via an unknown mechanism. This cytotoxin was shown to induce ER stress in murine cells (186). As described in section 5.1.2, ER stress impacts intracellular protein production and trafficking (219). Monocytic cells possess intracellular stores of pro-IL-1 $\beta$  and pro-IL-18 (238,239). However, *de novo* synthesis and release of both cytokines would be affected during ER stress, preventing release of additional cytokines. In this way, excessive secretion of SLO would i) lyse host phagocytes, ii) interfere with cytokine/chemokine secretion, and iii) inhibit/delay recruitment of additional phagocytes. Thus, this cytotoxin provides different immune evasion mechanisms.

Data on GAS-DC interaction is scarce and mainly derived from work with murine models. Cytokines/chemokines derived from myeloid cells are crucial effector molecules in infections. They are involved in recruitment of immune cells and induction of an adaptive immune response. Through tissue passage, GAS can adopt a hyper-virulent phenotype mediated by mutations of genes encoding the CovR/S TCS. Here, we show that *in vitro* infections of monocytic cells with such hyper-virulent strains result in abrogated release of IL-8 and IL-18. This phenotype was reversible upon inhibition of caspase-8. In conclusion, this study provides insights into the interaction of hyper-virulent GAS strains with human moDCs. While we did not observe an impact of GAS phenotype on systemic concentrations of IL-18, local effects of abrogated IL-18 secretion are still unknown and require further studies.



### 5.3 Neutrophil-derived Reactive Agents Induce a Transient SpeB Negative Phenotype in *Streptococcus pyogenes*

GAS isolated from NSTI patient tissue biopsies frequently display a mixed phenotype, consisting of SpeB positive (SpeB<sup>+</sup>) and SpeB negative (SpeB<sup>-</sup>) colonies (210). This phenotype can stem from genetic mutations in regulatory components, giving rise to hyper-virulent clones (117,212,240) or other still unknown mechanisms. SpeB itself is involved in many infectious processes: it can degrade cytokines, immunoglobulins, or complement factors to evade phagocytosis while also degrading bacterial factors like the M-protein or SLO to avoid detection (96). The aim of Paper III was to further characterize the hyper-virulent GAS phenotype, with a focus on SpeB<sup>-</sup> phenotype.

#### 5.3.1 Loss of SpeB in GAS Recovered from Tissue Biopsies Is Reversible

To characterize the phenotype of GAS recovered from tissue biopsies in regards to SpeB secretion, colonies were plated on casein agar. Presence of clear hydrolysis zones around the colonies indicates secretion of active SpeB. Biopsies frequently contained a mixture of both SpeB<sup>+</sup> and SpeB<sup>-</sup> clones (Paper III, Fig. 1A). Loss of SpeB secretion has been associated with genetic mutations of transcriptional regulators *covR/S* or *ropB*, giving rise to hyper-virulent clones, or *speB* itself (116,123,240). Whole genome sequencing revealed that some strains contained mutations in *covS* or *ropB* (Paper III, Fig. S2-4). However, passage of SpeB<sup>-</sup> clones without mutational inactivation of *covS* or *ropB* in THY restored SpeB secretion (Paper III, Fig. 1B), indicating that the host environment induces this transient phenotype.

#### 5.3.2 Neutrophil-derived ROS Induce SpeB<sup>-</sup> Phenotype

Correlation of SpeB<sup>-</sup> phenotype with inflammatory markers, IL-8 and HMGB1, as well as markers for neutrophil infiltration and degranulation in tissue biopsies revealed positive correlation of all markers with bacterial load and increasing numbers of SpeB<sup>-</sup> clones (Paper III, Fig. 1C-F). HMGB1 is a nuclear protein that is released by necrotic or injured cells. It was shown to be highly expressed in tissue biopsies of NSTI patients and serves as a chemoattractant for neutrophils (189,241). To confirm that a neutrophil-derived factor induces the transient SpeB<sup>-</sup> phenotype, isolated human neutrophils were infected with four different GAS strains showing stable SpeB phenotypes. Colonies recovered from neutrophil infections showed a mixed phenotype (Paper III, Fig. 2D-F), confirming that a neutrophil-derived factor induces transient SpeB negativity. Single colony proteomics and gene expression analysis of SpeB<sup>-</sup> colonies revealed transcription of *speB* and higher intracellular abundance of SpeB as compared to SpeB<sup>+</sup> colonies, suggesting impaired secretion of SpeB (Paper III, Fig. 3).

Neutrophils have different mechanisms to kill bacteria. To analyze the impact of oxidative burst on SpeB secretion, GAS strain 5448 was exposed to different concentrations of ROS, namely H<sub>2</sub>O<sub>2</sub> and HOCl. Exposure to sub-lethal concentrations of both species induced a switch to SpeB<sup>-</sup> phenotype in 30-70% of colonies (Paper III, Fig. 4A-D). To confirm involvement of ROS in the SpeB phenotype switch in neutrophils, infections were repeated in presence of an MPO inhibitor. MPO is the primary source of HOCl in neutrophils (42). The observed effects on SpeB secretion were time- and concentration-dependent: low concentrations of the inhibitor led to initially higher killing and fewer SpeB<sup>-</sup> colonies. However, this was reversed with continued infection, as shown by less killing and more SpeB<sup>+</sup> colonies. Higher concentrations of the inhibitor led to more killing and more colonies remaining SpeB<sup>+</sup> (Paper III, Fig. 4E-F). In general, ROS can induce oxidation of the functional cysteine in cysteine proteases, rendering them non-functional (242). To prove that ROS did not affect SpeB activity, SpeB activity was assessed in presence/absence of H<sub>2</sub>O<sub>2</sub>. No effect of H<sub>2</sub>O<sub>2</sub> on SpeB activity was observed (Paper III, Fig. 4H-J).

To confirm a role for MPO *in vivo*, NSTI patient tissue biopsies with known SpeB background were stained for MPO and GAS: Although comparable bacterial loads were detected in tissue biopsies of infections with SpeB<sup>+</sup> and SpeB<sup>-</sup> clones, higher levels of MPO were detected in biopsies of infections with SpeB<sup>-</sup> clones (Paper III, Fig. 5A-C). In a clinical context, the release of MPO is associated with hyper-inflammation and high levels of MPO were found in patients suffering from sepsis (243–245). Overall, this shift in SpeB phenotype points to neutrophils as potential bacterial reservoirs when SpeB secretion is impaired, or MPO is inhibited.

### 5.3.3 Increased Neutrophil Degranulation in Infections with Hyper-virulent 5448AP

Neutrophil infections with stable SpeB<sup>-</sup> strain 5448AP led to continuous intracellular bacterial replication (Paper III, Fig. S13A), which was also observed for strain 8003 (Paper III, Fig. 2D). Both strains have *covR/S* mutations, inactivating the TCS (118) (Paper III, Fig. S2-4). SpeB negativity was also associated with higher neutrophil degranulation, as shown in proteomic analysis of neutrophil secretome. SpeB<sup>-</sup> 5448AP induced a higher release of granule proteins as compared to SpeB<sup>+</sup> 5448 (Paper III, Fig. 6A-H). While lack of SpeB seems beneficial in terms of bacterial survival inside neutrophils, increased release of antimicrobial granule contents and enzymes can cause further tissue damage. In addition, inactivating mutations of *covR/S* and the associated loss of SpeB are also associated with impaired neutrophil recruitment, as shown by suppressed secretion of IL-8 in 5448AP infections of other myeloid cells (Paper II, Fig. 2). Hyper-inflammation and extensive tissue damage in NSTIs are partially derived from influx and excessive degranulation of neutrophils (48, 49). Reduced IL-8 levels due to activity of SpyCEP were shown to reduce neutrophil recruitment. In addition, hyper-

virulent GAS strains were previously shown to have improved intracellular survival in neutrophils and induce excessive degranulation (50, 51). This indicates, that hyper-virulent GAS not only impair recruitment of neutrophils, but also influence how neutrophils respond to GAS.

In conclusion, the role of SpeB in GAS pathogenesis remains controversial. On the one hand, SpeB provides protection from the immune system by degrading antimicrobial compounds like LL-37 (209) and impairing phagocytosis by degrading C3b (246) and immunoglobulins (247). On the other hand, SpeB also cleaves the precursors of IL-1 $\beta$  (240,248) and IL-18 (139) into their respective mature forms. These cytokines have potent proinflammatory effects and induce an immune response. The majority of isolates recovered from infections encode for *speB* and lack of active SpeB secretion is, in most cases, associated with mutational inactivation of transcriptional regulators (249). This study has shown that GAS adopt a transient SpeB<sup>-</sup> phenotype, to improve survival within neutrophils. Neutrophil-derived ROS drive loss of SpeB secretion, and inhibition of MPO reverses the phenotype switch. These insights into GAS fitness in the soft tissue might provide a new potential target for the treatment of NSTIs.

## 6. CONCLUSIONS

This thesis aimed to elucidate and provide a better understanding of factors influencing myeloid cells' response to infections. Myeloid cells are crucial first responders to infections. In addition to clearing the pathogen, they secrete cytokines to recruit further immune cells, initiate an effective adaptive immune response and eventually resolve the infection. Metal-based implants are widely used in arthroplasty and are well-known factors affecting immune cells' function and phenotype. Both *S. aureus* and GAS are Gram-positive human commensals that can cause severe disease. GAS, in particular, have developed multiple mechanisms to evade and manipulate the human immune system. Understanding the underlying disease mechanisms and contributions of individual virulence factors provides targets to improve existing therapies/materials or develop new ones.

### **Paper I**

CoCrMo alloys are biomaterials widely used in arthroplasty. They have been linked to the development of ALTRs, which are characterized by tissue necrosis, extensive inflammation, and macrophage infiltration. Macrophages are tissue-resident cells that phagocytose foreign particles, including implant-derived wear particles, in order to clear them. While inflammation caused by implant-derived particles is well studied, the effects of metal ions on the cellular phenotype and functionality of monocytes/macrophages remain elusive. In this study, isolated human monocytes were exposed to pathologic concentrations of  $\text{Co}^{2+}$  or  $\text{Cr}^{3+}$  ions *in vitro*, and cell phenotype, as well as response to infection, were analyzed:

- i. Local peri-implant tissue is exposed to Co and Cr with evident macrophage infiltration
- ii. Exposure to high concentrations of  $\text{Co}^{2+}$  induces differentiation to macrophages with a metal-specific imprint
- iii.  $\text{Co}^{2+}$  or  $\text{Cr}^{3+}$  do not induce activation of exposed macrophages
- iv.  $\text{Co}^{2+}$  and  $\text{Cr}^{3+}$  ions inhibit macrophage response to *S. aureus* infection

These findings demonstrate that implant-derived metal ions impact macrophage phenotype and functionality. While exposure to  $\text{Cr}^{3+}$  had only minor effects on macrophage phenotype, exposure to  $\text{Co}^{2+}$  led to almost complete loss of surface CD14 and CD16, as well as decreased HLA-DR expression. In addition, exposure to  $\text{Co}^{2+}$  impaired phagocytosis of *S. aureus*. Both metal ions inhibit cellular activation of macrophages.

---

## Paper II

GAS can adopt a hyper-virulent phenotype within the host. This is generally mediated by dysfunctional CovR/S. DCs are key components of the host's immune response. They present antigens and secrete cytokines to shape the T cell response. As knowledge on the DC-GAS interaction is scarce, this study aimed to investigate the cytokine response to hyper-virulent GAS variants. Therefore, moDCs were infected with different GAS variants, and cytokine profiling was performed:

- i. GAS harboring dysfunctional CovR/S suppress IL-8 and IL-18 secretion by human monocytic cells
- ii. DC maturation is not impaired by hyper-virulent GAS
- iii. Caspase-8 inhibition restores secretion of IL-8 and IL-18 in moDCs infected with hyper-virulent GAS
- iv. Infections of moDCs with 5448AP result in higher caspase-8 activity
- v. Dysfunctional CovR/S has no impact on systemic IL-18 in NSTI patients
- vi. Secretion of IL-1 $\beta$  and IL-18 by moDCs is increased in infections with a SLO knockout

These results show that infections with GAS strains harboring dysfunctional CovR/S result in abrogated secretion of IL-8 and IL-18 by monocytic cells. This suppression is mainly mediated by a caspase-8-dependent mechanism. While dysfunctional CovR/S had no impact on systemic IL-18 concentrations in NSTI patients, the effects on local tissue concentrations are still unknown and require further studies.

## Paper III

The secreted streptococcal protease SpeB is highly conserved and well-studied virulence factor. SpeB retains a controversial role in pathogenesis and severity of GAS infections. In NSTI patient biopsies as well as *in vitro* experiments, it was shown that:

- i. The host environment induces transient loss of SpeB secretion
- ii. Reversible loss of SpeB proteolytic activity is associated with tissue pathology and inflammation
- iii. ROS derived from neutrophils drive the transient SpeB<sup>-</sup> phenotype
- iv. Presence of MPO is enhanced in tissue biopsies with increased SpeB<sup>-</sup> variants
- v. SpeB<sup>-</sup> variants induce higher neutrophil degranulation than SpeB<sup>+</sup> strains

Irreversible loss of SpeB secretion is commonly caused by mutation of *covR/S* or *ropB*. These results show that GAS can transiently abrogate SpeB secretion in response to neutrophil-derived ROS. SpeB<sup>-</sup> variants induce extensive neutrophil degranulation and replicate

## CONCLUSIONS

---

intracellularly. Extensive neutrophil degranulation drives hyper-inflammatory conditions and tissue damage, both hallmarks of NSTIs. MPO inhibition partially restored secretion of SpeB and improved killing of GAS by neutrophils.

---

## 7. REFERENCES

1. Mogensen TH. Pathogen Recognition and Inflammatory Signaling in Innate Immune Defenses. *Clin Microbiol Rev.* 2009 Apr;22(2):240–73.
2. Thaiss CA, Zmora N, Levy M, Elinav E. The microbiome and innate immunity. *Nature.* 2016 Jul;535(7610):65–74.
3. Fitzgerald KA, Kagan JC. Toll-like Receptors and the Control of Immunity. *Cell.* 2020 Mar 19;180(6):1044–66.
4. Taguchi T, Mukai K. Innate immunity signalling and membrane trafficking. *Curr Opin Cell Biol.* 2019 Aug 1;59:1–7.
5. Garlanda C, Jaillon S. The Interleukin-1 Family. In: Ratcliffe MJH, editor. *Encyclopedia of Immunobiology* [Internet]. Oxford: Academic Press; 2016 [cited 2023 Oct 17]. p. 438–46. Available from: <https://www.sciencedirect.com/science/article/pii/B9780123742797100013>
6. Nakanishi K, Yoshimoto T, Tsutsui H, Okamura H. Interleukin-18 Regulates Both Th1 and Th2 Responses. *Annu Rev Immunol.* 2001;19(1):423–74.
7. Hatscher L, Amon L, Heger L, Dudziak D. Inflammasomes in dendritic cells: Friend or foe? *Immunol Lett.* 2021 Jun 1;234:16–32.
8. Yasuda K, Nakanishi K, Tsutsui H. Interleukin-18 in Health and Disease. *Int J Mol Sci.* 2019 Jan;20(3):649.
9. Maelfait J, Vercammen E, Janssens S, Schotte P, Haegman M, Magez S, et al. Stimulation of Toll-like receptor 3 and 4 induces interleukin-1 $\beta$  maturation by caspase-8. *J Exp Med.* 2008 Aug 25;205(9):1967–73.
10. Antonopoulos C, El Sanadi C, Kaiser WJ, Mocarski ES, Dubyak GR. Proapoptotic Chemotherapeutic Drugs Induce Noncanonical Processing and Release of IL-1 $\beta$  via Caspase-8 in Dendritic Cells. *J Immunol.* 2013 Nov 1;191(9):4789–803.
11. Gaidt MM, Hornung V. Alternative inflammasome activation enables IL-1 $\beta$  release from living cells. *Curr Opin Immunol.* 2017 Feb 1;44:7–13.
12. Gringhuis SI, Kaptein TM, Wevers BA, Theelen B, van der Vlist M, Boekhout T, et al. Dectin-1 is an extracellular pathogen sensor for the induction and processing of IL-1 $\beta$  via a noncanonical caspase-8 inflammasome. *Nat Immunol.* 2012 Mar;13(3):246–54.
13. Bossaller L, Chiang PI, Schmidt-Lauber C, Ganesan S, Kaiser WJ, Rathinam VAK, et al. Cutting Edge: FAS (CD95) Mediates Noncanonical IL-1 $\beta$  and IL-18 Maturation via Caspase-8 in an RIP3-Independent Manner. *J Immunol.* 2012 Dec 15;189(12):5508–12.
14. Goswami S, Anandhan S, Raychaudhuri D, Sharma P. Myeloid cell-targeted therapies for solid tumours. *Nat Rev Immunol.* 2023 Feb;23(2):106–20.
15. Varol C, Mildner A, Jung S. Macrophages: Development and Tissue Specialization. *Annu Rev Immunol.* 2015;33(1):643–75.
16. Mildner A, Yona S, Jung S. Chapter Three - A Close Encounter of the Third Kind: Monocyte-Derived Cells. In: Murphy KM, Merad M, editors. *Advances in Immunology* [Internet]. Academic Press; 2013 [cited 2023 Oct 17]. p. 69–103. (Development and Function of Myeloid Subsets; vol. 120). Available from: <https://www.sciencedirect.com/science/article/pii/B978012417028500003X>
17. Stuart LM, Ezekowitz RAB. Phagocytosis: Elegant Complexity. *Immunity.* 2005 May 1;22(5):539–50.
18. Wynn TA, Vannella KM. Macrophages in Tissue Repair, Regeneration, and Fibrosis. *Immunity.* 2016 Mar 15;44(3):450–62.
19. Gray JL, Farber DL. Tissue-Resident Immune Cells in Humans. *Annu Rev Immunol.* 2022;40(1):195–220.
20. Cabeza-Cabrerizo M, Cardoso A, Minutti CM, Pereira da Costa M, Reis e Sousa C. Dendritic Cells Revisited. *Annu Rev Immunol.* 2021;39(1):131–66.
21. Bošnjak B, Do KTH, Förster R, Hammerschmidt SI. Imaging dendritic cell functions\*. *Immunol Rev.* 2022;306(1):137–63.
22. Del Prete A, Salvi V, Soriani A, Laffranchi M, Sozio F, Bosisio D, et al. Dendritic cell subsets in cancer immunity and tumor antigen sensing. *Cell Mol Immunol.* 2023 May;20(5):432–47.
23. Collin M, Bigley V. Human dendritic cell subsets: an update. *Immunology.* 2018;154(1):3–20.
24. Swiecki M, Colonna M. The multifaceted biology of plasmacytoid dendritic cells. *Nat Rev Immunol.* 2015 Aug;15(8):471–85.
25. Zhou LJ, Tedder TF. CD14+ blood monocytes can differentiate into functionally mature CD83+ dendritic cells. *Proc Natl Acad Sci.* 1996 Mar 19;93(6):2588–92.

## REFERENCES

---

26. Randolph GJ, Beaulieu S, Lebecque S, Steinman RM, Muller WA. Differentiation of Monocytes into Dendritic Cells in a Model of Transendothelial Trafficking. *Science*. 1998 Oct 16;282(5388):480–3.
27. Randolph GJ, Inaba K, Robbiani DF, Steinman RM, Muller WA. Differentiation of Phagocytic Monocytes into Lymph Node Dendritic Cells In Vivo. *Immunity*. 1999 Dec 1;11(6):753–61.
28. Ziegler-Heitbrock L, Ancuta P, Crowe S, Dalod M, Grau V, Hart DN, et al. Nomenclature of monocytes and dendritic cells in blood. *Blood*. 2010 Oct 21;116(16):e74–80.
29. Döhrmann S, Cole JN, Nizet V. Conquering Neutrophils. *PLOS Pathog*. 2016 Jul 28;12(7):e1005682.
30. Witko-Sarsat V, Rieu P, Descamps-Latscha B, Lesavre P, Halbwachs-Mecarelli L. Neutrophils: Molecules, Functions and Pathophysiological Aspects. *Lab Invest*. 2000 May;80(5):617–53.
31. Mayadas TN, Cullere X, Lowell CA. The Multifaceted Functions of Neutrophils. *Annu Rev Pathol Mech Dis*. 2014;9(1):181–218.
32. Bardeel BW, Kenny EF, Sollberger G, Zychlinsky A. The Balancing Act of Neutrophils. *Cell Host Microbe*. 2014 May 14;15(5):526–36.
33. Rørvig S, Østergaard O, Heegaard NHH, Borregaard N. Proteome profiling of human neutrophil granule subsets, secretory vesicles, and cell membrane: correlation with transcriptome profiling of neutrophil precursors. *J Leukoc Biol*. 2013 Oct 1;94(4):711–21.
34. Lominadze G, Powell DW, Luerman GC, Link AJ, Ward RA, McLeish KR. Proteomic Analysis of Human Neutrophil Granules \* S. *Mol Cell Proteomics*. 2005 Oct 1;4(10):1503–21.
35. Amulic B, Cazalet C, Hayes GL, Metzler KD, Zychlinsky A. Neutrophil Function: From Mechanisms to Disease. *Annu Rev Immunol*. 2012;30(1):459–89.
36. Lacy P. Mechanisms of Degranulation in Neutrophils. *Allergy Asthma Clin Immunol*. 2006 Sep 15;2(3):98.
37. Calafat J, Janssen H, Ihl-Bäckdahl MS, Zuurbier AEM, Knol EF, Egesten A. Human Monocytes and Neutrophils Store Transforming Growth Factor- $\alpha$  in a Subpopulation of Cytoplasmic Granules. *Blood*. 1997 Aug 1;90(3):1255–66.
38. Sheshachalam A, Srivastava N, Mitchell T, Lacy P, Eitzen G. Granule Protein Processing and Regulated Secretion in Neutrophils. *Front Immunol [Internet]*. 2014 [cited 2023 Oct 16];5. Available from: <https://www.frontiersin.org/articles/10.3389/fimmu.2014.00448>
39. Clark SR, Ma AC, Tavener SA, McDonald B, Goodarzi Z, Kelly MM, et al. Platelet TLR4 activates neutrophil extracellular traps to ensnare bacteria in septic blood. *Nat Med*. 2007 Apr;13(4):463–9.
40. Winterbourn CC, Kettle AJ, Hampton MB. Reactive Oxygen Species and Neutrophil Function. *Annu Rev Biochem*. 2016;85(1):765–92.
41. Winterbourn CC. Toxicity of iron and hydrogen peroxide: the Fenton reaction. *Toxicol Lett*. 1995 Dec 1;82–83:969–74.
42. Nauseef WM. Myeloperoxidase in human neutrophil host defence. *Cell Microbiol*. 2014;16(8):1146–55.
43. Peacock SJ, de Silva I, Lowy FD. What determines nasal carriage of *Staphylococcus aureus*? *Trends Microbiol*. 2001 Dec;9(12):605–10.
44. van Belkum A, Melles DC, Nouwen J, van Leeuwen WB, van Wamel W, Vos MC, et al. Co-evolutionary aspects of human colonisation and infection by *Staphylococcus aureus*. *Infect Genet Evol J Mol Epidemiol Evol Genet Infect Dis*. 2009 Jan;9(1):32–47.
45. Tong SYC, Davis JS, Eichenberger E, Holland TL, Fowler VG. *Staphylococcus aureus* Infections: Epidemiology, Pathophysiology, Clinical Manifestations, and Management. *Clin Microbiol Rev*. 2015 Jul;28(3):603–61.
46. Lee AS, de Lencastre H, Garau J, Kluytmans J, Malhotra-Kumar S, Peschel A, et al. Methicillin-resistant *Staphylococcus aureus*. *Nat Rev Dis Primer*. 2018 May 31;4(1):1–23.
47. Chambers HF, Deleo FR. Waves of resistance: *Staphylococcus aureus* in the antibiotic era. *Nat Rev Microbiol*. 2009 Sep;7(9):629–41.
48. DeLeo FR, Otto M, Kreiswirth BN, Chambers HF. Community-associated methicillin-resistant *Staphylococcus aureus*. *Lancet Lond Engl*. 2010 May 1;375(9725):1557–68.
49. Shumba P, Mairpady Shambat S, Siemens N. The Role of Streptococcal and Staphylococcal Exotoxins and Proteases in Human Necrotizing Soft Tissue Infections. *Toxins [Internet]*. 2019 Jun 11 [cited 2019 Sep 15];11(6). Available from: <https://www.ncbi.nlm.nih.gov/pmc/articles/PMC6628391/>
50. Tam K, Torres VJ. *Staphylococcus aureus* Secreted Toxins & Extracellular Enzymes. *Microbiol Spectr [Internet]*. 2019 Mar [cited 2020 May 8];7(2). Available from: <https://www.ncbi.nlm.nih.gov/pmc/articles/PMC6422052/>



51. Spaan AN, Henry T, van Rooijen WJM, Perret M, Badiou C, Aerts PC, et al. The staphylococcal toxin Panton-Valentine Leukocidin targets human C5a receptors. *Cell Host Microbe*. 2013 May 15;13(5):584–94.
52. Wilke GA, Bubeck Wardenburg J. Role of a disintegrin and metalloprotease 10 in *Staphylococcus aureus* alpha-hemolysin-mediated cellular injury. *Proc Natl Acad Sci U S A*. 2010 Jul 27;107(30):13473–8.
53. Reyes-Robles T, Alonzo F, Kozhaya L, Lacy DB, Unutmaz D, Torres VJ. *Staphylococcus aureus* leukotoxin ED targets the chemokine receptors CXCR1 and CXCR2 to kill leukocytes and promote infection. *Cell Host Microbe*. 2013 Oct 16;14(4):453–9.
54. DuMont AL, Yoong P, Day CJ, Alonzo F, McDonald WH, Jennings MP, et al. *Staphylococcus aureus* LukAB cytotoxin kills human neutrophils by targeting the CD11b subunit of the integrin Mac-1. *Proc Natl Acad Sci U S A*. 2013 Jun 25;110(26):10794–9.
55. Berends ETM, Zheng X, Zwack EE, Ménager MM, Cammer M, Shopsin B, et al. *Staphylococcus aureus* Impairs the Function of and Kills Human Dendritic Cells via the LukAB Toxin. *mBio*. 2019 02;10(1).
56. Josse J, Laurent F, Diot A. Staphylococcal Adhesion and Host Cell Invasion: Fibronectin-Binding and Other Mechanisms. *Front Microbiol* [Internet]. 2017 [cited 2023 Oct 18];8. Available from: <https://www.frontiersin.org/articles/10.3389/fmicb.2017.02433>
57. Tuchscher L, Löffler B, Proctor RA. Persistence of *Staphylococcus aureus*: Multiple Metabolic Pathways Impact the Expression of Virulence Factors in Small-Colony Variants (SCVs). *Front Microbiol* [Internet]. 2020 [cited 2023 Oct 18];11. Available from: <https://www.frontiersin.org/articles/10.3389/fmicb.2020.01028>
58. Fraunholz M, Sinha B. Intracellular staphylococcus aureus: Live-in and let die. *Front Cell Infect Microbiol* [Internet]. 2012 Apr 24 [cited 2020 Mar 19];2. Available from: <https://www.ncbi.nlm.nih.gov/pmc/articles/PMC3417557/>
59. Proctor RA, von Eiff C, Kahl BC, Becker K, McNamara P, Herrmann M, et al. Small colony variants: a pathogenic form of bacteria that facilitates persistent and recurrent infections. *Nat Rev Microbiol*. 2006 Apr;4(4):295–305.
60. Learmonth ID, Young C, Rorabeck C. The operation of the century: total hip replacement. *The Lancet*. 2007 Oct 27;370(9597):1508–19.
61. Kurtz S, Ong K, Lau E, Mowat F, Halpern M. Projections of Primary and Revision Hip and Knee Arthroplasty in the United States from 2005 to 2030. *JBJS*. 2007 Apr;89(4):780.
62. Perino G, Martino ID, Zhang L, Xia Z, Gallo J, Natu S, et al. The contribution of the histopathological examination to the diagnosis of adverse local tissue reactions in arthroplasty. *EFORT Open Rev*. 2021 Jun 28;6(6):399–419.
63. Liu Z, Liu H, Powden R, Hughes L, Qi D, Francis W, et al. Combination of cobalt, chromium and titanium nanoparticles increases cytotoxicity in vitro and pro-inflammatory cytokines in vivo. *J Orthop Transl*. 2023 Jan 1;38:203–12.
64. Catelas I, Petit A, Vali H, Fragiskatos C, Meilleur R, Zukor DJ, et al. Quantitative analysis of macrophage apoptosis vs. necrosis induced by cobalt and chromium ions in vitro. *Biomaterials*. 2005 May 1;26(15):2441–53.
65. Eltit F, Wang Q, Wang R. Mechanisms of Adverse Local Tissue Reactions to Hip Implants. *Front Bioeng Biotechnol* [Internet]. 2019 [cited 2023 Oct 18];7. Available from: <https://www.frontiersin.org/articles/10.3389/fbioe.2019.00176>
66. Nyga A, Hart A, Tetley TD. Importance of the HIF pathway in cobalt nanoparticle-induced cytotoxicity and inflammation in human macrophages. *Nanotoxicology*. 2015 Oct 3;9(7):905–17.
67. Jämsen E, Pajarinen J, Kouri VP, Rahikkala A, Goodman SB, Manninen M, et al. Tumor necrosis factor primes and metal particles activate the NLRP3 inflammasome in human primary macrophages. *Acta Biomater*. 2020 May 1;108:347–57.
68. Matharu GS, Judge A, Murray DW, Pandit HG. Outcomes After Metal-on-metal Hip Revision Surgery Depend on the Reason for Failure: A Propensity Score-matched Study. *Clin Orthop Relat Res*. 2018 Feb;476(2):245.
69. Matharu GS, Pynsent PB, Sumathi VP, Mittal S, Buckley CD, Dunlop DJ, et al. Predictors of time to revision and clinical outcomes following revision of metal-on-metal hip replacements for adverse reaction to metal debris. *Bone Jt J*. 2014 Dec 1;96-B(12):1600–9.
70. Munro JT, Masri BA, Duncan CP, Garbuz DS. High Complication Rate After Revision of Large-head Metal-on-metal Total Hip Arthroplasty. *Clin Orthop Relat Res*. 2014 Feb 1;472(2):523–8.
71. Bonner B, Arauz P, Klemm C, Kwon YM. Outcome of Re-Revision Surgery for Adverse Local Tissue Reaction in Metal-on-Polyethylene and Metal-on-Metal Total Hip Arthroplasty. *J Arthroplasty*. 2020 Jun 1;35(6):S284–8.

72. Liukkonen RJ, Honkanen M, Reito AP, Skyttä ET, Karpelin M, Eskelinen AP. Trends in Revision Hip Arthroplasty for Prosthetic Joint Infection: A Single-Center Study of 423 Hips at a High-Volume Center Between 2008 and 2021. *J Arthroplasty*. 2023 Jun 1;38(6):1151–9.
73. Patel R. Periprosthetic Joint Infection. *N Engl J Med*. 2023 Jan 19;388(3):251–62.
74. Tande AJ, Patel R. Prosthetic Joint Infection. *Clin Microbiol Rev*. 2014 Apr;27(2):302–45.
75. Benito N, Mur I, Ribera A, Soriano A, Rodríguez-Pardo D, Sorlí L, et al. The Different Microbial Etiology of Prosthetic Joint Infections according to Route of Acquisition and Time after Prosthesis Implantation, Including the Role of Multidrug-Resistant Organisms. *J Clin Med*. 2019 May;8(5):673.
76. Tai DBG, Patel R, Abdel MP, Berbari EF, Tande AJ. Microbiology of hip and knee periprosthetic joint infections: a database study. *Clin Microbiol Infect*. 2022 Feb 1;28(2):255–9.
77. Triffault-Fillit C, Ferry T, Laurent F, Pradat P, Dupieux C, Conrad A, et al. Microbiologic epidemiology depending on time to occurrence of prosthetic joint infection: a prospective cohort study. *Clin Microbiol Infect*. 2019 Mar 1;25(3):353–8.
78. Saavedra-Lozano J, Falup-Pecurariu O, Faust SN, Girschick H, Hartwig N, Kaplan S, et al. Bone and Joint Infections. *Pediatr Infect Dis J*. 2017 Aug;36(8):788.
79. Chang JS, Haddad FS. Revision total hip arthroplasty for metal-on-metal failure. *J Clin Orthop Trauma*. 2020 Jan 1;11(1):9–15.
80. Kurtz SM, Lau EC, Son MS, Chang ET, Zimmerli W, Parvizi J. Are We Winning or Losing the Battle With Periprosthetic Joint Infection: Trends in Periprosthetic Joint Infection and Mortality Risk for the Medicare Population. *J Arthroplasty*. 2018 Oct 1;33(10):3238–45.
81. Dale H, Høvdning P, Tveit SM, Graff JB, Lutro O, Schrama JC, et al. Increasing but levelling out risk of revision due to infection after total hip arthroplasty: a study on 108,854 primary THAs in the Norwegian Arthroplasty Register from 2005 to 2019. *Acta Orthop*. 92(2):208–14.
82. Matharu GS, Judge A, Murray DW, Pandit HG. Outcomes following revision surgery performed for adverse reactions to metal debris in non-metal-on-metal hip arthroplasty patients: Analysis of 185 revisions from the National Joint Registry for England and Wales. *Bone Jt Res*. 2017 Jul 1;6(7):405–13.
83. Wyles CC, Van Demark RE, Sierra RJ, Trousdale RT. High Rate of Infection After Aseptic Revision of Failed Metal-on-Metal Total Hip Arthroplasty. *Clin Orthop Relat Res*. 2014 Feb 1;472(2):509–16.
84. Izakovicova P, Borens O, Trampuz A. Periprosthetic joint infection: current concepts and outlook. *EFORT Open Rev*. 2019 Jul 29;4(7):482–94.
85. Kong L, Cao J, Zhang Y, Ding W, Shen Y. Risk factors for periprosthetic joint infection following primary total hip or knee arthroplasty: a meta-analysis. *Int Wound J*. 2017;14(3):529–36.
86. Collaborative (MAC)1a\* TMA. Risk Factors for Periprosthetic Joint Infection Following Primary Total Hip Arthroplasty: A 15-Year, Population-Based Cohort Study. *JBJS*. 2020 Mar 18;102(6):503.
87. Renz N, Trampuz A, Perka C, Rakow A. Outcome and Failure Analysis of 132 Episodes of Hematogenous Periprosthetic Joint Infections—A Cohort Study. *Open Forum Infect Dis*. 2022 Apr 1;9(4):ofac094.
88. Walker MJ, Barnett TC, McArthur JD, Cole JN, Gillen CM, Henningham A, et al. Disease Manifestations and Pathogenic Mechanisms of Group A Streptococcus. *Clin Microbiol Rev*. 2014 Apr;27(2):264–301.
89. Lancefield RC. THE ANTIGENIC COMPLEX OF STREPTOCOCCUS HÆMOLYTICUS: I. DEMONSTRATION OF A TYPE-SPECIFIC SUBSTANCE IN EXTRACTS OF STREPTOCOCCUS HÆMOLYTICUS. *J Exp Med*. 1928 Jan 1;47(1):91–103.
90. Steer AC, Lamagni T, Curtis N, Carapetis JR. Invasive Group A Streptococcal Disease. *Drugs*. 2012 Sep 1;72(9):1213–27.
91. Carapetis JR, Steer AC, Mulholland EK, Weber M. The global burden of group A streptococcal diseases. *Lancet Infect Dis*. 2005 Nov;5(11):685–94.
92. Olsen RJ, Shelburne SA, Musser JM. Molecular mechanisms underlying group A streptococcal pathogenesis. *Cell Microbiol*. 2009;11(1):1–12.
93. McMillan DJ, Drèze PA, Vu T, Bessen DE, Guglielmini J, Steer AC, et al. Updated model of group A Streptococcus M proteins based on a comprehensive worldwide study. *Clin Microbiol Infect*. 2013 May 1;19(5):E222–9.
94. Lynskey NN, Jauneikaite E, Li HK, Zhi X, Turner CE, Mosavie M, et al. Emergence of dominant toxigenic M1T1 Streptococcus pyogenes clone during increased scarlet fever activity in England: a population-based molecular epidemiological study. *Lancet Infect Dis*. 2019 Nov 1;19(11):1209–18.
95. van der Putten BCL, Vlamincxx BJM, de Gier B, Freudenburg-de Graaf W, van Sorge NM. Group A Streptococcal Meningitis With the M1UK Variant in the Netherlands. *JAMA*. 2023 May 23;329(20):1791–2.

96. Brouwer S, Rivera-Hernandez T, Curren BF, Harbison-Price N, De Oliveira DMP, Jespersen MG, et al. Pathogenesis, epidemiology and control of Group A Streptococcus infection. *Nat Rev Microbiol*. 2023 Jul;21(7):431–47.
97. Anaya DA, McMahon K, Nathens AB, Sullivan SR, Foy H, Bulger E. Predictors of mortality and limb loss in necrotizing soft tissue infections. *Arch Surg Chic Ill 1960*. 2005 Feb;140(2):151–7; discussion 158.
98. Madsen MB, Skrede S, Perner A, Arnell P, Nekludov M, Bruun T, et al. Patient's characteristics and outcomes in necrotising soft-tissue infections: results from a Scandinavian, multicentre, prospective cohort study. *Intensive Care Med*. 2019 Sep;45(9):1241–51.
99. Morgan MS. Diagnosis and management of necrotising fasciitis: a multiparametric approach. *J Hosp Infect*. 2010 Aug 1;75(4):249–57.
100. Harbrecht BG, Nash NA. Necrotizing Soft Tissue Infections: A Review. *Surg Infect*. 2016 Oct;17(5):503–9.
101. Stevens DL, Bryant AE. Necrotizing Soft-Tissue Infections. *N Engl J Med*. 2017 Dec 7;377(23):2253–65.
102. Bruun T, Rath E, Madsen MB, Oppegaard O, Nekludov M, Arnell P, et al. Risk Factors and Predictors of Mortality in Streptococcal Necrotizing Soft-tissue Infections: A Multicenter Prospective Study. *Clin Infect Dis*. 2021 Jan 15;72(2):293–300.
103. Low DE. Toxic shock syndrome: major advances in pathogenesis, but not treatment. *Crit Care Clin*. 2013 Jul;29(3):651–75.
104. Stevens DL, Bisno AL, Chambers HF, Dellinger EP, Goldstein EJC, Gorbach SL, et al. Practice guidelines for the diagnosis and management of skin and soft tissue infections: 2014 update by the Infectious Diseases Society of America. *Clin Infect Dis Off Publ Infect Dis Soc Am*. 2014 Jul 15;59(2):e10-52.
105. Carapetis JR, Jacoby P, Carville K, Ang SJJ, Curtis N, Andrews R. Effectiveness of Clindamycin and Intravenous Immunoglobulin, and Risk of Disease in Contacts, in Invasive Group A Streptococcal Infections. *Clin Infect Dis*. 2014 Aug 1;59(3):358–65.
106. Schmitz M, Roux X, Huttner B, Pugin J. Streptococcal toxic shock syndrome in the intensive care unit. *Ann Intensive Care*. 2018 Sep 17;8(1):88.
107. Hedetoft M, Bennett MH, Hyldegaard O. Adjunctive hyperbaric oxygen treatment for necrotising soft-tissue infections: A systematic review and meta-analysis. *Diving Hyperb Med*. 2021 Mar 31;51(1):34–43.
108. Kachroo P, Eraso JM, Beres SB, Olsen RJ, Zhu L, Nasser W, et al. Integrated analysis of population genomics, transcriptomics and virulence provides novel insights into Streptococcus pyogenes pathogenesis. *Nat Genet*. 2019 Mar;51(3):548–59.
109. Nasser W, Beres SB, Olsen RJ, Dean MA, Rice KA, Long SW, et al. Evolutionary pathway to increased virulence and epidemic group A Streptococcus disease derived from 3,615 genome sequences. *Proc Natl Acad Sci*. 2014 Apr 29;111(17):E1768–76.
110. Beres SB, Carroll RK, Shea PR, Sitkiewicz I, Martinez-Gutierrez JC, Low DE, et al. Molecular complexity of successive bacterial epidemics deconvoluted by comparative pathogenomics. *Proc Natl Acad Sci*. 2010 Mar 2;107(9):4371–6.
111. Loughman JA, Caparon M. Regulation of SpeB in Streptococcus pyogenes by pH and NaCl: a Model for In Vivo Gene Expression. *J Bacteriol*. 2006 Jan 15;188(2):399–408.
112. Dalton TL, Scott JR. CovS Inactivates CovR and Is Required for Growth under Conditions of General Stress in Streptococcus pyogenes. *J Bacteriol*. 2004 Jun 15;186(12):3928–37.
113. Do H, Makthal N, VanderWal AR, Saavedra MO, Olsen RJ, Musser JM, et al. Environmental pH and peptide signaling control virulence of Streptococcus pyogenes via a quorum-sensing pathway. *Nat Commun*. 2019 Jun 13;10(1):2586.
114. Horstmann N, Tran CN, Flores AR, Shelburne SA. Hyperphosphorylation of the Group A Streptococcal Control of Virulence Regulator Increases Promoter Occupancy Specifically at Virulence Factor-Encoding Genes. *J Bacteriol*. 2023 Jun 8;205(6):e00118-23.
115. Horstmann N, Myers KS, Tran CN, Flores AR, Iii SAS. CovS inactivation reduces CovR promoter binding at diverse virulence factor encoding genes in group A Streptococcus. *PLOS Pathog*. 2022 Feb 18;18(2):e1010341.
116. Graham MR, Smoot LM, Migliaccio CAL, Virtaneva K, Sturdevant DE, Porcella SF, et al. Virulence control in group A Streptococcus by a two-component gene regulatory system: Global expression profiling and in vivo infection modeling. *Proc Natl Acad Sci*. 2002 Oct 15;99(21):13855–60.
117. Kansal RG, McGeer A, Low DE, Norrby-Teglund A, Kotb M. Inverse Relation between Disease Severity and Expression of the Streptococcal Cysteine Protease, SpeB, among Clonal M1T1

## REFERENCES

---

- Isolates Recovered from Invasive Group A Streptococcal Infection Cases. *Infect Immun*. 2000 Nov;68(11):6362–9.
118. Walker MJ, Hollands A, Sanderson-Smith ML, Cole JN, Kirk JK, Henningham A, et al. DNase Sda1 provides selection pressure for a switch to invasive group A streptococcal infection. *Nat Med*. 2007 Aug;13(8):981–5.
  119. Levin JC, Wessels MR. Identification of *csrR/csrS*, a genetic locus that regulates hyaluronic acid capsule synthesis in group A *Streptococcus*. *Mol Microbiol*. 1998;30(1):209–19.
  120. Turner CE, Kurupati P, Jones MD, Edwards RJ, Sriskandan S. Emerging Role of the Interleukin-8 Cleaving Enzyme SpyCEP in Clinical *Streptococcus pyogenes* Infection. *J Infect Dis*. 2009 Aug 1;200(4):555–63.
  121. Engleberg NC, Heath A, Miller A, Rivera C, DiRita VJ. Spontaneous Mutations in the CsrRS Two-Component Regulatory System of *Streptococcus pyogenes* Result in Enhanced Virulence in a Murine Model of Skin and Soft Tissue Infection. *J Infect Dis*. 2001 Apr 1;183(7):1043–54.
  122. Sumbly P, Whitney AR, Graviss EA, DeLeo FR, Musser JM. Genome-Wide Analysis of Group A *Streptococci* Reveals a Mutation That Modulates Global Phenotype and Disease Specificity. *PLOS Pathog*. 2006 Jan 27;2(1):e5.
  123. Neely MN, Lyon WR, Runft DL, Caparon M. Role of RopB in Growth Phase Expression of the SpeB Cysteine Protease of *Streptococcus pyogenes*. *J Bacteriol*. 2003 Sep;185(17):5166–74.
  124. Elliott SD. A PROTEOLYTIC ENZYME PRODUCED BY GROUP A STREPTOCOCCI WITH SPECIAL REFERENCE TO ITS EFFECT ON THE TYPE-SPECIFIC M ANTIGEN. *J Exp Med*. 1945 Jun 1;81(6):573–92.
  125. Carroll RK, Musser JM. From transcription to activation: how group A streptococcus, the flesh-eating pathogen, regulates SpeB cysteine protease production. *Mol Microbiol*. 2011;81(3):588–601.
  126. Liu TY, Elliott SD. Activation of Streptococcal Proteinase and its Zymogen by Bacterial Cell Walls. *Nature*. 1965 Apr;206(4979):33–4.
  127. Chen CY, Luo SC, Kuo CF, Lin YS, Wu JJ, Lin MT, et al. Maturation Processing and Characterization of Streptopain \*. *J Biol Chem*. 2003 May 9;278(19):17336–43.
  128. Kapur V, Topouzis S, Majesky MW, Li LL, Hamrick MR, Hamill RJ, et al. A conserved *Streptococcus pyogenes* extracellular cysteine protease cleaves human fibronectin and degrades vitronectin. *Microb Pathog*. 1993 Nov;15(5):327–46.
  129. Sumitomo T, Nakata M, Higashino M, Terao Y, Kawabata S. Group A Streptococcal Cysteine Protease Cleaves Epithelial Junctions and Contributes to Bacterial Translocation \*. *J Biol Chem*. 2013 May 10;288(19):13317–24.
  130. Terao Y, Mori Y, Yamaguchi M, Shimizu Y, Ooe K, Hamada S, et al. Group A streptococcal cysteine protease degrades C3 (C3b) and contributes to evasion of innate immunity. *J Biol Chem*. 2008 Mar 7;283(10):6253–60.
  131. Schmidtchen A, Frick IM, Andersson E, Tapper H, Björck L. Proteinases of common pathogenic bacteria degrade and inactivate the antibacterial peptide LL-37. *Mol Microbiol*. 2002;46(1):157–68.
  132. Nelson DC, Garbe J, Collin M. Cysteine proteinase SpeB from *Streptococcus pyogenes* – a potent modifier of immunologically important host and bacterial proteins. 2011 Dec 1;392(12):1077–88.
  133. Gerlach D, Ozegowski JH, Knöll H, Köhler W. [Isolation and characterization of erythrotoxic toxins. VIII. Purification of a biologically active protein of the molecular weight 10,000 (LMP-10k) from filtrates of *Streptococcus pyogenes*, strain NY-5. Relationship to erythrotoxic toxin type A]. *Zentralbl Bakteriell Mikrobiol Hyg [A]*. 1986 Feb;261(1):75–84.
  134. Gerlach D, Reichardt W, Fleischer B, Schmidt KH. Separation of mitogenic and pyrogenic activities from so-called erythrotoxic toxin type B (*Streptococcal Proteinase*). *Zentralblatt Für Bakteriell*. 1994 Mar 1;280(4):507–14.
  135. Uhlmann J, Siemens N, Kai-Larsen Y, Fiedler T, Bergman P, Johansson L, et al. Phosphoglycerate Kinase—A Novel Streptococcal Factor Involved in Neutrophil Activation and Degranulation. *J Infect Dis*. 2016 Dec 15;214(12):1876–83.
  136. Barnett TC, Liebl D, Seymour LM, Gillen CM, Lim JY, LaRock CN, et al. The Globally Disseminated M1T1 Clone of Group A *Streptococcus* Evades Autophagy for Intracellular Replication. *Cell Host Microbe*. 2013 Dec 11;14(6):675–82.
  137. Egesten A, Olin AI, Linge HM, Yadav M, Mörgelin M, Karlsson A, et al. SpeB of *Streptococcus pyogenes* differentially modulates antibacterial and receptor activating properties of human chemokines. *PloS One*. 2009;4(3):e4769.
  138. Kapur V, Majesky MW, Li LL, Black RA, Musser JM. Cleavage of interleukin 1 beta (IL-1 beta) precursor to produce active IL-1 beta by a conserved extracellular cysteine protease from *Streptococcus pyogenes*. *Proc Natl Acad Sci U S A*. 1993 Aug 15;90(16):7676–80.

139. Johnson AF, Sands JS, Trivedi KM, Russell R, LaRock DL, LaRock CN. Constitutive secretion of pro-IL-18 allows keratinocytes to initiate inflammation during bacterial infection. *PLOS Pathog.* 2023 Apr 17;19(4):e1011321.
140. Macleod T, Ainscough JS, Hesse C, Konzok S, Braun A, Buhl AL, et al. The Proinflammatory Cytokine IL-36 $\gamma$  Is a Global Discriminator of Harmless Microbes and Invasive Pathogens within Epithelial Tissues. *Cell Rep [Internet]*. 2020 Dec 15 [cited 2023 Oct 10];33(11). Available from: [https://www.cell.com/cell-reports/abstract/S2211-1247\(20\)31504-7](https://www.cell.com/cell-reports/abstract/S2211-1247(20)31504-7)
141. Deng W, Bai Y, Deng F, Pan Y, Mei S, Zheng Z, et al. Streptococcal pyrogenic exotoxin B cleaves GSDMA and triggers pyroptosis. *Nature*. 2022 Feb;602(7897):496–502.
142. LaRock DL, Johnson AF, Wilde S, Sands JS, Monteiro MP, LaRock CN. Group A Streptococcus induces GSDMA-dependent pyroptosis in keratinocytes. *Nature*. 2022 May;605(7910):527–31.
143. Maamary PG, Sanderson-Smith ML, Aziz RK, Hollands A, Cole JN, McKay FC, et al. Parameters Governing Invasive Disease Propensity of Non-M1 Serotype Group A Streptococci. *J Innate Immun.* 2010 Sep 2;2(6):596–606.
144. Trigger for group A streptococcal M1T1 invasive disease. [cited 2023 Oct 10]; Available from: <https://faseb.onlinelibrary.wiley.com/doi/10.1096/fj.06-5804fje>
145. Federle MJ, McIver KS, Scott JR. A Response Regulator That Represses Transcription of Several Virulence Operons in the Group A Streptococcus. *J Bacteriol.* 1999 Jun 15;181(12):3649–57.
146. Hurst JR, Shannon BA, Craig HC, Rishi A, Tuffs SW, McCormick JK. The Streptococcus pyogenes hyaluronic acid capsule promotes experimental nasal and skin infection by preventing neutrophil-mediated clearance. *PLOS Pathog.* 2022 Nov 30;18(11):e1011013.
147. Wessels MR. Capsular Polysaccharide of Group A Streptococcus. *Microbiol Spectr.* 2019 Jan;7(1).
148. Cywes C, Wessels MR. Group A Streptococcus tissue invasion by CD44-mediated cell signalling. *Nature*. 2001 Dec;414(6864):648–52.
149. Flores AR, Jewell BE, Fittipaldi N, Beres SB, Musser JM. Human Disease Isolates of Serotype M4 and M22 Group A Streptococcus Lack Genes Required for Hyaluronic Acid Capsule Biosynthesis. *mBio*. 2012 Nov 6;3(6):10.1128/mbio.00413-12.
150. Turner CE, Abbott J, Lamagni T, Holden MTG, David S, Jones MD, et al. Emergence of a New Highly Successful Acapsular Group A Streptococcus Clade of Genotype emm89 in the United Kingdom. *mBio*. 2015 Jul 14;6(4):10.1128/mbio.00622-15.
151. Turner CE, Holden MTG, Blane B, Horner C, Peacock SJ, Sriskandan S. The Emergence of Successful Streptococcus pyogenes Lineages through Convergent Pathways of Capsule Loss and Recombination Directing High Toxin Expression. *mBio*. 2019 Dec 10;10(6):10.1128/mbio.02521-19.
152. Flores AR, Chase McNeil J, Shah B, Van Beneden C, Shelburne SA III. Capsule-Negative emm Types Are an Increasing Cause of Pediatric Group A Streptococcal Infections at a Large Pediatric Hospital in Texas. *J Pediatr Infect Dis Soc.* 2019 Jul 1;8(3):244–50.
153. Döhrmann S, LaRock CN, Anderson EL, Cole JN, Ryali B, Stewart C, et al. Group A Streptococcal M1 Protein Provides Resistance against the Antimicrobial Activity of Histones. *Sci Rep.* 2017 21;7:43039.
154. Ryan PA, Pancholi V, Fischetti VA. Group A Streptococci Bind to Mucin and Human Pharyngeal Cells through Sialic Acid-Containing Receptors. *Infect Immun.* 2001 Dec;69(12):7402–12.
155. De Oliveira DMP, Hartley-Tassell L, Everest-Dass A, Day CJ, Dabbs RA, Ve T, et al. Blood Group Antigen Recognition via the Group A Streptococcal M Protein Mediates Host Colonization. *mBio*. 2017 Jan 24;8(1):10.1128/mbio.02237-16.
156. Okada N, Liszewski MK, Atkinson JP, Caparon M. Membrane cofactor protein (CD46) is a keratinocyte receptor for the M protein of the group A streptococcus. *Proc Natl Acad Sci.* 1995 Mar 28;92(7):2489–93.
157. Valderrama JA, Riestra AM, Gao NJ, LaRock CN, Gupta N, Ali SR, et al. Group A streptococcal M protein activates the NLRP3 inflammasome. *Nat Microbiol.* 2017 Oct;2(10):1425–34.
158. Richter J, Monteleone MM, Cork AJ, Barnett TC, Nizet V, Brouwer S, et al. Streptolysins are the primary inflammasome activators in macrophages during Streptococcus pyogenes infection. *Immunol Cell Biol.* 2021;99(10):1040–52.
159. Sumbly P, Porcella SF, Madrigal AG, Barbian KD, Virtaneva K, Ricklefs SM, et al. Evolutionary Origin and Emergence of a Highly Successful Clone of Serotype M1 Group A Streptococcus Involved Multiple Horizontal Gene Transfer Events. *J Infect Dis.* 2005 Sep 1;192(5):771–82.

## REFERENCES

---

160. Ikebe T, Ato M, Matsumura T, Hasegawa H, Sata T, Kobayashi K, et al. Highly Frequent Mutations in Negative Regulators of Multiple Virulence Genes in Group A Streptococcal Toxic Shock Syndrome Isolates. *PLOS Pathog*. 2010 Apr 1;6(4):e1000832.
161. Ato M, Ikebe T, Kawabata H, Takemori T, Watanabe H. Incompetence of Neutrophils to Invasive Group A streptococcus Is Attributed to Induction of Plural Virulence Factors by Dysfunction of a Regulator. *PLOS ONE*. 2008 Oct 21;3(10):e3455.
162. Breiman RF, Davis JP, Facklam RR, Gray BM, Hoge CW, Kaplan EL, et al. Defining the Group A Streptococcal Toxic Shock Syndrome: Rationale and Consensus Definition. *JAMA*. 1993 Jan 20;269(3):390–1.
163. Lappin E, Ferguson AJ. Gram-positive toxic shock syndromes. *Lancet Infect Dis*. 2009 May 1;9(5):281–90.
164. McCormick JK, Yarwood JM, Schlievert PM. Toxic Shock Syndrome and Bacterial Superantigens: An Update. *Annu Rev Microbiol*. 2001;55(1):77–104.
165. Shannon BA, McCormick JK, Schlievert PM. Toxins and Superantigens of Group A Streptococci. *Microbiol Spectr*. 2019 Feb 8;7(1):10.1128/microbiolspec.gpp3-0054–2018.
166. Kasper KJ, Zeppa JJ, Wakabayashi AT, Xu SX, Mazzuca DM, Welch I, et al. Bacterial Superantigens Promote Acute Nasopharyngeal Infection by *Streptococcus pyogenes* in a Human MHC Class II-Dependent Manner. *PLOS Pathog*. 2014 May 29;10(5):e1004155.
167. Brouwer S, Barnett TC, Ly D, Kasper KJ, De Oliveira DMP, Rivera-Hernandez T, et al. Prophage exotoxins enhance colonization fitness in epidemic scarlet fever-causing *Streptococcus pyogenes*. *Nat Commun*. 2020 Oct 6;11(1):5018.
168. Emgård J, Bergsten H, McCormick JK, Barrantes I, Skrede S, Sandberg JK, et al. MAIT Cells Are Major Contributors to the Cytokine Response in Group A Streptococcal Toxic Shock Syndrome. *Proc Natl Acad Sci*. 2019 Dec 17;116(51):25923–31.
169. Davies MR, Keller N, Brouwer S, Jespersen MG, Cork AJ, Hayes AJ, et al. Detection of *Streptococcus pyogenes* M1UK in Australia and characterization of the mutation driving enhanced expression of superantigen SpeA. *Nat Commun*. 2023 Feb 24;14(1):1051.
170. Bisno AL, Stevens DL. Streptococcal Infections of Skin and Soft Tissues. *N Engl J Med*. 1996 Jan 25;334(4):240–6.
171. Shewell LK, Day CJ, Jen FEC, Haselhorst T, Atack JM, Reijneveld JF, et al. All major cholesterol-dependent cytolysins use glycans as cellular receptors. *Sci Adv*. 2020 May;6(21):eaaz4926.
172. Flaherty RA, Puricelli JM, Higashi DL, Park CJ, Lee SW. Streptolysin S Promotes Programmed Cell Death and Enhances Inflammatory Signaling in Epithelial Keratinocytes during Group A Streptococcus Infection. *Infect Immun*. 2015 Sep 10;83(10):4118–33.
173. Molloy EM, Cotter PD, Hill C, Mitchell DA, Ross RP. Streptolysin S-like virulence factors: the continuing saga. *Nat Rev Microbiol*. 2011 Sep;9(9):670–81.
174. Goldmann O, Sastalla I, Wos-Oxley M, Rohde M, Medina E. *Streptococcus pyogenes* induces oncosis in macrophages through the activation of an inflammatory programmed cell death pathway. *Cell Microbiol*. 2009;11(1):138–55.
175. Timmer AM, Timmer JC, Pence MA, Hsu LC, Ghochani M, Frey TG, et al. Streptolysin O promotes group A *Streptococcus* immune evasion by accelerated macrophage apoptosis. *J Biol Chem*. 2009 Jan 9;284(2):862–71.
176. Kimoto H, Fujii Y, Yokota Y, Taketo A. Molecular characterization of NADase-streptolysin O operon of hemolytic streptococci. *Biochim Biophys Acta BBA - Gene Struct Expr*. 2005 Jan 11;1681(2):134–49.
177. Velarde JJ, O’Seaghdha M, Baddal B, Bastiat-Sempe B, Wessels MR. Binding of NAD<sup>+</sup>-Glycohydrolase to Streptolysin O Stabilizes Both Toxins and Promotes Virulence of Group A *Streptococcus*. *mBio*. 2017 Sep 12;8(5):10.1128/mbio.01382-17.
178. Michos A, Gryllos I, Håkansson A, Srivastava A, Kokkotou E, Wessels MR. Enhancement of Streptolysin O Activity and Intrinsic Cytotoxic Effects of the Group A Streptococcal Toxin, NAD-Glycohydrolase \*. *J Biol Chem*. 2006 Mar 24;281(12):8216–23.
179. Magassa N, Chandrasekaran S, Caparon MG. *Streptococcus pyogenes* cytolysin-mediated translocation does not require pore formation by streptolysin O. *EMBO Rep*. 2010 May;11(5):400–5.
180. Velarde JJ, Piai A, Lichtenstein IJ, Lynskey NN, Chou JJ, Wessels MR. Structure of the *Streptococcus pyogenes* NAD<sup>+</sup> Glycohydrolase Translocation Domain and Its Essential Role in Toxin Binding to Oropharyngeal Keratinocytes. *J Bacteriol*. 2022 Jan 18;204(1):e00366-21.

181. Chandrasekaran S, Caparon MG. The NADase-Negative Variant of the *Streptococcus pyogenes* Toxin NAD<sup>+</sup> Glycohydrolase Induces JNK1-Mediated Programmed Cellular Necrosis. *mBio*. 2016 Feb 2;7(1):10.1128/mbio.02215-15.
182. Zhu L, Olsen RJ, Lee JD, Porter AR, DeLeo FR, Musser JM. Contribution of Secreted NADase and Streptolysin O to the Pathogenesis of Epidemic Serotype M1 *Streptococcus pyogenes* Infections. *Am J Pathol*. 2017 Mar 1;187(3):605–13.
183. Bastiat-Sempe B, Love JF, Lomayeva N, Wessels MR. Streptolysin O and NAD-Glycohydrolase Prevent Phagolysosome Acidification and Promote Group A *Streptococcus* Survival in Macrophages. *mBio*. 2014 Sep 16;5(5):10.1128/mbio.01690-14.
184. O'Seaghdha M, Wessels MR. Streptolysin O and its Co-Toxin NAD-glycohydrolase Protect Group A *Streptococcus* from Xenophagic Killing. *PLOS Pathog*. 2013 Jun 6;9(6):e1003394.
185. Nozawa T, Iibushi J, Toh H, Minowa-Nozawa A, Murase K, Aikawa C, et al. Intracellular Group A *Streptococcus* Induces Golgi Fragmentation To Impair Host Defenses through Streptolysin O and NAD-Glycohydrolase. *mBio*. 2021 Feb 9;12(1):10.1128/mbio.01974-20.
186. Vajjala A, Biswas D, Tay WH, Hanski E, Kline KA. Streptolysin-induced endoplasmic reticulum stress promotes group A *Streptococcal* host-associated biofilm formation and necrotising fasciitis. *Cell Microbiol*. 2019;21(1):e12956.
187. Mover E, Bolarin JS, Valfridsson C, Velarde J, Skrede S, Nekludov M, et al. Interplay between human STING genotype and bacterial NADase activity regulates inter-individual disease variability. *Nat Commun*. 2023 Jul 6;14(1):4008.
188. Zhu L, Olsen RJ, Nasser W, Beres SB, Vuopio J, Kristinsson KG, et al. A molecular trigger for intercontinental epidemics of group A *Streptococcus*. *J Clin Invest*. 2015 Sep 1;125(9):3545–59.
189. Johansson L, Snäll J, Sendi P, Linnér A, Thulin P, Linder A, et al. HMGB1 in severe soft tissue infections caused by *Streptococcus pyogenes*. *Front Cell Infect Microbiol* [Internet]. 2014 [cited 2023 Oct 19];4. Available from: <https://www.frontiersin.org/articles/10.3389/fcimb.2014.00004>
190. Johansson L, Linnér A, Sundén-Cullberg J, Hagggar A, Herwald H, Loré K, et al. Neutrophil-Derived Hyperresistinemia in Severe Acute *Streptococcal* Infections<sup>1</sup>. *J Immunol*. 2009 Sep 15;183(6):4047–54.
191. Snäll J, Linnér A, Uhlmann J, Siemens N, Ibold H, Janos M, et al. Differential neutrophil responses to bacterial stimuli: *Streptococcal* strains are potent inducers of heparin-binding protein and resistin-release. *Sci Rep*. 2016 Feb 18;6(1):21288.
192. Remington A, Turner CE. The DNases of pathogenic Lancefield streptococci. *Microbiology*. 2018;164(3):242–50.
193. Sumbly P, Barbian KD, Gardner DJ, Whitney AR, Welty DM, Long RD, et al. Extracellular deoxyribonuclease made by group A *Streptococcus* assists pathogenesis by enhancing evasion of the innate immune response. *Proc Natl Acad Sci*. 2005 Feb;102(5):1679–84.
194. Buchanan JT, Simpson AJ, Aziz RK, Liu GY, Kristian SA, Kotb M, et al. DNase expression allows the pathogen group A *Streptococcus* to escape killing in neutrophil extracellular traps. *Curr Biol CB*. 2006 Feb 21;16(4):396–400.
195. Tanaka M, Kinoshita-Daitoku R, Kiga K, Sanada T, Zhu B, Okano T, et al. Group A *Streptococcus* establishes pharynx infection by degrading the deoxyribonucleic acid of neutrophil extracellular traps. *Sci Rep*. 2020 Feb 24;10(1):3251.
196. Keller N, Woytschak J, Heeb LEM, Maggio EM, Shambat SM, Snäll J, et al. Group A *Streptococcal* DNase Sda1 Impairs Plasmacytoid Dendritic Cells' Type 1 Interferon Response. *J Invest Dermatol*. 2019 Jun 1;139(6):1284–93.
197. Uchiyama S, Andreoni F, Schuepbach RA, Nizet V, Zinkernagel AS. DNase Sda1 Allows Invasive M1T1 Group A *Streptococcus* to Prevent TLR9-Dependent Recognition. *PLOS Pathog*. 2012 Jun 14;8(6):e1002736.
198. Zinkernagel AS, Timmer AM, Pence MA, Locke JB, Buchanan JT, Turner CE, et al. The IL-8 Protease SpyCEP/ScpC of Group A *Streptococcus* Promotes Resistance to Neutrophil Killing. *Cell Host Microbe*. 2008 Aug 14;4(2):170–8.
199. Kurupati P, Turner CE, Tziona I, Lawrenson RA, Alam FM, Nohadani M, et al. Chemokine-cleaving *Streptococcus pyogenes* protease SpyCEP is necessary and sufficient for bacterial dissemination within soft tissues and the respiratory tract. *Mol Microbiol*. 2010 Jun;76(6):1387–97.
200. Edwards RJ, Taylor GW, Ferguson M, Murray S, Rendell N, Wrigley A, et al. Specific C-Terminal Cleavage and Inactivation of Interleukin-8 by Invasive Disease Isolates of *Streptococcus pyogenes*. *J Infect Dis*. 2005 Sep 1;192(5):783–90.
201. Uchiyama S, Döhrmann S, Timmer AM, Dixit N, Ghochani M, Bhandari T, et al. Streptolysin O Rapidly Impairs Neutrophil Oxidative Burst and Antibacterial Responses to Group A *Streptococcus*. *Front Immunol*. 2015;6:581.

## REFERENCES

---

202. Pinho-Ribeiro FA, Baddal B, Haarsma R, O'Seaghda M, Yang NJ, Blake KJ, et al. Blocking Neuronal Signaling to Immune Cells Treats Streptococcal Invasive Infection. *Cell*. 2018 May 17;173(5):1083-1097.e22.
203. Loof TG, Rohde M, Chhatwal GS, Jung S, Medina E. The contribution of dendritic cells to host defenses against *Streptococcus pyogenes*. *J Infect Dis*. 2007 Dec 15;196(12):1794–803.
204. Loof TG, Goldmann O, Medina E. Immune recognition of *Streptococcus pyogenes* by dendritic cells. *Infect Immun*. 2008 Jun;76(6):2785–92.
205. Veckman V, Julkunen I. *Streptococcus pyogenes* activates human plasmacytoid and myeloid dendritic cells. *J Leukoc Biol*. 2008 Feb;83(2):296–304.
206. Cortés G, Wessels MR. Inhibition of dendritic cell maturation by group A *Streptococcus*. *J Infect Dis*. 2009 Oct 1;200(7):1152–61.
207. Langshaw EL, Reynolds S, Ozberk V, Dooley J, Calcutt A, Zaman M, et al. Streptolysin O Deficiency in *Streptococcus pyogenes* M1T1 covR/S Mutant Strain Attenuates Virulence in In Vitro and In Vivo Infection Models. *mBio*. 2023 Feb 6;14(1):e03488-22.
208. Kaul R, McGeer A, Low DE, Green K, Schwartz B. Population-based surveillance for group A streptococcal necrotizing fasciitis: Clinical features, prognostic indicators, and microbiologic analysis of seventy-seven cases. Ontario Group A Streptococcal Study. *Am J Med*. 1997 Jul;103(1):18–24.
209. Johansson L, Thulin P, Sendi P, Hertzén E, Linder A, Åkesson P, et al. Cathelicidin LL-37 in Severe *Streptococcus pyogenes* Soft Tissue Infections in Humans. *Infect Immun*. 2008 Aug;76(8):3399–404.
210. Siemens N, Chakrakodi B, Shambat SM, Morgan M, Bergsten H, Hyldegaard O, et al. Biofilm in group A streptococcal necrotizing soft tissue infections. *JCI Insight*. 2016 07;1(10):e87882.
211. Skutlaberg DH, Wiker HG, Mylvaganam H, The INFECT Study Group, Norrby-Teglund A, Skrede S. Consistent Biofilm Formation by *Streptococcus pyogenes* emm 1 Isolated From Patients With Necrotizing Soft Tissue Infections. *Front Microbiol* [Internet]. 2022 [cited 2023 Oct 9];13. Available from: <https://www.frontiersin.org/articles/10.3389/fmicb.2022.822243>
212. Kazmi SU, Kansal R, Aziz RK, Hooshdaran M, Norrby-Teglund A, Low DE, et al. Reciprocal, Temporal Expression of SpeA and SpeB by Invasive M1T1 Group A Streptococcal Isolates In Vivo. *Infect Immun*. 2001 Aug;69(8):4988–95.
213. Baude J, Bastien S, Gillet Y, Leblanc P, Itzek A, Tristan A, et al. Necrotizing Soft Tissue Infection *Staphylococcus aureus* but not *S. pyogenes* Isolates Display High Rates of Internalization and Cytotoxicity Toward Human Myoblasts. *J Infect Dis*. 2019 Jul 19;220(4):710–9.
214. Mairpady Shambat S, Siemens N, Monk IR, Mohan DB, Mukundan S, Krishnan KC, et al. A point mutation in AgrC determines cytotoxic or colonizing properties associated with phenotypic variants of ST22 MRSA strains. *Sci Rep*. 2016 Aug 11;6(1):31360.
215. Tang-Huau TL, Gueguen P, Goudot C, Durand M, Bohec M, Baulande S, et al. Human in vivo-generated monocyte-derived dendritic cells and macrophages cross-present antigens through a vacuolar pathway. *Nat Commun*. 2018 Jul 2;9(1):2570.
216. Horev-Azaria L, Baldi G, Beno D, Bonacchi D, Golla-Schindler U, Kirkpatrick JC, et al. Predictive Toxicology of cobalt ferrite nanoparticles: comparative in-vitro study of different cellular models using methods of knowledge discovery from data. *Part Fibre Toxicol*. 2013 Jul 29;10(1):32.
217. Rakow A, Schoon J, Dienelt A, John T, Textor M, Duda G, et al. Influence of particulate and dissociated metal-on-metal hip endoprosthesis wear on mesenchymal stromal cells in vivo and in vitro. *Biomaterials*. 2016 Aug 1;98:31–40.
218. Scharf B, Clement CC, Zolla V, Perino G, Yan B, Elci SG, et al. Molecular analysis of chromium and cobalt-related toxicity. *Sci Rep*. 2014 Jul 17;4(1):5729.
219. Bettigole SE, Glimcher LH. Endoplasmic Reticulum Stress in Immunity. *Annu Rev Immunol*. 2015;33(1):107–38.
220. Loeffler H, Jonitz-Heincke A, Peters K, Mueller-Hilke B, Fiedler T, Bader R, et al. Comparison of Inflammatory Effects in THP-1 Monocytes and Macrophages after Exposure to Metal Ions. *Materials*. 2020 Jan;13(5):1150.
221. Posada OM, Tate RJ, Grant MH. Effects of CoCr metal wear debris generated from metal-on-metal hip implants and Co ions on human monocyte-like U937 cells. *Toxicol In Vitro*. 2015 Mar 1;29(2):271–80.
222. Nagarajan S, Chesla S, Cobern L, Anderson P, Zhu C, Selvaraj P. Ligand Binding and Phagocytosis by CD16 (Fc  $\gamma$  Receptor III) Isoforms: PHAGOCYTOTIC SIGNALING BY ASSOCIATED  $\zeta$  AND  $\gamma$  SUBUNITS IN CHINESE HAMSTER OVARY CELLS (\*). *J Biol Chem*. 1995 Oct 27;270(43):25762–70.



223. Verkaik NJ, de Vogel CP, Boelens HA, Grumann D, Hoogenboezem T, Vink C, et al. Anti-Staphylococcal Humoral Immune Response in Persistent Nasal Carriers and Noncarriers of *Staphylococcus aureus*. *J Infect Dis*. 2009 Mar 1;199(5):625–32.
224. Ben Mkaddem S, Aloulou M, Benhamou M, Monteiro RC. Role of FcγRIIIA (CD16) in IVIg-Mediated Anti-Inflammatory Function. *J Clin Immunol*. 2014 Jul 1;34(1):46–50.
225. Aloulou M, Ben Mkaddem S, Biarnes-Pelicot M, Boussetta T, Souchet H, Rossato E, et al. IgG1 and IVIg induce inhibitory ITAM signaling through FcγRIII controlling inflammatory responses. *Blood*. 2012 Mar 29;119(13):3084–96.
226. Stoodley P, Nistico L, Johnson S, Lasko LA, Baratz M, Gahlot V, et al. Direct Demonstration of Viable *Staphylococcus aureus* Biofilms in an Infected Total Joint Arthroplasty: A Case Report. *JBJS*. 2008 Aug 1;90(8):1751.
227. Ghosh C, Luong G, Sun Y. A snapshot of the PD-1/PD-L1 pathway. *J Cancer*. 2021 Mar 5;12(9):2735–46.
228. Møllergaard M, Skovbakke SL, Jepsen SD, Panagiotopoulou N, Hansen ABR, Tian W, et al. Clinical *Staphylococcus aureus* inhibits human T-cell activity through interaction with the PD-1 receptor. *mBio*. 2023 Oct 5;14(5):e01349-23.
229. Chella Krishnan K, Mukundan S, Landero Figueroa JA, Caruso JA, Kotb M. Metal-Mediated Modulation of Streptococcal Cysteine Protease Activity and Its Biological Implications. *Infect Immun*. 2014 Jun 23;82(7):2992–3001.
230. Norrby-Teglund A, Thulin P, Gan BS, Kotb M, McGeer A, Andersson J, et al. Evidence for Superantigen Involvement in Severe Group A Streptococcal Tissue Infections. *J Infect Dis*. 2001 Oct 1;184(7):853–60.
231. Medina LMP, Rath E, Jahagirdar S, Bruun T, Madsen MB, Strålin K, et al. Discriminatory plasma biomarkers predict specific clinical phenotypes of necrotizing soft-tissue infections. *J Clin Invest* [Internet]. 2021 Jul 15 [cited 2023 Nov 23];131(14). Available from: <https://www.jci.org/articles/view/149523>
232. Sedimbi SK, Häggglöf T, Karlsson MCI. IL-18 in inflammatory and autoimmune disease. *Cell Mol Life Sci*. 2013 Dec 1;70(24):4795–808.
233. Ren H, Yang H, Yang X, Zhang G, Rong X, Huang J, et al. *Brucella* Outer Membrane Lipoproteins 19 and 16 Differentially Induce Interleukin-18 Response or Pyroptosis in Human Monocytic Cells. *J Infect Dis*. 2021 Dec 15;224(12):2148–59.
234. Mandal R, Barrón JC, Kostova I, Becker S, Strebhardt K. Caspase-8: The double-edged sword. *Biochim Biophys Acta BBA - Rev Cancer*. 2020 Apr 1;1873(2):188357.
235. Parrish AB, Freel CD, Kornbluth S. Cellular Mechanisms Controlling Caspase Activation and Function. *Cold Spring Harb Perspect Biol*. 2013 Jan 6;5(6):a008672.
236. Anderson J, Imran S, Frost HR, Azzopardi KI, Jalali S, Novakovic B, et al. Immune signature of acute pharyngitis in a *Streptococcus pyogenes* human challenge trial. *Nat Commun*. 2022 Feb 9;13(1):769.
237. Kak G, Raza M, Tiwari BK. Interferon-gamma (IFN-γ): Exploring its implications in infectious diseases. *Biomol Concepts*. 2018 Jan 1;9(1):64–79.
238. Perregaux DG, McNiff P, Laliberte R, Conklyn M, Gabel CA. ATP Acts as an Agonist to Promote Stimulus-Induced Secretion of IL-1β and IL-18 in Human Blood. *J Immunol*. 2000 Oct 15;165(8):4615–23.
239. Mehta VB, Hart J, Wewers MD. ATP-stimulated Release of Interleukin (IL)-1β and IL-18 Requires Priming by Lipopolysaccharide and Is Independent of Caspase-1 Cleavage\*. *J Biol Chem*. 2001 Feb 9;276(6):3820–6.
240. Aziz RK, Pabst MJ, Jeng A, Kansal R, Low DE, Nizet V, et al. Invasive M1T1 group A *Streptococcus* undergoes a phase-shift in vivo to prevent proteolytic degradation of multiple virulence factors by SpeB. *Mol Microbiol*. 2004 Jan;51(1):123–34.
241. Deng M, Scott MJ, Fan J, Billiar TR. Location is the key to function: HMGB1 in sepsis and trauma-induced inflammation. *J Leukoc Biol*. 2019 Jul 1;106(1):161–9.
242. Davies MJ. Protein oxidation and peroxidation. *Biochem J*. 2016 Mar 29;473(7):805–25.
243. van der Veen BS, de Winther MPJ, Heeringa P. Myeloperoxidase: Molecular Mechanisms of Action and Their Relevance to Human Health and Disease. *Antioxid Redox Signal*. 2009 Nov;11(11):2899–937.
244. Schrijver IT, Kemperman H, Roest M, Kesecioglu J, de Lange DW. Myeloperoxidase can differentiate between sepsis and non-infectious SIRS and predicts mortality in intensive care patients with SIRS. *Intensive Care Med Exp*. 2017 Sep 15;5(1):43.

## REFERENCES

---

245. Bonaventura A, Carbone F, Vecchié A, Meessen J, Ferraris S, Beck E, et al. The role of resistin and myeloperoxidase in severe sepsis and septic shock: Results from the ALBIOS trial. *Eur J Clin Invest.* 2020;50(10):e13333.
246. Kuo CF, Lin YS, Chuang WJ, Wu JJ, Tsao N. Degradation of Complement 3 by Streptococcal Pyrogenic Exotoxin B Inhibits Complement Activation and Neutrophil Opsonophagocytosis. *Infect Immun.* 2008 Mar;76(3):1163–9.
247. Eriksson A, Norgren M. Cleavage of Antigen-Bound Immunoglobulin G by SpeB Contributes to Streptococcal Persistence in Opsonizing Blood. *Infect Immun.* 2003 Jan;71(1):211–7.
248. LaRock CN, Todd J, LaRock DL, Olson J, O'Donoghue AJ, Robertson AAB, et al. IL-1 $\beta$  is an innate immune sensor of microbial proteolysis. *Sci Immunol.* 2016 Aug 19;1(2):eaah3539–eaah3539.
249. Olsen RJ, Raghuram A, Cantu C, Hartman MH, Jimenez FE, Lee S, et al. The Majority of 9,729 Group A Streptococcus Strains Causing Disease Secrete SpeB Cysteine Protease: Pathogenesis Implications. *Infect Immun.* 2015 Nov 10;83(12):4750–8.

## 8. APPENDIX

### i. Eigenständigkeitserklärung

Hiermit erkläre ich, dass diese Arbeit bisher von mir weder an der Mathematisch-Naturwissenschaftlichen Fakultät der Universität Greifswald noch einer anderen wissenschaftlichen Einrichtung zum Zwecke der Promotion eingereicht wurde.

Ferner erkläre ich, dass ich diese Arbeit selbstständig verfasst und keine anderen als die darin angegebenen Hilfsmittel und Hilfen benutzt und keine Textabschnitte eines Dritten ohne Kennzeichnung übernommen habe.

Greifswald, 08.12.2023

.....

Lea Tölken

ii. Curriculum Vitae

*Personal Details*

Name: Lea Alessandra Tölken  
Date of birth: February 08, 1996  
Place of birth: Bremerhaven

*Education*

02/2020 to present **PhD student** at the Interfaculty Institute for Genetics and Functional Genome Research, Department of Molecular Genetics and Infection Biology; Research Group "Infectious Diseases"

10/2017 to 08/2020 Master of Science in Biochemistry, University of Greifswald  
Master Thesis: Group G streptococcal defense mechanisms in skin infections

08/2018 to 12/2018 Visiting student at the University of Manitoba, Winnipeg, MB; Canada

10/2014 to 11/2017 Bachelor of Science in Biochemistry, University of Greifswald  
Bachelor Thesis: Influence of fatty acids on the cardiolipin-composition and proliferation of human T cells

08/2006 to 07/2014 General university entrance qualification at the Gymnasium Wesermünde, Bremerhaven

*Additional Skills*

Languages German (native), English (fluent in speaking and writing)  
Certificates Qualification for laboratory animal experiments acc. to FELASA category B

Greifswald, 08.12.2023

.....  
Lea Tölken

---

iii. Publications and conference contributions

a) Papers and Manuscripts Not Included in this Thesis

Antje D. Paulikat, **Lea A. Tölken**, Lana H. Jachmann, Gerhard Burchhardt, Sven Hammerschmidt, Nikolai Siemens; *Streptococcus pneumoniae* Impairs Maturation of Human Dendritic Cells and Consequent Activation of CD4<sup>+</sup> T Cells via Pneumolysin; J Innate Immun; 2 September 2022; 14 (5): 569–580. <https://doi.org/10.1159/000522339>

Fabian Cuypers, Alexander Schäfer, Sebastian B. Skorka, Surabhi Surabhi, **Lea A. Tölken**, Antje D. Paulikat, Thomas P. Kohler, Saskia A. Otto, Thomas C. Mettenleiter, Sven Hammerschmidt, Ulrike Blohm, Nikolai Siemens; Innate immune responses at the asymptomatic stage of influenza A viral infections of *Streptococcus pneumoniae* colonized and non-colonized mice.; Scientific Reports. 2021;11(1):20609. <https://doi.org/10.1038/s41598-021-00211-y>

**Lea A. Tölken**#, Antje D. Paulikat#, Fabian Cuypers, Sebastian B. Skorka, Sven Hammerschmidt, Nikolai Siemens; Cytokine Profiling in Influenza A Virus and Staphylococcal (Co-)Infections. Infectious Microbes & Diseases 4(4):p 161-167, December 2022. | DOI: 10.1097/IM9.000000000000108. # equal contribution

**Lea A. Tölken**#, Janine V. Neufend#, Oddvar Oppegaard, Karen Methling, Kirsten Moll, Sylvio Redanz, Miriam M.D. Katsburg, Murtadha Q. Ali, Patience Shumba, Bernd Kreikemeyer, Steinar Skrede, Marcus Fulde, Anna Norrby-Teglund, Michael Lalk, Bård R. Kittang, Nikolai Siemens; Streptokinase reduces *Streptococcus dysgalactiae* subsp. *equisimilis* biofilm formation; submitted to BMC Microbiology; # equal contribution

b) Conference Contributions

International Joint Meeting Infection Biology and Antibiotics 2022; oral presentation: Hyper-virulent *Streptococcus pyogenes* impairs interleukin-18 response in human immune cells of myeloid lineage

21st Lancefield International Symposium for Streptococci and Streptococcal Diseases 2022, Stockholm; poster presentation: Hyper-virulent *Streptococcus pyogenes* impairs interleukin-18 response in human immune cells of myeloid lineage

2nd Summer School on "Infection Biology, Greifswald; oral presentation: Hyper-virulent *Streptococcus pyogenes* impairs interleukin-18 response in human immune cells of myeloid lineage

5th German Pneumococcal & Streptococcal Symposium 2023, Hannover; oral presentation: Hyper-virulent *Streptococcus pyogenes* impairs interleukin-18 response in human immune cells of myeloid lineage via a caspase-mediated mechanism

#### iv. Danksagung

Wie dem einen oder anderen aufgefallen sein könnte bin ich kein Freund vieler Worte. Mein Dank gilt allen, die mir in den letzten vier Jahren zur Seite gestanden haben! Besonders bei folgenden Leuten möchte ich mich von Herzen bedanken:

Bei Nikolai Siemens für die Möglichkeit an den vielfältigen und interessanten Projekten zu arbeiten, die nun in dieser Arbeit enthalten sind. Vielen Dank für deinen Einsatz und deine motivierenden Worte während der letzten vier Jahre!

Bei allen Mitarbeitern der Abteilung für molekulare Genetik und Infektionsbiologie für ihre Hilfsbereitschaft und Unterstützung während der letzten vier Jahre.

Bei meinen Mit-Doktoranden, die jederzeit ein offenes Ohr hatten und mir immer mit Rat und Tat zur Seite gestanden haben. Danke für Kaffeepausen, mehr oder weniger wissenschaftliche Diskussionen und einfach witzige Unterhaltungen, die meine Zeit hier unvergesslich gemacht haben.

Bei meiner Familie und meinen Freunden, die mir jederzeit zur Seite gestanden haben. Danke für eure immerwährende Geduld und eure bedingungslose Unterstützung während dieser Zeit.

Danke!





## PAPER I

# **Cobalt and Chromium Ions Impair Macrophage Response to *Staphylococcus aureus* Infection**

Lea A. Tölken, Georgi I. Wassilew, Daniel Grolimund, Timm Weitkamp, Bernhard Hesse,  
Anastasia Rakow, Nikolai Siemens, and Janosch Schoon

Accepted manuscript in ACS Biomaterials Science & Engineering, 2023 December 06

### Author Contributions:

Conceptualization: **LAT**, NS, JS; Data curation: **LAT**, NS, JS; Formal analysis: **LAT**, NS, JS;  
Funding acquisition: NS, GIW, JS; Investigation: **LAT**, NS, JS, BH, TW, AR, DG; Methodology:  
NS, JS, BH, TW, DG; Project administration: NS, JS; Resources: GIW, NS, JS; Software: GIW,  
NS, JS; Supervision: NS, JS; Validation: **LAT**, GIW, AR, NS, JS; Visualization: **LAT**, NS, JS;  
Writing - original draft: **LAT**, NS, JS; Writing - review & editing: **LAT**, GIW, AR, NS, JS, TW, BH,  
DG.

.....  
Prof. Dr. Nikolai Siemens

.....  
Lea Tölken



# Cobalt and chromium ions impair macrophage response to *Staphylococcus aureus* infection

*Lea A. Tölken<sup>a</sup>, Georgi I. Wassilew<sup>b</sup>, Daniel Grolimund<sup>c</sup>, Timm Weitkamp<sup>d</sup>, Bernhard Hesse<sup>e,f</sup>,  
Anastasia Rakow<sup>b</sup>, Nikolai Siemens<sup>a, ‡, \*</sup>, and Janosch Schoon<sup>b, ‡, \*</sup>*

<sup>a</sup> Department of Molecular Genetics and Infection Biology, University of Greifswald,  
Greifswald, 17489, Germany.

<sup>b</sup> Center for Orthopaedics, Trauma Surgery and Rehabilitation Medicine, University Medicine  
Greifswald, Greifswald, 17475, Germany

<sup>c</sup> Swiss Light Source, Paul Scherrer Institute, Villigen-PSI, 5232, Switzerland

<sup>d</sup> Synchrotron SOLEIL, Saint-Aubin, 91190, France

<sup>e</sup> Xploraytion GmbH, Berlin, 10625, Germany

<sup>f</sup> ESRF-The European Synchrotron, Grenoble, 38000, France

## Abstract

Cobalt-chromium-molybdenum (CoCrMo) alloys are routinely used in arthroplasty. CoCrMo wear particles and ions derived from arthroplasty implants lead to macrophage-driven adverse local tissue reactions, which have been linked to an increased risk of periprosthetic joint infection after revision arthroplasty. While metal-induced cytotoxicity is well characterized in human macrophages, direct effects on their functionality have remained elusive. Synchrotron radiation x-ray microtomography and x-ray fluorescence mapping indicated that peri-implant tissues harvested during aseptic revision of different arthroplasty implants are exposed to Co and Cr in situ. Confocal laser scanning microscopy revealed that macrophage influx is predominant in patient tissue. While in vitro exposure to Cr<sup>3+</sup> had only minor effects on monocytes/macrophage phenotype, pathologic concentrations of Co<sup>2+</sup> significantly impaired both, monocytes/macrophage phenotype and functionality. High concentrations of Co<sup>2+</sup> led to a shift in macrophage subsets and loss of surface markers including CD14 and CD16. Both, Co<sup>2+</sup> and Cr<sup>3+</sup> impaired macrophage responses to *Staphylococcus aureus* infection and particularly Co<sup>2+</sup>-exposed macrophages showed decreased phagocytic activity. These findings demonstrate the immunosuppressive effects of locally elevated metal ions on the innate immune response and supports further investigations, including studies exploring whether Co<sup>2+</sup> and Cr<sup>3+</sup> or CoCrMo alloys per se expose the patients to a higher risk of infections post revision arthroplasty.

**Keywords:** macrophages, *Staphylococcus aureus*, arthroplasty, cobalt, chromium, periprosthetic joint infection

## 1. Introduction

Arthroplasty is a successful surgical procedure for the treatment of patients suffering from chronic pain due to degenerative joint disease. Complications that usually occur in the late postoperative course due to tissue inflammation caused by material degradation and release or infections lead to revisions of implants. Cobalt-chromium-molybdenum (CoCrMo) metal alloys are metallic biomaterials widely used in arthroplasty. Multiple studies have indicated adverse effects of wear particles and metal ions released from CoCrMo alloys. These adverse local tissue reactions (ALTRs), such as tissue necrosis and pseudotumor formation, are characterized by lymphocyte and macrophage infiltration<sup>1</sup>. Two specific types of necrosis occur in ALTRs, namely, (i) necrosis predominantly through death of macrophages and (ii) tissue necrosis characterized by cell death of stromal elements<sup>2</sup>. *In vitro* data indicate that macrophage necrosis and not apoptosis is the predominant type of cell death following exposure to high concentrations of Co<sup>2+</sup><sup>3</sup>. Widely accepted mechanisms posit that phagocytosis of arthroprosthetic metal particles activates the NLRP3 inflammasome and that the cellular damage caused by metal ions result in the release of proinflammatory cytokines, subsequently giving rise to the inflammatory responses observed in ALTRs<sup>4-6</sup>. The proinflammatory environment has been held responsible for the differentiation of macrophages to bone resorbing osteoclasts and their activation, hence for the onset of periprosthetic osteolysis<sup>7</sup>. In clinical context, exposure to Co<sup>2+</sup> and Cr<sup>3+</sup> has been associated with early implant revision and increased rates of secondary revision, due to aseptic implant loosening and/or periprosthetic joint infections (PJI)<sup>8-13</sup>. Factors such as metal-induced cytotoxicity as well as ALTRs are believed to create an environment favorable to bacterial infections<sup>14-15</sup>.

Previous studies have shown that peri-implant tissues, including bone marrow, are exposed to Co- and Cr-containing particles<sup>2, 16-18</sup> and that these metals are present in the particulate as well

as in the dissociated state<sup>19</sup>. The comparison between *in vitro* corrosion and tribocorrosion showed that the dissolution of Co occurred primarily in tribocorrosive conditions, suggesting that the mechanism responsible for particle release affects their Co content<sup>20</sup>. *Ex vivo* analyses of the elemental composition of CoCrMo particles in periprosthetic bone marrow have revealed that Co content depends on their size<sup>21</sup>. The comparison of elemental ratios of CoCrMo-derived particles with the composition of the implanted bulk alloy showed that particle degradation results in the release of Co ions<sup>21</sup>, reaching local pathologic concentrations exceeding 10 µg/mL<sup>19</sup>. Besides CoCr alloy particles, trivalent Cr salts and oxides have been shown to be the predominant state of Cr in periprosthetic tissue collected during revisions of metal-on-metal hip implants<sup>18</sup>. Notably, Co has only been found co-localized with Cr in the elemental states, indicating that dissociated Co is released during the wear process or due to dealloying by passive or cell mediated degradation processes<sup>17-18, 21</sup>. Consequently, dissociated Co and Cr can cross cellular barriers leading to systemic exposure<sup>22-24</sup>.

Besides ALTRs, PJIs are devastating complications of arthroplasty, requiring revision surgery with partial or total exchange or explantation of the implant, debridement of necrotic and infected tissues, and effective antimicrobial treatment<sup>25-28</sup>. The incidence of PJIs is constantly increasing during the last decades. However, certain referral centers, particularly in Scandinavia, are reporting that the incidence appears to have levelled out after 2010<sup>14, 29-30</sup>. *Staphylococcus aureus* is one of the major causes of bone and joint infections<sup>31-32</sup> including PJIs<sup>33-35</sup>. Being held responsible for up to 28% of PJIs, makes it one of the most prevalent pathogens in revision arthroplasty<sup>36-38</sup>.

As part of the innate immune axis, macrophages are of crucial importance in initiating immediate response to highly inflammatory conditions and particularly infections. Tissue-resident macrophages are the first responders. They are involved in tissue-homeostasis, clearance of

cellular debris as well as pathogens, and metallic particles, among others.<sup>39-40</sup> As a result of inflammation, the limited number of resident macrophages is depleted, circulating monocytes influx into the tissue and differentiate to macrophages<sup>41</sup>. High influx of macrophages is commonly detected in peri-implant tissue, especially in ALTRs, and macrophages often co-localize with metal particles<sup>2</sup>. Metal particles as well as ions have been shown to impact macrophage viability<sup>42</sup>, migration<sup>43</sup>, and activation<sup>1</sup>. However, the pathogen-macrophage interplay following metal exposure has remained unknown.

Thus, the aims of this study were to evaluate whether exposure to Co and Cr and subsequent macrophage influx is evident at the time of aseptic arthroplasty implant revision and to analyze the impact of Co and Cr ions on human primary monocytes/macrophages including markers associated with infections and the ability of these cells to respond to subsequent *S. aureus* infection. We show that macrophages change their phenotype post Co<sup>2+</sup> exposure. More strikingly, Co<sup>2+</sup> affect expression of various surface markers and impair overall macrophage response to *S. aureus* infection. In contrast, Cr<sup>3+</sup> does not significantly affect monocyte/macrophage phenotype, but the response to infection.

## 2. Materials and Methods

### 2.1 Patient recruitment and sampling

The independent ethics committee (IEC) of the University Medicine Greifswald approved the study (BB 178/20 and BB 014/14) in accordance with the World Medical Association Declaration of Helsinki. All patients gave written informed consent to participate in this study. All experiments were carried out in accordance with the approved guidelines. Peri-implant soft tissue samples were collected during aseptic arthroplasty implant revisions. Buffy coats obtained from healthy blood donors were anonymously provided by the blood bank at the University Medicine Greifswald.

### 2.2 Synchrotron radiation x-ray computed tomography

Peri-implant soft tissue samples were fixed in phosphate buffered saline (PBS, BIO SELL) containing 4 % v/v formaldehyde (Carl Roth). Following overnight fixation, the specimens were placed in 2 ml screw-top tubes filled with PBS containing 100 U/mL penicillin and 1 µg/mL streptomycin (both Gibco). The specimens were scanned using Synchrotron radiation micro-computed tomography (SR-µCT) at the Anatomix beamline at the Synchrotron SOLEIL; the beamline and its instrumentation are described elsewhere <sup>44-45</sup>. In brief, the voxel size was 3.07 µm<sup>3</sup>, the central energy of the filtered white X-ray beam was around 40 keV. Each scan involved a slight offset of the rotation axis in relation to the detector field of view, aiming to enlarge the diameter of the reconstructed volume. For each scan, between 3,000 and 4,000 projections were acquired, each with an exposure time of 50 ms per projection. For the reconstruction of tomographic data, the standard pipeline implemented at the beamline was used; it is based on the PyHST2 framework. A Paganin phase-retrieval filter with a kernel length (“Paganin length” in PyHST2) of 138 µm was applied to facilitate data analysis.



Further data analysis and visualization of the tomographic reconstructions was performed using the AVIZO software (Thermo Fisher Scientific). For the segmentation of metallic particles, the 3D images were thresholded selecting a value above the gray-values corresponding to mineralized tissue. Subsequently, only particles larger than 4 voxels were considered as metal particles.

### 2.3 Synchrotron radiation x-ray fluorescence mapping

Parts of the fixed specimens (see 2.2) were dehydrated for 24 h in each step by an ascending ethanol gradient (70%, 80%, 96%, and 100%). After completing dehydration by incubation with xylene (Th. Geyer) for 3 h, the specimens were embedded in paraffin and 10  $\mu\text{m}$  sections were prepared. The sections were placed between two pieces of a 4  $\mu\text{m}$  thin ultralene foil (Spex SamplePrep) and mounted on custom-made sample holders. Synchrotron radiation micro x-ray fluorescence (SR- $\mu\text{XRF}$ ) mapping was performed at the microXAS beamline of the Swiss Light Source (Paul Scherrer Institute). Monochromatic excitation radiation of 9.8 keV (above Zn K-edge) was selected using a double crystal monochromator equipped with Si(111) crystals. The primary beam was focused by two orthogonal reflective mirrors ('Kirkpatrick-Baez geometry') down to a spot size of 1  $\mu\text{m}$  x 2  $\mu\text{m}$  (h x v). XRF spectra were collected using silicon drift detectors systems. Chemical images were recorded in 'on-the-fly' mode, with a pixel size of 20  $\mu\text{m}$  x 20  $\mu\text{m}$  to obtain overviews for further selection of regions of interest to be scanned with a pixel size of 2  $\mu\text{m}$  x 2  $\mu\text{m}$ . XRF spectra obtained for each individual pixel were deconvoluted using the software PyMCA<sup>46</sup>.

### 2.4 Histology, Immunostaining and laser scanning microscopy

The paraffin embedded tissue samples used for sectioning and subsequent SR-XRF analyses were additionally sectioned for histology (5  $\mu\text{m}$ ) and for immunostaining (10  $\mu\text{m}$ ). The sections were mounted on glass slides, dried overnight at 60 °C and dewaxed with xylene prior to

rehydration by ethanol gradient (100%, 96%, 80%, 70%) and water. The section adjacent to the section used for immunostaining were stained with hematoxylin and eosin (both Carl Roth) by the “progressive method”<sup>47</sup>. For immunostaining, antigen retrieval was performed by heating the slides in a microwave submersed in citrate buffer (pH 6.0, Sigma Aldrich) until boiling followed by 10 min at a sub-boiling temperature (95-98 °C). Tissue sections were permeabilized with 1% saponin in PBS for 30 min at room temperature. Sections were blocked using 2.5% fetal calf serum (Gibco) and 2.5% normal goat serum (Abcam) in PBS for 30 min at room temperature. Sections were stained overnight at 4 °C using titrated amounts of fluorophore-labeled antibodies. Sections were washed with PBS containing 1% saponin between each staining step. The following antibodies were used for immunofluorescence analysis (clone, fluorophore; all BioLegend): CD68 (Y1/82A, AlexaFlour647), CD45 /2D1, AlexaFlour700), CD14 (HCD14, AlexaFlour594) and HLA-DR (L243, AlexaFlour488). The staining was visualized using a Leica DMI8 CS Premium confocal laser scanning microscope (Leica).

## 2.5 Isolation of human monocytes and in vitro metal exposure

Human monocytes were isolated from buffy coats using CD14 S-pluriBead antihuman beads (PluriSelect) according to manufacturer’s instructions. Cobalt (II) chloride hexahydrate and chromium (III) chloride hexahydrate (both Sigma Aldrich) were dissolved in human AB serum (PAN-Biotech) at a stock concentration of 10 mg×mL<sup>-1</sup> Co<sup>2+</sup> or 10 mg/mL Cr<sup>3+</sup> and 10 mg×mL<sup>-1</sup> Co<sup>2+</sup> plus 10 mg×mL<sup>-1</sup> Cr<sup>3+</sup> and incubated overnight at 37 °C. Pre-incubation was performed to emulate in vivo formation of ion complexes of biomacromolecules. Isolated monocytes were exposed to metal salt solutions for 48 h at 37 °C and 5% CO<sub>2</sub> (final concentrations: 1 µg×mL<sup>-1</sup> and 10 µg×mL<sup>-1</sup> or of each in combination). Pure human AB serum served as control.

## 2.6 Bacterial strain

*S. aureus* strain 6005<sup>48</sup> was grown overnight at 37 °C in casein hydrolysate and yeast extract medium with agitation<sup>49</sup>. To mimic initial low grade infections, a multiplicity of infection (MOI) of 1 was used.

### 2.7 Infection of monocytes/macrophages

Stimulated monocytes were infected with *S. aureus* 6005 at a MOI of 1 for 1 h. Extracellular bacteria were killed by addition of antibiotics (400 µg×mL<sup>-1</sup> gentamicin/ 2 µg×mL<sup>-1</sup> lysostaphin, both Sigma Aldrich). For flow cytometry, infected monocytes were incubated for an additional 23 h at 37 °C and 5% CO<sub>2</sub>. For assessing intracellular bacterial counts, monocytes were infected as described above. One hour after addition of antibiotics, cells were washed, lysed, and intracellular bacteria were plated on blood agar plates (Oxoid).

### 2.8 Flow cytometry

Dead cells were stained using the Zombie Aqua Fixable Viability Kit (BioLegend) according to the manufacturer's instructions. Human TruStain FcX (BioLegend) was used according to the manufacturer's instructions to block unspecific binding of immunoglobulins. Extracellular markers were stained by incubating the cells with titrated amounts of monoclonal antibodies at 4 °C for 30 min. Cells were fixed and permeabilized using Cyto-Fast Fix/Perm Buffer Set (BioLegend). Intracellular markers were stained using titrated amounts of monoclonal antibodies at 4 °C for 30 min. Cells were washed between each staining step. Antibodies and clones directed against the following markers were used (clone, fluorophore; all BioLegend): CD14 (63D3, BV750 or HCD14, PE/Cy7), CD16 (B73.1, PE/Dazzle594), HLA-DR (LN3, FITC), CD38 (HB-7, PerCP), CD86 (BU63, PE/Cy7), PD-L1 (29E.2A3, APC) and CD68 (Y1/82A, BV421). The gating strategy is shown in the Supporting Information. (Figure S1). Data were acquired using a

FACSAriaIII flow cytometer and FACS DIVA 8.0 Software (both BD Biosciences) and analyzed using FCS Express 7 Software (De Novo Software).

## 2.8 Quantitative reverse transcription PCR analysis

Total RNA was isolated using RiboPure RNA purification Kit (Ambion) according to manufacturer's guidelines. cDNA synthesis was performed using the Superscript first-strand synthesis system for RT-PCR (Invitrogen). The real-time PCR amplification was performed with iTaq Universal SYBR Green Supermix kit (Biorad) using a StepOnePlus sequence detection system (Applied Biosystems). The levels of  $\beta$ -actin transcription (h\_beta-actin\_for: 5'-CTCTTCCAGCCTTCCTTCCT-3', h\_beta-actin\_rev: 5'-AGCACTGTGTTGGCGTACAG-3' (both Eurofins)) were used for normalization. The following commercially available primers were used (Name (Cat.#); all Qiagen): Hs\_HLA\_DRA\_1\_SG (QT00089383), Hs\_CD68\_1\_SG (QT00037184), Hs\_PPARG\_1\_SG (QT00029841), Hs\_STAT1\_1\_SG (QT00074123), Hs\_IRF5\_1\_SG (QT00092736).

## 2.10 Statistics

Statistical significance of differences was determined using the Kruskal-Wallis test with Dunn's multiple comparison posttest. Data plotting and exploratory analyses were performed using GraphPad Prism version 8. A *p* value below 0.05 was considered statistically significant. The analyses included all samples and data, and individual values are presented for all data points. The PyMCA software was used to perform RGB imaging, heatmap imaging, and peak spectra analyzes of the XRF data<sup>46</sup>.

### 3. Results

#### 3.1 Local metal exposure and macrophage influx in patient tissue

To evaluate whether patients are locally exposed to Co- and Cr-containing degradation products, peri-implant tissue samples were collected during aseptic revision surgery of hip, knee and ankle arthroplasty implants (n=3) (Figure 1A,B).

Histological analysis of the tissue samples revealed ALTR indicated by immune cell infiltration accompanied by numerous metal particles (Figure 1C). Spatially resolved multi-element mapping by SR- $\mu$ XRF showed local exposure in all three cases analyzed, characterized by Co- and Cr-containing particles of heterogeneous elemental composition (Figure 1D). The highest Co and Cr signals were detected in peri-implant tissue collected during revision total hip arthroplasty, with minor Co content i.e. only few regions indicating co-localized Co and Cr, pointing towards local Co dissolution. XRF-spectra of the soft tissue sample, harvested during revision total knee arthroplasty of an exposed versus non-exposed volume indicated arthroprosthetic degradation products characterized by co-localized Co and Cr. The soft tissue sample harvested during revision ankle arthroplasty was characterized by bone residues indicated by high calcium levels. Co-localized Co and Cr were found to be abundant in soft tissue surrounding osteolytic bone.

Since elemental analyses using SR- $\mu$ XRF are limited to only a small region of interest, parts of the tissue samples were additionally scanned using SR- $\mu$ CT to evaluate whether metal debris is distributed throughout the tissue samples. These analyses indicated that exposure to particles of different sizes is evident (Figure 2). Segmentation of micron-sized particles ( $>116 \mu\text{m}^3$ ) revealed a particle count of 842/250  $\text{mm}^3$ , 1435/250  $\text{mm}^3$ , and 104/250  $\text{mm}^3$  in peri-implant tissue collected during revision surgery of a hip, knee, and ankle arthroplasty implant, respectively.

Taken together, local Co and Cr exposure was evident at the time of revisions of standard hip, knee, and ankle arthroplasty implants and metal debris are distributed throughout the analyzed peri-implant tissue samples.

To confirm that infiltrating immune cells are macrophages, sections of nine patients (n=9), including the tree mentioned above, were immuno-stained (CD45 – leukocyte common antigen; CD68 – mainly expressed by macrophages; CD14 – mainly expressed by monocytic cells) and visualized via confocal laser scanning microscopy (CLSM). Highly auto-fluorescent metal particles were detected in tissues of all patients (Figure 3A). Areas with extensive macrophage infiltration were evident in seven out of nine patient tissues analyzed (Figure 3B). All macrophages stained positive for CD14 (Figure 3B). In many cases, macrophages and metal particles co-localized, indicating potential phagocytosis (Figure 3B, lower panel).

### 3.2 Exposure of monocytes to metal ions initiates macrophage differentiation with a metal-specific imprint

After proving that local exposure to Co and Cr and infiltration of macrophages at the time of aseptic revision of various arthroplasty implants is evident in peri-implant tissue, we next evaluated the effects of Co and Cr ion exposure on human monocytes/macrophages. To this end, primary monocytes were exposed to 1 or 10  $\mu\text{g}\times\text{mL}^{-1}$  of  $\text{Co}^{2+}$ ,  $\text{Cr}^{3+}$  or both metal ions for 48 h and cell phenotype was analyzed via flow cytometry. In all conditions, monocytes differentiated to macrophages ( $\text{CD68}^+\text{HLA-DR}^+$ ; Fig. S1). Although the viability of cells dropped following 48 h exposure to high concentrations of  $\text{Co}^{2+}$ , it did not reach statistical significance compared to non-exposed cells (Figure 4A). Subsequent analyses of surface-expressed CD14, a co-receptor of TLR4, allowed for discrimination of two subsets:  $\text{CD68}^+\text{CD14}^+$  and  $\text{CD68}^+\text{CD14}^-$  cells

(Figure 4B). Exposure of monocytes to  $10 \mu\text{g}\times\text{mL}^{-1} \text{Co}^{2+}$  alone or  $\text{Co}^{2+}/\text{Cr}^{3+}$  combination resulted in a shift from  $\text{CD68}^+\text{CD14}^+$  to mainly  $\text{CD68}^+\text{CD14}^-$  subset (Figure 4B). The subset distribution remained unchanged in all other conditions as compared to untreated cells (Figure 4B). Notably, this result was in contrast to the tissue analyses showing exclusively  $\text{CD14}^+$  macrophages (Figure 3B). Therefore, the two subsets were further analyzed for presence of intracellular CD14. Irrespective of the prior analyses dividing macrophages in  $\text{CD68}^+\text{CD14}^+$  and  $\text{CD68}^+\text{CD14}^-$  populations, all cells stained positive for intracellular CD14 (Figures 4C and S2). Therefore, these two subsets are referred to as  $\text{CD68}^+\text{CD14}^{\text{do}+}$  (CD14 double positive) and  $\text{CD68}^+\text{CD14}^{\text{in}+}$  (intracellular  $\text{CD14}^+$ ) in the following. However, both subsets were characterized by reduced expression of intracellular CD14 (Figure S2). Next, expression of CD16 (FC $\gamma$ RIII) was analyzed. Exposure to high concentrations of  $\text{Co}^{2+}$  resulted in an almost complete loss of CD16 on the cell surface (Figure 4D).

Next, stimulatory potential of metal ions towards macrophages was assessed. No activation of macrophages (CD38) in response to any condition was observed (Figure 5A). Irrespective of the macrophage subset, surface expression of HLA-DR was significantly decreased in response to high  $\text{Co}^{2+}$  concentrations, including co-exposure to  $\text{Co}^{2+}/\text{Cr}^{3+}$  (Figure 5B). In contrast, PD-L1 expression remained unaffected in all conditions (Figure 5C).

### 3.3 Cobalt and chromium ions inhibit macrophage response to *Staphylococcus aureus* infections

Next, the responsiveness of metal exposed macrophages towards subsequent *S. aureus* infections was assessed. Since *S. aureus* is a common cause of PJIs, a MSSA strain 6005 was used. In brief, human primary monocytes were exposed to metal ions for 24 h, subsequently infected with 6005 for 1 h, extracellular bacteria were killed, and macrophage responsiveness was analyzed

after 23 additional hours of infection. To match the peri-implant tissue environment, metal exposure continued through the entire series of infections.

First, phagocytic activity was analyzed by plating intracellular bacteria. Macrophages exposed to  $10 \mu\text{g}\times\text{mL}^{-1} \text{Co}^{2+}$  alone or in combination with  $\text{Cr}^{3+}$  showed significantly reduced bacterial phagocytosis (Figure 6A). To exclude potential metal ion mediated bactericidal effects, 6005 strain was directly exposed to  $10 \mu\text{g}\times\text{mL}^{-1}$  of metal ions. No effects were observed (Figure S3).

Subsequently, macrophage phenotype was analyzed in response to infections. Overall, no additional *S. aureus*-mediated cytotoxicity towards macrophages was noted (Figure 6B). Furthermore, the subsets distribution ( $\text{CD68}^+\text{CD14}^{\text{do}+}$  and  $\text{CD68}^+\text{CD14}^{\text{in}+}$ ) followed the previously observed metal-mediated phenotype and remained unaffected in all infectious conditions (Figure 6C). Irrespective of infections, general exposure of cells to high concentrations of  $\text{Co}^{2+}$  resulted in almost complete loss of CD16 on the cell surface. Of note, infected macrophages exposed to low concentrations of  $\text{Co}^{2+}$  showed comparable reduction of CD16 expression (Figure 6D). A similar trend was observed in infections of macrophages with prior  $\text{Cr}^{3+}$  treatment (Figure 6D).

In addition, the activation of macrophages was analyzed. While expansion of  $\text{CD38}^+$  cells was noted in response to infections of naïve cells, all metal ions completely suppressed this activation, irrespective of the type or concentration used (Figure 7A). Overall, no upregulation of HLA-DR expression in response to infection was detected (Figure 7B). In contrast, infection of macrophages led to an upregulation of PD-L1 expression in almost all conditions (Figure 7C). This effect was diminished in infected macrophages which were exposed to  $10 \mu\text{g} \times \text{mL}^{-1}$  of  $\text{Co}^{2+}$  alone or in combination with  $\text{Cr}^{3+}$  (Figure 6c).



Next, gene expression of different transcription factors and surface markers involved in macrophage activation in response to infection was analyzed. Since mostly single stimulations with high metal ion concentrations, and particularly  $\text{Co}^{2+}$ , had pronounced effects on macrophage responses, only  $10 \mu\text{g}\times\text{mL}^{-1}$  of  $\text{Co}^{2+}$  or  $\text{Cr}^{3+}$  prior to infection were used. *CD68* mRNA expression, indicative of monocytes to macrophages differentiation, was confirmed in all conditions (Figure S4A). The pro-inflammatory transcriptional factor *STAT1* was upregulated in *S. aureus* infections, while expression of anti-inflammatory *PPAR $\gamma$*  was reduced. In contrast, metal-exposed macrophages expressed similar levels of both transcriptional factors as compared to the unstimulated controls (Figure S4B-C). *IRF5* expression was unaffected in all conditions tested (Figure S4D). In congruence with the flow cytometry analyses, *HLA-DR* mRNA levels were reduced particularly in response to  $\text{Co}^{2+}$  stimulations irrespective of infections (Figure S4E).

#### 4. Discussion

Metal particles and ions derived from orthopedic implants containing CoCrMo can cause ALTRs<sup>2, 50</sup>. Tissue necrosis and influx of lymphocytes and macrophages are regularly observed in neoplastic tissue specimens from patients undergoing aseptic arthroplasty implant revision. Macrophages are crucial first-responders to infection and arthroprosthetic particles. They clear pathogens and debris and recruit additional immune cells through release of chemoattractants. Metal particles and ions were shown to significantly affect macrophage viability<sup>51</sup>. Here, we show that macrophages infiltrate peri-implant tissue of Co/Cr-exposed patients and change their phenotype post Co<sup>2+</sup> exposure. More strikingly, Co<sup>2+</sup> affect expression of various infection-associated surface markers and impair overall macrophage response to *S. aureus* infection. In contrast, Cr<sup>3+</sup> does not significantly affect macrophage phenotype, but the response to infection. The SR- $\mu$ XRF and SR- $\mu$ CT analyses presented here clearly demonstrate that peri-implant tissues, obtained at the time of revision of different implants, are exposed to Co and Cr. In earlier studies, we demonstrated that Co and Cr in peri-implant tissue and fluid obtained during hip arthroplasty implant revisions are present in the particulate and also in the dissociated state<sup>19, 52</sup>, with concentrations of up to 25  $\mu\text{g}\times\text{mL}^{-1}$  of Cr and 7  $\mu\text{g}\times\text{mL}^{-1}$  of Co in periprosthetic tissue and 9  $\mu\text{g}\times\text{mL}^{-1}$  of Cr and 15  $\mu\text{g}\times\text{mL}^{-1}$  of Co in synovial fluid. These data and other studies emphasize not only that the concentrations used for cell stimulations in the present study emulate a clinically relevant exposure scenario but also that Co and Cr released from arthroplasty implants are characterized by a multitude of physicochemical properties<sup>16-18, 21, 53</sup>, resulting in an interplay of biologically active metal ions and immunogenic particles<sup>16, 54-55</sup>. Dense metal aggregation commonly results in tissue inflammation characterized by influx of macrophages and lymphocytes<sup>2</sup>. Detailed CLSM analyses of patient tissue identified mainly macrophages (CD45<sup>+</sup>CD68<sup>+</sup> cells),

which often co-localized with metal particles. Subsequently, we determined the phenotype and functionality of macrophages in a series of *in vitro* experiments using human primary cells. Most studies focus on cytotoxicity of Co and Cr ions and particles towards different cell types, *e.g.* fibroblasts, lymphocytes and different monocytic cell lines<sup>1</sup>. Especially Co was shown to be cytotoxic and necrosis was identified as a predominant type of cell death<sup>42,56</sup>. While Co<sup>2+</sup> induced cytolytic events in THP1 macrophages, Cr<sup>3+</sup> did not<sup>51</sup>. This is in line with our results on human primary monocytes/macrophages showing that high concentrations of Co<sup>2+</sup> are cytotoxic and Cr<sup>3+</sup> are not. Characterization of macrophages revealed a substantial shift of subsets from CD68<sup>+</sup>CD14<sup>do+</sup> to CD68<sup>+</sup>CD14<sup>in+</sup> in response to high Co<sup>2+</sup> concentrations. The later completely lacked the surface deposition of CD14.

Macrophages phagocytose metal particles. The acidic pH in the phagolysosome leads to release of Co<sup>2+</sup> from Co particles, due to increased solubility of this element at low pH<sup>57</sup>. Consequently, Co<sup>2+</sup> induce oxidative stress and reactive oxygen species (ROS) production in macrophages<sup>51,58</sup>. Excessive ROS production is in turn linked to impaired macrophage migration<sup>43</sup>. Although speculative, Co<sup>2+</sup>-mediated stress might impair intracellular protein transport from the ER to Golgi apparatus, leading to a loss of surface CD14 as well as other markers, including the observed lack of CD16 in our experimental setup, as intracellular stores are not transported to the cell membrane anymore<sup>59</sup>.

Studies have shown that THP1 and U937 monocytic cell lines upregulate transcription of genes encoding for cytokines/chemokines (*IL1B*, *CXCL8*)<sup>51</sup>, or release cytokines (IL-6, TNF $\alpha$ , IFN- $\gamma$ )<sup>60</sup> in response to metal exposure. Consequently, this phenomenon has been referred to as “activation”. In contrast to those two studies, we did not observe activation of macrophages in response to metal ions, since none of the key cellular markers analyzed (CD38, HLA-DR, PD-L1)

were upregulated. Even down-regulation of HLA-DR in response to high  $\text{Co}^{2+}$  concentrations was noted, which was confirmed on mRNA level. This immunosuppression is further confirmed in infection experiments under constant metal ion exposure.  $\text{Co}^{2+}$  and  $\text{Cr}^{3+}$  severely impaired the cellular response to infection. While *S. aureus* infection of naïve cells resulted in expansion of  $\text{CD38}^+$  cells, all metal conditions suppressed this effect. In addition, no upregulation of HLA-DR was observed and PD-L1 up-regulation was exclusively impaired when high concentrations of  $\text{Co}^{2+}$  were used. PD-L1 is a checkpoint inhibitor that binds to PD-1 on T cells. Interaction of these molecules controls T cell activation by preventing excessive proliferation<sup>40</sup>. Our surface markers data is further supported by mRNA expression analyses of transcriptional factors. STAT1, a pro-inflammatory transcriptional regulator, expression was exclusively upregulated in *S. aureus* infections without prior metal exposure, while  $\text{PPAR}\gamma$ , which is rather suppressed under infectious conditions, was down-regulated. In contrast, mRNA expression of these regulators in metal exposed cells remained at the levels of unstimulated controls. Therefore, our data support the concept that local exposure to  $\text{Co}^{2+}$  and  $\text{Cr}^{3+}$  in human peri-implant tissues suppresses critical immune functions of professional phagocytes and therefore predisposes patients to an increased risk of peri-implant infections, as seen in patients with ALTR<sup>13, 15, 25-27</sup>. This hypothesis is further supported by our observation that high concentrations of  $\text{Co}^{2+}$  resulted in lack of CD16 deposition on macrophage surface. CD16 is a  $\text{Fc}\gamma\text{III}$  receptor that facilitates phagocytosis of bacteria<sup>61</sup>. Both, lack of surface associated CD14 as well as CD16 potentially explain the observed reduced bacterial phagocytosis. Of note, *S. aureus* growth itself was not affected by the metal concentrations, suggesting that it might form biofilms in PJIs<sup>34-35, 62-64</sup>. PJIs occur in up to 4% of revision arthroplasties<sup>25</sup>. It was reported that the presence of a foreign body and local metal release reduce the infectivity dose of *S. aureus*<sup>65</sup>. Furthermore, a limited number of animal studies revealed

reduced phagocytic and bactericidal activities of tissue infiltrating granulocytes induced by non-phagocytosable foreign bodies, while circulating neutrophils retained the activities<sup>66-67</sup>. Our *in vitro* data support these findings and underline the need for additional investigations analyzing *ex vivo* metal-mediated local immunosuppressive effects and their consequences for potential local infections. In addition, further prospective clinical studies are warranted.

## 5. Conclusions

In conclusion, our results provide evidence that exposure to Co- and Cr-ions inhibits essential immune functions of professional phagocytes. This finding potentially explains the increased risk of PJI following revision arthroplasty. CoCrMo is a metallic biomaterial constantly used in orthopedic surgery. Degradation of this applied metallic biomaterial leading to systemic and local metal exposure and ALTR is a clinically well-known scenario. Based on our data, a risk assessment for PJI, especially for infections with *S. aureus*, after the use of CoCrMo-containing arthroplasty implants in prospectively designed studies seems indicated. In addition, *in vitro* studies on Co and Cr in the particulate state and *ex vivo* studies on the classical pro- and anti-inflammatory phenotype as well as functionality of macrophages locally exposed to metal ions and particles should be performed. Our data support a better understanding of the local tissue response after material degradation and add weight to the risk and benefit evaluation of CoCrMo routinely used in arthroplasty. Possible long-term effects of metal-based biomaterial degradation including the risk of infection should be considered.

## Figures and Figure Captions

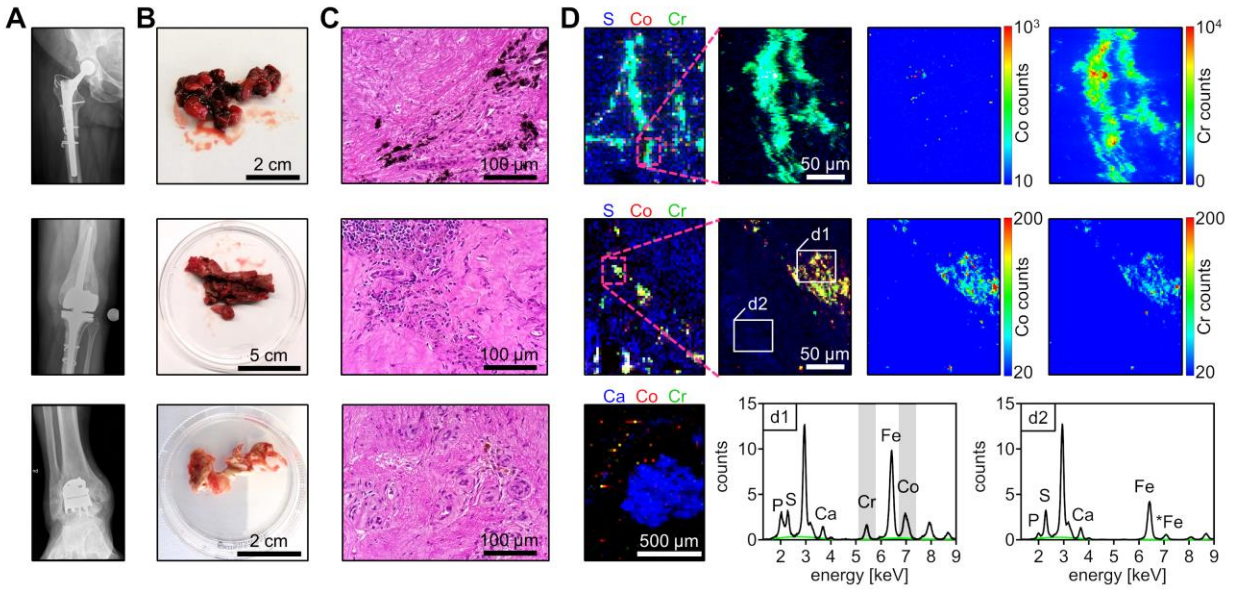


Figure 1. Histological evaluation and multi-element detection of peri-implant tissue collected from three patients undergoing arthroplasty implant revision. The respective samples, tissue stains and XRF maps are arranged horizontally. (A) From top to bottom: Anteroposterior radiographs taken before revision of hip, knee and ankle arthroplasty implants. (B) Peri-implant soft tissue samples. (C) Hematoxylin and eosin staining of tissue sections. (D) RGB imaging, heatmaps of the Co and Cr signals, and spectra of XRF maps of tissue sections at 20  $\mu\text{m}$  steps (left) and 2  $\mu\text{m}$  steps (right). RGB images (2  $\mu\text{m}$  steps) depict the same region depicted by heatmaps.

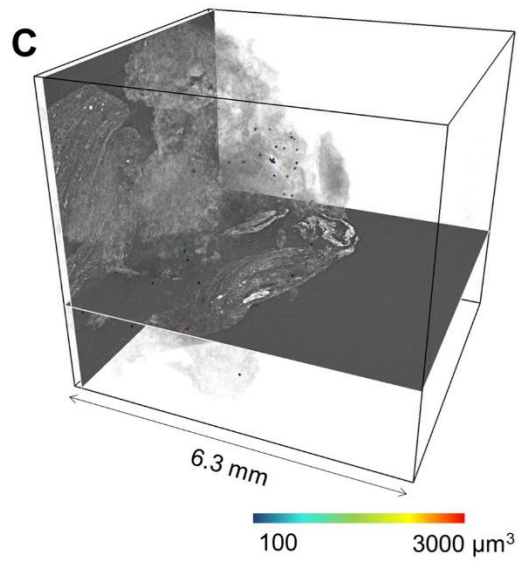
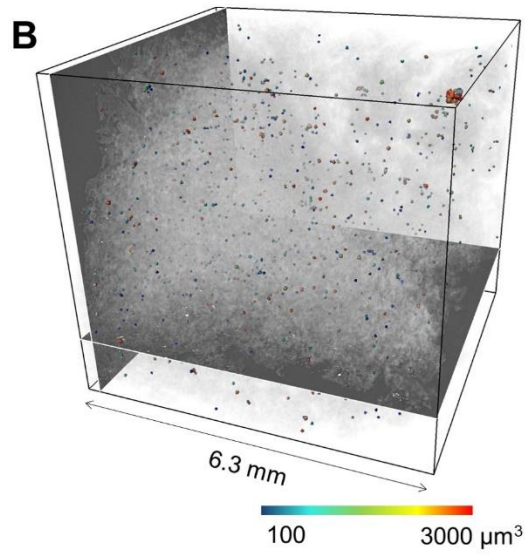
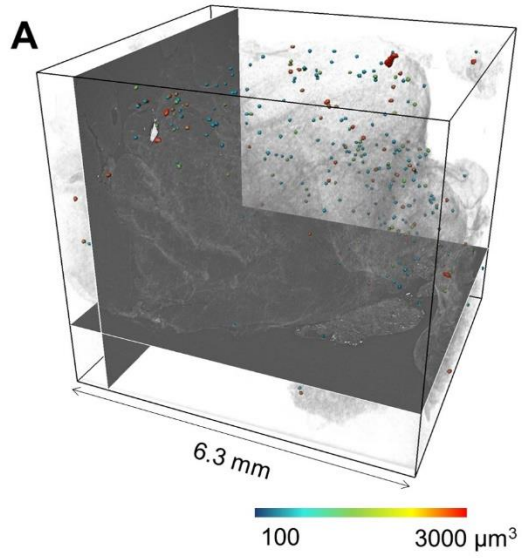




Figure 2. Renderings of SR- $\mu$ CT data and segmentation of micron-sized debris in peri-implant tissue samples collected during revision surgery of a hip arthroplasty implant (A), knee arthroplasty implant (B) and ankle arthroplasty implant (C). The colors of the debris particles and the color bars indicate the volume of each particle. Please note that for the visualization, the particles have been dilated using a 3D spherical structuring element of 5 voxels in diameter to enhance the visibility of the particle distribution. The gray transparent cloud-like features are soft-tissue structures.

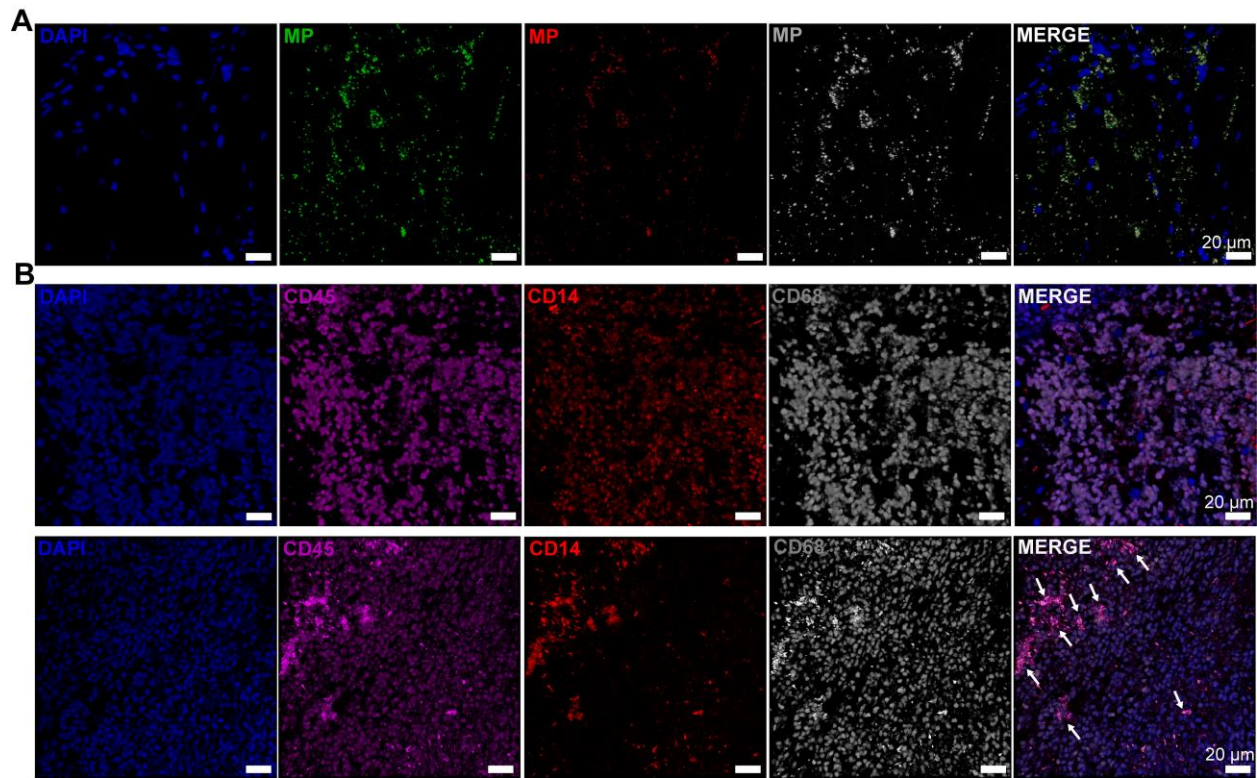


Figure 3. Macrophage infiltration in peri-implant tissue visualized by positive CD45/CD68/CD14 staining and CLSM. (A) Representative reconstruction of CLSM micrographs visualizing highly auto-fluorescent metal particles (MP) and (B) macrophages (n=9). Arrows indicate metal particles associated with macrophages.

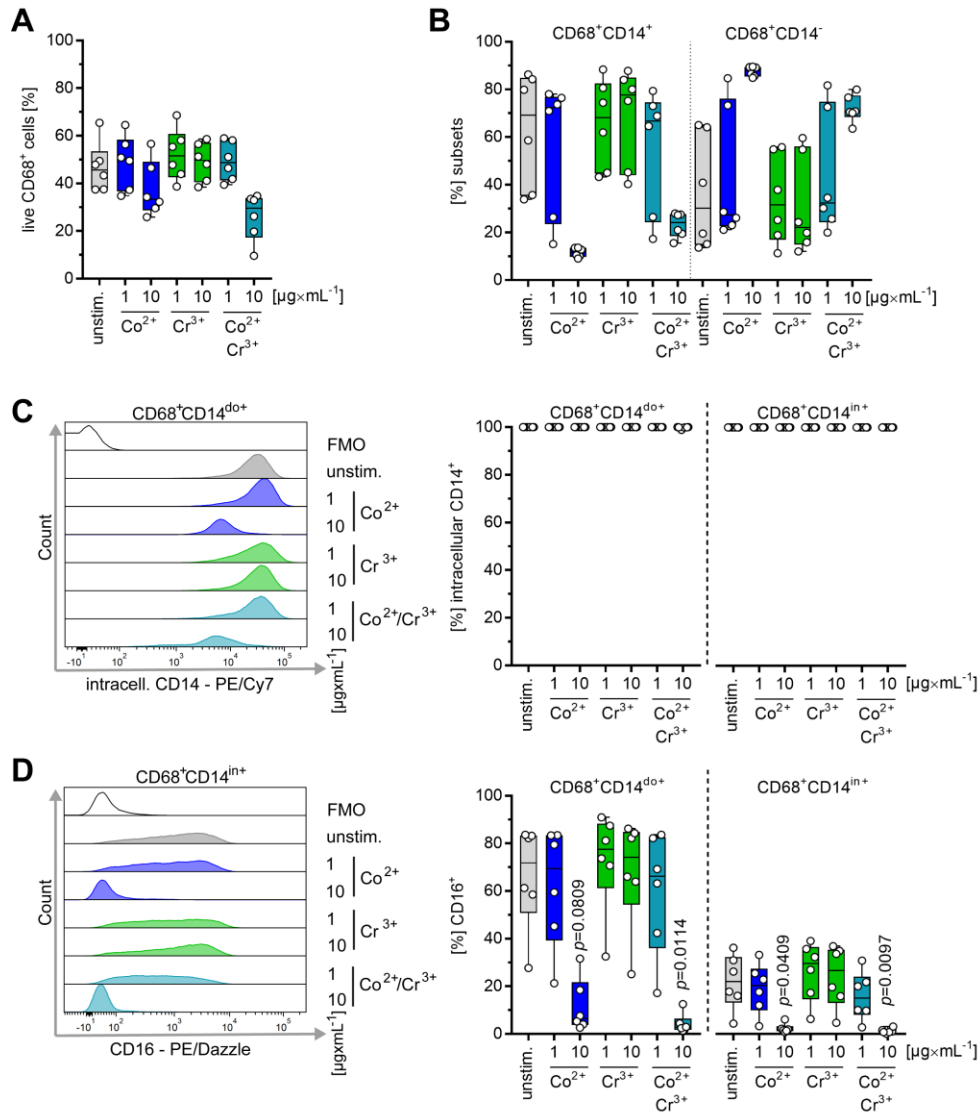


Figure 4. Metal-induced imprint of macrophage populations. Human primary monocytes were exposed to 1 or 10  $\mu\text{g}\times\text{mL}^{-1}$  of  $\text{Co}^{2+}$ ,  $\text{Cr}^{3+}$  alone or in combination for 48 h. Macrophage viability (A) and subsets (B-D) were analyzed via flow cytometry ( $n=6$ ). Representative histograms are shown in C and D (left panels). (B) Macrophage subsets were evaluated based on intracellular CD68 and extracellular CD14 positivity. (C) Detailed assessment of the subsets was performed based on frequencies of cells, which stained positive for intracellular CD14 ( $\text{CD14}^+$ ) and (D) extracellular CD16 ( $\text{CD16}^+$ ). The data are displayed as box plots. Each dot represents one independent experiment with cells from one donor. The level of significance was determined using Kruskal-Wallis test with Dunn's posttest. FMO, fluorescence minus one; unstim., unstimulated control.

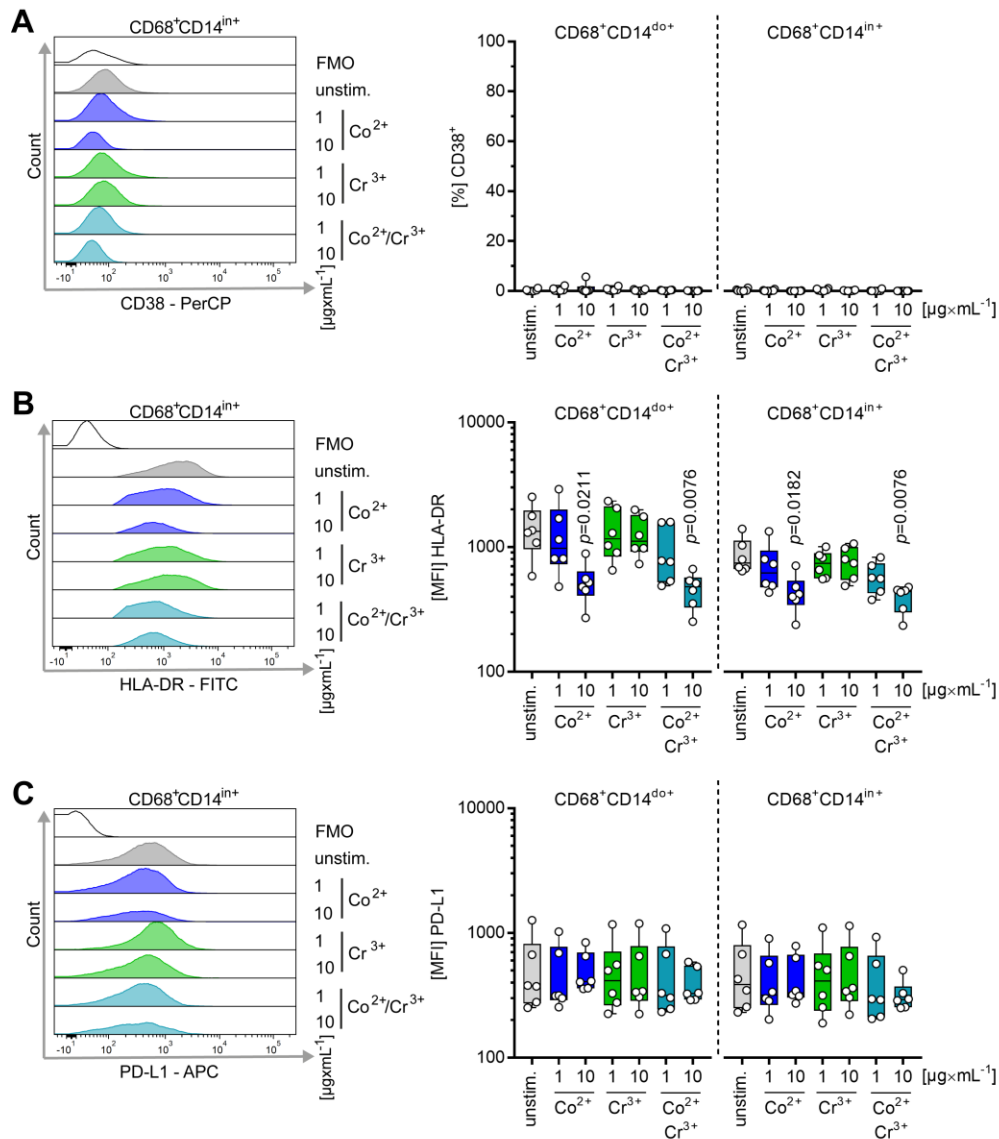


Figure 5. Metal-exposure decreases surface-expression of HLA-DR on macrophages. Human primary monocytes were exposed to 1 or 10  $\mu\text{g}\times\text{mL}^{-1}$  of Co<sup>2+</sup>, Cr<sup>3+</sup> alone or in combination for 48 h and macrophage subsets (A-C) was analyzed via flow cytometry (n=6). Representative histograms are shown in A-C (left panels). The macrophage response to infection and metal exposure was evaluated based on frequencies of CD38<sup>+</sup> (A) as well as expression of HLA-DR (B) and PD-L1 (C). The data are displayed as box plots. Each dot represents one independent experiment with cells from one donor. The level of significance was determined using Kruskal-Wallis test with Dunn's posttest. FMO, fluorescence minus one; unstim., unstimulated control.

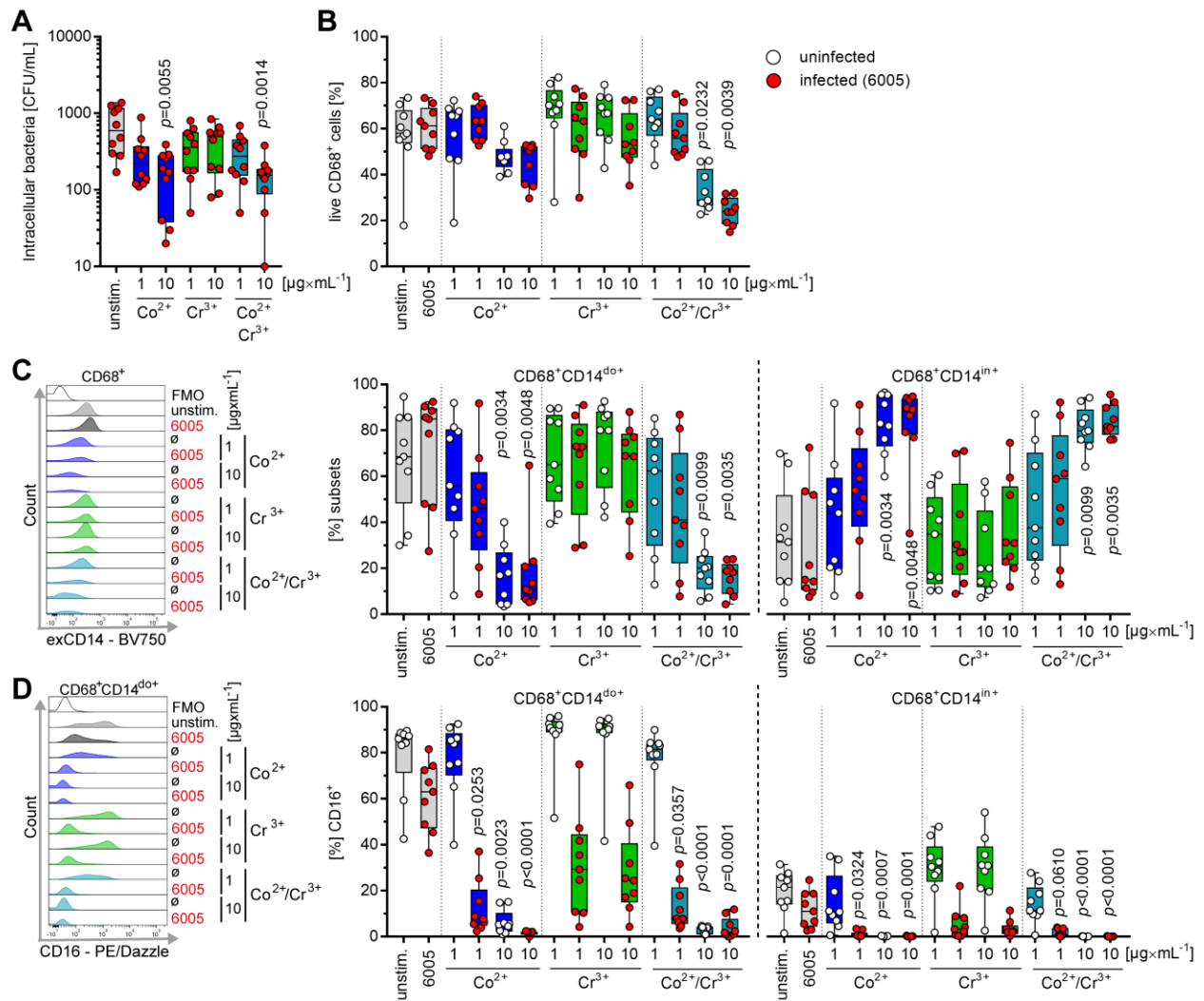


Figure 6. Reduced phagocytosis of bacteria in Co<sup>2+</sup>-exposed cells. Human macrophages were exposed to 1 or 10  $\mu\text{g}\times\text{mL}^{-1}$  of Co<sup>2+</sup> or Cr<sup>3+</sup> alone or in combination for 24 h. Metal-exposed cells were infected with *S. aureus* 6005 (MOI 1). Extracellular bacteria were killed by substituting the media with antibiotics. Viable intracellular bacteria were determined 2 h post infection (A). Macrophage viability (B) and subsets (C-D) were analyzed via flow cytometry after a total of 48 h of metal treatment with 24 h of infection (n=10). Representative histograms are shown in left panels of C and D. (C) Analyses of macrophage subsets in response to infections. (D) Frequencies of CD16 positive cells in response to infections. The data are displayed as box plots. Each dot represents one independent experiment with cells from one donor. The level of significance was determined using Kruskal-Wallis test with Dunn's posttest. FMO, fluorescence minus one; unstim., unstimulated control.

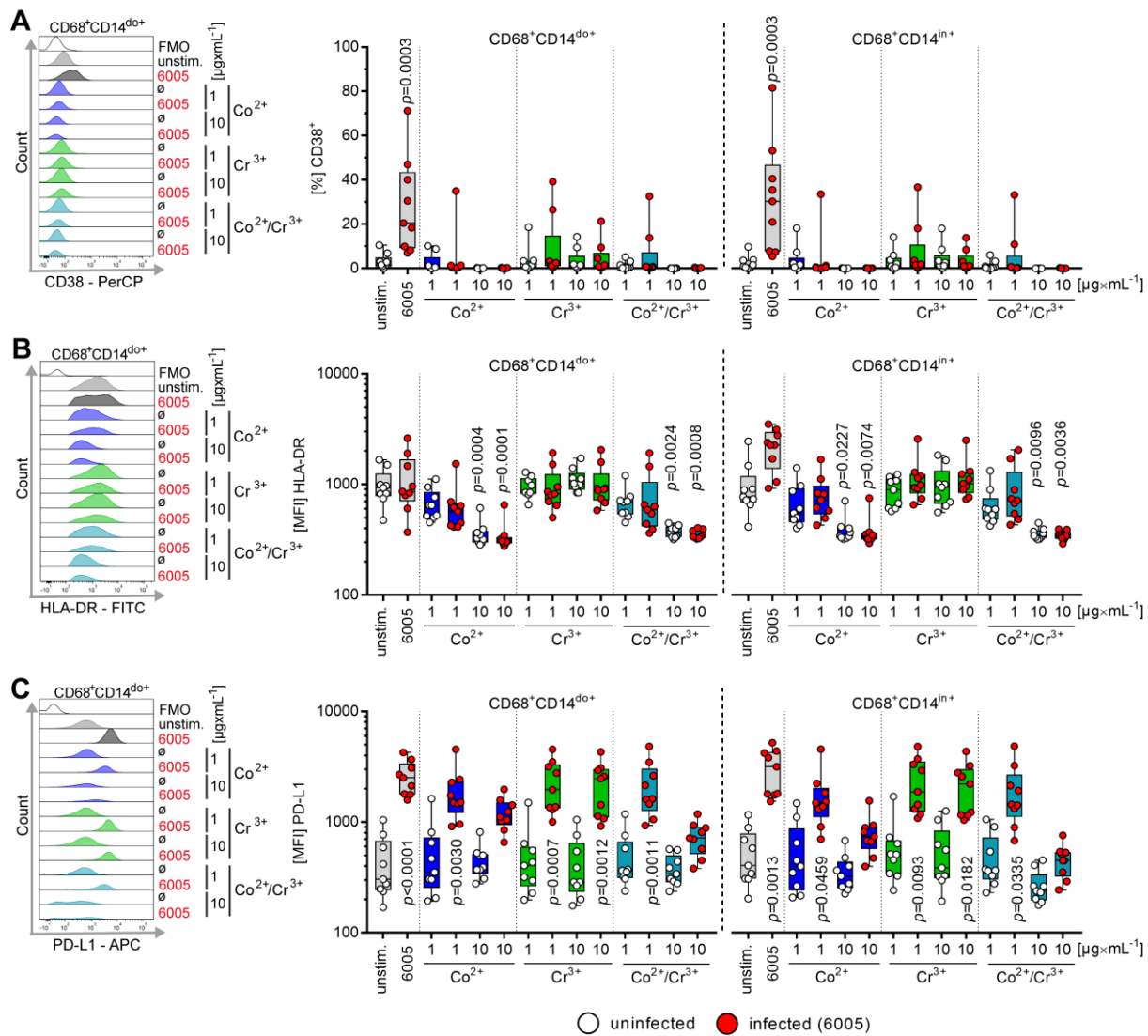


Figure 7. Metal-exposed cells are less responsive to *S. aureus* infections. Human monocytes were exposed to 1 or 10 µg×mL<sup>-1</sup> of Co<sup>2+</sup> or Cr<sup>3+</sup> alone or in combination for 24 h and metal-exposed cells were infected with *S. aureus* 6005 (MOI 1). Macrophage phenotype (A-C) was analyzed via flow cytometry after a total of 48 h of metal treatment, which included 24 h of infection (n=10). Representative histograms are shown in left panels of A-C. The phenotype was evaluated based on frequencies of CD38<sup>+</sup> (A) as well as expression of HLA-DR (B) and PD-L1 (C) on macrophage surface. The data are displayed as box plots. Each dot represents one independent experiment with cells from one donor. The level of significance was determined using Kruskal-Wallis test with Dunn's posttest. FMO, fluorescence minus one; unstim., unstimulated control.

## ASSOCIATED CONTENT

### Supporting Information.

The following files are available free of charge:

Extended results: Figure S1. Gating strategy used to identify human monocytes/macrophages; Figure S2. Intracellular CD14 expression in macrophages; Figure S3. The impact of metal ions on *Staphylococcus aureus* vitality; Figure S4. Gene expression analyses in macrophages.

## AUTHOR INFORMATION

### Corresponding Authors

‡ equal contribution

\* Nikolai Siemens, Email: [nikolai.siemens@uni-greifswald.de](mailto:nikolai.siemens@uni-greifswald.de). \* Janosch Schoon, Email: [janosch.schoon@med.uni-greifswald.de](mailto:janosch.schoon@med.uni-greifswald.de)

### Author Contributions

Conceptualization: LAT, NS, JS; Data curation: LAT, NS, JS; Formal analysis: LAT, NS, JS; Funding acquisition: NS, GIW, JS; Investigation: LAT, NS, JS, BH, TW, AR, DG.; Methodology: NS, JS, BH, TW, DG; Project administration: NS, JS; Resources: GIW, NS, JS; Software: GIW, NS, JS; Supervision: NS, JS; Validation: LAT, GIW, AR, NS, JS; Visualization: LAT, NS, JS; Writing - original draft: LAT, NS, JS; Writing - review & editing: LAT, GIW, AR, NS, JS, TW, BH, DG.

### Funding Sources

This work was supported by German Research Foundation (DFG; grants 407176682 to NS, 492903360 to NS, and INST 292/151-1 FUGG – 447143887 for the purchase of CLSM). JS

received the Domagk Master Class (DMC) scholarship funded by the University Medicine Greifswald.

## Notes

Declaration of competing interest: GIW serves as consultant for Mathys AG and receives institutional funding and research support from Mathys AG and Smith & Nephew. These companies did not financially support this study, had no role in study design, sample collection, data collection and analysis, decision to publish, or preparation of the manuscript. All other authors declare no competing interest.

## ACKNOWLEDGMENT

This study was supported with beamtime at Synchrotron SOLEIL (ANATOMIX, proposal number: 20220776) and Swiss Light Source (microXAS, proposal number: 20201651). ANATOMIX is an Equipment of Excellence (EQUIPEX) funded by the *Investments for the Future* program of the French National Research Agency (ANR), project *NanoimagesX*, grant no. [ANR-11-EQPX-0031](#). The authors would like to thank D. Stobbe, L. Berndt, and K. Barnekow for expert technical support. The authors gratefully acknowledge support during SR- $\mu$ CT data analyses by Dr. E. Bortel and acquisition by Dr. C. Seim, Dr. E. Bortel, and Javier Gerber as well as during SR-XRF data acquisition by Dr. F. Ferreira Sanchez, Dr. C. Seim, and L. Schweitzer. Furthermore, the authors would like to thank PD Dr. Dr. J. Reichert, Dr. A. Hofer, Dr. U. Schietsch, and Dr. A. Springer for intraoperative sample harvesting. All patients are gratefully acknowledged for their participation in the study.

## ABBREVIATIONS



ALTR, adverse local tissue reaction; CLSM, confocal laser scanning microscopy; CoCrMo, Cobalt-chromium-molybdenum; FMO, fluorescence minus one; PBS, phosphate buffered saline, PJI, periprosthetic joint infection; SR- $\mu$ CT, synchrotron radiation micro-computed tomography; SR- $\mu$ XRF, synchrotron radiation micro x-ray fluorescence analyses

## REFERENCES

1. Liu, Z.; Liu, H.; Vowden, R.; Hughes, L.; Qi, D.; Francis, W.; Perino, G.; Pink, R.; Xiao, J.; Li, B.; Xia, Z., Combination of cobalt, chromium and titanium nanoparticles increases cytotoxicity in vitro and pro-inflammatory cytokines in vivo. *Journal of Orthopaedic Translation* **2023**, *38*, 203-212.
2. Perino, G.; De Martino, I.; Zhang, L.; Xia, Z.; Gallo, J.; Natu, S.; Langton, D.; Huber, M.; Rakow, A.; Schoon, J.; Gomez-Barrena, E.; Krenn, V., The contribution of the histopathological examination to the diagnosis of adverse local tissue reactions in arthroplasty. *EFORT Open Rev* **2021**, *6* (6), 399-419.
3. Catelas, I.; Petit, A.; Vali, H.; Fragiskatos, C.; Meilleur, R.; Zukor, D. J.; Antoniou, J.; Huk, O. L., Quantitative analysis of macrophage apoptosis vs. necrosis induced by cobalt and chromium ions in vitro. *Biomaterials* **2005**, *26* (15), 2441-2453.
4. Eltit, F.; Wang, Q.; Wang, R., Mechanisms of adverse local tissue reactions to hip implants. *Frontiers in bioengineering and biotechnology* **2019**, *7*, 176.
5. Nyga, A.; Hart, A.; Tetley, T. D., Importance of the HIF pathway in cobalt nanoparticle-induced cytotoxicity and inflammation in human macrophages. *Nanotoxicology* **2015**, *9* (7), 905-917.
6. Jämsen, E.; Pajarinen, J.; Kouri, V.-P.; Rahikkala, A.; Goodman, S. B.; Manninen, M.; Nordström, D. C.; Eklund, K. K.; Nurmi, K., Tumor necrosis factor primes and metal particles activate the NLRP3 inflammasome in human primary macrophages. *Acta biomaterialia* **2020**, *108*, 347-357.
7. Couto, M.; Vasconcelos, D. P.; Sousa, D. M.; Sousa, B.; Conceição, F.; Neto, E.; Lamghari, M.; Alves, C. J., The mechanisms underlying the biological response to wear debris in periprosthetic inflammation. *Frontiers in Materials* **2020**, *7*, 274.
8. Bonner, B.; Arauz, P.; Klemm, C.; Kwon, Y.-M., Outcome of re-revision surgery for adverse local tissue reaction in metal-on-polyethylene and metal-on-metal total hip arthroplasty. *The Journal of arthroplasty* **2020**, *35* (6), S284-S288.
9. Munro, J. T.; Masri, B. A.; Duncan, C. P.; Garbuz, D. S., High Complication Rate After Revision of Large-head Metal-on-metal Total Hip Arthroplasty. *Clinical Orthopaedics and Related Research*® **2014**, *472* (2), 523-528.
10. Matharu, G. S.; Pynsent, P. B.; Sumathi, V. P.; Mittal, S.; Buckley, C. D.; Dunlop, D. J.; Revell, P. A.; Revell, M. P., Predictors of time to revision and clinical outcomes following revision of metal-on-metal hip replacements for adverse reaction to metal debris. *The Bone & Joint Journal* **2014**, *96-B* (12), 1600-1609.
11. Matharu, G. S.; Judge, A.; Murray, D. W.; Pandit, H. G., Outcomes After Metal-on-metal Hip Revision Surgery Depend on the Reason for Failure: A Propensity Score-matched Study. *Clinical Orthopaedics and Related Research*® **2018**, *476* (2).
12. Grammatopoulos, G.; Pandit, H.; Kwon, Y. M.; Gundle, R.; McLardy-Smith, P.; Beard, D. J.; Murray, D. W.; Gill, H. S., Hip resurfacings revised for inflammatory pseudotumour have a poor outcome. *The Journal of Bone & Joint Surgery British Volume* **2009**, *91-B* (8), 1019-1024.
13. Wyles, C. C.; Van Demark, R. E.; Sierra, R. J.; Trousdale, R. T., High Rate of Infection After Aseptic Revision of Failed Metal-on-Metal Total Hip Arthroplasty. *Clinical Orthopaedics and Related Research*® **2014**, *472* (2), 509-516.

14. Chang, J. S.; Haddad, F. S., Revision total hip arthroplasty for metal-on-metal failure. *Journal of Clinical Orthopaedics and Trauma* **2020**, *11* (1), 9-15.
15. Matharu, G. S.; Judge, A.; Murray, D. W.; Pandit, H. G., Outcomes following revision surgery performed for adverse reactions to metal debris in non-metal-on-metal hip arthroplasty patients. *Bone & Joint Research* **2017**, *6* (7), 405-413.
16. Schulze, F.; Perino, G.; Rakow, A.; Wassilew, G.; Schoon, J., Noninfectious tissue interactions at periprosthetic interfaces. *Die Orthopädie* **2023**, 1-10.
17. Schoon, J.; Hesse, B.; Rakow, A.; Ort, M. J.; Lagrange, A.; Jacobi, D.; Winter, A.; Huesker, K.; Reinke, S.; Cotte, M.; Tucoulou, R.; Marx, U.; Perka, C.; Duda, G. N.; Geissler, S., Metal-Specific Biomaterial Accumulation in Human Peri-Implant Bone and Bone Marrow. *Adv Sci* **2020**, *7* (20), 2000412.
18. Morrell, A. P.; Floyd, H.; JF, W. M.; Grover, L. M.; Castillo-Michel, H.; Davis, E. T.; Parker, J. E.; Martin, R. A.; Addison, O., Improving our understanding of metal implant failures: Multiscale chemical imaging of exogenous metals in ex-vivo biological tissues. *Acta biomaterialia* **2019**, *98*, 284-293.
19. Rakow, A.; Schoon, J.; Dienelt, A.; John, T.; Textor, M.; Duda, G.; Perka, C.; Schulze, F.; Ode, A., Influence of particulate and dissociated metal-on-metal hip endoprosthesis wear on mesenchymal stromal cells in vivo and in vitro. *Biomaterials* **2016**, *98*, 31-40.
20. Espallargas, N.; Torres, C.; Muñoz, A. I., A metal ion release study of CoCrMo exposed to corrosion and tribocorrosion conditions in simulated body fluids. *Wear* **2015**, *332*, 669-678.
21. Schoon, J.; Hesse, B.; Tucoulou, R.; Geissler, S.; Ort, M.; Duda, G. N.; Perka, C.; Wassilew, G. I.; Perino, G.; Rakow, A., Synchrotron-based characterization of arthroprosthetic CoCrMo particles in human bone marrow. *J Mater Sci Mater Med* **2022**, *33* (6), 54.
22. Gkiatas, I.; Sharma, A. K.; Greenberg, A.; Duncan, S. T.; Chalmers, B. P.; Sculco, P. K., Serum metal ion levels in modular dual mobility acetabular components: a systematic review. *Journal of Orthopaedics* **2020**, *21*, 432-437.
23. Rakow, A.; Schoon, J., Systemic effects of metals released from arthroplasty implants—a brief summary. *Zeitschrift für Orthopädie und Unfallchirurgie* **2020**, *158* (05), 501-507.
24. Bradberry, S.; Wilkinson, J.; Ferner, R., Systemic toxicity related to metal hip prostheses. *Clinical toxicology* **2014**, *52* (8), 837-847.
25. Izakovicova, P.; Borens, O.; Trampuz, A., Periprosthetic joint infection: current concepts and outlook. *EFORT Open Rev* **2019**, *4* (7), 482-494.
26. Kong, L.; Cao, J.; Zhang, Y.; Ding, W.; Shen, Y., Risk factors for periprosthetic joint infection following primary total hip or knee arthroplasty: a meta-analysis. *Int Wound J* **2017**, *14* (3), 529-536.
27. McMaster Arthroplasty, C., Risk Factors for Periprosthetic Joint Infection Following Primary Total Hip Arthroplasty: A 15-Year, Population-Based Cohort Study. *J Bone Joint Surg Am* **2020**, *102* (6), 503-509.
28. Renz, N.; Trampuz, A.; Perka, C.; Rakow, A. In *Outcome and Failure Analysis of 132 Episodes of Hematogenous Periprosthetic Joint Infections—A Cohort Study*, Open Forum Infectious Diseases, Oxford University Press US: 2022; p ofac094.
29. Dale, H.; Hovding, P.; Tveit, S. M.; Graff, J. B.; Lutro, O.; Schrama, J. C.; Wik, T. S.; Skramm, I.; Westberg, M.; Fenstad, A. M.; Hallan, G.; Engesaeter, L. B.; Furnes, O., Increasing but levelling out risk of revision due to infection after total hip arthroplasty: a study on 108,854 primary THAs in the Norwegian Arthroplasty Register from 2005 to 2019. *Acta Orthop* **2021**, *92* (2), 208-214.

30. Kurtz, S. M.; Lau, E. C.; Son, M. S.; Chang, E. T.; Zimmerli, W.; Parvizi, J., Are We Winning or Losing the Battle With Periprosthetic Joint Infection: Trends in Periprosthetic Joint Infection and Mortality Risk for the Medicare Population. *J Arthroplasty* **2018**, *33* (10), 3238-3245.
31. Saavedra-Lozano, J.; Falup-Pecurariu, O.; Faust, S. N.; Girschick, H.; Hartwig, N.; Kaplan, S.; Lorrot, M.; Mantadakis, E.; Peltola, H.; Rojo, P.; Zaoutis, T.; LeMair, A., Bone and Joint Infections. *The Pediatric Infectious Disease Journal* **2017**, *36* (8), 788-799.
32. Tong, S. Y.; Davis, J. S.; Eichenberger, E.; Holland, T. L.; Fowler Jr, V. G., Staphylococcus aureus infections: epidemiology, pathophysiology, clinical manifestations, and management. *Clinical microbiology reviews* **2015**, *28* (3), 603-661.
33. Liukkonen, R.; Honkanen, M.; Reito, A.; Skyttä, E.; Karppelin, M.; Eskelinen, A., Trends in Revision Hip Arthroplasty for Prosthetic Joint Infection: A Single-Center Study of 423 Hips at a High-Volume Center between 2008 and 2021. *The Journal of Arthroplasty*.
34. Patel, R., Periprosthetic Joint Infection. *New England Journal of Medicine* **2023**, *388* (3), 251-262.
35. Tande, A. J.; Patel, R., Prosthetic Joint Infection. *Clinical Microbiology Reviews* **2014**, *27* (2), 302-345.
36. Benito, N.; Mur, I.; Ribera, A.; Soriano, A.; Rodriguez-Pardo, D.; Sorli, L.; Cobo, J.; Fernandez-Sampedro, M.; Del Toro, M. D.; Guio, L.; Praena, J.; Bahamonde, A.; Riera, M.; Esteban, J.; Baraia-Etxaburu, J. M.; Martinez-Alvarez, J.; Jover-Saenz, A.; Duenas, C.; Ramos, A.; Sobrino, B.; Euba, G.; Morata, L.; Pigrau, C.; Horcajada, J. P.; Coll, P.; Crusi, X.; Ariza, J.; Reipi Group for the Study of Prosthetic Joint Infections / Geio, S., The Different Microbial Etiology of Prosthetic Joint Infections according to Route of Acquisition and Time after Prosthesis Implantation, Including the Role of Multidrug-Resistant Organisms. *J Clin Med* **2019**, *8* (5).
37. Tai, D. B. G.; Patel, R.; Abdel, M. P.; Berbari, E. F.; Tande, A. J., Microbiology of hip and knee periprosthetic joint infections: a database study. *Clin Microbiol Infect* **2022**, *28* (2), 255-259.
38. Triffault-Fillit, C.; Ferry, T.; Laurent, F.; Pradat, P.; Dupieux, C.; Conrad, A.; Becker, A.; Lustig, S.; Fessy, M. H.; Chidiac, C.; Valour, F.; Lyon, B. J. I. S. G., Microbiologic epidemiology depending on time to occurrence of prosthetic joint infection: a prospective cohort study. *Clin Microbiol Infect* **2019**, *25* (3), 353-358.
39. Nich, C.; Takakubo, Y.; Pajarinen, J.; Ainola, M.; Salem, A.; Sillat, T.; Rao, A. J.; Raska, M.; Tamaki, Y.; Takagi, M.; Konttinen, Y. T.; Goodman, S. B.; Gallo, J., Macrophages—Key cells in the response to wear debris from joint replacements. *Journal of Biomedical Materials Research Part A* **2013**, *101* (10), 3033-3045.
40. Locati, M.; Curtale, G.; Mantovani, A., Diversity, Mechanisms, and Significance of Macrophage Plasticity. *Annual Review of Pathology: Mechanisms of Disease* **2020**, *15* (1), 123-147.
41. Gentek, R.; Molawi, K.; Sieweke, M. H., Tissue macrophage identity and self-renewal. *Immunological Reviews* **2014**, *262* (1), 56-73.
42. Horev-Azaria, L.; Kirkpatrick, C. J.; Korenstein, R.; Marche, P. N.; Maimon, O.; Ponti, J.; Romano, R.; Rossi, F.; Golla-Schindler, U.; Sommer, D.; Uboldi, C.; Unger, R. E.; Villiers, C., Predictive Toxicology of Cobalt Nanoparticles and Ions: Comparative In Vitro Study of Different Cellular Models Using Methods of Knowledge Discovery from Data. *Toxicological Sciences* **2011**, *122* (2), 489-501.

43. Xu, J.; Yang, J.; Nyga, A.; Ehteramyan, M.; Moraga, A.; Wu, Y.; Zeng, L.; Knight, M. M.; Shelton, J. C., Cobalt (II) ions and nanoparticles induce macrophage retention by ROS-mediated down-regulation of RhoA expression. *Acta biomaterialia* **2018**, *72*, 434-446.
44. Weitkamp, T.; Scheel, M.; Perrin, J.; Daniel, G.; King, A.; Le Roux, V.; Giorgetta, J.; Carcy, A.; Langlois, F.; Desjardins, K. In *Microtomography on the ANATOMIX beamline at Synchrotron SOLEIL*, Journal of Physics: Conference Series, IOP Publishing: 2022; p 012122.
45. Weitkamp, T.; Scheel, M.; Giorgetta, J.; Joyet, V.; Le Roux, V.; Cauchon, G.; Moreno, T.; Polack, F.; Thompson, A.; Samama, J. In *The tomography beamline ANATOMIX at Synchrotron SOLEIL*, Journal of Physics: Conference Series, IOP Publishing: 2017; p 012037.
46. Solé, V. A.; Papillon, E.; Cotte, M.; Walter, P.; Susini, J., A multiplatform code for the analysis of energy-dispersive X-ray fluorescence spectra. *Spectrochimica Acta Part B: Atomic Spectroscopy* **2007**, *62* (1), 63-68.
47. Wick, M. R. In *The hematoxylin and eosin stain in anatomic pathology—An often-neglected focus of quality assurance in the laboratory*, Seminars in diagnostic pathology, Elsevier: 2019; pp 303-311.
48. Baude, J.; Bastien, S.; Gillet, Y.; Leblanc, P.; Itzek, A.; Tristan, A.; Bes, M.; Duguez, S.; Moreau, K.; Diep, B. A.; Norrby-Teglund, A.; Henry, T.; Vandenesch, F.; Group, I. S., Necrotizing Soft Tissue Infection Staphylococcus aureus but not S. pyogenes Isolates Display High Rates of Internalization and Cytotoxicity Toward Human Myoblasts. *The Journal of Infectious Diseases* **2019**, *220* (4), 710-719.
49. Mairpady Shambat, S.; Siemens, N.; Monk, I. R.; Mohan, D. B.; Mukundan, S.; Krishnan, K. C.; Prabhakara, S.; Snall, J.; Kearns, A.; Vandenesch, F.; Svensson, M.; Kotb, M.; Gopal, B.; Arakere, G.; Norrby-Teglund, A., A point mutation in AgrC determines cytotoxic or colonizing properties associated with phenotypic variants of ST22 MRSA strains. *Sci Rep* **2016**, *6*, 31360.
50. Krenn, V.; Perino, G., Histological Diagnosis of Implant-Associated Pathologies. In *Histological Diagnosis of Implant-Associated Pathologies*, Krenn, V.; Perino, G., Eds. Springer Berlin Heidelberg: Berlin, Heidelberg, 2017; pp 1-44.
51. Loeffler, H.; Jonitz-Heincke, A.; Peters, K.; Mueller-Hilke, B.; Fiedler, T.; Bader, R.; Klinder, A., Comparison of Inflammatory Effects in THP-1 Monocytes and Macrophages after Exposure to Metal Ions. *Materials* **2020**, *13* (5), 1150.
52. Schoon, J.; Geißler, S.; Traeger, J.; Luch, A.; Tentschert, J.; Perino, G.; Schulze, F.; Duda, G. N.; Perka, C.; Rakow, A., Multi-elemental nanoparticle exposure after tantalum component failure in hip arthroplasty: in-depth analysis of a single case. *Nanomedicine: Nanotechnology, Biology and Medicine* **2017**, *13* (8), 2415-2423.
53. Xia, Z.; Ricciardi, B. F.; Liu, Z.; von Ruhland, C.; Ward, M.; Lord, A.; Hughes, L.; Goldring, S. R.; Purdue, E.; Murray, D., Nano-analyses of wear particles from metal-on-metal and non-metal-on-metal dual modular neck hip arthroplasty. *Nanomedicine: Nanotechnology, Biology and Medicine* **2017**, *13* (3), 1205-1217.
54. Perino, G.; Sunitsch, S.; Huber, M.; Ramirez, D.; Gallo, J.; Vaculova, J.; Natu, S.; Kretzer, J.; Müller, S.; Thomas, P., Diagnostic guidelines for the histological particle algorithm in the periprosthetic neo-synovial tissue. *BMC clinical pathology* **2018**, *18* (1), 1-22.
55. Pearson, M. J.; Williams, R. L.; Floyd, H.; Bodansky, D.; Grover, L. M.; Davis, E. T.; Lord, J. M., The effects of cobalt–chromium–molybdenum wear debris in vitro on serum cytokine profiles and T cell repertoire. *Biomaterials* **2015**, *67*, 232-239.

56. Granchi, D.; Cenni, E.; Ciapetti, G.; Savarino, L.; Stea, S.; Gamberini, S.; Gori, A.; Pizzoferrato, A., Cell death induced by metal ions: necrosis or apoptosis? *Journal of materials science: materials in medicine* **1998**, *9*, 31-37.
57. Posada, O. M.; Tate, R. J.; Meek, R. M. D.; Grant, M. H. In Vitro Analyses of the Toxicity, Immunological, and Gene Expression Effects of Cobalt-Chromium Alloy Wear Debris and Co Ions Derived from Metal-on-Metal Hip Implants *Lubricants* [Online], 2015, p. 539-568.
58. Scharf, B.; Clement, C. C.; Zolla, V.; Perino, G.; Yan, B.; Elci, S. G.; Purdue, E.; Goldring, S.; Macaluso, F.; Cobelli, N.; Vachet, R. W.; Santambrogio, L., Molecular analysis of chromium and cobalt-related toxicity. *Scientific Reports* **2014**, *4* (1), 5729.
59. Yoshioka, N.; Taniguchi, Y.; Yoshida, A. Y. A.; Nakata, K.; Nishizawa, T.; Inagawa, H.; Kohchi, C.; Soma, G.-I., Intracellular Localization of CD14 Protein in Intestinal Macrophages. *Anticancer Research* **2009**, *29* (3), 865.
60. Posada, O. M.; Tate, R. J.; Grant, M. H., Effects of CoCr metal wear debris generated from metal-on-metal hip implants and Co ions on human monocyte-like U937 cells. *Toxicology in Vitro* **2015**, *29* (2), 271-280.
61. Nagarajan, S.; Chesla, S.; Cobern, L.; Anderson, P.; Zhu, C.; Selvaraj, P., Ligand Binding and Phagocytosis by CD16 (Fc  $\gamma$ 3 Receptor III) Isoforms: PHAGOCYTOTIC SIGNALING BY ASSOCIATED  $\alpha$  AND  $\beta$  SUBUNITS IN CHINESE HAMSTER OVARY CELLS ( $\alpha$ 2217). *Journal of Biological Chemistry* **1995**, *270* (43), 25762-25770.
62. Frank Kristi, L.; Hanssen Arlen, D.; Patel, R., icaA Is Not a Useful Diagnostic Marker for Prosthetic Joint Infection. *Journal of Clinical Microbiology* **2004**, *42* (10), 4846-4849.
63. Lu, Y.; Cai, W.-j.; Ren, Z.; Han, P. The Role of Staphylococcal Biofilm on the Surface of Implants in Orthopedic Infection *Microorganisms* [Online], 2022.
64. Yamada, K. J.; Heim, C. E.; Xi, X.; Attri, K. S.; Wang, D.; Zhang, W.; Singh, P. K.; Bronich, T. K.; Kielian, T., Monocyte metabolic reprogramming promotes pro-inflammatory activity and Staphylococcus aureus biofilm clearance. *PLOS Pathogens* **2020**, *16* (3), e1008354.
65. Gbejuade, H. O.; Lovering, A. M.; Webb, J. C., The role of microbial biofilms in prosthetic joint infections. *Acta Orthop* **2015**, *86* (2), 147-58.
66. Zimmerli, W.; Lew, P. D.; Waldvogel, F. A., Pathogenesis of foreign body infection. Evidence for a local granulocyte defect. *J Clin Invest* **1984**, *73* (4), 1191-200.
67. Zimmerli, W.; Waldvogel, F. A.; Vaudaux, P.; Nydegger, U. E., Pathogenesis of foreign body infection: description and characteristics of an animal model. *J Infect Dis* **1982**, *146* (4), 487-97.

## TOC

# Cobalt and chromium ions impair macrophage response to *Staphylococcus aureus* infection

Lea A. Tölken<sup>a</sup>, Georgi I. Wassilew<sup>b</sup>, Daniel Grolimund<sup>c</sup>, Timm Weitkamp<sup>d</sup>, Bernhard Hesse<sup>e,f</sup>,  
Anastasia Rakow<sup>b</sup>, Nikolai Siemens<sup>a, ‡, \*</sup>, and Janosch Schoon<sup>b, ‡, \*</sup>

<sup>a</sup> Department of Molecular Genetics and Infection Biology, University of Greifswald, Greifswald, 17489, Germany.

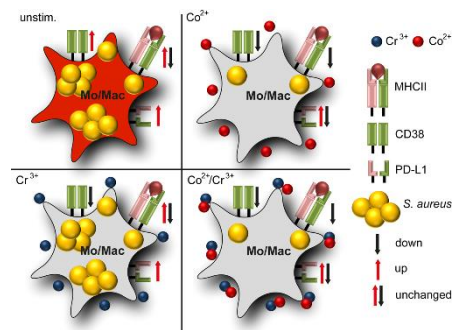
<sup>b</sup> Center for Orthopaedics, Trauma Surgery and Rehabilitation Medicine, University Medicine Greifswald, Greifswald, 17475, Germany

<sup>c</sup> Swiss Light Source, Paul Scherrer Institute, Villigen-PSI, 5232, Switzerland

<sup>d</sup> Synchrotron SOLEIL, Saint-Aubin, 91190, France

<sup>e</sup> Xploraytion GmbH, Berlin, 10625, Germany

<sup>f</sup> ESRF-The European Synchrotron, Grenoble, 38000, France



# Supporting Information

## Cobalt and chromium ions impair macrophage response to *Staphylococcus aureus* infection

*Lea A. Tölken<sup>a</sup>, Georgi I. Wassilew<sup>b</sup>, Daniel Grolimund<sup>c</sup>, Timm Weitkamp<sup>d</sup>, Bernhard Hesse<sup>e,f</sup>, Anastasia Rakow<sup>b</sup>, Nikolai Siemens<sup>a, ‡\*</sup>, and Janosch Schoon<sup>b, ‡\*</sup>*

<sup>a</sup> Department of Molecular Genetics and Infection Biology, University of Greifswald,  
Greifswald, 17489, Germany.

<sup>b</sup> Center for Orthopaedics, Trauma Surgery and Rehabilitation Medicine, University  
Medicine Greifswald, Greifswald, 17475, Germany

<sup>c</sup> Swiss Light Source, Paul Scherrer Institute, Villigen-PSI, 5232, Switzerland

<sup>d</sup> Synchrotron SOLEIL, Saint-Aubin, 91190, France

<sup>e</sup> Xploraytion GmbH, Berlin, 10625, Germany

<sup>f</sup> ESRF-The European Synchrotron, Grenoble, 38000, France



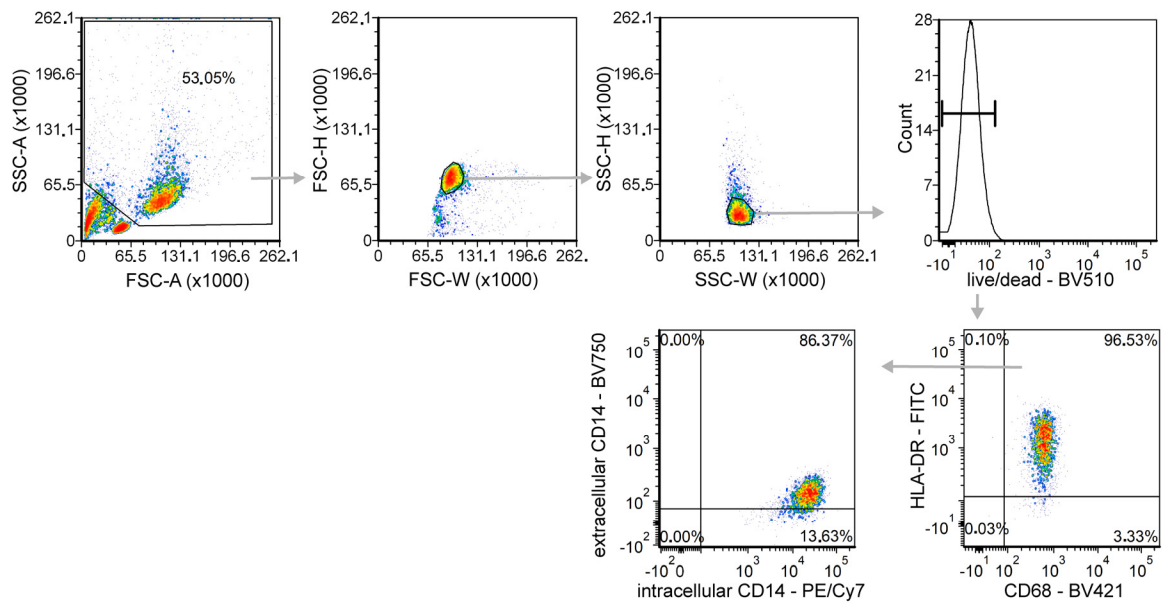


Figure S1. Gating strategy used to identify human monocytes/macrophages. Doublets were excluded by consecutive gating of FSC-H/FSC-W and SSC-H/SSC-W. Dead cells were excluded by using the Zombie Aqua™ Fixable Viability Kit. Monocytes/macrophages were selected based on the expression of HLA-DR and CD68. Macrophage subsets were further distinguished based on expression of intracellular and extracellular CD14.

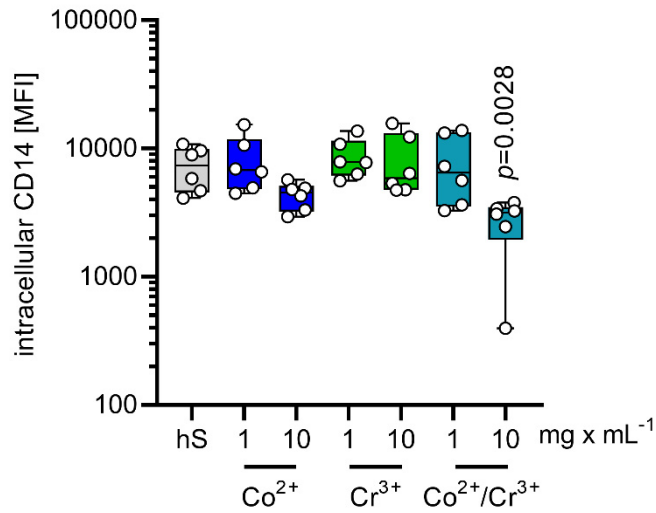


Figure S2. Intracellular CD14 expression in macrophages. Human primary monocytes were exposed to 1 or 10  $\mu\text{g}\times\text{mL}^{-1}$  of  $\text{Co}^{2+}$ ,  $\text{Cr}^{3+}$  alone or in combination for 48 h and expression of intracellular CD14 was analyzed via flow cytometry (n=6). The data are displayed as box plots. Each dot represents one independent experiment with cells from one donor. The level of significance was determined using Kruskal-Wallis test with Dunn's posttest. FMO, fluorescence minus one; unstim., unstimulated control.

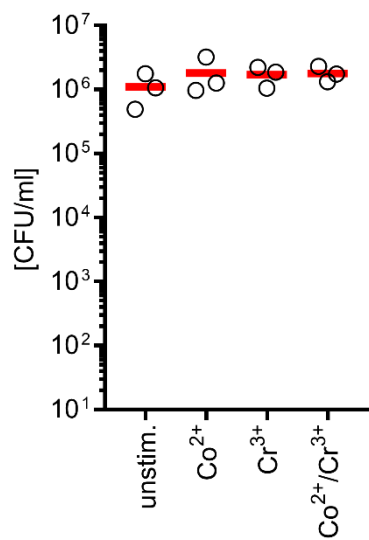


Figure S3. The impact of  $10 \mu\text{g}\times\text{mL}^{-1}$  of indicated metal ions on *Staphylococcus aureus* vitality. In short,  $1\times 10^6$  bacteria were incubated with  $10 \mu\text{g}\times\text{mL}^{-1}$  of indicated metal ions for 1 h at  $37^\circ\text{C}$ . Viable bacteria were plated on blood agar plates (n=3). unstim., unstimulated control.

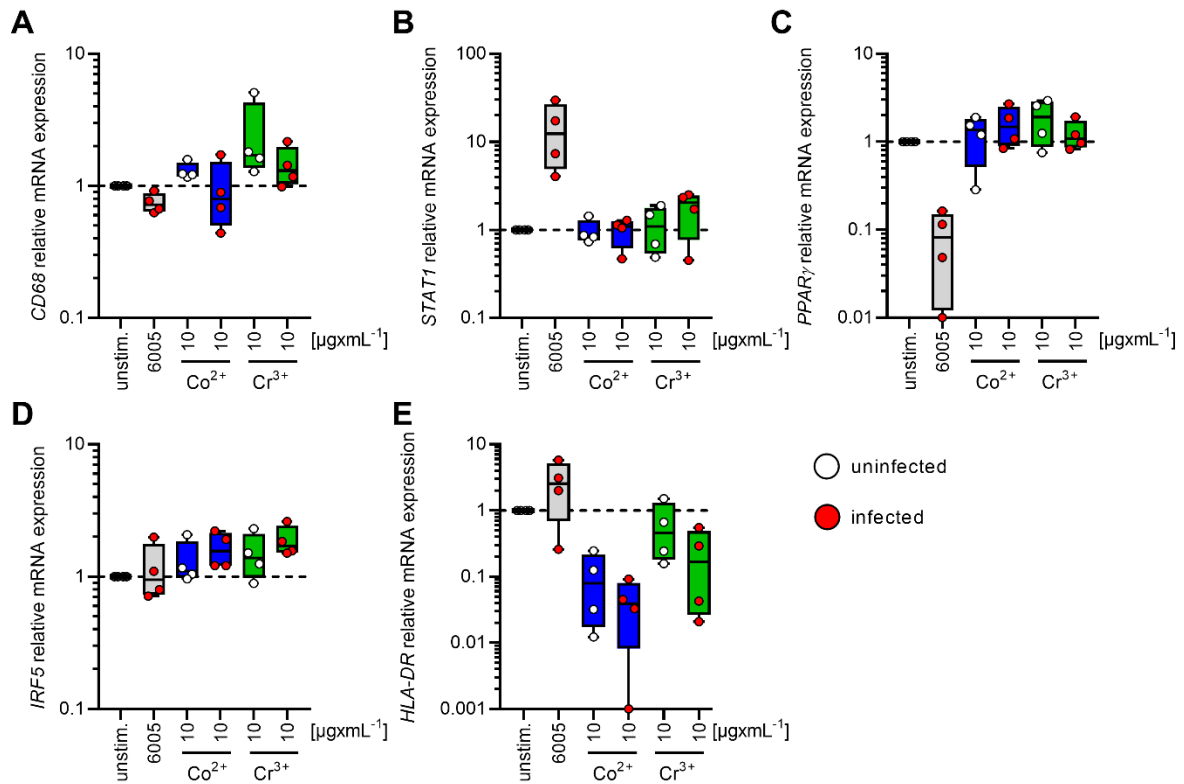


Figure S4. Gene expression analyses in macrophages. Human primary monocytes were exposed to 10  $\mu\text{g}\times\text{mL}^{-1}$  of  $\text{Co}^{2+}$  or  $\text{Cr}^{3+}$  for 48 h. Metal-exposed cells were infected with *S. aureus* 6005 (MOI 1). Extracellular bacteria were killed by substituting the media with antibiotics. Gene expression of genes encoding for *CD68* (A), *STAT1* (B), *PPAR $\gamma$*  (C), *IRF5* (D), and *HLA-DR* (E) are shown. The data are displayed as box plots. Each dot represents one independent experiment with cells from one donor (n=4). unstim., unstimulated control.





## PAPER II

# **Reduced Interleukin-18 Secretion by Human Monocytic Cells in Response to Infections with Hyper-virulent *Streptococcus pyogenes***

Lea A. Tölken, Antje D. Paulikat, Lana H. Jachmann, Alexander Reder, Manuela Gesell Salazar, Laura M. Palma Medina, Stephan Michalik, Uwe Völker, Mattias Svensson, Anna Norrby-Teglund, Katharina J. Hoff, Michael Lammers, and Nikolai Siemens

Submitted to Journal of Biomedical Science, 2023 December 08

Author contributions:

Conceptualization: **LAT**, NS; Methodology: **LAT**, ADP, LHJ, AR, MGS, KJH, ML, NS; investigation: **LAT**, ADP, LHJ, AR, MGS, MS, LMPM, SM, UV, ANT, KJH, ML, NS; visualization: **LAT**, ADP, LHJ, MGS, KJH, ML, NS; funding acquisition: NS; project administration: ANT, NS; supervision: NS; writing-original draft: **LAT**, NS; writing-review & editing: **LAT**, ADP, LHJ, AR, MGS, LMPM, SM, UV, MS, ANT, KJH, ML, NS.

.....  
Prof. Dr. Nikolai Siemens

.....  
Lea Tölken





1 **Reduced interleukin-18 secretion by human monocytic cells in response to**  
2 **infections with hyper-virulent *Streptococcus pyogenes***

3

4 Lea A. Tölken<sup>1</sup>, Antje D. Paulikat<sup>1</sup>, Lana H. Jachmann<sup>1</sup>, Alexander Reder<sup>2</sup>, Manuela Gesell Salazar<sup>2</sup>,  
5 Laura M. Palma Medina<sup>3</sup>, Stephan Michalik<sup>2</sup>, Uwe Völker<sup>2</sup>, Mattias Svensson<sup>3</sup>, Anna Norrby-Teglund<sup>3</sup>,  
6 Katharina J. Hoff<sup>4</sup>, Michael Lammers<sup>5</sup>, and Nikolai Siemens<sup>1#</sup>

7

8 <sup>1</sup>Department of Molecular Genetics and Infection Biology, University of Greifswald, Greifswald, Germany

9 <sup>2</sup>Department of Functional Genomics, University Medicine Greifswald, Greifswald, Germany.

10 <sup>3</sup>Center for Infectious Medicine, Karolinska Institutet, Karolinska University Hospital, Huddinge, Sweden

11 <sup>4</sup>Institute of Mathematics and Computer Science, University of Greifswald, Greifswald, Germany

12 <sup>5</sup>Department of Synthetic and Structural Biochemistry, Institute of Biochemistry, University of Greifswald,  
13 Greifswald, Germany

14

15 #Correspondence: Nikolai Siemens; Email: [nikolai.siemens@uni-greifswald.de](mailto:nikolai.siemens@uni-greifswald.de)

16 **Abstract**

17 **Background** *Streptococcus pyogenes* (group A streptococcus, GAS) causes a variety of diseases  
18 ranging from mild superficial infections of the throat and skin to severe invasive infections, such as  
19 necrotizing soft tissue infections (NSTIs). Tissue passage of GAS often results in mutations within the  
20 genes encoding for control of virulence (Cov)R/S two component system leading to a hyper-virulent  
21 phenotype. Dendritic cells (DCs) are innate immune sentinels specialized in antigen uptake and  
22 subsequent T cell priming. This study aimed to analyze cytokine release by DCs in response to wild-  
23 type and natural *covR/S* mutant infections.

24 **Methods** Human primary monocytes, macrophages, and monocyte-derived (mo)DCs were used. DC  
25 maturation and release of pro-inflammatory cytokines in response to infections with wild-type and  
26 *covR/S* mutants were assessed via flow cytometry.

27 **Results** *In vitro* infections of moDCs and other monocytic cells with natural GAS *covR/S* mutants  
28 resulted in reduced secretion of IL-8 and IL-18 as compared to wild-type infections. In contrast, moDC  
29 maturation remained unaffected. Inhibition of caspase-8 restored secretion of both molecules. Knock-  
30 out of streptolysin O in GAS strain with unaffected CovR/S even further elevated the IL-18 secretion by  
31 moDCs. Of 67 fully sequenced NSTI GAS isolates, 28 harbored mutations resulting in dysfunctional  
32 CovR/S. However, analyses of plasma IL-8 and IL-18 levels did not correlate with presence or absence  
33 of such mutations.

34 **Conclusions** Our data demonstrate that strains, which harbor *covR/S* mutations interfere with IL-18  
35 response in monocytic cells by utilizing the caspase-8 axis. Future experiments aim to identify the  
36 underlying mechanism and consequences for NSTI patients.

37

38 **Keywords:** *Streptococcus pyogenes*, dendritic cells, interleukin-18, CovR/S, necrotizing soft tissue  
39 infection

## 40 **Background**

41 *Streptococcus pyogenes* (group A streptococcus, GAS) causes a variety of human diseases ranging  
42 from mild superficial to severe invasive infections, including necrotizing soft tissue infections (NSTIs).  
43 Globally, invasive GAS infections are estimated to cause approx. 500,000 deaths annually [12]. NSTIs  
44 encompass necrosis of any layer of the skin and soft tissue compartment and are often associated with  
45 systemic toxicity. Despite prompt antibiotic treatment, intensive care, and extensive surgical intervention  
46 [2], the morbidity and mortality of such infections remain substantial [39,56]. While microbial etiologies  
47 of NSTIs are diverse, GAS are among the main causative pathogens of monomicrobial NSTIs [10,39].  
48 In a recent Scandinavian prospective multicenter study INFECT, 31% of surgically confirmed NSTI  
49 cases were caused by GAS [11,39].

50 In the host, GAS can adopt a hyper-virulent phenotype, often mediated by inactivating mutations within  
51 genes encoding for the two component system (TCS) control of virulence (Cov)R/S [17,20,57,58,65].  
52 Strains possessing *covR/S* mutations are frequently isolated from patients suffering from invasive GAS  
53 infections [5,26,39,60]. In mouse studies, GAS hyper-virulence is characterized by induction of  
54 excessive inflammation through increased superantigenic activity [6]. However, immunosuppressive  
55 effects, including impaired neutrophil responses, are also reported [62]. The CovR/S system consists of  
56 the histidine kinase CovS and the response regulator CovR. CovS senses environmental signals  
57 including pH acidification [18,25]. Upon activation, CovS phosphorylates CovR at D53. Phosphorylated  
58 CovR binds DNA and activates or represses transcription of several target genes [18,25]. CovR/S  
59 regulates up to 15% of the GAS genome and is a transcriptional suppressor of several key virulence  
60 factors, including the hyaluronic acid capsule, M protein, and cholesterol-dependent cytolysin  
61 streptolysin O (SLO). Consequently, inactivating mutations in *covR/S* result in higher expression of these  
62 virulence factors, among others [14,57].

63 Dendritic cells (DCs) are sentinel leukocytes and proficient antigen presenting cells (APCs). They bridge  
64 the innate and adaptive arms of the immune system by presenting processed antigens to T cells [54].  
65 After ingestion of pathogens, DCs mature, migrate to the secondary lymph nodes, and present antigens  
66 to T cells via major histocompatibility complex (MHC) class II molecules [55]. In addition, DCs express  
67 co-stimulatory molecules and secrete cytokines to shape the direction of T cell priming and  
68 differentiation [41]. Only limited data exists on DC-GAS interactions. In murine models, it was shown  
69 that DCs are essential to limit GAS spread to the lymph nodes [38]. Furthermore, *in vitro* studies have

70 demonstrated that GAS inhibit DC maturation in a capsule- and/or SLO-dependent manner and induce  
71 significant cell death [15,35]. In addition, the streptococcal DNase Sda1 was found to impair  
72 plasmacytoid dendritic cell recruitment by reducing IFN-1 levels at the tissue site of infection [34].

73 DCs and other myeloid cells of monocytic lineage are major sources of cytokine/chemokine production  
74 for an appropriate response to infections. In addition to interleukin (IL)-8, a potent neutrophil  
75 chemoattractant, DCs secrete IL-1 $\beta$  and IL-18. Both IL-1-family cytokines are stored intracellularly as  
76 inactive precursors. Processing and release occur upon activation of the NLRP3 inflammasome. The  
77 associated active executioner caspase-1 cleaves the precursors into the respective mature cytokines.  
78 Subsequently, the release is mediated through caspase-1 processed gasdermin D pores [23]. The  
79 secreted GAS cysteine protease SpeB was shown to cleave pro-IL-1 $\beta$  and pro-IL-18 into their respective  
80 mature forms [28,36]. Both cytokines have strong pro-inflammatory effects and play crucial roles in  
81 invasive GAS infections. IL-1 $\beta$  network was identified as a key network involved in susceptibility to GAS  
82 NSTIs [13]. IL-18 is crucial for activation of mucosa associated invariant T (MAIT) cells and subsequent  
83 interferon (IFN)- $\gamma$  secretion [43,66]. Excessive MAIT cell activation through IL-12/IL-18 was linked to  
84 pathological cytokine storm underlying STSS [19], which is a common complication of NSTIs [44,46].

85 To date, data on GAS-DCs interactions are scarce and mainly derived from murine studies. Thus, we  
86 investigated the cytokine response of human monocyte-derived (mo)DCs and other cells to infections  
87 with either wild-type GAS or natural *covR/S* mutants. All cells of monocytic lineage infected with *covR/S*  
88 mutants secreted significantly less IL-8 and IL-18 as compared to wild-type infections. Inhibition of host  
89 initiator caspase-8 restored the secretion of both cytokines in response to infections. Validation of  
90 systemic plasma IL-18 levels in patients did not show differences based on bacterial *CovR/S*  
91 assignment.

## 92 **Methods**

### 93 **Bacterial and strains**

94 The following GAS strains were used: NSTI/STSS strains 5448, 5626, 8003, and 8157 (provided by  
95 Donald E. Low, Mount Sinai Hospital, Toronto, Canada) [27,33], 2002 and 2006 from the INFECT cohort  
96 [51], MGAS5005 [57], 5448AP [65], 5448 $\Delta$ *emm1* [37], and 5448 $\Delta$ *slo* [61]. All strains were cultured in  
97 Todd-Hewitt broth (Carl Roth) supplemented with 1.5% (w/v) yeast extract (Carl Roth) at 37°C.  
98 Hemolytic activity of GAS stationary culture supernatants was assessed as previously described [35].

99

### 100 **Isolation of human monocytes and generation of dendritic cells and macrophages**

101 Human monocytes were isolated from buffy coats using CD14 S-pluriBead antihuman beads  
102 (PluriSelect) or EasySep Human CD14 Positive Selection Kit II (Stemcell technologies) according to  
103 manufacturer's instructions. The moDCs were generated by culturing monocytes for 5 d in RPMI1640  
104 (Cytivia) medium supplemented with 10% (v/v) heat inactivated fetal calf serum (FCS; Thermo Fisher),  
105 89 ng $\times$ mL<sup>-1</sup> GM-CSF, and 22 ng $\times$ mL<sup>-1</sup> IL-4 (both Immunotools). Medium was exchanged on day 3.

106 The monocyte-derived macrophages were generated by culturing monocytes in RPMI1640 (Cytivia)  
107 medium supplemented with 10% (v/v) heat inactivated FCS (Thermo Fisher) and 25 ng $\times$ mL<sup>-1</sup> GM-CSF  
108 (Immunotools) for 7 d. Medium was exchanged on days 3 and 5.

109

### 110 **Infections of myeloid cells**

111 All infections were performed in RPMI1640 complete media. 1 $\times$ 10<sup>5</sup> monocytes, 2 $\times$ 10<sup>5</sup> monocyte-derived  
112 macrophages, or 1 $\times$ 10<sup>5</sup> moDCs were infected with GAS at a multiplicity of infection (MOI) 10 for 1 h.  
113 Next, extracellular bacteria were killed by addition of RPMI1640 containing antibiotics (100  $\mu$ g $\times$ mL<sup>-1</sup>  
114 streptomycin, 100 IU $\times$ mL<sup>-1</sup> penicillin G (Hyclone)). After a total of 23 h infection, supernatants were  
115 collected and stored at -80°C until further analyses. The moDCs were directly prepared for flow  
116 cytometry.

117 For assessing intracellular bacterial survival kinetics,  $2 \times 10^5$  moDCs were infected, as described above.  
118 After addition of antibiotics, the cells were washed, lysed, and intracellular bacteria plated on blood agar  
119 plates (Oxoid).

120 For inhibition studies, moDCs were pre-treated with inhibitors targeting different caspases: caspase-3  
121 (Cas3/7-Inhibitor I (CAS 220509-74-0), Sigma Aldrich, 500 nM; Ac-DEVD-cho (Invivogen), 40  $\mu$ M),  
122 caspase-8 (z-IETD-fmk (Invivogen), 40  $\mu$ M), or pan-caspase inhibitor (z-VAD-fmk, (Invivogen), 40  $\mu$ M).  
123 moDCs were pre-treated with the respective inhibitors for 1 h at 37°C and subsequently infected as  
124 described above. Inhibition of caspases remained through the entire course of infections. DMSO served  
125 as solvent control.

126

### 127 **Flow cytometry**

128 Dead cells were labeled using the Zombie Aqua Fixable Viability Kit (BioLegend). Unspecific binding of  
129 immunoglobulins was blocked by using Human TruStain FcX (BioLegend) according to the  
130 manufacturer's instructions. Incubations of cells with titrated amounts of monoclonal antibodies were  
131 carried out for 30 min at 4°C in the dark. Cells were washed between each staining step and fixed using  
132 the Cyto-Fast Fix/Perm Buffer Set (BioLegend). Antibodies and clones directed against the following  
133 markers were used (target, clone, fluorochrome, all Bio-Legend): CD209 (9E9A8, APC), CD209 (9E9A8,  
134 BV421), CD40 (5C3, Alexa Fluor700), CD80 (2D10, BV711), CD86 (BU63, PE/Cyanine7), CD83  
135 (HB15e, BV421) and HLA-DR (L243, FITC). The gating strategy is shown in Figure S1. Data were  
136 acquired using a FACS Aria III flow cytometer and FACS DIVA 8.0 Software (both BD Biosciences, San  
137 Jose, CA, USA) and analyzed using FCS Express 7 Software (De Novo Software).

138

### 139 **Cytokine measurements**

140 Cytokine concentrations in cell culture supernatants were measured via LEGENDPlex human  
141 inflammation panel (13-plex) kit or custom panel (3-plex: IL-1 $\beta$ , IL-8, IL18) (both BioLegend) according  
142 to the manufacturer's instructions. Data were acquired with a FACS Aria III flow cytometer using FACS  
143 DIVA Software (both BD Bioscience) and analyzed using LEGENDPlex software (BioLegend).

144 Furthermore, previously published cytokine levels in acute plasma from NSTI patients from the infect  
145 cohort [46] was reanalyzed.

146

### 147 **Caspase activity measurements**

148 Caspase 8 activity was measured using the Caspase-Glo® 8 Assay Systems (Promega) according to  
149 manufacturer's instructions. Caspase 3 activity was measured using the Magic Red Caspase 3/7 Kit  
150 (BioRad) according to manufacturer's instructions.

151

### 152 **Bioinformatic analysis**

153 Analyses of CovR and CovS sequences were performed as described previously [51]. In brief, genes  
154 were identified via BLAST (v. 2.9.0+) using a custom Python script. Mutations were automatically  
155 identified using Python (Reference sequence CovS: WP\_002991036.1, CovR: WP\_002991052.1).  
156 Predictions of CovR/S functionality (Table S1) were based on literature review (Table S2) or predicted  
157 protein structures using AlphaFold2 [29,30]. Previously published patient cytokine data [46] and whole  
158 genome sequences [60] of the GAS strains were retrieved from the INFECT cohort and reanalyzed.

159

### 160 **Proteomic Analysis**

161 Infected moDC pellets were resuspended in 100 µl Tris-HCl (5 mM pH 7.4 containing 5% SDS) and  
162 immediately disrupted using a Dismembrator (Retsch) at 2,600 rpm for 3 min (in a 4.8 ml Teflon vessel  
163 precooled in liquid nitrogen with an 8 mm diameter steel ball). Next, the cell powder was resuspended  
164 with 400 µl of preheated (95°C) Tris-HCl buffer (5 mM, pH 7.4) and the viscous lysate was transferred  
165 into a fresh 1.5 ml low bind pre-lubricated Eppendorf tube and shaken for 1 min at 95°C and 1,400 rpm.  
166 The lysate was cooled to RT and 2 µl of a 1 M MgCl<sub>2</sub> stock solution (final conc. 4 mM MgCl<sub>2</sub>) was added.  
167 Next, 1 µl of a 1:100 diluted benzonase (Pierce Universal Nuclease; Pierce) stock solution (final 0.005  
168 U/µl) was added and mixed by short vortexing. The samples were incubated in an ultrasonic bath at RT  
169 for 5 min until the viscous lysate was liquefied by complete degradation of DNA and RNA. The raw  
170 lysates were centrifuged (17,000 g; RT; 30 min). After centrifugation, the protein lysate was transferred  
171 into a fresh 1.5 ml low bind pre-lubricated Eppendorf tube, and the pelleted cell debris was discarded.

172 The protein concentration of the samples was determined using the Micro BCA Protein Assay Kit  
173 following the manufacturer's protocol (Pierce). Samples were stored at -80°C until further use. Sample  
174 preparation for mass spectrometry measurements was performed using the SP3 protocol as previously  
175 described [8].

176 LC-MS/MS analyses of tryptic peptide solutions were carried out on a reverse phase HPLC  
177 chromatography system (Ultimate 3000 nano-LC system, Thermo Fisher Scientific) coupled to a Q  
178 Exactive™ Exploris 480 mass spectrometer (Thermo Fisher Scientific) in data-independent acquisition  
179 mode. Data analyses were performed in Spectronaut version 17 (Biognosys AG), based on a database  
180 search against a Uniprot/Swissprot database limited to 20,375 human entries (version 2022\_01) using  
181 trypsin/P digest rule with maximum number of two missed cleavages, methionine oxidation as variable  
182 modifications (for details see Table S3). Further DIA-MS data analysis was carried out in R (R Version  
183 4.2.0) using the tidyverse (version 1.3.1), factomineR (version 2.4.0) and PECA package (version  
184 1.32.0) with a paired reproducibility-optimized test statistic (ROTS) [50,59] as described by Cuypers *et*  
185 *al* [16].

186

## 187 **Statistics**

188 Statistical significance of differences was determined using Kruskal-Wallis test with Dunn's multiple  
189 comparison posttest or Mann-Whitney *U* test. Statistics were performed using GraphPad Prism version  
190 8. A *p* value less than 0.05 was considered significant.



## 191 **Results**

### 192 **Reduced release of IL-8 and IL-18 by myeloid cells in response to infections with GAS harboring** 193 **dysfunctional CovR/S**

194 To assess the pro-inflammatory response by moDCs, cells were infected with four GAS strains harboring  
195 functional CovR/S (CovR/S<sup>+</sup>; 2006, 5448, 5626, 8157) or four *covS* mutant strains carrying non-  
196 functional CovR/S (CovR/S<sup>-</sup>; 2002, MGAS5005, 5448AP, 8003) and IL1 $\beta$ , IL-8 as well as IL-18 release  
197 in response to infections was measured. The sequences as well as CovR/S functionality of the  
198 respective strains were previously assessed [51] (Table S1) and confirmed via SpeB proteolytic activity  
199 on casein agar plates (Fig. S2). While moDCs readily secreted equal amounts of IL-1 $\beta$  in response to  
200 all infections (Fig. 1A), IL-18 as well as IL-8 levels were significantly less in infections with CovR/S<sup>-</sup> as  
201 compared to CovR/S<sup>+</sup> strains (Fig. 1B-C).

202 To evaluate whether (i) this observation is restricted to moDCs and (ii) to exclude potential impact of  
203 genomic variations between the GAS strains, moDCs, monocytes, and monocyte-derived macrophages  
204 were infected with *emm1* STSS isolate 5448 and its corresponding *covS* mutant 5448AP [65] and the  
205 release of multiple cytokines in response to infections was assessed (Fig. 2, Fig. S3). Irrespective of the  
206 CovR/S variant used for infections, all three cell types released comparable levels of IFN- $\gamma$ , tumor  
207 necrosis factor (TNF)- $\alpha$ , MCP-1, IL-6, IL-10, IL-12p70, and IL-23 (Fig. 2A-C; Fig. S3). Notably, of the  
208 two inflammasome-related cytokines, only IL-1 $\beta$  release was equally induced (Fig. 2D). In contrast, IL-  
209 18 secretion in 5448AP infections remained at the levels of uninfected controls (Fig. 2E). Furthermore,  
210 similar results were noted for IL-8 release (Fig. 2F).

211

### 212 **Infected dendritic cells clear intracellular bacteria and mature irrespective of GAS CovR/S** 213 **phenotype**

214 Next, we assessed whether 5448AP infections would also have an effect on DC maturation. Since  
215 CovR/S inactivation has been reported to increase surface abundance of M-protein [58], an *emm*-  
216 knockout strain was included in this series of experiments. MoDCs were infected with 5448, 5448AP, or  
217 5448 $\Delta$ *emm1* and bacterial intracellular survival (Fig. S4) and moDC maturation were assessed  
218 (Fig. 3A). Irrespective of the strain used, moDCs remained viable (Fig. 3B) and eliminated all bacteria  
219 within 24 h of total infection time. No differences in GAS uptake were noted (Fig. S4). Furthermore,

220 moDCs readily matured in all infectious conditions to the levels of LPS stimulations, characterized by  
221 increased frequencies of CD80 and CD83 positive cells as well as upregulation of CD40, CD86, and  
222 HLA-DR on the surface (Fig. 3A-G).

223 To assess potential differences on a global level, whole proteome of moDCs infected with 5448 or  
224 5448AP was quantitatively profiled by mass spectrometry at 6 and 24 h post infection. Uninfected  
225 moDCs at respective time points served as controls. In total, 5857 protein groups were identified. For  
226 quantification, 4801 protein groups identified by the presence of two or more peptides and observed in  
227 at least half of the experiments for each condition were used. Principal component analysis (PCA)  
228 revealed that uninfected controls (6 and 24 h) and both 6 h infections with 5448 and 5448AP clustered  
229 together (Fig. 3H). Furthermore, rather a donor specific proteome signature with no obvious impact of  
230 infections was noted at 6 h (Fig. S5; Table S4) suggesting that 6 h of infection are too short to induce  
231 maturation. In contrast, the moDC proteomes of both 24 h infections were different from uninfected  
232 moDC and separated in the PCA (Fig. 3H). Statistical analyses revealed a general infection specific  
233 signature. However, no major differences were observed between 5448 and 5448AP infections (Fig. S6,  
234 Table S4). Furthermore, IL-18 as well as IL-8 were not detected within moDCs (Table S4).

235

### 236 **Caspase-8 inhibition restores secretion of IL-8 and IL-18 by moDCs in 5448AP infections**

237 Since reduction of IL-8 levels in GAS infections by action of either SpyCEP [63,68] or Nga [45] is well  
238 established, we further focused on IL-18 secretion by moDCs. The IL-18 amino acid sequence contains  
239 predicted cleavage sites for executioner proteases, including caspase-1 and caspase-3 [49]. Processing  
240 of IL-18 by caspase-3 was shown to yield biologically inactive fragments [48]. To investigate whether  
241 inhibition of caspase-3 or its upstream initiator caspase-8 would restore the moDCs ability to secrete IL-  
242 18 (and potentially IL-8), moDCs were pre-treated with specific inhibitors of caspase-3, caspase-8, or a  
243 pan-caspase inhibitor. Subsequently, pre-treated moDCs were infected with 5448AP, and multiple  
244 inflammatory cytokines were measured in supernatants. No cytokine secretion in response to inhibitors  
245 or its solvent, DMSO, was noted (Fig. S7). Caspase-3, caspase-8, or pan-caspase inhibition did not alter  
246 secretion of IFN- $\alpha$ 2, IFN- $\gamma$ , MCP-1, IL-6, IL-10, IL-12p70 or IL-23, as elevated levels of these cytokines  
247 were detected in all infection conditions (Fig. 4, Fig. S7). Furthermore, IL-1 $\beta$  secretion in response to all  
248 5448AP infections remained at the levels of 5448 infections (Fig. 4A-B). Notably, in the presence of

249 caspase-8 as well as pan-caspase inhibitors, the levels of IL-18 increased in response to 5448AP  
250 infections, reaching the levels of 5448 infection control (Fig. 4A, 4C). A similar trend was also observed  
251 for IL-8 (Fig. 4A, 4D), particularly when caspase-8 inhibitor was used.

252

### 253 **Infections of moDCs with 5448AP result in higher caspase-8 activity**

254 Since caspase-8 inhibition restored the secretion of IL-8 and IL-18 in response to 5448AP infections, its  
255 intracellular abundance was assessed in moDCs. Executioner caspase-3 was also analyzed.  
256 Irrespective of the strain used for the infections, moDCs equally responded by upregulating the  
257 expression of both caspases at 24 h post infection (Fig. 5A-B; Table S4). However, total protein  
258 abundance does not reflect its activity. Therefore, moDCs were infected with both strains and caspase-  
259 8 activity was assessed at different time points of infection. Luminescence-based measurement over a  
260 period of 8 h revealed a stable increase of caspase-8 activity in response to 5448AP infections (Fig. 5C)  
261 In contrast, 5448 infections rather suppressed caspase-8 activity. Assessment of its activity in several  
262 donors confirmed the initial result. While 5448AP infections activated caspase-8, 5448 infections did not  
263 (Fig. 5D). Downstream assessment of executioner caspase-3 activity via flow cytometry showed that  
264 only a negligible percentage of infected moDCs were positive for active caspase-3 (Fig. 5E).

265

### 266 **Impact of dysfunctional CovR/S on systemic cytokine levels in NSTI patients**

267 As both, the IL-1 $\beta$  network [13] and the IL-12/IL-18 axis [19] are closely linked to NSTIs and STSS, the  
268 CovR/S phenotype of GAS isolates collected during the INFECT study was determined and correlated  
269 to previously measured plasma concentrations of IL-8, IL-1 $\beta$ , and IL-18 [46]. In total, *covS* and *covR*  
270 genes of 67 isolates were analyzed and amino acid sequences were predicted (Table S1). The majority  
271 of mutations leading to amino acid substitution or truncated proteins were identified in *CovS* (Table S1).  
272 To assess the functionality of different CovR/S variants, literature review (Table S2) and protein  
273 structure predictions using AlphaFold2 (Fig. S8) were performed [29,30]. Twenty-eight strains were  
274 predicted to harbor dysfunctional CovR/S (Table S1, Fig. S8; please refer to the figure legend of Fig. S8  
275 for detailed description of the functionality assignment). Next, the CovR/S phenotype was matched to  
276 plasma cytokine concentrations of respective patients. Irrespective of functional or dysfunctional CovR/S  
277 of the infective GAS, equal systemic concentrations of IL-8, IL-1 $\beta$ , and IL-18 (Fig. 6A-C) were detected

278 in patient's plasma. As the IL-12/IL-18 axis is also linked to development of STSS, patients were grouped  
279 based on clinical presentation, with and without septic shock. These analyses revealed that patients  
280 suffering from septic shock have significantly higher systemic IL-8 or IL-1 $\beta$  plasma levels if they are  
281 infected with CovR/S<sup>+</sup> or CovR/S<sup>-</sup> strains, respectively (Fig. 6D-E). No differences in systemic IL-18  
282 levels between patient groups were observed (Fig. 6F).

283

#### 284 **Secretion of IL-1 $\beta$ and IL-18 by moDCs is increased in infections with 5448 $\Delta$ s/o**

285 SLO is a known inducer of apoptotic program in myeloid cells, which requires activation of caspase-8  
286 [61]. Since SLO was previously shown to (i) impact maturation of murine DCs, (ii) to interfere with  
287 caspases [15,35], and (iii) its expression is under CovR/S control [57], we hypothesized that SLO might  
288 be responsible for impaired secretion of IL-18 by moDCs. First, hemolytic activity of stationary culture  
289 supernatants of 5448 and 5448AP was measured. This revealed significantly higher hemolytic activity  
290 of 5448AP supernatants as compared to 5448 (Fig. 7A). Several attempts to construct a *s/o*-knock-out  
291 in 5448AP background was unsuccessful. We therefore hypothesized that infections of moDCs with  
292 5448 $\Delta$ s/o strain would further increase IL-18 response as compared to 5448 wild-type infections.  
293 Therefore, cells were infected with 5448 and its corresponding 5448 $\Delta$ s/o. Deletion of SLO had no  
294 obvious impact on moDC viability (Fig. 7B). Furthermore, moDCs matured in response to all infections  
295 characterized by increased frequencies of CD83<sup>+</sup> (Fig. 7C) and CD86<sup>+</sup> (Fig. 7D) cells as well as increased  
296 expression of surface HLA-DR (Fig. 7E). Analyses of cytokines revealed an equal IL-8 response  
297 (Fig. 7F). In contrast, IL-1 $\beta$  (Fig. 7G) and IL-18 (Fig. 7H) secretion were significantly higher in 5448 $\Delta$ s/o  
298 as compared to wild-type infections.

## 299 Discussion

300 Myeloid cells are crucial responders to infections, responsible for pathogen clearance, recruitment of  
301 other immune cells, and shaping the T cell response through secretion of a plethora of cytokines and  
302 chemokines. They are the primary sources of IL-1 family cytokines IL-1 $\beta$  and IL-18 as well as potent  
303 producers of the main human neutrophil chemoattractant IL-8 [23]. Bacteria, including GAS, have  
304 developed multiple phenotypic and genetic adaptations to evade the host immune system effector  
305 mechanisms. In this study, we show that infections with GAS strains harboring dysfunctional CovR/S  
306 result in reduced secretion of IL-8 and IL-18 by monocytic cells. This phenomenon is mainly mediated  
307 by a caspase-8-dependent mechanism.

308 GAS have developed several ways to adapt to the host environment. Enhanced mutational rates in the  
309 *covR/S* genes often mediate the switch to a hyper-virulent phenotype [65]. CovS senses environmental  
310 signals and phosphorylates the bound response regulator CovR. Phosphorylated CovR dissociates from  
311 CovS, binds to its target DNA sequences, and either activates or represses transcription of target genes  
312 [18,25]. Not every mutation in *covR* or *covS* will lead to dysfunctional TCS [47]. However, loss of function  
313 mutations are often associated with increased virulence [17] due to de-repression of transcription of  
314 several virulence factors, which is particularly pronounced in *emm1* strains [6,24,32]. Of 67 strains  
315 analyzed in this study, 28 isolates possessed mutations, which were experimentally validated or  
316 predicted to negatively affect the functionality of the TCS resulting in a hyper-virulent phenotype. In such  
317 strains, increased levels of key virulence factors, including the capsule, M protein, SpyCEP, and Nga  
318 were reported [57,58].

319 The cell-envelope protease SpyCEP was shown to cleave human IL-8, resulting in decreased local  
320 levels and consequently impaired neutrophil recruitment to the site of infection [53,63,68]. In addition,  
321 induction of ER stress and Golgi fragmentation by the NAD-glycohydrolase Nga was shown to reduce  
322 secretion of IL-8 by GAS-infected macrophages [45]. Furthermore, Nga activity inhibits type I interferon  
323 production in macrophages via suppression of STING signaling, which also correlates with increased  
324 disease severity in NSTI patients [42]. The results of this study are in line with previous observations.  
325 However, our data indicates that streptococcal SpyCEP and Nga are not the only factors responsible  
326 for the abrogated IL-8 secretion, as inhibition of initiator caspase-8 restored IL-8 release by moDCs.  
327 This suggests that particularly host factors play also a role in the observed phenotype.

328 Strains harboring dysfunctional CovR/S were also shown to produce increased levels of SLO [31,35,58].  
329 SLO forms pores in membranes of phagocytes [67], mediates bacterial escape from phagosomes, and  
330 induces macrophage death [61]. In addition, SLO is essential for Nga translocation across the plasma  
331 membrane into the host cell cytosol. Consequently, Nga depletes cellular energy stores and interferes  
332 with cytokine secretion [42,45]. STSS isolates were shown to produce significantly more SLO than  
333 strains derived from non-invasive infections, emphasizing a crucial role for this cytolysin in invasive  
334 diseases [7,26]. Much of the knowledge about DC-GAS interactions is derived from work with murine  
335 cells or prolonged infection times. In such settings, DCs infected with a CovR/S dysfunctional and high-  
336 SLO secreting 5448AP strain showed impaired maturation and significant cell death [15,35]. Our results  
337 are in stark contrast to these previous findings mostly due to the following reasons: (i) short initial  
338 infections which were not exceeding one hour and (ii) immediate depletion of extracellular bacterial  
339 supply through antibiotic treatment. Even in such setting, IL-18 secretion by infected monocytic cells  
340 was impaired. SLO is a known inducer of apoptotic program through activation of the initiator caspase-  
341 8 [61]. Although speculative, increased production of SLO by phagocytosed GAS might lead to the  
342 observed increased activation of caspase-8. Consequently, caspase-8 or a downstream-protease other  
343 than caspase-3 might cleave IL-18, which results in the observed abrogated IL-18 secretion. Although  
344 we were not able to construct a *slo*-knockout in 5448AP background, our data supports the concept that  
345 SLO interferes with the cytokine axis, since moDCs infected with 5448 $\Delta$ *slo* secreted high amounts of  
346 IL-1 $\beta$  and IL-18, even exceeding the levels of wild-type infections.

347 The role of the IL-1 $\beta$  network in NSTIs is well established [13]. Furthermore, the IL-12/IL-18 axis has  
348 been linked to the pathological MAIT cell activation and development of STSS [19,44,46]. Although we  
349 did not detect differences in systemic IL-18 levels in patients, local tissue concentrations might differ  
350 due to a mix of GAS clones, which are usually recovered from NSTI tissue biopsies [52]. Reduced local  
351 IL-18 levels could potentially delay activation of resident or recruited MAIT cells characterized by  
352 reduced IFN- $\gamma$  production. Nonetheless, hyper-virulent GAS harboring *covR/S* mutations produce  
353 increased amounts of superantigens [58], which might potentially negate the IL-18 effect. In general,  
354 myeloid cells are the primary sources of IL-1 $\beta$  and IL-18 [23] and elevated levels of both cytokines were  
355 found locally and systemically in a pharyngitis human challenge trial as well as increased frequencies  
356 of circulating monocytes and DCs [3]. In our *in vitro* experimental setup, strains harboring dysfunctional  
357 CovR/S exclusively suppressed IL-18 release by myeloid cells. Notably, these two cytokines are

358 commonly considered to be processed and released together. Thus, little is known about their differential  
359 processing. Canonical maturation and release are mediated by inflammasome-associated executioner  
360 caspase-1. However, other non-canonical inflammasomes as well as proteases can process both  
361 cytokines [66]. In addition, cell death pathways mediate caspase-1 and/or caspase-8 dependent release  
362 of IL-1 $\beta$  [64] and caspase-8 is able to substitute for loss of caspase-1 dependent processing of IL-18  
363 [4,9,21,22,40]. Furthermore, cleavage of pro- and mature IL-18 via caspase-3 was shown to yield  
364 biologically inactive fragments [1,48]. In this study, inhibition of caspase-8 restored secretion of IL-18 in  
365 infections with hyper-virulent GAS, while inhibition of caspase-3 did not. This suggests that either  
366 caspase-8 or an unknown factor downstream is responsible for this effect, which is also supported by  
367 the fact that caspase-8 activity was exclusively increased in 5448AP infections.

368

## 369 **Conclusions**

370 Cytokines/chemokines derived from myeloid cells are crucial effector molecules in infections. Through  
371 tissue passage, GAS adopt a hyper-virulent phenotype mediated by mutations of genes encoding the  
372 CovR/S TCS. Here, we show that *in vitro* infections of monocytic cells with such hyper-virulent strains  
373 result in abrogated release of IL-8 and IL-18. To our knowledge, this is the first report that provides  
374 evidence of IL-18 suppression by hyper-virulent GAS strains in cells of monocytic lineage and warrants  
375 further experimental studies to identify host as well as bacterial factors which are used to interfere with  
376 the immune response.

377 **Abbreviations**

378 GAS: Group A streptococcus; NSTI: necrotizing skin and soft tissue infection; TCS: two component  
379 system; STSS: streptococcal toxic shock syndrome; SLO: streptolysin O; (mo)DC: (monocyte-derived)  
380 dendritic cell; IL: interleukin; IFN: interferon; MAIT: mucosa associated invariant T cell; CD: cluster of  
381 differentiation

382 **Supplementary information**

383 Additional file 1: Figures S1-8; Tables S2, S3, S5; Table legends S1, S4

384 Additional file 2: Tables S1, S4

385

386 **Declarations**

387 **Patient material and blood samples**

388 This study reanalyzed previously published plasma cytokine levels and whole genome sequences of  
389 GAS strains retrieved from the INFECT patient cohort consisting of patients with NSTI (INFECT study;  
390 ClinicalTrials.gov, NCT01790698).

391 Buffy coats of blood provided by the blood bank at the University Medicine Greifswald were used. The  
392 buffy coats were provided anonymously. The ethical research committee at the University Medicine  
393 Greifswald approved the study (Ref. No. BB 014/14). All experiments were carried out in accordance  
394 with the approved guidelines.

395

396 **Consent for publication**

397 Not applicable

398

399 **Availability of data and materials**

400 All data associated with this study are presented in the manuscript and supplementary material. Whole  
401 genome sequencing data of GAS strains are available at the European Nucleotide Archive (ENA) under



402 the reference number PRJNA524111. The mass spectrometry proteomics data have been deposited to  
403 the Mass Spectrometry Interactive Virtual Environment (MassIVE) with the dataset identifier  
404 MSV000093585.

405

#### 406 **Competing interests**

407 All authors declare no competing interests.

408

#### 409 **Funding**

410 This research was supported by the German Research Foundation (DFG; grants 492903360 and  
411 503880638 to NS), the European Union Seventh Framework Programme (FP7/2007-2013) under the  
412 grant agreement 305340 (INFECT project); the Swedish Governmental Agency for Innovation Systems  
413 (VINNOVA) under the frame of NordForsk (project no. 90456, PerAID), the Swedish Research Council.

414

#### 415 **Author Contributions**

416 Conceptualization: LAT, NS; methodology: LAT, ADP, LHJ, AR, MGS, KJH, ML, NS; investigation: LAT,  
417 ADP, LHJ, AR, MGS, MS, LMPM, SM, UV, ANT, KJH, ML, NS; visualization: LAT, ADP, LHJ, MGS,  
418 KJH, ML, NS; funding acquisition: NS; project administration: ANT, NS; supervision: NS; writing-original  
419 draft: LAT, NS; writing-review & editing: LAT, ADP, LHJ, AR, MGS, LMPM, SM, UV, MS, ANT, KJH, ML,  
420 NS.

421

#### 422 **Acknowledgment**

423 We thank Karsta Barnekow and Max Sittner for expert technical assistance. We thank all clinical  
424 partners of the INFECT consortium.

425 **References**

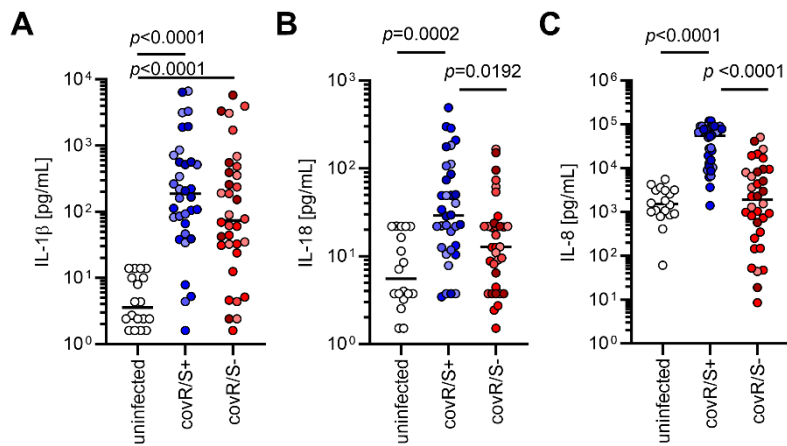
- 426 1. Akita K., Ohtsuki T., Nukada Y., Tanimoto T., Namba M., Okura T., Takakura-Yamamoto R.,  
 427 Torigoe K., Gu Y., Su M.S.S., Fujii M., Satoh-Itoh M., Yamamoto K., Kohno K., Ikeda M. and  
 428 Kurimoto M. Involvement of Caspase-1 and Caspase-3 in the Production and Processing of  
 429 Mature Human Interleukin 18 in Monocytic THP.1 Cells\*. *Journal of Biological Chemistry*  
 430 272(42):26595-26603, 1997.
- 431 2. Anaya D.A., McMahon K., Nathens A.B., Sullivan S.R., Foy H. and Bulger E. Predictors of  
 432 Mortality and Limb Loss in Necrotizing Soft Tissue Infections. *Archives of Surgery* 140(2):151-  
 433 157, 2005.
- 434 3. Anderson J., Imran S., Frost H.R., Azzopardi K.I., Jalali S., Novakovic B., Osowicki J., Steer A.C.,  
 435 Licciardi P.V. and Pellicci D.G. Immune signature of acute pharyngitis in a *Streptococcus*  
 436 *pyogenes* human challenge trial. *Nature Communications* 13(1):769, 2022.
- 437 4. Antonopoulos C., El Sanadi C., Kaiser W.J., Mocarski E.S. and Dubyak G.R. Proapoptotic  
 438 Chemotherapeutic Drugs Induce Noncanonical Processing and Release of IL-1 $\beta$  via Caspase-8  
 439 in Dendritic Cells. *The Journal of Immunology* 191(9):4789-4803, 2013.
- 440 5. Ato M., Ikebe T., Kawabata H., Takemori T. and Watanabe H. Incompetence of Neutrophils to  
 441 Invasive Group A streptococcus Is Attributed to Induction of Plural Virulence Factors by  
 442 Dysfunction of a Regulator. *PLOS ONE* 3(10):e3455, 2008.
- 443 6. Aziz R.K., Pabst M.J., Jeng A., Kansal R., Low D.E., Nizet V. and Kotb M. Invasive M1T1 group A  
 444 *Streptococcus* undergoes a phase-shift in vivo to prevent proteolytic degradation of multiple  
 445 virulence factors by SpeB. *Molecular Microbiology* 51(1):123-134, 2004.
- 446 7. Bisno A.L. and Stevens D.L. *Streptococcal Infections of Skin and Soft Tissues*. *New England*  
 447 *Journal of Medicine* 334(4):240-246, 1996.
- 448 8. Blankenburg S., Hentschker C., Nagel A., Hildebrandt P., Michalik S., Dittmar D., Surmann K.  
 449 and Volker U. Improving Proteome Coverage for Small Sample Amounts: An Advanced Method  
 450 for Proteomics Approaches with Low Bacterial Cell Numbers. *Proteomics* 19(23):e1900192,  
 451 2019.
- 452 9. Bossaller L., Chiang P.-I., Schmidt-Lauber C., Ganesan S., Kaiser W.J., Rathinam V.A.K., Mocarski  
 453 E.S., Subramanian D., Green D.R., Silverman N., Fitzgerald K.A., Marshak-Rothstein A. and Latz  
 454 E. Cutting Edge: FAS (CD95) Mediates Noncanonical IL-1 $\beta$  and IL-18 Maturation via Caspase-8  
 455 in an RIP3-Independent Manner. *The Journal of Immunology* 189(12):5508-5512, 2012.
- 456 10. Bruun T., Kittang B.R., de Hoog B.J., Aardal S., Flaatten H.K., Langeland N., Mylvaganam H.,  
 457 Vindenes H.A. and Skrede S. Necrotizing soft tissue infections caused by *Streptococcus*  
 458 *pyogenes* and *Streptococcus dysgalactiae* subsp. *equisimilis* of  
 459 groups C and G in western Norway. *Clinical Microbiology and Infection* 19(12):E545-E550,  
 460 2013.
- 461 11. Bruun T., Rath E., Madsen M.B., Oppegaard O., Nekludov M., Arnell P., Karlsson Y., Babbar A.,  
 462 Bergey F., Itzek A., Hyldegaard O., Norrby-Teglund A., Skrede S. and Group I.S. Risk Factors and  
 463 Predictors of Mortality in Streptococcal Necrotizing Soft-tissue Infections: A Multicenter  
 464 Prospective Study. *Clinical Infectious Diseases* 72(2):293-300, 2020.
- 465 12. Carapetis J.R., Steer A.C., Mulholland E.K. and Weber M. The global burden of group A  
 466 streptococcal diseases. *The Lancet Infectious Diseases* 5(11):685-694, 2005.
- 467 13. Chella Krishnan K., Mukundan S., Alagarsamy J., Hur J., Nookala S., Siemens N., Svensson M.,  
 468 Hyldegaard O., Norrby-Teglund A. and Kotb M. Genetic Architecture of Group A Streptococcal  
 469 Necrotizing Soft Tissue Infections in the Mouse. *PLoS Pathog* 12(7):e1005732, 2016.
- 470 14. Cole J.N., Pence M.A., Köckritz-Blickwede M.v., Hollands A., Gallo R.L., Walker M.J. and Nizet  
 471 V. M Protein and Hyaluronic Acid Capsule Are Essential for *In Vivo* Selection of  
 472 *covRS* Mutations Characteristic of Invasive Serotype M1T1 Group A  
 473 *Streptococcus*. *mBio* 1(4):10.1128/mbio.00191-00110, 2010.
- 474 15. Cortés G. and Wessels M.R. Inhibition of Dendritic Cell Maturation by Group A *Streptococcus*.  
 475 *The Journal of Infectious Diseases* 200(7):1152-1161, 2009.

- 476 16. Cuypers F., Klabunde B., Gesell Salazar M., Surabhi S., Skorka S.B., Burchhardt G., Michalik S.,  
477 Thiele T., Rohde M., Volker U., Hammerschmidt S. and Siemens N. Adenosine Triphosphate  
478 Neutralizes Pneumolysin-Induced Neutrophil Activation. *J Infect Dis* 222(10):1702-1712, 2020.
- 479 17. Dalton T.L., Hobb R.I. and Scott J.R. Analysis of the role of CovR and CovS in the dissemination  
480 of *Streptococcus pyogenes* in invasive skin disease. *Microbial Pathogenesis* 40(5):221-227,  
481 2006.
- 482 18. Dalton T.L. and Scott J.R. CovS Inactivates CovR and Is Required for Growth under Conditions  
483 of General Stress in *Streptococcus pyogenes*. *Journal of Bacteriology* 186(12):3928-  
484 3937, 2004.
- 485 19. Emgård J., Bergsten H., McCormick J.K., Barrantes I., Skrede S., Sandberg J.K. and Norrby-  
486 Teglund A. MAIT Cells Are Major Contributors to the Cytokine Response in Group A  
487 Streptococcal Toxic Shock Syndrome. *Proceedings of the National Academy of Sciences*  
488 116(51):25923-25931, 2019.
- 489 20. Engleberg N.C., Heath A., Miller A., Rivera C. and DiRita V.J. Spontaneous Mutations in the  
490 CsrRS Two-Component Regulatory System of *Streptococcus pyogenes* Result in Enhanced  
491 Virulence in a Murine Model of Skin and Soft Tissue Infection. *The Journal of Infectious*  
492 *Diseases* 183(7):1043-1054, 2001.
- 493 21. Gaidt M.M. and Hornung V. Alternative inflammasome activation enables IL-1 $\beta$  release from  
494 living cells. *Current Opinion in Immunology* 44:7-13, 2017.
- 495 22. Gringhuis S.I., Kaptein T.M., Wevers B.A., Theelen B., van der Vlist M., Boekhout T. and  
496 Geijtenbeek T.B.H. Dectin-1 is an extracellular pathogen sensor for the induction and  
497 processing of IL-1 $\beta$  via a noncanonical caspase-8 inflammasome. *Nature Immunology*  
498 13(3):246-254, 2012.
- 499 23. Hatscher L., Amon L., Heger L. and Dudziak D. Inflammasomes in dendritic cells: Friend or foe?  
500 *Immunology Letters* 234:16-32, 2021.
- 501 24. Hollands A., Pence M.A., Timmer A.M., Osvath S.R., Turnbull L., Whitchurch C.B., Walker M.J.  
502 and Nizet V. Genetic Switch to Hypervirulence Reduces Colonization Phenotypes of the  
503 Globally Disseminated Group A *Streptococcus* M1T1 Clone. *The Journal of Infectious Diseases*  
504 202(1):11-19, 2010.
- 505 25. Horstmann N., Tran C.N., Brumlow C., DebRoy S., Yao H., Noguera Gonzalez G., Makthal N.,  
506 Kumaraswami M. and Shelburne S.A. Phosphatase activity of the control of virulence sensor  
507 kinase CovS is critical for the pathogenesis of group A streptococcus. *PLOS Pathogens*  
508 14(10):e1007354, 2018.
- 509 26. Ikebe T., Ato M., Matsumura T., Hasegawa H., Sata T., Kobayashi K. and Watanabe H. Highly  
510 Frequent Mutations in Negative Regulators of Multiple Virulence Genes in Group A  
511 Streptococcal Toxic Shock Syndrome Isolates. *PLOS Pathogens* 6(4):e1000832, 2010.
- 512 27. Johansson L., Thulin P., Sendi P., Hertzén E., Linder A., Åkesson P., Low D.E., Agerberth B. and  
513 Norrby-Teglund A. Cathelicidin LL-37 in Severe *Streptococcus pyogenes* Soft Tissue  
514 Infections in Humans. *Infection and Immunity* 76(8):3399-3404, 2008.
- 515 28. Johnson A.F., Sands J.S., Trivedi K.M., Russell R., LaRock D.L. and LaRock C.N. Constitutive  
516 secretion of pro-IL-18 allows keratinocytes to initiate inflammation during bacterial infection.  
517 *PLOS Pathogens* 19(4):e1011321, 2023.
- 518 29. Jumper J., Evans R., Pritzel A., Green T., Figurnov M., Ronneberger O., Tunyasuvunakool K.,  
519 Bates R., Zidek A., Potapenko A., Bridgland A., Meyer C., Kohl S.A.A., Ballard A.J., Cowie A.,  
520 Romera-Paredes B., Nikolov S., Jain R., Adler J., Back T., Petersen S., Reiman D., Clancy E.,  
521 Zielinski M., Steinegger M., Pacholska M., Berghammer T., Bodenstein S., Silver D., Vinyals O.,  
522 Senior A.W., Kavukcuoglu K., Kohli P. and Hassabis D. Highly accurate protein structure  
523 prediction with AlphaFold. *Nature* 596(7873):583-589, 2021.
- 524 30. Jumper J. and Hassabis D. Protein structure predictions to atomic accuracy with AlphaFold. *Nat*  
525 *Methods* 19(1):11-12, 2022.
- 526 31. Kansal R.G., Datta V., Aziz R.K., Abdeltawab N.F., Rowe S. and Kotb M. Dissection of the  
527 Molecular Basis for Hypervirulence of an In Vivo—Selected Phenotype of the Widely

- 528 Disseminated M1T1 Strain of Group A Streptococcus Bacteria. *The Journal of Infectious*  
529 *Diseases* 201(6):855-865, 2010.
- 530 32. Kansal Rita G., McGeer A., Low Donald E., Norrby-Teglund A. and Kotb M. Inverse Relation  
531 between Disease Severity and Expression of the Streptococcal Cysteine Protease, SpeB, among  
532 Clonal M1T1 Isolates Recovered from Invasive Group A Streptococcal Infection Cases. *Infection*  
533 *and Immunity* 68(11):6362-6369, 2000.
- 534 33. Kaul R., McGeer A., Low D.E., Green K., Schwartz B. and Simor A.E. Population-Based  
535 Surveillance for Group A Streptococcal Necrotizing Fasciitis: Clinical Features, Prognostic  
536 Indicators, and Microbiologic Analysis of Seventy-Seven Cases. *The American Journal of*  
537 *Medicine* 103(1):18-24, 1997.
- 538 34. Keller N., Woytschak J., Heeb L.E.M., Marques Maggio E., Mairpady Shambat S., Snall J.,  
539 Hyldegaard O., Boyman O., Norrby-Teglund A. and Zinkernagel A.S. Group A Streptococcal  
540 DNase Sda1 Impairs Plasmacytoid Dendritic Cells' Type 1 Interferon Response. *J Invest*  
541 *Dermatol* 139(6):1284-1293, 2019.
- 542 35. Langshaw Emma L., Reynolds S., Ozberk V., Dooley J., Calcutt A., Zaman M., Walker Mark J.,  
543 Batzloff Michael R., Davies Mark R., Good Michael F. and Pandey M. Streptolysin O Deficiency  
544 in *Streptococcus pyogenes* M1T1 covR/S Mutant Strain Attenuates Virulence in In Vitro and In  
545 Vivo Infection Models. *mBio* 14(1):e03488-03422, 2023.
- 546 36. LaRock C.N., Todd J., LaRock D.L., Olson J., O'Donoghue A.J., Robertson A.A.B., Cooper M.A.,  
547 Hoffman H.M. and Nizet V. IL-1 $\beta$  is an innate immune sensor of microbial proteolysis. *Science*  
548 *Immunology* 1(2):eaah3539-eaah3539, 2016.
- 549 37. Lauth X., von Köckritz-Blickwede M., McNamara C.W., Myskowski S., Zinkernagel A.S., Beall B.,  
550 Ghosh P., Gallo R.L. and Nizet V. M1 Protein Allows Group A Streptococcal Survival in  
551 Phagocyte Extracellular Traps through Cathelicidin Inhibition. *Journal of Innate Immunity*  
552 1(3):202-214, 2009.
- 553 38. Loof T.G., Rohde M., Chhatwal G.S., Jung S. and Medina E. The Contribution of Dendritic Cells  
554 to Host Defenses against *Streptococcus pyogenes*. *The Journal of Infectious Diseases*  
555 196(12):1794-1803, 2007.
- 556 39. Madsen M.B., Skrede S., Perner A., Arnell P., Nekludov M., Bruun T., Karlsson Y., Hansen M.B.,  
557 Polzik P., Hedetoft M., Rosén A., Saccenti E., Bergey F., Martins dos Santos V.A.P., Bidstrup D.,  
558 Bærnthsen N.F., Frendø G.H., Jansen E.C., Madsen L.B., Müller R.B., Pedersen E.M.J., Petersen  
559 M.W., Ravn F., Smidt-Nielsen I.F.G., Wahl A.M., Wulffeld S., Aronsson S., Rosemar A., Trogen  
560 J., Nedrebø T., Oppegaard O., Rath E., Sævik M., Norrby-Teglund A., Hyldegaard O. and group  
561 I.s. Patient's characteristics and outcomes in necrotising soft-tissue infections: results from a  
562 Scandinavian, multicentre, prospective cohort study. *Intensive Care Medicine* 45(9):1241-  
563 1251, 2019.
- 564 40. Maelfait J., Vercammen E., Janssens S., Schotte P., Haegman M., Magez S. and Beyaert R.  
565 Stimulation of Toll-like receptor 3 and 4 induces interleukin-1 $\beta$  maturation by caspase-8.  
566 *Journal of Experimental Medicine* 205(9):1967-1973, 2008.
- 567 41. Mellman I. Dendritic Cells: Master Regulators of the Immune Response. *Cancer Immunology*  
568 *Research* 1(3):145-149, 2013.
- 569 42. Mover E., Bolarin J.S., Valfridsson C., Velarde J., Skrede S., Nekludov M., Hyldegaard O., Arnell  
570 P., Svensson M., Norrby-Teglund A., Cho K.H., Elhaik E., Wessels M.R., Råberg L. and Carlsson  
571 F. Interplay between human STING genotype and bacterial NADase activity regulates inter-  
572 individual disease variability. *Nature Communications* 14(1):4008, 2023.
- 573 43. Nakanishi K., Yoshimoto T., Tsutsui H. and Okamura H. Interleukin-18 Regulates Both Th1 and  
574 Th2 Responses. *Annual Review of Immunology* 19(1):423-474, 2001.
- 575 44. Norrby-Teglund A., Thulin P., Gan B.S., Kotb M., McGeer A., Andersson J. and Low D.E. Evidence  
576 for Superantigen Involvement in Severe Group A Streptococcal Tissue Infections. *The Journal*  
577 *of Infectious Diseases* 184(7):853-860, 2001.
- 578 45. Nozawa T., Iibushi J., Toh H., Minowa-Nozawa A., Murase K., Aikawa C. and Nakagawa I.  
579 Intracellular Group A Streptococcus Induces Golgi Fragmentation To Impair Host Defenses

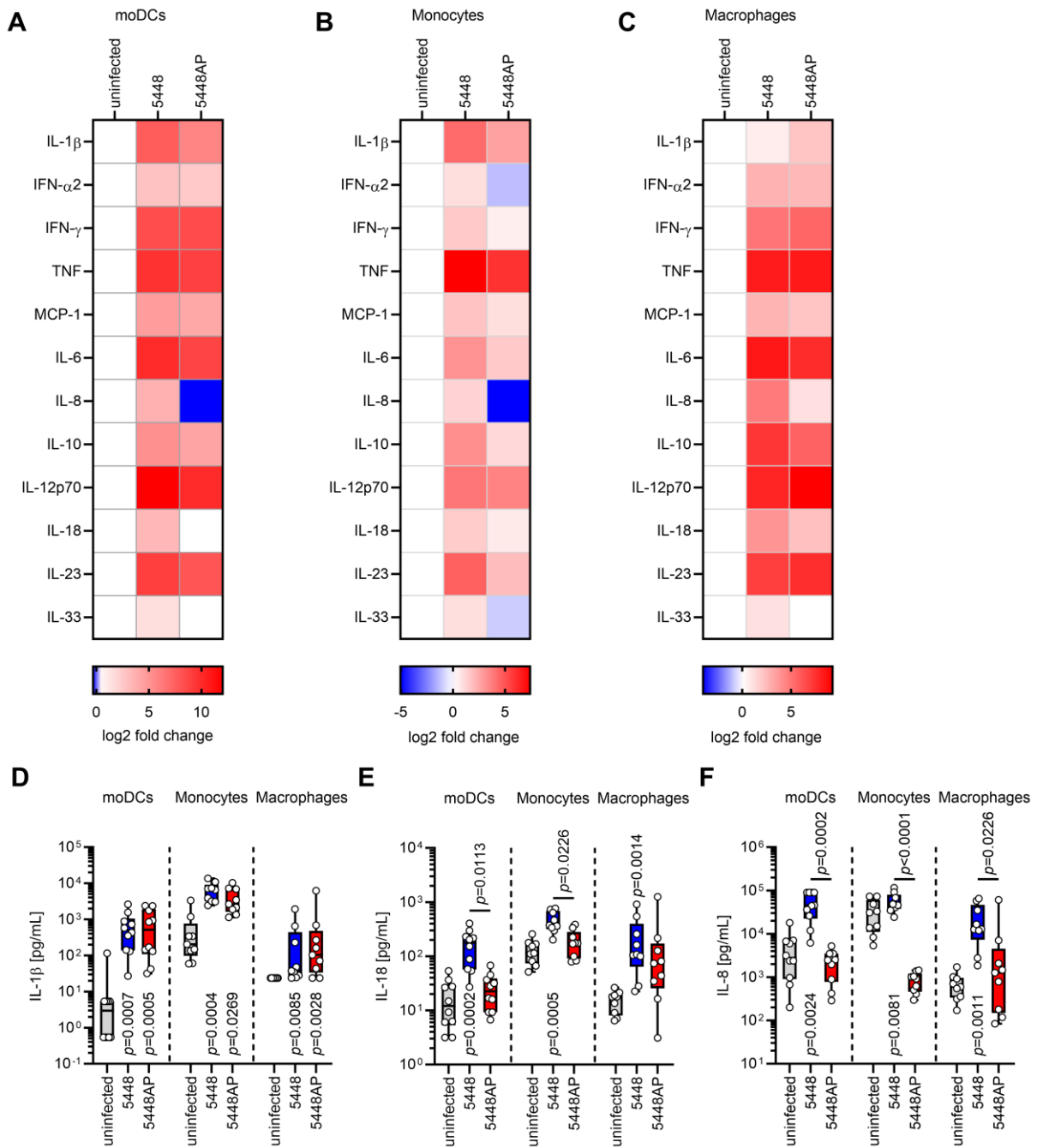
- 580 through Streptolysin O and NAD-Glycohydrolase. *mBio* 12(1):10.1128/mbio.01974-01920,  
581 2021.
- 582 46. Palma Medina L.M., Rath E., Jahagirdar S., Bruun T., Madsen M.B., Stralin K., Unge C., Hansen  
583 M.B., Arnell P., Nekludov M., Hyldegaard O., Lourda M., Santos V., Saccenti E., Skrede S.,  
584 Svensson M. and Norrby-Teglund A. Discriminatory plasma biomarkers predict specific clinical  
585 phenotypes of necrotizing soft-tissue infections. *J Clin Invest* 131(14), 2021.
- 586 47. Plainvert C., Rosinski-Chupin I., Weckel A., Lambert C., Touak G., Sauvage E., Poyart C., Glaser  
587 P. and Fouet A. A Novel CovS Variant Harbored by a Colonization Strain Reduces *Streptococcus*  
588 *pyogenes* Virulence. *Journal of Bacteriology* 205(4):e00039-00023, 2023.
- 589 48. Ren H., Yang H., Yang X., Zhang G., Rong X., Huang J., Zhang L., Fu Y., Allain J.-P., Li C. and Wang  
590 W. *Brucella* Outer Membrane Lipoproteins 19 and 16 Differentially Induce Interleukin-18  
591 Response or Pyroptosis in Human Monocytic Cells. *The Journal of Infectious Diseases*  
592 224(12):2148-2159, 2021.
- 593 49. Sedimbi S.K., Hägglöf T. and Karlsson M.C.I. IL-18 in inflammatory and autoimmune disease.  
594 *Cellular and Molecular Life Sciences* 70(24):4795-4808, 2013.
- 595 50. Seyednasrollah F., Rantanen K., Jaakkola P. and Elo L.L. ROTS: reproducible RNA-seq biomarker  
596 detector-prognostic markers for clear cell renal cell cancer. *Nucleic Acids Res* 44(1):e1, 2016.
- 597 51. Shumba P., Sura T., Moll K., Chakrakodi B., Tolken L.A., Hossmann J., Hoff K.J., Hyldegaard O.,  
598 Nekludov M., Svensson M., Arnell P., Skrede S., Group I.S., Norrby-Teglund A. and Siemens N.  
599 Neutrophil-derived reactive agents induce a transient SpeB negative phenotype in  
600 *Streptococcus pyogenes*. *J Biomed Sci* 30(1):52, 2023.
- 601 52. Siemens N., Chakrakodi B., Shambat S.M., Morgan M., Bergsten H., Hyldegaard O., Skrede S.,  
602 Arnell P., Madsen M.B., Johansson L., Group I.S., Juarez J., Bosnjak L., Morgelin M., Svensson  
603 M. and Norrby-Teglund A. Biofilm in group A streptococcal necrotizing soft tissue infections.  
604 *JCI Insight* 1(10):e87882, 2016.
- 605 53. Soderholm A.T., Barnett T.C., Korn O., Rivera-Hernandez T., Seymour L.M., Schulz B.L., Nizet  
606 V., Wells C.A., Sweet M.J. and Walker M.J. Group A *Streptococcus* M1T1 Intracellular Infection  
607 of Primary Tonsil Epithelial Cells Dampens Levels of Secreted IL-8 Through the Action of  
608 SpyCEP. *Frontiers in Cellular and Infection Microbiology* 8, 2018.
- 609 54. Steinman R.M. and Banchereau J. Taking dendritic cells into medicine. *Nature* 449(7161):419-  
610 426, 2007.
- 611 55. Steinman R.M. and Nussenzweig M.C. Avoiding horror autotoxicus: The importance of  
612 dendritic cells in peripheral T cell tolerance. *Proceedings of the National Academy of Sciences*  
613 99(1):351-358, 2002.
- 614 56. Stevens D.L. and Bryant A.E. Necrotizing Soft-Tissue Infections. *New England Journal of*  
615 *Medicine* 377(23):2253-2265, 2017.
- 616 57. Sumbly P., Porcella S.F., Madrigal A.G., Barbian K.D., Virtaneva K., Ricklefs S.M., Sturdevant D.E.,  
617 Graham M.R., Vuopio-Varkila J., Hoe N.P. and Musser J.M. Evolutionary Origin and Emergence  
618 of a Highly Successful Clone of Serotype M1 Group A *Streptococcus* Involved Multiple  
619 Horizontal Gene Transfer Events. *The Journal of Infectious Diseases* 192(5):771-782, 2005.
- 620 58. Sumbly P., Whitney A.R., Graviss E.A., DeLeo F.R. and Musser J.M. Genome-Wide Analysis of  
621 Group A *Streptococci* Reveals a Mutation That Modulates Global Phenotype and Disease  
622 Specificity. *PLOS Pathogens* 2(1):e5, 2006.
- 623 59. Suomi T. and Elo L.L. Enhanced differential expression statistics for data-independent  
624 acquisition proteomics. *Sci Rep* 7(1):5869, 2017.
- 625 60. Thänert R., Itzek A., Hoßmann J., Hamisch D., Madsen M.B., Hyldegaard O., Skrede S., Bruun  
626 T., Norrby-Teglund A., Oppegaard O., Rath E., Nedrebø T., Arnell P., Rosen A., Polzik P., Hansen  
627 M.B., Svensson M., Snäll J., Karlsson Y., Nekludov M., Medina E., Pieper D.H. and group I.S.  
628 Molecular profiling of tissue biopsies reveals unique signatures associated with streptococcal  
629 necrotizing soft tissue infections. *Nature Communications* 10(1):3846, 2019.
- 630 61. Timmer A.M., Timmer J.C., Pence M.A., Hsu L.-C., Ghochani M., Frey T.G., Karin M., Salvesen  
631 G.S. and Nizet V. Streptolysin O Promotes Group A *Streptococcus* Immune Evasion

- 632 by Accelerated Macrophage Apoptosis \*. *Journal of Biological Chemistry* 284(2):862-871,  
633 2009.
- 634 62. Tsatsaronis J.A., Ly D., Pupovac A., Goldmann O., Rohde M., Taylor J.M., Walker M.J., Medina  
635 E. and Sanderson-Smith M.L. Group A *Streptococcus* Modulates Host Inflammation by  
636 Manipulating Polymorphonuclear Leukocyte Cell Death Responses. *Journal of Innate Immunity*  
637 7(6):612-622, 2015.
- 638 63. Turner C.E., Kurupati P., Jones M.D., Edwards R.J. and Sriskandan S. Emerging Role of the  
639 Interleukin-8 Cleaving Enzyme SpyCEP in Clinical *Streptococcus pyogenes* Infection. *The*  
640 *Journal of Infectious Diseases* 200(4):555-563, 2009.
- 641 64. Vince James E., Wong W.W.-L., Gentle I., Lawlor Kate E., Allam R., O'Reilly L., Mason K., Gross  
642 O., Ma S., Guarda G., Anderton H., Castillo R., Häcker G., Silke J. and Tschopp J. Inhibitor of  
643 Apoptosis Proteins Limit RIP3 Kinase-Dependent Interleukin-1 Activation. *Immunity* 36(2):215-  
644 227, 2012.
- 645 65. Walker M.J., Hollands A., Sanderson-Smith M.L., Cole J.N., Kirk J.K., Henningham A., McArthur  
646 J.D., Dinkla K., Aziz R.K., Kansal R.G., Simpson A.J., Buchanan J.T., Chhatwal G.S., Kotb M. and  
647 Nizet V. DNase Sda1 provides selection pressure for a switch to invasive group A streptococcal  
648 infection. *Nature Medicine* 13(8):981-985, 2007.
- 649 66. Yasuda K., Nakanishi K. and Tsutsui H. Interleukin-18 in Health and Disease. *International*  
650 *Journal of Molecular Sciences*, 2019.
- 651 67. Zhu L., Olsen R.J., Lee J.D., Porter A.R., DeLeo F.R. and Musser J.M. Contribution of Secreted  
652 NADase and Streptolysin O to the Pathogenesis of Epidemic Serotype M1 *Streptococcus*  
653 *pyogenes* Infections. *The American Journal of Pathology* 187(3):605-613, 2017.
- 654 68. Zinkernagel A.S., Timmer A.M., Pence M.A., Locke J.B., Buchanan J.T., Turner C.E., Mishalian I.,  
655 Sriskandan S., Hanski E. and Nizet V. The IL-8 Protease SpyCEP/ScpC of Group A  
656 *Streptococcus* Promotes Resistance to Neutrophil Killing. *Cell Host & Microbe*  
657 4(2):170-178, 2008.
- 658



659

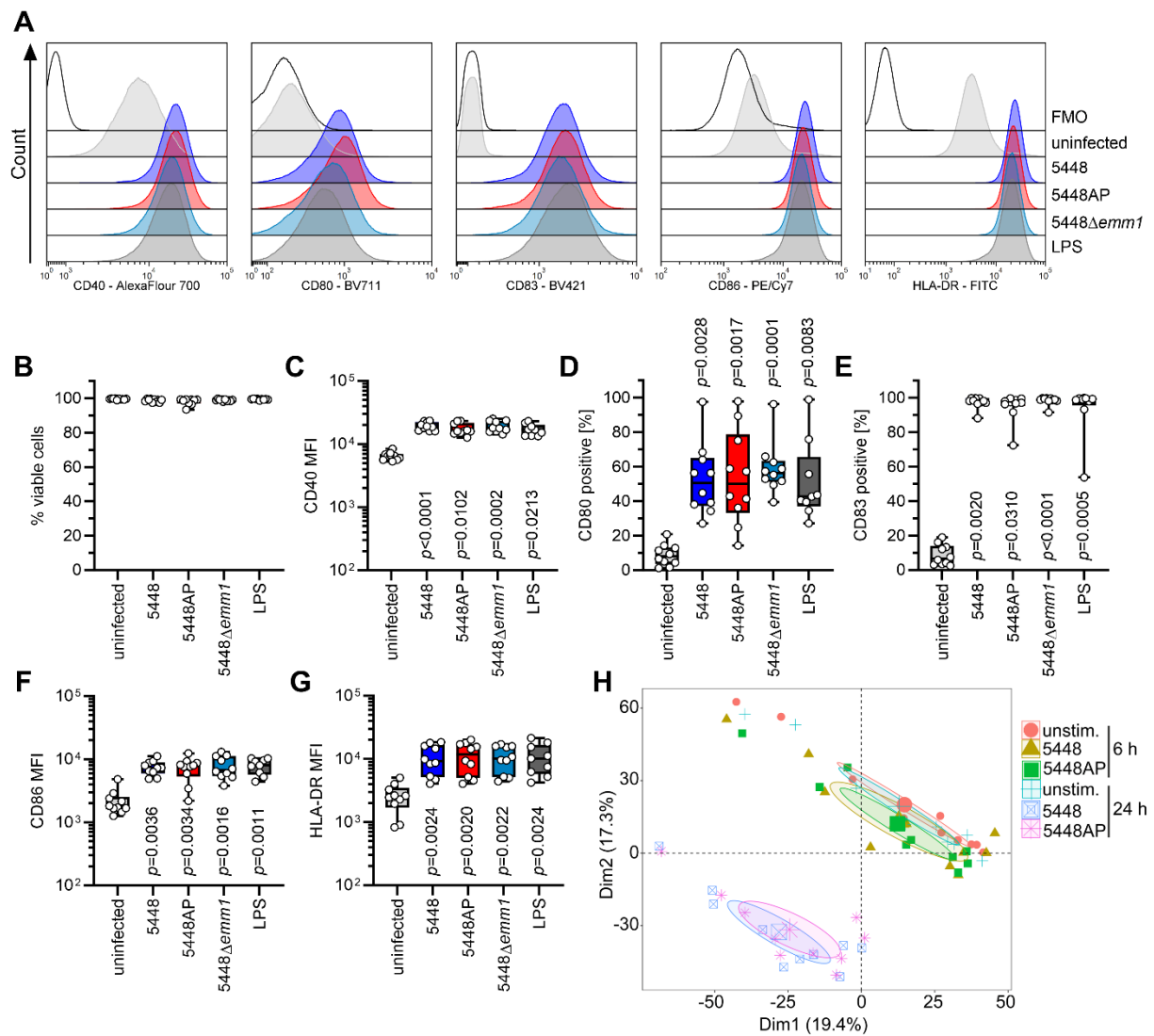
660 **Fig. 1** MoDCs infected with GAS strains harboring dysfunctional CovR/S secrete less IL-8 and IL-18.  
 661 MoDCs were infected with four strains possessing functional CovR/S (5448, 5626, 2006, 8157) or four  
 662 strains possessing non-functional CovR/S (5448AP, 2002, 5005, 8003) as assessed by sequence  
 663 analyses and SpeB proteolytic assay. The concentrations of IL-1 $\beta$  (A), IL-18 (B), and IL-8 (C) were  
 664 measured in supernatants of (un)infected moDCs. Each dot represents one independent experiment  
 665 with cells from one donor ( $n \geq 8$ ). Horizontal lines denote median values. The level of significance was  
 666 determined using Kruskal-Wallis test with Dunn's post test. Different shades of color represent infections  
 667 with different strains.



668

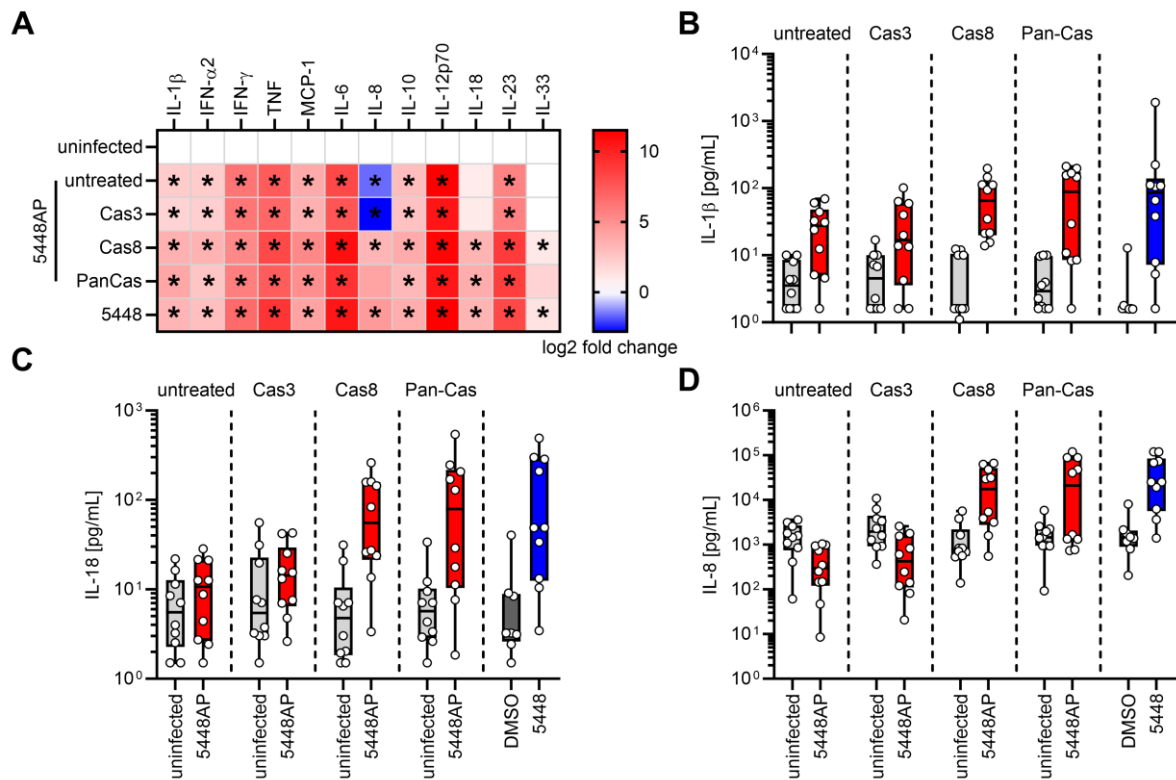
669 **Fig. 2** Monocytic cells infected with 5448AP secrete less IL-18 and IL-8. MoDCs (A), monocytes (B), or  
 670 monocyte-derived macrophages (C) were infected with 5448 or 5448AP and cytokine secretion was  
 671 measured via a multiplex assay ( $n \geq 8$ ). The heatmaps represent the log<sub>2</sub> fold change of cytokine  
 672 concentration in relation to the uninfected controls (A-C). Original data are displayed in D-F and Fig. S3.  
 673 Original data of IL-1 $\beta$  (D), IL-18 (E), and IL-8 (F) concentration in supernatants of (un)infected moDCs,  
 674 monocytes, and monocyte-derived macrophages. The data in (D-F) are displayed as box plots. Each  
 675 dot represents one independent experiment with cells from one donor ( $n \geq 8$ ). The level of significance  
 676 was determined using Kruskal-Wallis test with Dunn's posttest.





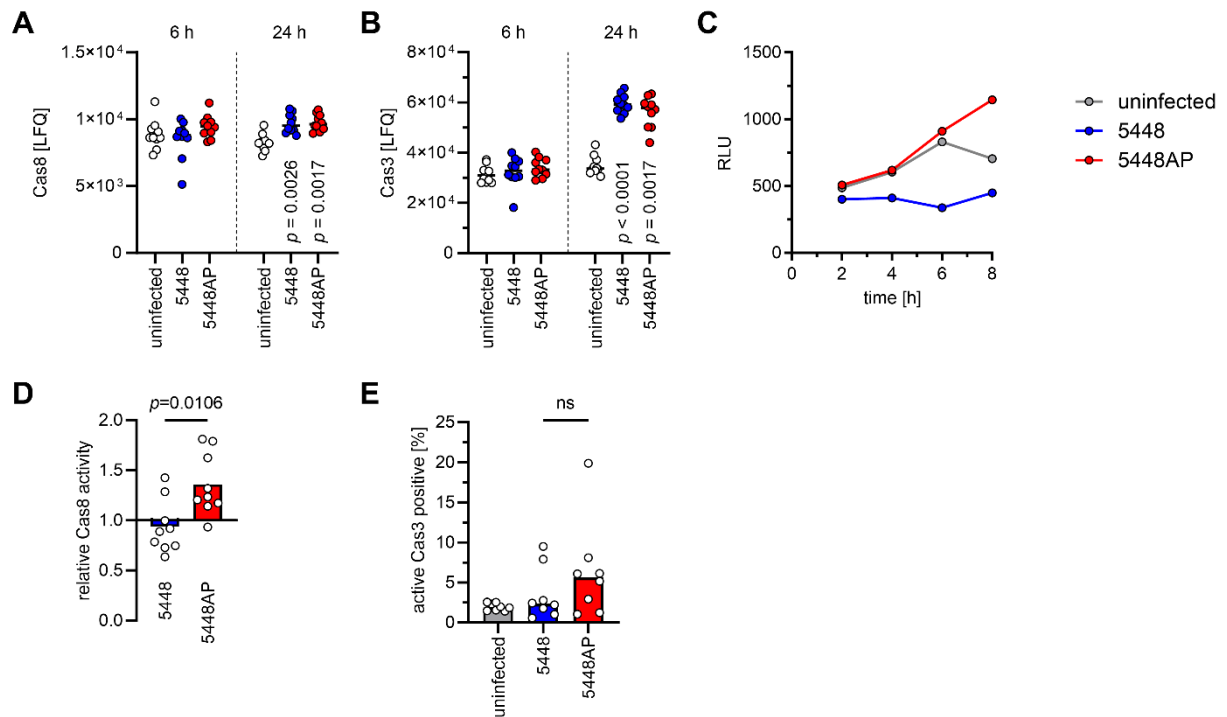
677

678 **Fig. 3** 5448AP does not impair DC maturation. MoDC were infected with 5448, 5448AP, or 5448 $\Delta$ emm1  
 679 for 1 h. Extracellular bacteria were killed by substituting the media with antibiotics for additional 23 h.  
 680 MoDC phenotype (**A**, **C-G**) and viability (**B**) were evaluated via flow cytometry. Representative  
 681 histograms for each marker are shown in (**A**). The maturation process was evaluated by assessing the  
 682 expression of CD40 (**B**), frequencies of CD80<sup>+</sup> (**D**) and CD83<sup>+</sup> (**E**) cells as well as CD86 (**F**) and HLA-  
 683 DR expression (**G**). (**H**) Principal component analysis of intracellular proteins 6 h and 24 h post infections  
 684 with indicated strains. Each dot represents one donor (n=10). The ellipses indicate the calculated 95%  
 685 probability region for a bivariate normal distribution with an average center of groups. The data in (B-G)  
 686 are displayed as box plots. Each dot represents one independent experiment with cells from one donor  
 687 (n=10). The level of significance was determined using the Kruskal-Wallis test with Dunn's posttest.  
 688 FMO, fluorescence minus one; MFI, mean fluorescence intensity.



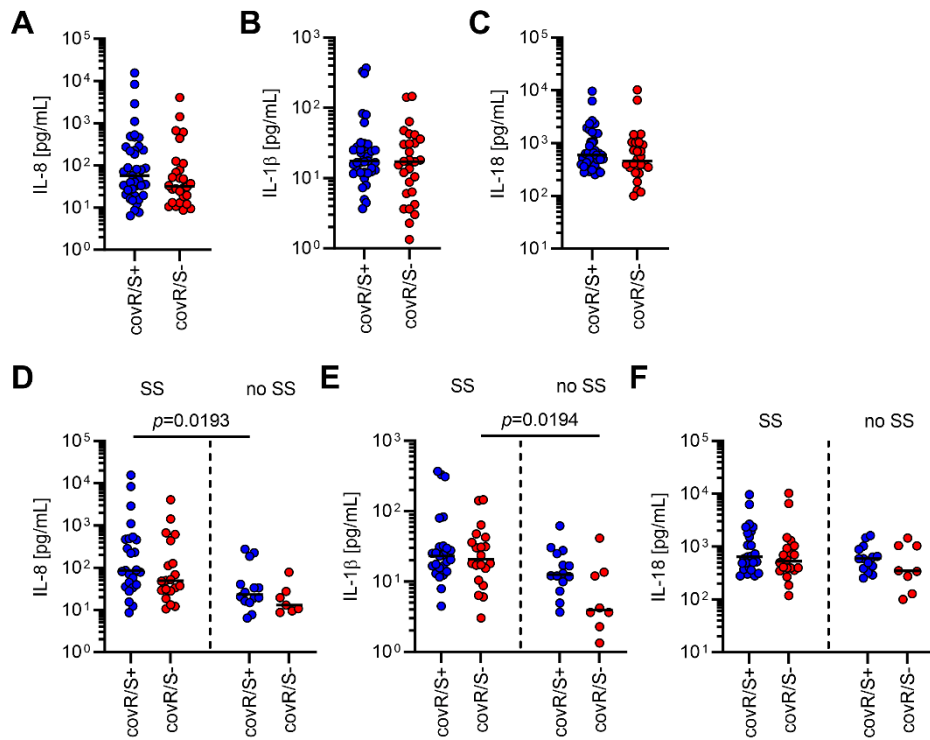
689

690 **Fig. 4** Inhibition of caspase-8 restores IL-18 and IL-8 secretion in 5448AP infections. MoDCs were  
 691 treated with caspase inhibitors (caspase-3: Cas3/7-Inhibitor I, Ac-DEVD-cho; caspase-8: z-IETD-fmk,  
 692 pan-caspase: z-VAD-fmk) and subsequently infected with 5448AP. Cytokine secretion by moDCs was  
 693 measured via a multiplex assay. **(A)** The heatmap represents the log<sub>2</sub> fold change of cytokine  
 694 concentration in relation to the respective uninfected controls. Original data are displayed in **B-D** and  
 695 Fig. S7. Original data of IL-1β **(B)**, IL-18 **(C)**, and IL-8 **(D)** concentration in supernatants of (un)infected  
 696 moDCs. The data in (B-D) are displayed as box plots. Each dot represents one independent experiment  
 697 with cells from one donor (n=10). A separate uninfected control with the respective inhibitor treatment  
 698 was performed for each 5448AP infection. Untreated: indicates 5448AP infection without inhibitors. Each  
 699 infection was compared to its respective uninfected controls. The level of significance was determined  
 700 using Mann-Whitney *U*-test. Exact statistical analysis is displayed in Table S5.



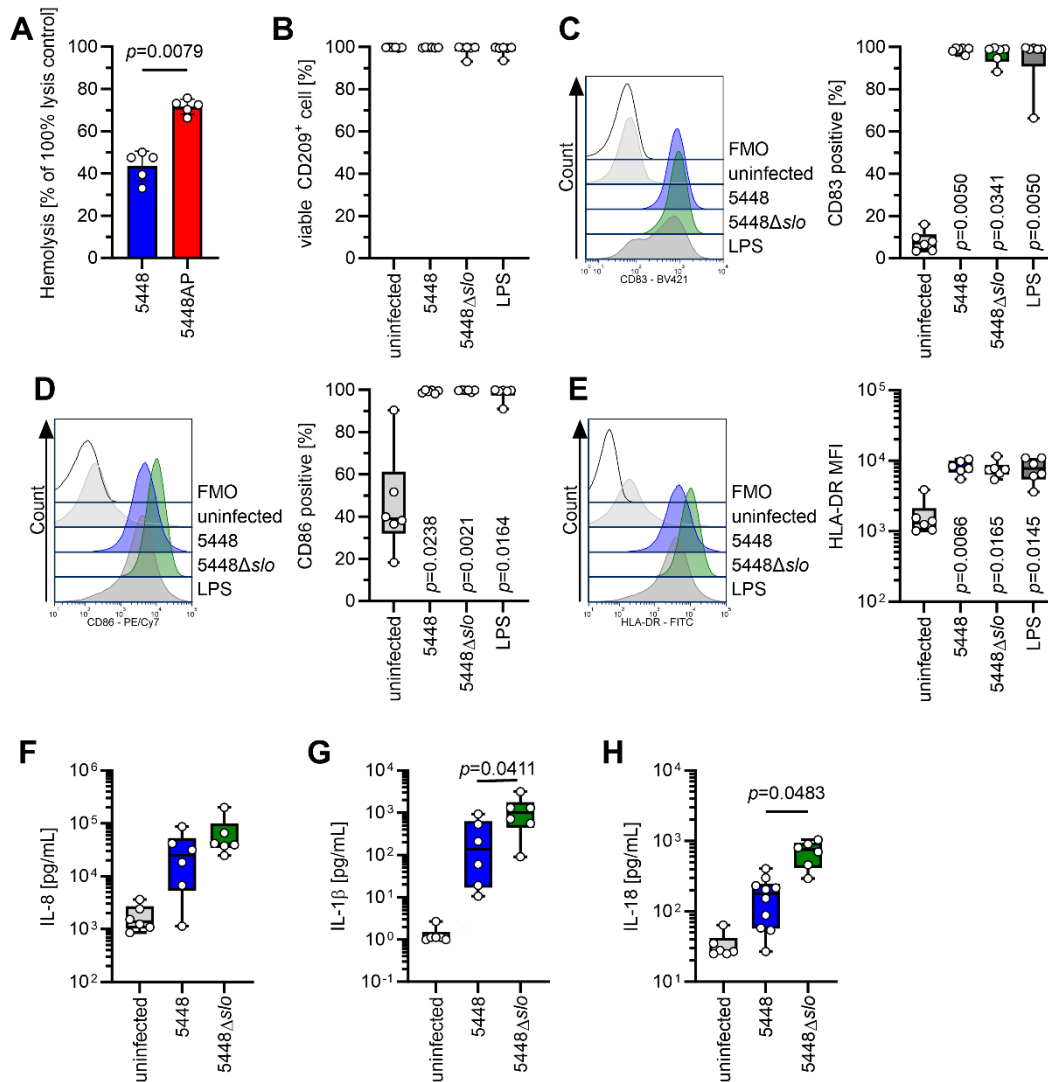
701

702 **Fig. 5** 5448AP-infected moDCs exhibit high caspase-8 activity. MoDCs were infected with 5448 or  
 703 5448AP. Relative abundance of caspase-8 (**A**) and caspase-3 (**B**) 6 h and 24 h post infection. Original  
 704 calculations are displayed in Table S3. (**C**) Caspase-8 activity of (un)infected moDCs as measured at  
 705 indicated time points by luminescence. (**D**) Relative caspase-8 activity at 8 h post infection. (**E**)  
 706 Frequencies of caspase-3<sup>+</sup> moDCs 8 h post infection. Each dot represents one independent experiment  
 707 with cells from one donor (n≥8). Horizontal lines in (A, B) denote median values. Bars in (D-E) denote  
 708 mean values. The level of significance was determined using Kruskal-Wallis test with Dunn's posttest in  
 709 (A, B, E) or Mann-Whitney *U*-test in (D). LFQ, label-free quantification intensities; RLU, relative light  
 710 units.



711

712 **Fig. 6** Cytokine/chemokine levels in plasma of NSTI patients. Levels of IL-8 (A), IL-1β (B), and IL-18 (C)  
 713 were previously determined in plasma of NSTI patients [46] and reanalyzed. Comparison of IL-8 (D), IL-  
 714 1β (E), and IL-18 (F) plasma concentrations between septic shock and no septic shock. Each dot  
 715 represents data from one patient. Horizontal lines denote median values. The level of significance was  
 716 determined using Kruskal-Wallis test with Dunn's posttest. SS, septic shock.



717

718 **Fig. 7** Knock-out of SLO in 5448 leads to elevated secretion of IL-1 $\beta$  and IL-18 by moDCs. (A) SLO  
 719 hemolytic activity in supernatants of 5448 and 5448AP strains. MoDCs were infected with 5448 or  
 720 5448 $\Delta$ s/o and moDC viability (B) and phenotype (C-E) were evaluated via flow cytometry. The  
 721 maturation process was evaluated by assessing the frequencies of CD83<sup>+</sup> (C) and CD86<sup>+</sup> (D)  
 722 as well as expression of HLA-DR (E). Representative histograms for each marker are shown in each  
 723 respective left panel. The concentrations of IL-8 (F), IL-1 $\beta$  (G), and IL-18 (H) were measured in  
 724 supernatants of (un)infected moDCs. The data in (B-H) are displayed as box plots. Each dot represents  
 725 one independent experiment with cells from one donor (n $\geq$ 6). The level of significance was determined  
 726 using Kruskal-Wallis test with Dunn's posttest. FMO, fluorescence minus one; MFI, mean fluorescence  
 727 intensity.

## Additional File 1

### Reduced interleukin-18 secretion by human monocytic cells in response to infections with hyper-virulent *Streptococcus pyogenes*

Lea A. Tölken<sup>1</sup>, Antje D. Paulikat<sup>1</sup>, Lana H. Jachmann<sup>1</sup>, Alexander Reder<sup>2</sup>, Manuela Gesell Salazar<sup>2</sup>, Laura M. Palma Medina<sup>3</sup>, Stephan Michalik<sup>2</sup>, Uwe Völker<sup>2</sup>, Mattias Svensson<sup>3</sup>, Anna Norrby-Teglund<sup>3</sup>, Katharina J. Hoff<sup>4</sup>, Michael Lammers<sup>5</sup>, and Nikolai Siemens<sup>1#</sup>

<sup>1</sup>Department of Molecular Genetics and Infection Biology, University of Greifswald, Greifswald, Germany

<sup>2</sup>Department of Functional Genomics, University Medicine Greifswald, Greifswald, Germany.

<sup>3</sup>Center for Infectious Medicine, Karolinska Institutet, Karolinska University Hospital, Huddinge, Sweden

<sup>4</sup>Institute of Mathematics and Computer Science, University of Greifswald, Greifswald, Germany

<sup>5</sup>Department of Synthetic and Structural Biochemistry, Institute of Biochemistry, University of Greifswald, Greifswald, Germany

#Correspondence: Nikolai Siemens; Email: [nikolai.siemens@uni-greifswald.de](mailto:nikolai.siemens@uni-greifswald.de)

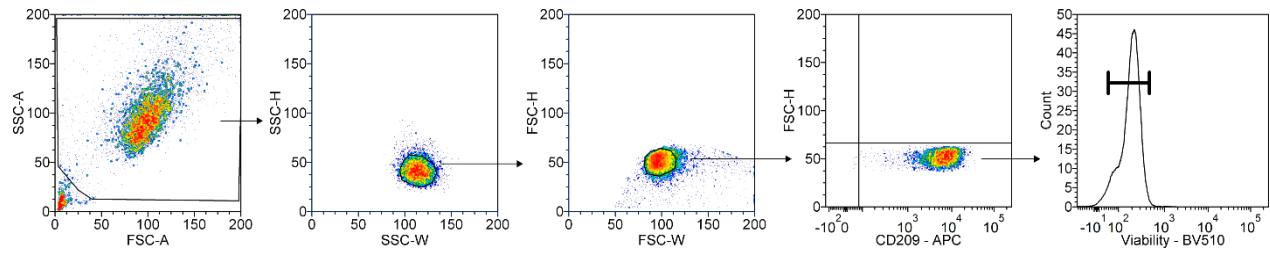


**Fig. S1** Gating strategy used to identify human moDCs. Doublets were excluded by consecutive gating of FSC-H/FSC-W and SSC-H/SSC-W. MoDCs were selected based on the expression of the specific moDC marker DC-SIGN (CD209). Dead cells were excluded by using the Zombie Aqua™ Fixable Viability Kit.

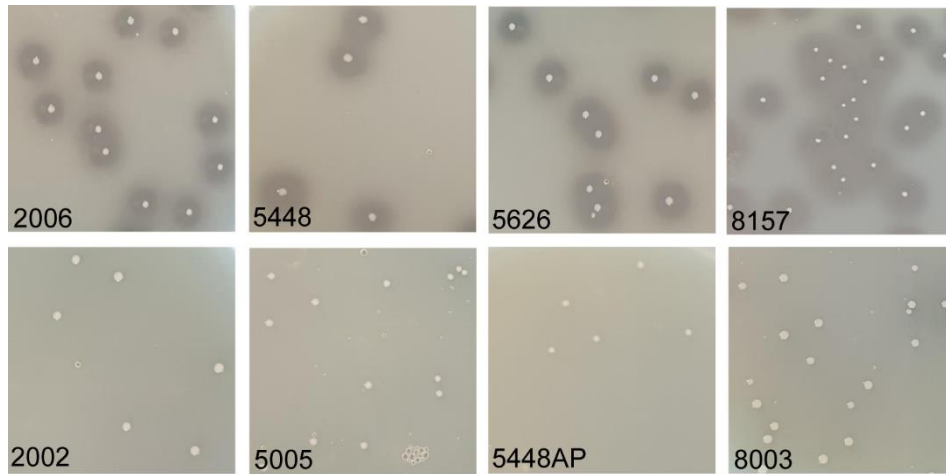


**Fig. S2** CovR/S TCS functionality as assessed via SpeB proteolytic activity on casein agar plates. Presence of hydrolysis zones around the colonies was categorized as CovR/S<sup>+</sup>. Lack of hydrolysis zones was categorized as CovR/S<sup>-</sup>.



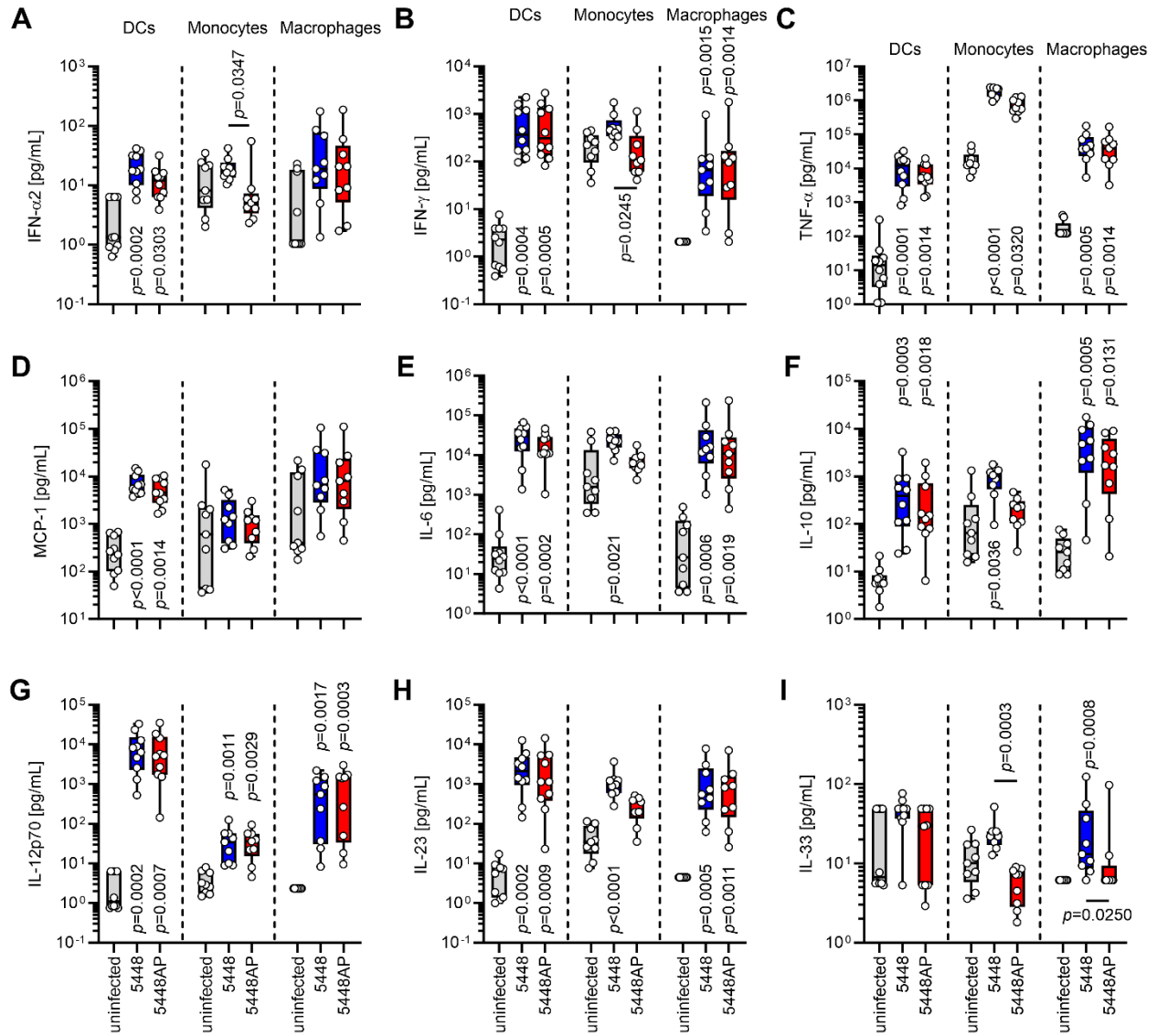


**Fig. S3** MoDCs, monocytes, or monocyte-derived macrophages were infected with 5448 or 5448AP and cytokine secretion by myeloid cells was measured via a multiplex assay ( $n \geq 8$ ). Displayed are concentrations of IFN- $\alpha$ 2 (A), IFN- $\gamma$  (B), TNF- $\alpha$  (C), MCP-1 (D), IL-6 (E), IL-10 (F), IL-12p70 (G), IL-23 (H), and IL-33 (I) in supernatants of (un)infected cells. The data are displayed as box plots. Each dot represents one independent experiment with cells from one donor ( $n \geq 8$ ). The level of significance was determined using Kruskal-Wallis test with Dunn's posttest.

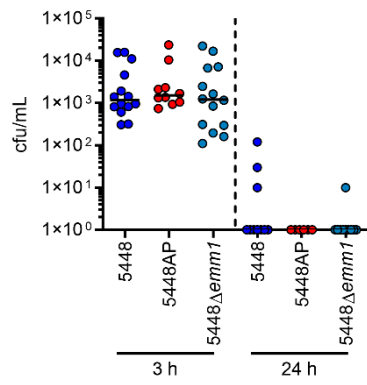


**Fig. S4** MoDCs eliminate intracellular GAS. Viable intracellular bacteria were determined at indicated time points post infections. Each dot represents one independent experiment with cells from one donor ( $n \geq 10$ ). Horizontal lines denote median value.

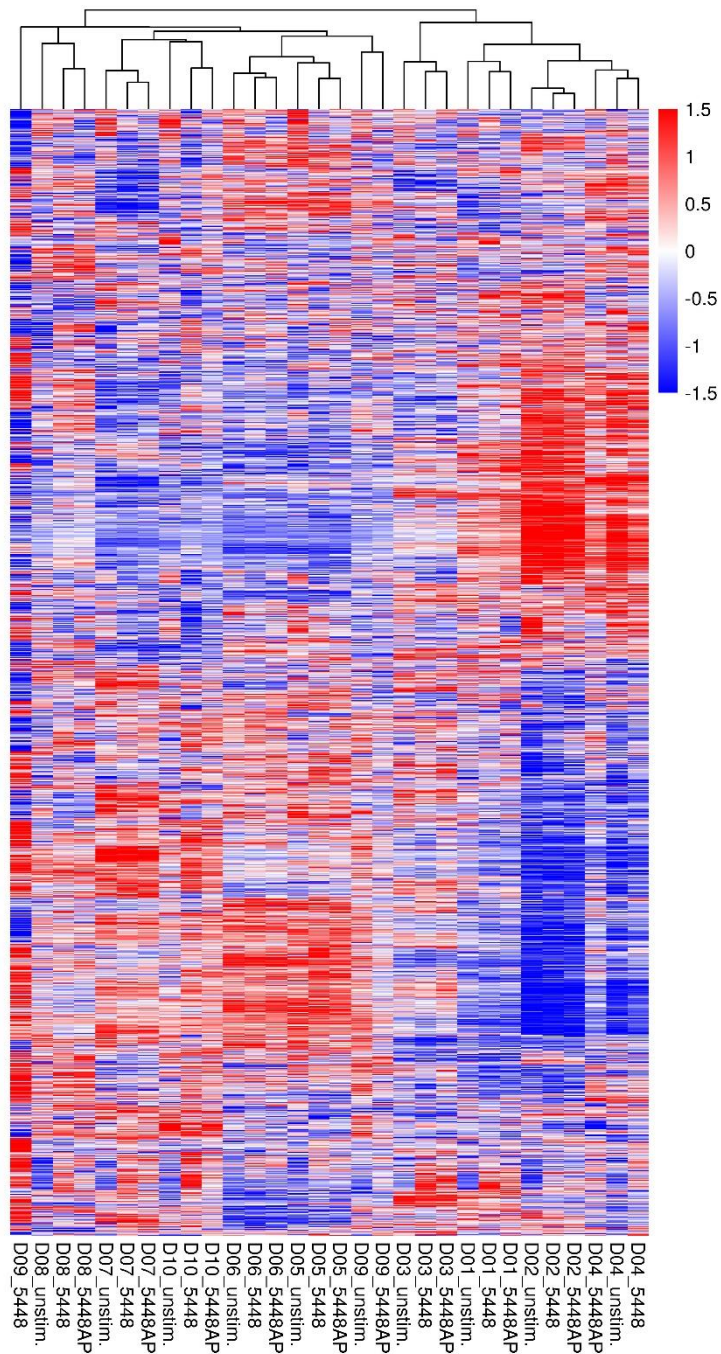


**Fig. S5** Heatmap (z-scored) depicting protein intensities (maxLFQ) in moDCs 6 h post infection. Each column represents one condition for one respective donor (n=10). In total, 5857 protein groups were identified. For quantification 4801 protein groups, identified with two or more peptides and found in 50% of the individual condition replicates, were used.



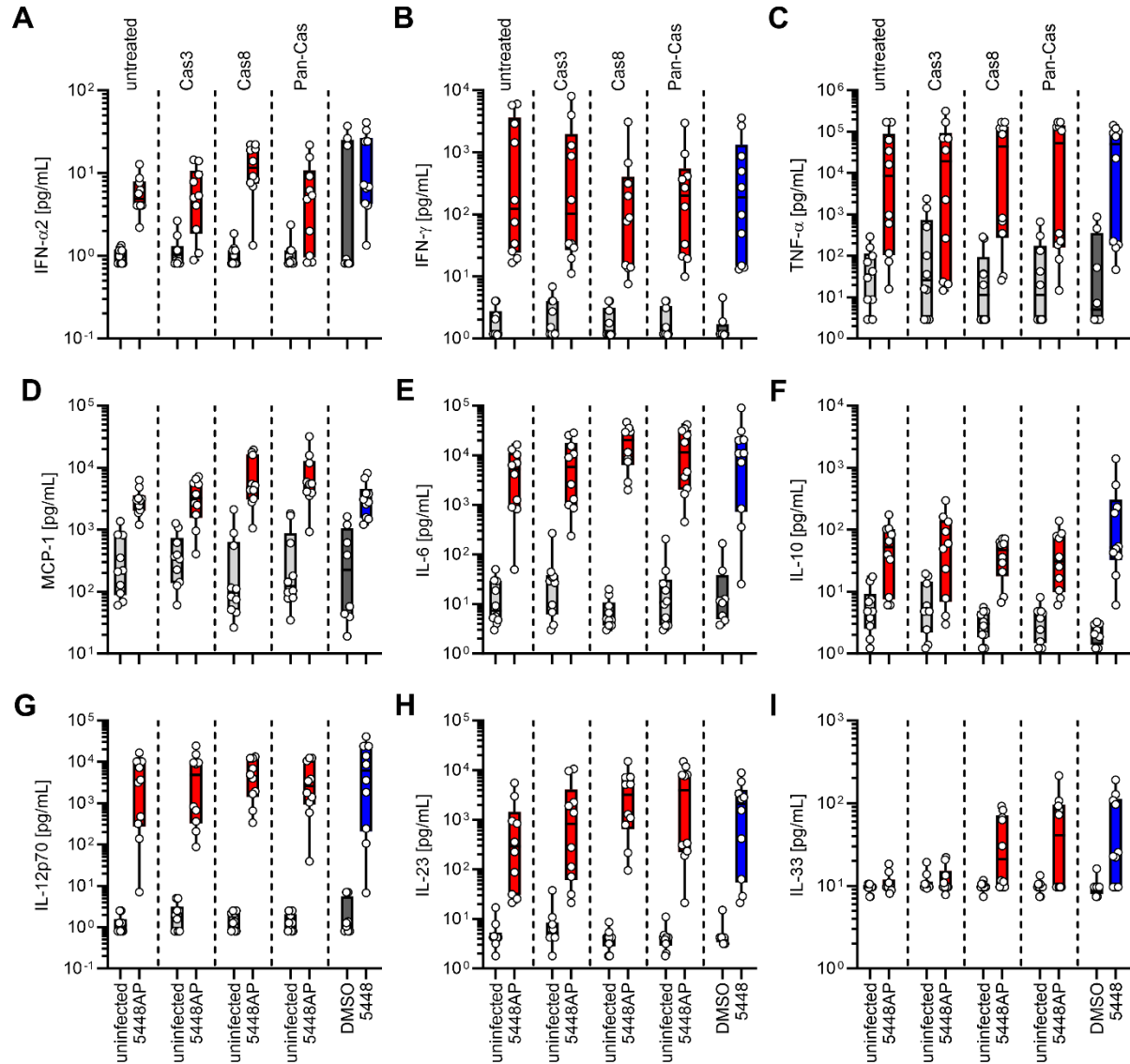


**Fig. S7** MoDCs were treated with caspase inhibitors (caspase-3: Cas3/7-Inhibitor I, Ac-DEVD-cho; caspase-8: z-IETD-fmk, pan-caspase: z-VAD-fmk) and subsequently infected with 5448AP. Cytokine secretion by moDCs was measured via a multiplex assay. The concentrations of IFN- $\alpha$ 2 (A), IFN- $\gamma$  (B), TNF- $\alpha$  (C), MCP-1 (D), IL-6 (E), IL-10 (F), IL-12p70 (G), IL-23 (H), and IL-33 (I) were measured in supernatants of (un)infected moDCs. The data are displayed as box plots. Each dot represents one independent experiment with cells from one donor ( $n=10$ ). A separate uninfected control with the respective inhibitor treatment was performed for each 5448AP infection. Untreated: indicates 5448AP infection without inhibitors. Each infection was compared to its respective uninfected controls. The level of significance was determined using Mann-Whitney U-test. Exact  $p$ -values are displayed in Table S1.



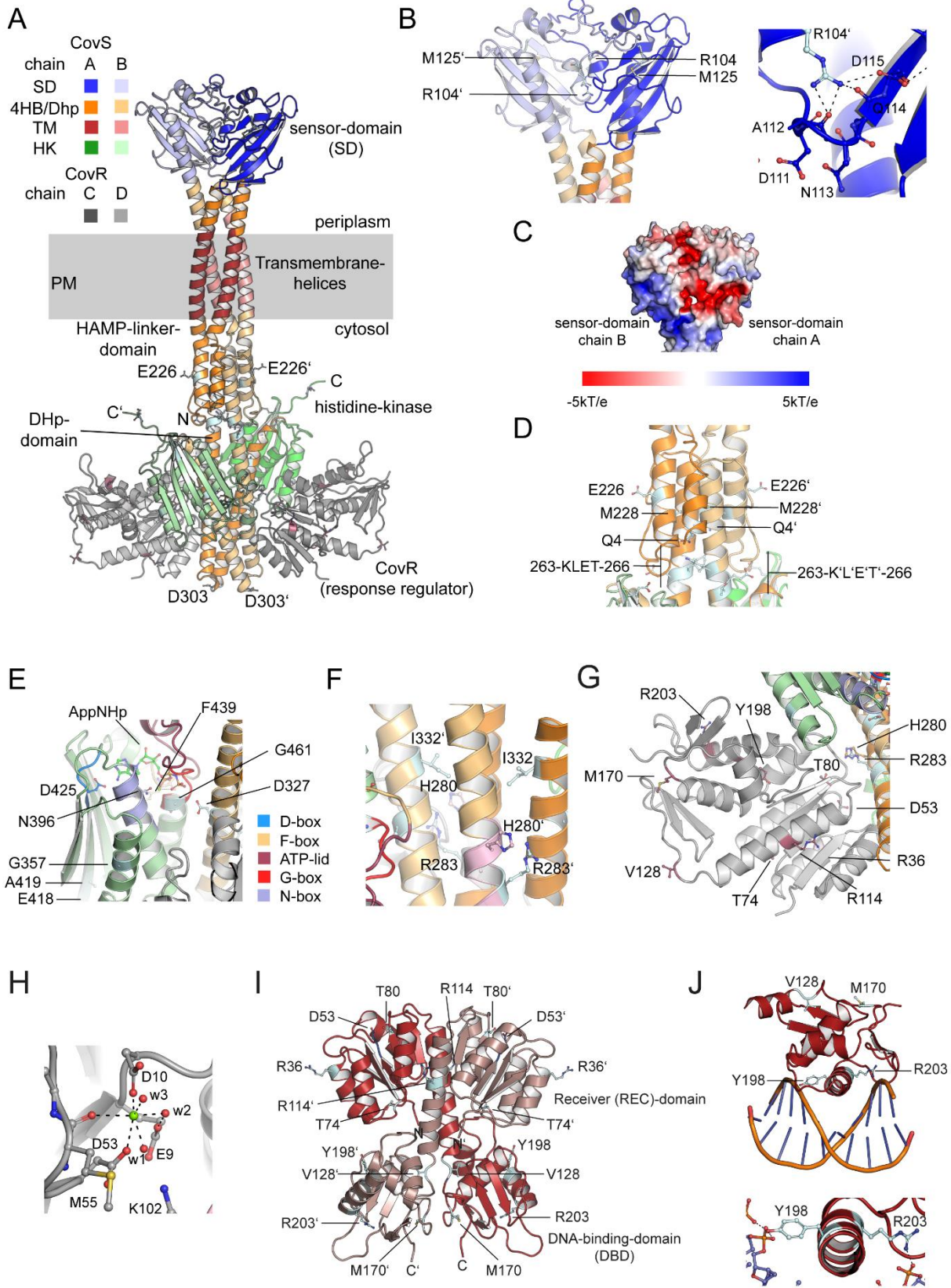


**Fig. S8: Structural analyses of the overall fold of the CovS/CovR histidine kinase response regulator complex by AlphaFold2.[5,6]**

**(A)** AlphaFold2 was used to predict the overall structure of the tetrameric CovR<sub>2</sub>•2CovS complex. As described for two-component signaling systems, the histidine kinase CovS dimerizes. It consists of a periplasmic sensor-domain (SD), a section that contains the transmembrane helices, a HAMP (histidine kinases, adenyl cyclases, methyl-accepting chemotaxis proteins and phosphatases)-linker-domain forming a four-helix bundle, a dimerization and histidine phosphotransfer (DHP)-domain containing the phosphorylated histidine residue (H280) and the histidine-kinase (HK)-domain containing the ATP-binding site. The response regulator CovR binds to the DHP-domain and HK-domain. Two molecules of CovS bind to a CovR-dimer. CovR is phosphorylated at an aspartate residue, D53, that induces dissociation from CovS to bind to the DNA. The structure shows that CovS is in a state incompatible with phosphorylation of H280 and transfer of the phosphoryl-group to D53, suggesting that activation of the sensor-domain by ligand binding, such as LL-37, or by a pH shift into the acidic range. The figure was created by PyMOL.[8]

**(B)** The sensor domain (SD) of the histidine kinase CovS dimerizes by formation of interactions of residues from chain A with residues of chain B. M125 and R104 were found to be mutated to isoleucine and histidine, respectively. Mutation of R104H would interfere with formation of several interactions. R104 from chain B/A forms an important salt bridge with the side chain of D115 of chain A/B, i.e. *in trans*, thereby interconnecting the dimer. Moreover, R104 of chain B/A forms hydrogen bonds to the main chain carbonyl of A112 and D111 of chain A/B, respectively. Asp115 is part of a large electrostatic network containing several acidic residues (right panel). The side chain of Asp115 shows an increased pK<sub>a</sub> value of 6.09 for chain A and of 5.85 for chain B, as determined by the APBS-PDB2PQR software suite.[7] This would allow alteration of the protonation state dependent of the pH and thereby to translate changes in the pH-value into altered conformations. It is postulated that CovS senses acidic shifts of the environmental pH to approximately pH 5.5. Upon protonation of the Asp115 side chains of chain A/B, formation of the salt bridge with R104 in chain B/A is abolished. This might result in alteration of the sensor-domain conformation that is further propagated into the cell, finally activating the histidine kinase activity. The impact of the mutation of M125I is less obvious. It might interfere with the conformation of the SD. The pK<sub>a</sub>-values were determined by the APBS-PDB2PQR software suite.[7] The figure was created by PyMOL.[8]

**(C)** The surface of the sensor-domain contains a strong acidic patch. The electrostatic surface potential is shown from -5kT/e (negatively charged, red) to +5kT/e (positively charged, blue). D115 of chain A is part of this acidic patch visible in this representation. The acidic patch of chain B is on the opposite surface area. The figure was created by the APBS plugin in PyMOL.[8]

**(D)** Residues that are mutated in CovS cluster at the transition from the HAMP-domain to the DHP-domain. The residues E226, M228, and Q4 were found to be mutated, and patch 163-KLET-266 was found to be deleted. This area is important to translate the extracellular activation of the sensor-domain (SD) into the activation of the histidine kinase (HK). To this end, a conformational change might be elicited that results in the rotation of the  $\alpha$ -helices of the HAMP- and DHP-domains that bring H280 located in DHP-domain in proximity to the ATP-bound to the HK-domain. Mutation of residues in this area might impair the signal-transduction from the sensor-domain to finally activate the histidine kinase. The figure was created by PyMOL.[8]

**(E)** Structural organization of the histidine kinase domain. The CovS HK-domain shows all sequence motifs essential for an active histidine kinase. The D-box contains an aspartate, i.e. D425, that directly contacts the exocyclic amino group of the adenine base at C6, thereby creating specificity for adenine nucleotides. The F-box as a central element contains F438. The ATP-lid covers the ATP-molecule. The G-box contains several glycine side chains. This sequence element contacts the  $\gamma$ - and  $\beta$ -phosphates and is similar to a P-loop described for other nucleotide binding proteins. It is needed for ATP-binding and forms an oxyanion hole to stabilize a negative charge occurring at the phosphate oxygen during catalysis. G461 within the G-box was found to be mutated to serine. This mutation might directly interfere with ATP/ADP-binding and might impair phosphoryl-group transfer. The stretch from E418 to K432 was found to be deleted. This will render the kinase inactive, as ATP/ADP-binding will be impaired and the HK-fold will be disrupted. Finally, the N-box contains a conserved asparagine, i.e. N396. N396 is involved in coordinating the bound Mg<sup>2+</sup>-ion needed for nucleotide binding and to allow the nucleophilic attack of the activated H280 for phosphoryl-group transfer. Mg<sup>2+</sup>-ATP was modelled by superimposing the CovS•CovR structure and the structure 4KP4 by PyMOL.[8] K399 of the N-box forms a salt bridge with D327 of the DHP-domain, thereby positioning the HK-domain in the conformation analyzed here. D327 within the DHP domain was found to be mutated to asparagine. Related histidine kinases have a glutamine at the analogous position. As asparagine and glutamine have similar physicochemical properties but are sterically different, an impact of CovS•CovR function cannot be excluded. Another mutation identified in the HK-domain is K498N at the C-terminus. This residue is solvent-exposed and might not directly affect CovS activity. K is a positively charged residue at physiological pH and might be important for solubility of CovS. Furthermore, lysines were known to be post-translationally modified, i.e. by lysine acetylation. Mutation of K498N would abolish this. The figure was created by PyMOL.[8].

**(F)** Closeup of the CovS DHP-domain showing position of I332 and the phosphoryl-group acceptor H280 and R283. I332 was found to be mutated to valine. Although this is an exchange of residues with similar physicochemical properties, both being hydrophobic

side chains, they are sterically different. As predicted by marcoil I332 is positioned at position "a" of the coiled-coil heptad repeat [2]. This means that it is directly involved in the formation of the interface of the coiled-coil structure. Exchange of I332 to V, therefore, might affect the coiled-coil structure. As a direct consequence this could affect the position of the phosphoryl-group acceptor H280 and E281 serving as hydrogen bond acceptor orienting and activating H280 for nucleophilic attack on the  $\beta$ -phosphate of the ATP molecule. Notably, H280 shows a strongly reduced  $pK_a$  value of 2.09 (chain A)/2.10 (Chain B) compared to the free amino acid. This shows that H280 is deprotonated in this structural environment and able to act as a strong nucleophile during catalysis. R283 is postulated to be important for phosphoryl-group transfer by contacting the negatively-charged ATP-phosphoryl groups. Similar to an arginine-finger in small GTP-binding proteins, this might improve the nucleophilic attack of H280 on the  $\beta$ -phosphate by neutralizing the negative charge emerging in the transition state of catalysis. Besides, R383 contacts H280. Deletion of R283 affects the  $pK_a$  of H280, shifting it to 5.24 (chain A)/5.18 (chain B). This shows that deletion of R283 decreases nucleophilicity of H280. R283 was found to be deleted in CovS variants. While AlphaFold2 structure predictions (not shown) suggest that deletion of R283 does not affect CovS structure, it will impair catalytic activity of HK. The  $pK_a$ -values were determined by the APBS-PDB2PQR software suite.[7] The figure was created by PyMOL.[8]

**(G)** Structure of the response-regulator CovR bound to histidine kinase CovS. Residues found to be mutated in CovR are shown in dark red. R36 and V128 are positioned towards the solvent. It was found that R36 is mutated to cysteine. Mutation of a solvent exposed residue to cysteine might affect protein function by formation of cysteine disulfide bonds, if occurring under non-reducing conditions. M170 is solvent exposed but might also play a structural role. i.e. as hydrophobic amino acid and by acting hydrogen bond acceptor via bridging water molecules not visible in this structural model. T80 was found to be mutated to alanine. T80 is located not too far away from D53, the phosphoryl-group acceptor site in CovR. The hydroxyl-group at the side chain of T80 might play a structural role, i.e. via formation of hydrogen bonds with bridging water molecule. This cannot be achieved by an alanine side chain. If this manifests in CovS•CovR activity needs to be evaluated. R203 and Y198 are located within the CovR DNA-binding helix. In the CovS-bound state R203 is solvent exposed and Y198 might play a structural role via formation of hydrogen bonds between the side chain hydroxyl and bridging water molecules. The figure was created by PyMOL.[8]

**(H)** Superposition of the AlphaFold2 CovR•CovS structure with the structure of the response regulator CheY (PDB: 2CHE) suggests that the response-regulator CovR binds  $Mg^{2+}$ . The  $Mg^{2+}$ -binding site is totally conserved. The  $Mg^{2+}$  is hexacoordinated by three water molecules ( $w1$ ,  $w2$ ,  $w3$ ), the side chain of D110, the main chain carbonyl oxygen of M55 (N59 in CheY) and by the side chain of the phosphoryl-group acceptor D53. E9 positions  $w2$  by formation of a hydrogen bond. K102 contacts D53 by formation of a salt bridge. During catalysis the carboxylate of D53 would act as a nucleophile and performs an in-line attack to the phosphoimidazol ring of H280 with H280 acting as a leaving group. It is suggested that the bound  $Mg^{2+}$  stabilizes the pentavalent bipyramidal transition state during phosphoryl-transfer reactions. In analogy to CheY, K102 in CovR might be dispensable for the phosphoryl-transfer reaction. However, it might bind to the phosphorylated D53 carboxylate thereby eliciting conformational changes. This might result in dissociation of CovR from CovS adopting a conformation that allows CovR to bind to the target DNA sequence. The figure was created by PyMOL[8].

**(I)** Overall conformation of the non-complexed, non-phosphorylated CovR dimer as predicted by AlphaFold2. CovR can be separated in a C-terminal DNA-binding domain (aa129-227) with the DNA-binding helix containing R203 and Y198 and a N-terminal receiver (REC)-domain (4-117) that contains D53 that is phosphorylated by the histidine kinase of CovS in order to act as a transcriptional regulator. The conformation shown here is not compatible with DNA-binding at both DNA-binding sites. The figure was created by PyMOL.[8]

**(J)** Closeup of the DNA-binding site of CovR in complex with DNA. CovR was superimposed with 1GXP. CovR inserts an  $\alpha$ -helix into the major groove of the DNA. R203 and Y198 form contacts to the sugar-phosphate backbone. The side chain hydroxyl of Y198 forms a hydrogen bond with the phosphate of the DNA-backbone, R203 forms a salt bridge with the phosphate of the DNA-backbone. In this conformation, both residues would contribute to DNA-binding affinity but not to create sequence specificity. However, binding to DNA might alter the conformation and a crystal structure of CovS in complex with dsDNA would be needed to judge this. R203 was shown to be mutated to serine, which is not compatible with creating the interactions with DNA. Y198 was found to be deleted in CovR variants. Mutation of R203S will likely decrease binding affinity while possibly retaining some DNA-binding. However, deletion of Y198 will most likely result in variant not capable to bind DNA as all residues that mediate DNA-binding, i.e. R200, R203 and K205, are located C-terminally of Y198 and will not be properly oriented to allow DNA-binding. The figure was created by PyMOL[8]



**Table S2** Literature review on previously characterized *covR/S* mutations

<b>Amino acid substitutions</b>	<b>CovR/S phenotype</b>	<b>Reference</b>
I332V in CovS	functional	[3]
G461S in CovS	dysfunctional	[4]
E226G in CovS	dysfunctional	[4]
R203S in CovR	dysfunctional	[1]
M1I in CovS	dysfunctional	[10]
T214P in CovS	dysfunctional	[10]
truncation from aa300 in CovS	dysfunctional	[12]
truncation from aa202 in CovS	dysfunctional	[11]

**Table S3.** Parameters for mass spectrometry**reversed phase liquid chromatography (RPLC)**

<i>instrument</i>	Ultimate 3000 RSLC (Thermo Scientific)
<i>trap column</i>	75 $\mu\text{m}$ inner diameter, packed with 3 $\mu\text{m}$ C18 particles (Acclaim PepMap100, Thermo Scientific)
<i>analytical column</i>	Accucore 150-C18, (Thermo Fisher Scientific) 25 cm x 75 $\mu\text{m}$ , 2,6 $\mu\text{m}$ C18 particles, 150 $\text{\AA}$ pore size
<i>buffer system</i>	binary buffer system consisting of 0.1% acetic acid in HPLC-grade water (solvent A) and 100% ACN in 0.1% acetic acid (solvent B)
<i>flow rate</i>	300 nl/min
<i>gradient</i>	(0min-2% B 2min-5% B 10min-7% B 70min-25% B 75min-40% B 77min-90% B 83min-90% B 85min-2% B 95min-2%B
<i>column oven temperature</i>	40°C
<b>Mass spectrometry</b>	
<i>instrument</i>	Orbitrap Exploris 480
<i>electrospray</i>	Nanospray Flex™ Ion Source
<i>operation mode</i>	data-independent
<b>Full Scan Properties</b>	
<i>MS scan resolution</i>	120000
<i>AGC target</i>	3e6 (300%)
<i>maximum ion injection time for the MS scan</i>	60 ms
<i>Scan range</i>	350 to 1200 m/z
<i>Microscans</i>	1
<i>Polarity</i>	positive
<i>RF Lens</i>	50%
<i>Spectra data type</i>	profile
<b>Dia Properties (MS2)</b>	
<i>Resolution</i>	30,000

<i>maximum ion injection time for the MS/MS scans</i>	auto
<i>Normalized AGC target</i>	3E6
<i>Spectra data type</i>	profile
<i>Microscans</i>	1
<i>isolation window</i>	66
<i>Isolation window width</i>	13 m/z
<i>Window overlay</i>	2 m/z
<i>Fixed first mass</i>	200
<i>HCD collision energy</i>	30%

**Table S5** Exact *p*-values of statistical analysis of cytokine secretion by moDCs after caspase-inhibition (n=10). A separate uninfected control with the respective inhibitor treatment was performed for each 5448AP infection. The level of significance was determined using Mann-Whitney *U*-test.

	untreated vs. 5448AP	Cas3 Inh vs. 5448AP	Cas8 Inh vs. 5448AP	PanCas Inh vs. 5448AP	untreated vs. 5448
<b>IL-1<math>\beta</math></b>	<i>p</i> =0.0045	<i>p</i> =0.0385	<i>p</i> <0.0001	<i>p</i> =0.0055	<i>p</i> =0.0045
<b>IFN<math>\alpha</math></b>	<i>p</i> <0.0001	<i>p</i> =0.0019	<i>p</i> <0.0001	<i>p</i> =0.0094	<i>p</i> <0.0001
<b>IFN<math>\gamma</math></b>	<i>p</i> <0.0001	<i>p</i> <0.0001	<i>p</i> <0.0001	<i>p</i> <0.0001	<i>p</i> <0.0001
<b>TNF</b>	<i>p</i> =0.0020	<i>p</i> =0.0286	<i>p</i> =0.0007	<i>p</i> =0.0036	<i>p</i> =0.0007
<b>MCP-1</b>	<i>p</i> <0.0001	<i>p</i> =0.0002	<i>p</i> <0.0001	<i>p</i> <0.0001	<i>p</i> <0.0001
<b>IL-6</b>	<i>p</i> <0.0001	<i>p</i> <0.0001	<i>p</i> <0.0001	<i>p</i> <0.0001	<i>p</i> <0.0001
<b>IL-8</b>	<i>p</i> =0.0068	<i>p</i> =0.0115	<i>p</i> =0.0068	n.s.	<i>p</i> =0.0003
<b>IL-10</b>	<i>p</i> =0.0014	<i>p</i> =0.0109	<i>p</i> <0.0001	<i>p</i> <0.0001	<i>p</i> =0.0321
<b>IL-12p70</b>	<i>p</i> <0.0001	<i>p</i> <0.0001	<i>p</i> <0.0001	<i>p</i> <0.0001	<i>p</i> <0.0001
<b>IL-18</b>	n.s.	n.s.	<i>p</i> =0.0014	<i>p</i> =0.0084	<i>p</i> =0.0021
<b>IL-23</b>	<i>p</i> <0.0001	<i>p</i> <0.0001	<i>p</i> <0.0001	<i>p</i> <0.0001	<i>p</i> <0.0001
<b>IL-33</b>	n.s.	n.s.	<i>p</i> =0.0159	n.s.	<i>p</i> =0.0027

## **Table legends for Additional File 2.**

**Table S1** CovR/S phenotype of GAS isolates recovered from the INFECT cohort. Type of infection (poly-/monomicrobial), involvement of septic shock, CovR/CovS mutations as identified by bioinformatics, and CovR/S functionality. Data was published in [9] and re-analyzed based on CovR/S functionality. CovR/S functionality was assessed by literature review (Table S2) and protein structure prediction (Fig. S8). Yellow color indicates dysfunctional CovR/S system.

**Table S4** Statistical analyses of the abundance patterns of proteins of (un)infected moDCs 6 h and 24 h post indicated infections. Color code: blue:  $\log_2$  fold change below 0; red:  $\log_2$  fold change above 0.

## References

1. Dalton T.L. and Scott J.R. CovS Inactivates CovR and Is Required for Growth under Conditions of General Stress in *Streptococcus pyogenes*. *Journal of Bacteriology* 186(12):3928-3937, 2004.
2. Delorenzi M. and Speed T. An HMM model for coiled-coil domains and a comparison with PSSM-based predictions. *Bioinformatics* 18(4):617-625, 2002.
3. Horstmann N., Sahasrabhojane P., Saldaña M., Ajami N.J., Flores A.R., Sumbly P., Liu C.-G., Yao H., Su X., Thompson E. and Shelburne S.A. Characterization of the Effect of the Histidine Kinase CovS on Response Regulator Phosphorylation in Group A *Streptococcus*. *Infection and Immunity* 83(3):1068-1077, 2015.
4. Ikebe T., Ato M., Matsumura T., Hasegawa H., Sata T., Kobayashi K. and Watanabe H. Highly Frequent Mutations in Negative Regulators of Multiple Virulence Genes in Group A Streptococcal Toxic Shock Syndrome Isolates. *PLOS Pathogens* 6(4):e1000832, 2010.
5. Jumper J., Evans R., Pritzel A., Green T., Figurnov M., Ronneberger O., Tunyasuvunakool K., Bates R., Zidek A., Potapenko A., Bridgland A., Meyer C., Kohl S.A.A., Ballard A.J., Cowie A., Romera-Paredes B., Nikolov S., Jain R., Adler J., Back T., Petersen S., Reiman D., Clancy E., Zielinski M., Steinegger M., Pacholska M., Berghammer T., Bodenstein S., Silver D., Vinyals O., Senior A.W., Kavukcuoglu K., Kohli P. and Hassabis D. Highly accurate protein structure prediction with AlphaFold. *Nature* 596(7873):583-589, 2021.
6. Jumper J. and Hassabis D. Protein structure predictions to atomic accuracy with AlphaFold. *Nat Methods* 19(1):11-12, 2022.
7. Jurrus E., Engel D., Star K., Monson K., Brandi J., Felberg L.E., Brookes D.H., Wilson L., Chen J., Liles K., Chun M., Li P., Gohara D.W., Dolinsky T., Konecny R., Koes D.R., Nielsen J.E., Head-Gordon T., Geng W., Krasny R., Wei G.W., Holst M.J., McCammon J.A. and Baker N.A. Improvements to the APBS biomolecular solvation software suite. *Protein Sci* 27(1):112-128, 2018.
8. Madsen M.B., Skrede S., Perner A., Arnell P., Nekludov M., Bruun T., Karlsson Y., Hansen M.B., Polzik P., Hedetoft M., Rosén A., Saccanti E., Bergey F., Martins dos Santos V.A.P., Bidstrup D., Bærnthsen N.F., Frændø G.H., Jansen E.C., Madsen L.B., Müller R.B., Pedersen E.M.J., Petersen M.W., Ravn F., Smidt-Nielsen I.F.G., Wahl A.M., Wulffeld S., Aronsson S., Rosemar A., Trogen J., Nedrebø T., Oppegaard O., Rath E., Sævik M., Norrby-Teglund A., Hyldegaard O. and group I.s. Patient's characteristics and outcomes in necrotising soft-tissue infections: results from a Scandinavian, multicentre, prospective cohort study. *Intensive Care Medicine* 45(9):1241-1251, 2019.
9. Palma Medina L.M., Rath E., Jahagirdar S., Bruun T., Madsen M.B., Stralin K., Unge C., Hansen M.B., Arnell P., Nekludov M., Hyldegaard O., Lourda M., Santos V., Saccanti E., Skrede S., Svensson M. and Norrby-Teglund A. Discriminatory plasma biomarkers predict specific clinical phenotypes of necrotizing soft-tissue infections. *J Clin Invest* 131(14), 2021.
10. Shumba P., Sura T., Moll K., Chakrakodi B., Tolken L.A., Hossmann J., Hoff K.J., Hyldegaard O., Nekludov M., Svensson M., Arnell P., Skrede S., Group I.S., Norrby-Teglund A. and Siemens N. Neutrophil-derived reactive agents induce a transient SpeB negative phenotype in *Streptococcus pyogenes*. *J Biomed Sci* 30(1):52, 2023.
11. Sumbly P., Whitney A.R., Graviss E.A., DeLeo F.R. and Musser J.M. Genome-Wide Analysis of Group A Streptococci Reveals a Mutation That Modulates Global Phenotype and Disease Specificity. *PLOS Pathogens* 2(1):e5, 2006.
12. Walker M.J., Hollands A., Sanderson-Smith M.L., Cole J.N., Kirk J.K., Henningham A., McArthur J.D., Dinkla K., Aziz R.K., Kansal R.G., Simpson A.J., Buchanan J.T., Chhatwal G.S., Kotb M. and Nizet V. DNase Sda1 provides selection pressure for a switch to invasive group A streptococcal infection. *Nature Medicine* 13(8):981-985, 2007.







## PAPER III

# Neutrophil-derived Reactive Agents Induce a Transient SpeB Negative Phenotype in *Streptococcus pyogenes*

Patience Shumba, Thomas Sura, Kirsten Moll, Bhavya Chakrakodi, Lea A Tölken, Jörn Hoßmann, Katharina J Hoff, Ole Hyldegaard, Michael Nekludov, Mattias Svensson, Per Arnell, Steinar Skrede; INFECT Study Group; Anna Norrby-Teglund, Nikolai Siemens

Published in Journal of Biomedical Science, 2023 July 10

[doi.org/10.1186/s12929-023-00947-x](https://doi.org/10.1186/s12929-023-00947-x)

### Author contributions:

Conceptualization: PS, ANT, NS; Methodology: PS, TS, JH, KJH, OH, MN, PA, SS, ANT, NS; Investigation: PS, TS, KM, BC, **LAT**, JH, KJH, OH, MN, MS, PA, SS, NS; Visualization: PS, TS, KM, BC, **LAT**, JH, KJH, NS; Funding acquisition: ANT, NS; Project administration: ANT, NS; Supervision: ANT, NS; Writing—original draft: PS, TS, ANT, NS; Writing—review & editing: PS, TS, BC, **LAT**, KM, JH, KJH, OH, MN, MS, PA, SS, ANT, NS.

.....  
Prof. Dr. Nikolai Siemens

.....  
Lea Tölken




RESEARCH

Open Access



# Neutrophil-derived reactive agents induce a transient SpeB negative phenotype in *Streptococcus pyogenes*

Patience Shumba<sup>1</sup>, Thomas Sura<sup>2</sup>, Kirsten Moll<sup>3</sup>, Bhavya Chakrakodi<sup>3</sup>, Lea A. Tölken<sup>1</sup>, Jörn Hoßmann<sup>4</sup>, Katharina J. Hoff<sup>5</sup>, Ole Hyldegaard<sup>6,7</sup>, Michael Nekludov<sup>8</sup>, Mattias Svensson<sup>3</sup>, Per Arnell<sup>9</sup>, Steinar Skrede<sup>10,11</sup>, INFECT Study Group, Anna Norrby-Teglund<sup>3†</sup> and Nikolai Siemens<sup>1\*†</sup> 

## Abstract

**Background** *Streptococcus pyogenes* (group A streptococci; GAS) is the main causative pathogen of monomicrobial necrotizing soft tissue infections (NSTIs). To resist immuno-clearance, GAS adapt their genetic information and/or phenotype to the surrounding environment. Hyper-virulent streptococcal pyrogenic exotoxin B (SpeB) negative variants caused by *covRS* mutations are enriched during infection. A key driving force for this process is the bacterial Sda1 DNase.

**Methods** Bacterial infiltration, immune cell influx, tissue necrosis and inflammation in patient's biopsies were determined using immunohistochemistry. SpeB secretion and activity by GAS post infections or challenges with reactive agents were determined via Western blot or casein agar and proteolytic activity assays, respectively. Proteome of GAS single colonies and neutrophil secretome were profiled, using mass spectrometry.

**Results** Here, we identify another strategy resulting in SpeB-negative variants, namely reversible abrogation of SpeB secretion triggered by neutrophil effector molecules. Analysis of NSTI patient tissue biopsies revealed that tissue inflammation, neutrophil influx, and degranulation positively correlate with increasing frequency of SpeB-negative GAS clones. Using single colony proteomics, we show that GAS isolated directly from tissue express but do not secrete SpeB. Once the tissue pressure is lifted, GAS regain SpeB secreting function. Neutrophils were identified as the main immune cells responsible for the observed phenotype. Subsequent analyses identified hydrogen peroxide and hypochlorous acid as reactive agents driving this phenotypic GAS adaptation to the tissue environment. SpeB-negative GAS show improved survival within neutrophils and induce increased degranulation.

**Conclusions** Our findings provide new information about GAS fitness and heterogeneity in the soft tissue milieu and provide new potential targets for therapeutic intervention in NSTIs.

**Keywords** *Streptococcus pyogenes*, Necrotizing soft tissue infections, SpeB, Neutrophils

<sup>†</sup>Anna Norrby-Teglund and Nikolai Siemens contributed equally to this work.

\*Correspondence:

Nikolai Siemens

[nikolai.siemens@uni-greifswald.de](mailto:nikolai.siemens@uni-greifswald.de)

Full list of author information is available at the end of the article



## Introduction

Necrotizing soft tissue infections (NSTIs) are rapidly progressing infections of any layer of the skin or soft tissue. The infections are associated with significant morbidity and mortality [22, 39]. Extensive surgical interventions and even amputations are often required despite intensive care and prompt antibiotic therapy [1]. Based on the microbiological etiology, NSTIs are categorized into two main types: type 1 of polymicrobial and type 2 of monomicrobial nature [37]. *Streptococcus pyogenes* (group A streptococci [GAS]) is the major causative pathogen of NSTIs [3, 22]. GAS NSTIs are more frequent among younger individuals without comorbidities, preferably located to the extremities, and often complicated by streptococcal toxic shock syndrome (STSS) [4, 22, 41]. A recent Scandinavian prospective multicenter study called INFECT enrolled 409 surgically confirmed NSTI cases, among which 31% constituted GAS cases [4, 22].

Several studies have shown that GAS NSTIs are characterized by high bacterial load and a hyper-inflammatory response characterized by a massive infiltration of immune cells, including neutrophils and macrophages, and elevated levels of pro-inflammatory molecules [14, 15, 26, 27, 33, 42]. The ability of GAS to cause hyper-inflammation and tissue damage can be attributed to an arsenal of virulence factors. In light of neutrophil activation, several GAS virulence factors such as M-protein and phosphoglycerate kinase (PGK) have been identified as potent inducers of neutrophil activation and degranulation resulting in release of proteolytic enzymes and other effector molecules into the surrounding milieu and subsequent tissue damage [14, 15, 32, 33, 35, 38, 43]. Another important virulence factor is the streptococcal pyrogenic exotoxin B (SpeB), which is a cysteine protease targeting numerous important host substrates such as immunoglobulins, complement, antimicrobial peptides, and interleukin (IL)-1 $\beta$  [25, 37]. Notably, it also has endogenous substrates including several important virulence factors [37]. In the case of PGK, neutrophil activation is only evident in SpeB-negative variants [43]. Such variants have been ascribed hyper-virulent properties and reported to be enriched during infection through mutations in genes encoding CovR/S two-component system and stand-alone regulator RopB resulting in an irreversible loss of SpeB expression [13, 40].

Bacterial killing by neutrophils involves both non-oxidative and oxidative mechanisms. The latter of which is ensured through reactive oxygen species (ROS). ROS are generated via the NADPH oxidase and myeloperoxidase (MPO) systems [47]. Hydrogen peroxide (H<sub>2</sub>O<sub>2</sub>) is produced by spontaneous or dismutase driven conversion of superoxide. The subsequent MPO-catalysed oxidation of chlorine by H<sub>2</sub>O<sub>2</sub> results in formation of hypochlorous

acid (HOCl) [24]. MPO is highly abundant within azurophilic granules of neutrophils. Hence, HOCl can be found intracellularly within neutrophils as well as extracellularly [28].

The role of SpeB in NSTI remains elusive. In our previous report [33], we identified that NSTI patient tissue biopsies frequently contained a mixture of SpeB-positive (SpeB<sup>+</sup>) and SpeB-negative (SpeB<sup>-</sup>) clones as assessed by proteolytic assays. In this study, we further characterized these clones and through single colony proteomics, we show that the bacteria express but do not secrete SpeB. We further show that this phenotype is induced by the neutrophils, and particularly MPO-derived HOCl and its precursor, H<sub>2</sub>O<sub>2</sub>, resulting in SpeB-negative GAS clones that survive and multiply within neutrophils, induce excessive degranulation, and thereby contribute to tissue disruptive and hyper-inflammatory processes in NSTIs.

## Methods

### Bacterial strains

GAS 5448, 5626, 8003, and 8157 are NSTI isolates from Toronto, Canada (provided by Donald E. Low, Mount Sinai Hospital, Toronto, Canada) [16, 19]. All strains were cultured in Todd-Hewitt broth (Carl Roth) supplemented with 1.5% (w/v) yeast extract (Carl Roth) at 37 °C. GAS strains from the INFECT NSTI patients were recovered directly by culture from the tissue biopsies.

### SpeB expression and protease activity analyses

The SpeB protease activity was determined as described previously [34]. Briefly, the bacteria were grown in THY (16–18 h), centrifuged, the supernatants were collected and filtered (pore size, 0.20  $\mu$ m). Supernatants were incubated with 5 mM DTT for 30 min at 37 °C, after which *n*-benzoyl-proline-phenylalanine-arginine-*p*-nitroanilide hydrochloride (1 mM) and phosphate buffer (pH 6; 5 mM) were added and absorbance at 405 nm was detected. Experiments also included testing activity with addition of H<sub>2</sub>O<sub>2</sub> (10 and 100  $\mu$ M). Furthermore, SpeB secretion and activity were tested via casein digestion assay as described previously [21]. Serial dilutions of bacteria were plated on modified Columbia agar containing 3% (w/v) skim milk (both Sigma-Aldrich) following incubation under 37 °C and 5% CO<sub>2</sub> atmosphere for 24 h. SpeB<sup>+</sup> producers were characterized by a clearance zone around the colonies, whereas non-producers had no zone of clearance.

For Western blot analyses, bacterial supernatants were precipitated with 96% (v/v) ethanol over night at – 20 °C. Equal amounts of protein were incubated with sodium dodecyl sulfate loading buffer at 90 °C for 10 min. Proteins were separated using a 4–12% SDS-PAGE gel and transferred onto a nitrocellulose membrane. The

membrane was blocked with 5% (w/v) dry casein powder in 0.05% (v/v) Tween-20 Tris-buffered saline. The following antibodies were used for detection: anti-SpeB antibody (Abcam) and secondary anti-rabbit IgG horseradish peroxidase linked Fab fragment (GE Healthcare).

#### Antimicrobial testing

$1 \times 10^6$  CFU/ml of bacterial strains were exposed to different concentrations of clindamycin, benzylpenicillin (both Sigma-Aldrich), LL-37 (Invivogen), Lysozyme (Sigma-Aldrich), HNP-1 (Peprotech), MPO, resistin, HBP (R&D Systems), and  $H_2O_2$  (Sigma-Aldrich) for 3 h and plated in serial dilutions on casein agar plates. CFUs were analyzed after 24 h of incubation at 37 °C and 5%  $CO_2$ .

#### Human cells, culture conditions, and infections

The human keratinocyte cell line N/TERT-1 (a gift from J. Rheinwald and the Cell Culture Core of the Harvard Skin Disease Research Centre, Boston, MA, USA) was cultured in EpiLife medium (Invitrogen). Primary normal human dermal fibroblasts (NHDFs) were cultured in DMEM (Invitrogen) supplemented with 10% (v/v) FCS (Invitrogen). Human primary neutrophils were isolated from healthy donors using a density gradient centrifugation on Polymorphprep (Axis Shield). Neutrophil viability was assessed via trypan blue staining. After isolation, neutrophils were suspended in RPMI1640 medium (HyClone) supplemented with 10 mM L-glutamine, 25 mmol/l HEPES (all HyClone), and 5% (v/v) FCS. PBMCs were isolated from buffy coats by Lymphoprep (Axis-Shields) gradient centrifugation. Cells were allowed to adhere in cell culture flasks (Corning) for 30 min at 37 °C in serum free RPMI1640 media. The non-adherent cells were removed by washing with PBS (HyClone). Monocyte-derived macrophages were generated by culturing primary human monocytes isolated from peripheral blood of healthy donors in 6-well plates (Corning) for 9 days at a density of  $1 \times 10^6$  cells/well. Monocytes were differentiated to pro-inflammatory macrophages for 7 days in cell culture media containing GM-CSF (25 ng/ml), followed by two additional days of incubation with LPS (100 ng/ml). Media was changed every 2–3 days. All cells were cultured under 37 °C and 5%  $CO_2$  atmosphere.

All infections were performed at a multiplicity of infection (MOI) 10 in a final volume of 1 ml of the respective media. Adherence to and internalization into N/TERT-1 cells and NHDFs were quantified using the antibiotic protection assay [23]. Briefly, 24-well plates were inoculated with  $2.5 \times 10^5$  N/TERT-1 or NHDFs/well without antibiotics. The cells were allowed to grow to confluence. For the assay, cells were washed and infected with GAS (MOI 10). Two hours after infection, the viable counts of

bacteria (colony-forming units, CFU) released from lysed cells were determined by plating on blood agar. For the assessment of bacterial internalization, 2 h after infection, the cells were washed with PBS and incubated with media supplemented with benzylpenicillin ( $20 \mu\text{g ml}^{-1}$ ) and gentamicin ( $120 \mu\text{g ml}^{-1}$ ) for additional 2 or 4 h. Subsequently, the cells were washed, lysed, and the CFU counts were determined as described above. For the assessment of SpeB release and activity, intracellular bacteria were plated on casein agar plates.

$1 \times 10^6$  macrophages were infected for 2 h following 1 h of antibiotic treatment and  $5 \times 10^5$  neutrophils were infected for 1 h following antibiotic treatment. Assessment of intracellular bacterial numbers was performed as described above. For MPO inhibition, different concentrations of 4-aminobenzoic hydrazide (Sigma-Aldrich) were used: 25, 50 and 100  $\mu\text{M}$ . After isolation, neutrophils were suspended in RPMI media with MPO inhibitor and incubated at 37 °C for 30 min prior to infections. All infections were performed in the presence of the inhibitor. Bacterial survival was evaluated 1, 2 and 4 h post infections. For proteomics, all infections were performed in Hank's balanced salts solution (HBSS, Invitrogen). Neutrophil supernatants were collected and stored at  $-20$  °C until analysis.

#### Immunostaining and analysis of tissue biopsies

Patient biopsies were cryosectioned (5–8  $\mu\text{m}$ ) using a MICROM cryostat HM 560 MV (Zeiss), fixed in 2% (v/v) formaldehyde or ice-cold acetone, and immunostained as previously described [33, 35]. The following antibodies were used for immunohistochemistry: anti-human HMGB1 (clone EPR3507; Abcam), anti-human IL-8 (clone NAP-1; Invitrogen), anti-human resistin (clone 184,305; R&D systems), and anti-human neutrophil-elastase (clone NP57; DAKO). Biotinylated secondary antibodies included goat anti-mouse IgG and goat anti-rabbit IgG (both from Vector Laboratories). The immunohistochemically stained sections were analyzed by acquired computerized image analysis (ACIA) [20]. The cell area was defined by the hematoxylin counterstaining, and the results are presented as percent positively stained area  $\times$  mean intensity of positive staining.

The following antibodies were used for immunofluorescence analyses: anti-MPO (MAB3174; R&D), anti-GAS (9191; Abcam). Secondary antibodies included anti-mouse IgG AF488, anti-goat IgG AF594, and anti-rabbit IgG AF594 (all Invitrogen). IF-images were acquired with Olympus BXS1 microscope and Olympus cellSense software (Olympus) and/or Leica Stellaris 8 confocal laser scanning microscope (CLSM) and LasX software (Leica Microsystems). Four to six images were taken per biopsy. Analysis of the micrographs was performed in a

two-step procedure, which included an automated recognition of GAS and MPO stainings followed by a calculation of the stained area ( $\text{px}^2$ ). Each picture was manually checked and if necessary corrected after an automated recognition.

#### Whole genome sequencing and data processing

DNA extraction from GAS strains 5448, 5626, 8003, and 8157, whole genome sequencing, and analyses were performed as previously described [36]. Detailed description is provided in the Additional file 1.

#### Protein extraction, LC–MS/MS analyses, and data processing of single GAS colonies and neutrophil secretome

Neutrophil secretome was determined as previously described [8]. Detailed description of protein extraction, measurements, and analyses are provided in the Additional file 1.

#### Statistics

If not otherwise indicated, statistical significance of differences was determined using the 2-tailed Mann–Whitney *U* test. Multiple comparisons were done using Kruskal Wallis test with Dunn's post-test. Correlation analyses were determined using Spearman test. Statistics were performed using GraphPad Prism version 7 (GraphPad software). A *p*-value less than 0.05 was considered significant.

## Results

### Reversible loss of SpeB proteolytic activity by GAS is associated with tissue pathology and inflammation

Bacteria were isolated from tissue biopsies collected from GAS patients (Additional file 2: Table S1) through direct plating of tissue sections on casein agar plates to assess SpeB activity. These analyses confirmed previous observations that infected tissue harbors a mixture of SpeB<sup>+</sup> and SpeB<sup>-</sup> clones (Fig. 1A). The majority of successor generations of SpeB<sup>-</sup> clones returned to a wild-type-like SpeB<sup>+</sup> phenotype after cultivation in THY media (Fig. 1B and Additional file 1: Fig. S1). To confirm that the observed SpeB<sup>-</sup> phenotype is not linked to genetic variations within mutational hotspots (*covS*, *covR*, and *ropB*) or *speB*, comparative whole genome sequence analyses were performed. Although strains 2001, 2006, 6016, and 6018 were exclusively SpeB<sup>-</sup> post direct tissue isolation (Fig. 1A), no mutations in these strains were found. In general, the analyses of these hotspots revealed only minor variance on nucleotide and amino acid levels (Additional file 1: Fig. S2–S4). *CovR* amino acid sequences were 100% identical between all strains. In strain 2002, *covS* initiated with the rare start codon ATA [11] and a

frame shift causing single nucleotide deletion in position 381 was detected (Additional file 1: Fig. S2). Most of the mutations were found in strain 6028, e.g., mutations within *covS* leading to several amino acid substitutions and a notable deletion of 45 nucleotides (Additional file 1: Figs. S2 and S3). Furthermore, single mutations leading to amino acid substitution within *RopB* were found in strains 2002, 5004, 6026, and 6028 (Additional file 1: Fig. S4). *SpeB* gene itself was unaffected. Additional exemplary sequence analyses of other TCS kinases/regulators identified rather *emm*-type specific mutations resulting in conserved amino acid substitutions, which would most likely not affect *SpeB* expression (Additional file 2: Table S2). These results suggest that in addition to irreversible loss of *SpeB* expression due to mutations in *covR/S* or *ropB* regions, reversible abrogation of *SpeB* expression at protein or activity level occurs in the tissue setting.

The observation of heterogeneity in *SpeB* proteolytic activity led us to explore how this related to tissue inflammation and damage. For this purpose, biopsies collected from repeated surgeries at different sites of infection (e.g., fascia, soft tissue, and muscle) of 31 GAS NSTI patients were analyzed for the presence of markers of tissue necrosis [high-mobility-group-protein B1 (HMGB1)], inflammation (IL-8), neutrophil infiltration [neutrophil elastase (NE)], and neutrophil degranulation (resistin; Additional file 1: Fig. S5). Correlation analyses based on bacterial load and the percentage of SpeB<sup>-</sup> clones recovered from the respective tissue specimen with each of the markers were performed. All of the analyzed markers showed a positive correlation to bacterial load (Fig. 1C–F). Moreover, positive correlations between tissue necrosis, inflammation, and neutrophil infiltration as well as degranulation with increasing percentage of SpeB<sup>-</sup> clones, irrespective of their rise through genetic or phenotypic variations, were found (Fig. 1C–F).

### Intracellular GAS recovered from neutrophils show reversible loss of SpeB proteolytic activity

Based on our data showing the mixed *SpeB* phenotype particularly in the tissue milieu, we sought to identify which factors might be driving this process. Due to increased variability in *SpeB* phenotype of freshly isolated GAS NSTI strains, four well-characterized strains of the two dominant NSTI *emm1* and *emm3* types (*emm1* strains 5448 and 8157 and *emm3* strains 5626 and 8003) were selected. These strains displayed stable SpeB<sup>+</sup> and SpeB<sup>-</sup> phenotypes, respectively. All colonies of 5448, 8157 and 5626 showed a clearance zone, while colonies of 8003 did not. (Fig. 2A). Analyses of supernatants from overnight cultures showed that *SpeB* was readily detectable in 5448, 8157, and 5626 (Fig. 2B,



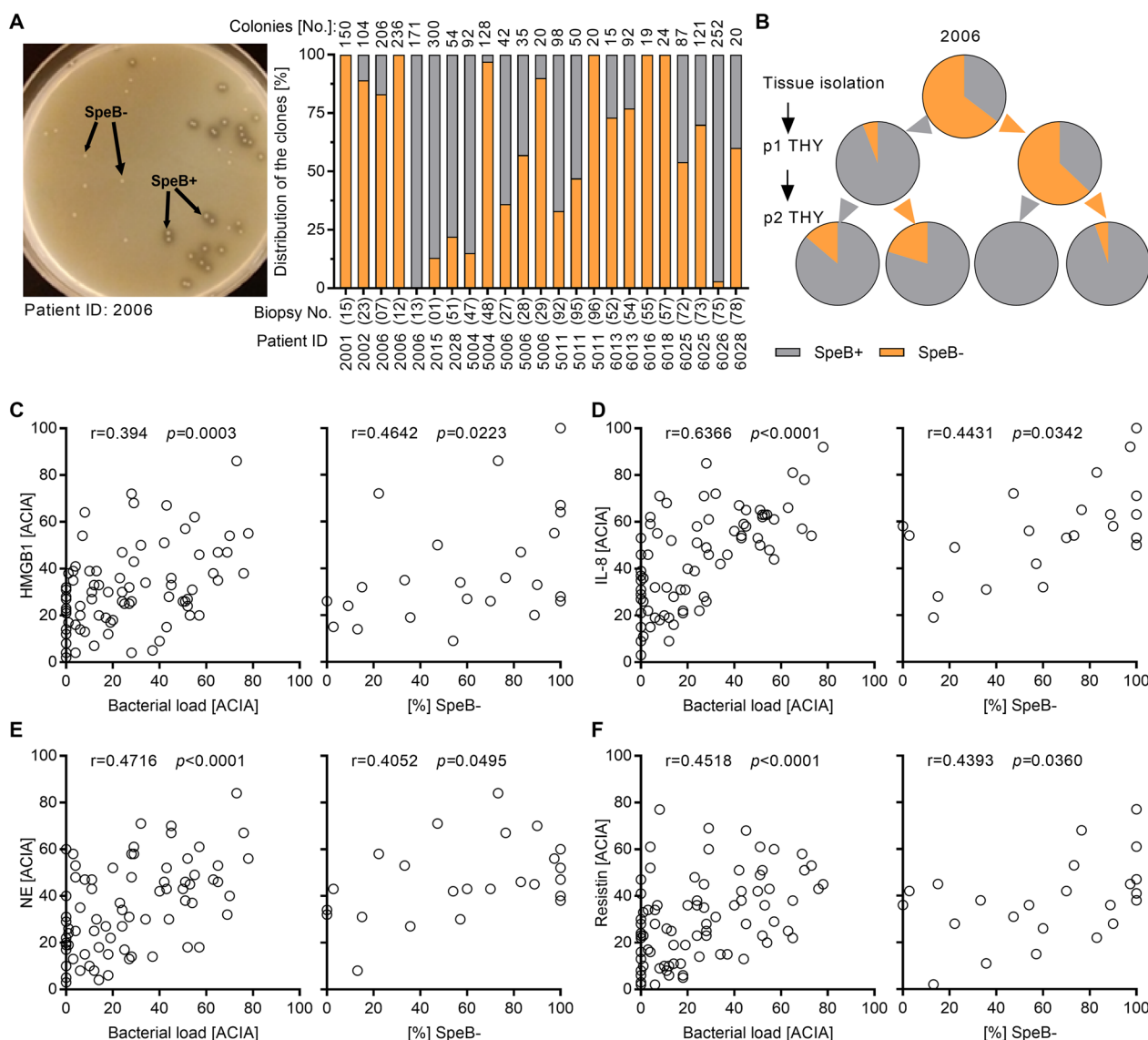


**Fig. 1** Reversible loss of SpeB is associated with tissue pathology and inflammation. **A** Distribution of SpeB<sup>+</sup> and SpeB<sup>-</sup> GAS clones directly isolated from NSTI patient tissue biopsies (n = 23). **B** Percentage of SpeB<sup>+</sup> and SpeB<sup>-</sup> GAS clones after the passage in THY media (p1, passage 1; p2, passage 2). Representative analysis of 2006 GAS patient isolate is shown. **C–G** Correlation analysis of bacterial load (left panel; n = 81 biopsies) or percentage of SpeB<sup>-</sup> clones (right panel; n = 23 biopsies) with the presence of HMGB1 (**C**), IL-8 (**D**), infiltrating neutrophils (**E**), and resistin (**F**) in patient biopsies. Correlation was determined using Spearman test. Semiquantitative acquired computerized image analyses (ACIA) of immuno-histochemical staining were performed as described in the methods section. The cell area was defined by the hematoxylin counterstaining, and the results are presented as percent positively stained area x mean intensity of positive staining

Additional file 1: Fig. S8). This was further verified in a SpeB proteolytic assay (Fig. 2C). Next, the strains' whole genome were sequenced and comparative analyses with annotated genomes of M1GAS (SF370, *emm1*) and MGAS315 (*emm3*) were performed. In general, rather low numbers of sequence variants were identified within the genomes (Additional file 1: Fig. S6). Analyses of mutational hotspots responsible for loss of SpeB expression identified a mutation in *covS* of 8003

strain resulting in T<sub>214</sub>P substitution (Additional file 1: Fig. S7).

Next, using the four strains with stable SpeB<sup>+</sup> and SpeB<sup>-</sup> phenotype, different human skin and soft tissue cell types, including keratinocytes, primary fibroblasts and immune cells (primary macrophages and neutrophils) were infected with GAS strains followed by assessment of infectivity, as well as SpeB activity by single colonies recovered from the intracellular compartment.

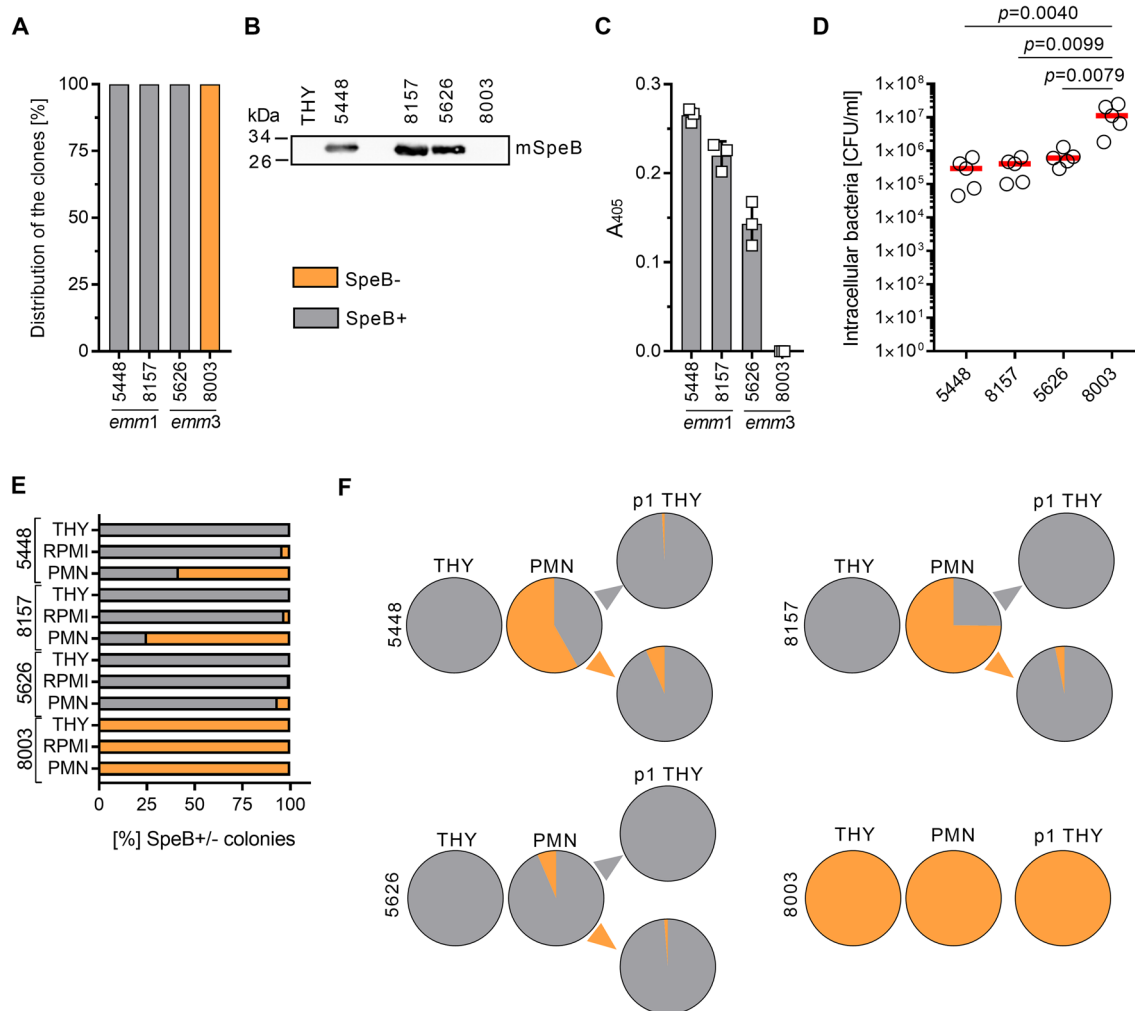


**Fig. 2** Human neutrophils induce loss of SpeB in GAS. **A** Assessment of SpeB positivity/negativity of indicated strains via casein agar assay. Mean percentage from four independent experiments is shown (n=4). **B** Representative image of Western-Blot analyses (n=3; mSpeB, mature SpeB) and **(C)** SpeB activity assay (n=3) of bacterial supernatants. GAS were grown over-night (16 h) in THY and sterile-filtered supernatants were used for the analyses. Original blot is shown in Additional file 1: Fig. S8. Each dot in **C** represents one independent experiment. Bars denote mean values  $\pm$ SD. **D** Intracellular bacterial counts after 1 h of neutrophil infection. Each dot represents an experiment with neutrophils from one donor. The horizontal lines denote median values (n=5). The level of significance was determined using Kruskal–Wallis test with Dunn’s multiple comparison post-test. **E** Assessment of SpeB positivity/negativity of indicated strains recovered from primary human neutrophils shown in **D**. Mean percentage of SpeB<sup>+</sup> and SpeB<sup>-</sup> clones from five independent experiments are shown (n=5). Bacteria incubated in RPMI and THY media served as controls. **F** Distribution of SpeB<sup>+</sup> and SpeB<sup>-</sup> clones post neutrophil (PMN) and subsequent THY media passage. Displayed are mean [%] of five independent experiments (n=5)

Since clindamycin and benzylpenicillin are used to treat GAS NSTIs, control experiments with these two antibiotics were also performed (Additional file 1: Fig. S9). No differences in adherence to or internalization into keratinocytes and fibroblasts between the strains were detected (Additional file 1: Fig. S9A-B and D-E). In contrast, while the bacteria were multiplying within keratinocytes, reduced numbers of bacteria were recovered from fibroblasts over time. Only minor effects on SpeB of these two cell types were seen (Additional file 1:

Fig. S9C, F). Next, primary macrophages and neutrophils were infected and intracellular bacteria were recovered. No differences in bacterial numbers were seen in macrophage infections (Additional file 1: Fig. S9G). In contrast, significantly higher numbers of SpeB<sup>-</sup> 8003 strain as compared to other three SpeB<sup>+</sup> stains were recovered from neutrophils (Fig. 2D). Infection of both myeloid cell types resulted in loss of SpeB activity on casein agar (Fig. 2E and Additional file 1: Fig. S9H). However, this phenotype was more pronounced in *emm1* strains,



where more than 50% of the colonies were SpeB<sup>-</sup> when exposed to neutrophils (Fig. 2E). Subsequent passaging of single colonies from neutrophil experiments showed that the majority of successor generations of SpeB<sup>-</sup> clones returned to a wild-type-like SpeB<sup>+</sup> phenotype (Fig. 2F). Bacteria exposed to minimal inhibitory concentrations of antibiotics retained its original SpeB<sup>+</sup> or SpeB<sup>-</sup> phenotype (Additional file 1: Fig. S9I-K). These results demonstrate that the reversible loss of SpeB activity is seen among intracellular GAS, particularly in neutrophils, and consequently, might represent an adaptation strategy of GAS to the intracellular environment of neutrophils.

### SpeB accumulates intracellularly in GAS as a response to intracellular environment of neutrophils

To verify if the SpeB<sup>-</sup> phenotype is characterized by the transient loss of SpeB expression, an impaired secretion or loss of proteolytic activity a series of experiments was performed.

First, relative *speB* transcription in single colonies of the 5448 strain post neutrophil infection was determined. *SpeB* transcription was detected in both SpeB<sup>+</sup> as well as in SpeB<sup>-</sup> colonies, albeit weaker in the latter (Fig. 3A).

Second, the proteome of SpeB<sup>+</sup> and SpeB<sup>-</sup> single colonies recovered from intracellular bacteria in neutrophils was quantitatively profiled by mass spectrometry. Bacteria cultured in THY media resulting in 100% SpeB<sup>+</sup> served as controls. In total, up-to 752 proteins were identified in single colonies (Additional file 2: Table S3). Principal component analysis showed that all three groups (THY vs. PMN SpeB<sup>+</sup> vs. PMN SpeB<sup>-</sup>) separate from each other, suggesting that each of them is characterized by a distinct proteome profile (Fig. 3B). Next, protein expression patterns of SpeB<sup>-</sup> colonies post neutrophil infections were compared either to SpeB<sup>+</sup> from the same experiment or to colonies from THY control (Fig. 3C, D). Notably, SpeB was found in all samples. In fact, SpeB<sup>-</sup> GAS colonies accumulated higher amounts of SpeB intracellularly, as compared to the SpeB<sup>+</sup> colonies or THY controls (Fig. 3C, D). Alignment of detected peptides with the amino acid sequence of SpeB revealed that SpeB zymogene was exclusively present intracellularly (Additional file 1: Figure S10). In addition, other secreted proteins, including DNaseB and immunogenic secreted protein 2 (Isp2) and surface anchored antiphagocytic M1 protein as well as C5a peptidase (ScpA), were found in higher abundance in SpeB<sup>-</sup> colonies. Identical experiments were performed with SpeB<sup>-</sup> 8003 strain. 8003 remained SpeB<sup>-</sup> post neutrophil challenge and SpeB was not detected (Additional file 1: Fig. S11 and Additional file 2: Table S4).

Third, we sought to determine which neutrophil-derived components might be responsible for the

observed reversible SpeB<sup>-</sup> phenotype. Therefore, an initial screen with strain 5448, which stably expresses and releases SpeB, was performed using antimicrobial peptides, lysozyme, and granule components (HBP and resistin). None of the tested agents had an impact on SpeB release/proteolytic activity by bacteria (Additional file 1: Fig. S12). Next, 5448 was exposed to different concentrations of hydrogen peroxide (H<sub>2</sub>O<sub>2</sub>). High concentrations of H<sub>2</sub>O<sub>2</sub> (1 mM) caused a 1-log reduction in bacterial counts, while no effect on CFU were noted in the presence of 10–100 μM (Fig. 4A). Exposure of 5448 strain to these sub-lethal concentrations of H<sub>2</sub>O<sub>2</sub> resulted in increased frequency of SpeB<sup>-</sup> clones in up to 32% of the total GAS population (Fig. 4B). Since MPO converts the majority of available H<sub>2</sub>O<sub>2</sub> intracellularly to HOCl, we next exposed strain 5448 to different concentrations of HOCl. Up to 70% of GAS did not secrete SpeB upon exposure to sub-lethal concentrations of HOCl (Fig. 4C, D). However, NaCl exposure, the source of Cl<sup>-</sup>, induced a similar bacterial phenotype although not to the same extent. To verify this result in a more complex setting, human primary neutrophils were infected with the 5448 strain in the presence of an MPO inhibitor and bacterial killing as well as SpeB positivity were assessed over time. To exclude potential masking effects due to the time-dependent delay in abrogated SpeB-secretion, 5448AP strain was used as a stable SpeB<sup>-</sup> control. In the infection model, reduced numbers of 5448 strain were recovered from neutrophils one-hour post infection (Fig. 4E). However, increased bacterial survival was noticed over a period of the next three hours if low concentrations of MPO-inhibitor (0–50 μM) were used. Four hours post infections almost equal numbers of bacteria compared to the initial infection inoculum were recovered (Fig. 4E). High concentrations of MPO inhibitor (100 μM) reversed this effect and an increased killing of bacteria was observed over time (Fig. 4E). In congruence with those observations, the amount of SpeB<sup>-</sup> clones significantly increased over the infection period. MPO-inhibition partially reversed this effect, particularly evident at 2 h post infections (Fig. 4F). In contrast, neutrophil infections with stable SpeB<sup>-</sup> 5448AP strain were characterized by a continuous intracellular multiplication (Additional file 1: Fig. S13A). As expected, 5448AP remained SpeB<sup>-</sup> over the entire period of infections (Fig. S13B). No MPO-inhibitor mediated effects on bacterial growth were observed (Additional file 1: Fig. S13C).

Finally, to assess whether the secretion or only the activity of SpeB were impaired by exposure of the bacteria to H<sub>2</sub>O<sub>2</sub> within neutrophils or in liquid cultures, 5448 strain was (i) plated on casein agar containing H<sub>2</sub>O<sub>2</sub> and (ii) SpeB presence as well as activity were determined in the presence/absence of H<sub>2</sub>O<sub>2</sub> in bacterial supernatants.

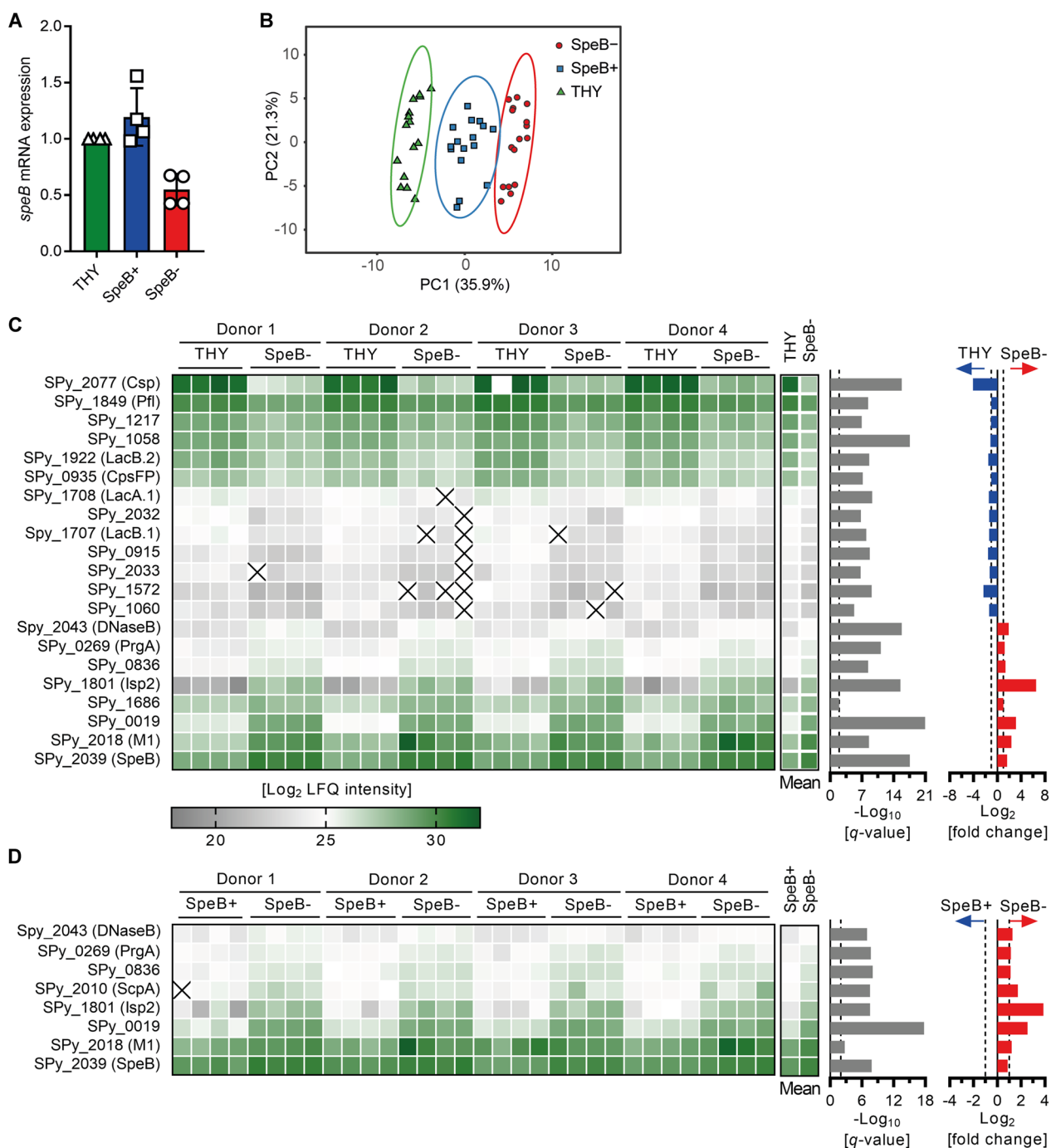


**Fig. 3** Distinct single colony proteome profile of GAS post neutrophil infection. **A** Relative *speB* mRNA expression in 5448 single colonies post neutrophil infections. Each dot represents one colony (n=4). Bars denote mean value  $\pm$  SD. **B** Principal component analysis of the proteome of single SpeB<sup>-</sup> and SpeB<sup>+</sup> colonies post neutrophil infections. GAS incubated in THY media, which remained 100% SpeB<sup>+</sup> were used as controls. Each dot represents proteome analysis of one GAS colony (n=16). **C, D** Heat map of differentially expressed proteins on a single colony level. Displayed are  $\text{Log}_2$  LFQ intensities (left panel),  $-\text{Log}_{10} q\text{-value}$  (middle panel), and  $\text{Log}_2$  fold change of the mean (right panel). Each column represents one single colony (four per condition and donor; n=16 in total). **C** Protein abundance of THY vs. SpeB<sup>-</sup> colonies and **D** SpeB<sup>+</sup> vs. SpeB<sup>-</sup> colonies are displayed (x, not detected)

These analyses revealed that  $H_2O_2$  does not impair SpeB activity but secretion in a subpopulation of the bacteria as shown via casein agar plating revealing negative colonies as well as Western blot analysis showing reduced levels of SpeB post  $H_2O_2$  treatment (Fig. 4G–J; Additional file 1: Fig. S14).

#### Enhanced neutrophil degranulation and presence of MPO in tissue biopsies with increased SpeB<sup>-</sup> variants

Since MPO converts major amounts of  $H_2O_2$  to HOCl, the presence of this molecule was determined in patient tissue biopsies based on the initial assessment of SpeB-positivity/negativity. Multiple tissue sections were stained for GAS and MPO, and analyzed microscopically (Fig. 5A, Additional file 1: Fig. S15). Confocal laser scanning microscopy (CLSM) and subsequent image analyses revealed that although equal bacterial load is detectable in both types of biopsies (SpeB<sup>-</sup> vs. SpeB<sup>+</sup>), higher amounts of MPO were detected in biopsies associated with SpeB<sup>-</sup> GAS clones (Fig. 5B, C). However, as evident by the micrographs, these biopsies are characterized by extensive necrosis resulting in a relatively diffuse DAPI staining (Fig. 5A). This is a characteristic of these infections and the biopsies represent tissue that are clinically indicated for surgical removal and will hence be associated with necrosis.

Both, *in vitro* as well as *ex vivo* analyses suggest that SpeB secretion is abrogated in GAS in response to  $H_2O_2$  and HOCl, which subsequently triggers increased neutrophil activation resulting in enhanced tissue pathology. Therefore, we next assessed neutrophil activation on a global level. Secretome composition of neutrophils post 5448 infections was quantitatively profiled by mass spectrometry. Again, to exclude time-dependent delay in abrogated SpeB secretion of this strain, the SpeB<sup>-</sup> 5448AP strain, which encodes truncated *covS* transcript effecting

expression of several virulence factors (Sda1, capsule, M1-protein) [45], was used as a control. To ensure that potential alterations in secretome composition and protein abundance were not caused by differences in cytotoxicity, LDH assay was performed. Although slightly increased cytolytic events were detected over time, no differences were seen between 5448 and 5448AP infections (Additional file 1: Fig. S16). Up to 495 secreted proteins/peptides were detected in neutrophil supernatants post infections (Additional file 2: Table S5), suggesting that both, SpeB<sup>+</sup> as well as SpeB<sup>-</sup> strains, activate neutrophils. However, granule content release was more pronounced in infections with SpeB<sup>-</sup> 5448AP strain over time (Fig. 6A, B). Comparison of neutrophil degranulation in response to 5448 vs. 5448AP strain showed that 103 proteins/peptides were more abundant in neutrophil secretome of SpeB<sup>-</sup> 5448AP infections (Fig. 6C–E). Among these, several tissue degrading enzymes, including neutrophil elastase (ELANE) and metalloproteases (MMP8, MMP9) were detected. PCA revealed that neutrophil secretome of both infections is distinct at 4 h post-infections (Fig. 6F). Subsequent pathway analyses by *Reactome* profiler showed that the SpeB<sup>-</sup> 5448AP strain activates several neutrophil specific pathways to a higher extent as compared to the 5448, including degranulation and immune responses (Fig. 6G, Additional file 2: Table S6). Sub-analyses of neutrophil cellular compartments showed that protein/peptides of all four granules were released in higher abundance in response to the SpeB<sup>-</sup> 5448AP infections (Fig. 6H).

#### Discussion

Phenotypic and genetic adaptations of GAS to the tissue environment are key survival mechanisms to establish a successful infection. In this study, we show that GAS reversibly abrogate SpeB secretion in the tissue setting

(See figure on next page.)

**Fig. 4**  $H_2O_2$  and HOCl impair SpeB secretion by GAS. **A** GAS 5448 strain was exposed to indicated concentration of hydrogen peroxide ( $H_2O_2$ ) and bacterial numbers were determined 1 h post stimulations. Each dot represents one independent experiment. Lines denote mean values ( $n=5$ ). **B** Assessment of SpeB positivity/negativity of 5448 strain post  $H_2O_2$  treatment as displayed in **A**. Mean percentage from five independent experiments is shown ( $n=5$ ). **C** GAS 5448 strain was exposed to indicated concentration of HOCl and bacterial numbers were determined 1 h post stimulations. Each dot represents one independent experiment. Lines denote mean values ( $n=5$ ). **D** Assessment of SpeB positivity/negativity of 5448 strain post HOCl treatment as displayed in **C**. Mean percentage from five independent experiments is shown ( $n=5$ ). **A–D** Untreated bacteria in THY media, acidified NaCl or  $Na_3PO_4$  served as controls. **E** Human primary neutrophils were infected with GAS strain 5448 and intracellular bacteria were determined by plating serial dilution of neutrophil lysates on casein agar plates post indicated time points. The MPO activity was inhibited by indicated concentrations of MPO inhibitor 30 min prior and during the entire infection period. Dots represent the median value  $\pm$  range of independent experiments with five donors ( $n=5$ ). **F** Assessment of SpeB positivity/negativity of 5448 strain recovered from primary human neutrophils shown in **E**. Mean percentages of SpeB<sup>+</sup> and SpeB<sup>-</sup> clones from five independent experiments are shown ( $n=5$ ). **G** Representative images of GAS 5448 directly plated on casein agar containing indicated concentrations of  $H_2O_2$  and **H** subsequent analyses. Mean percentage from four independent experiments is shown ( $n=4$ ). **I** SpeB activity assay ( $n=4$ ) of bacterial supernatants. GAS were grown over-night (16 h) in THY and sterile-filtered supernatants supplemented with indicated concentrations of  $H_2O_2$  were used for the analyses. **J** Western blot (upper left panel), silver staining of the loading control (upper lower panel), and image analyses (right panel) of GAS 5448 supernatants post exposure to indicated concentrations of  $H_2O_2$ . Representative images and analysis of three independent experiments are shown ( $n=3$ ). The level of significance between the groups of experiments presented in **A–H** was determined using Kruskal Wallis test with Dunn's posttest. The level of significance in **J** was determined using Friedman test

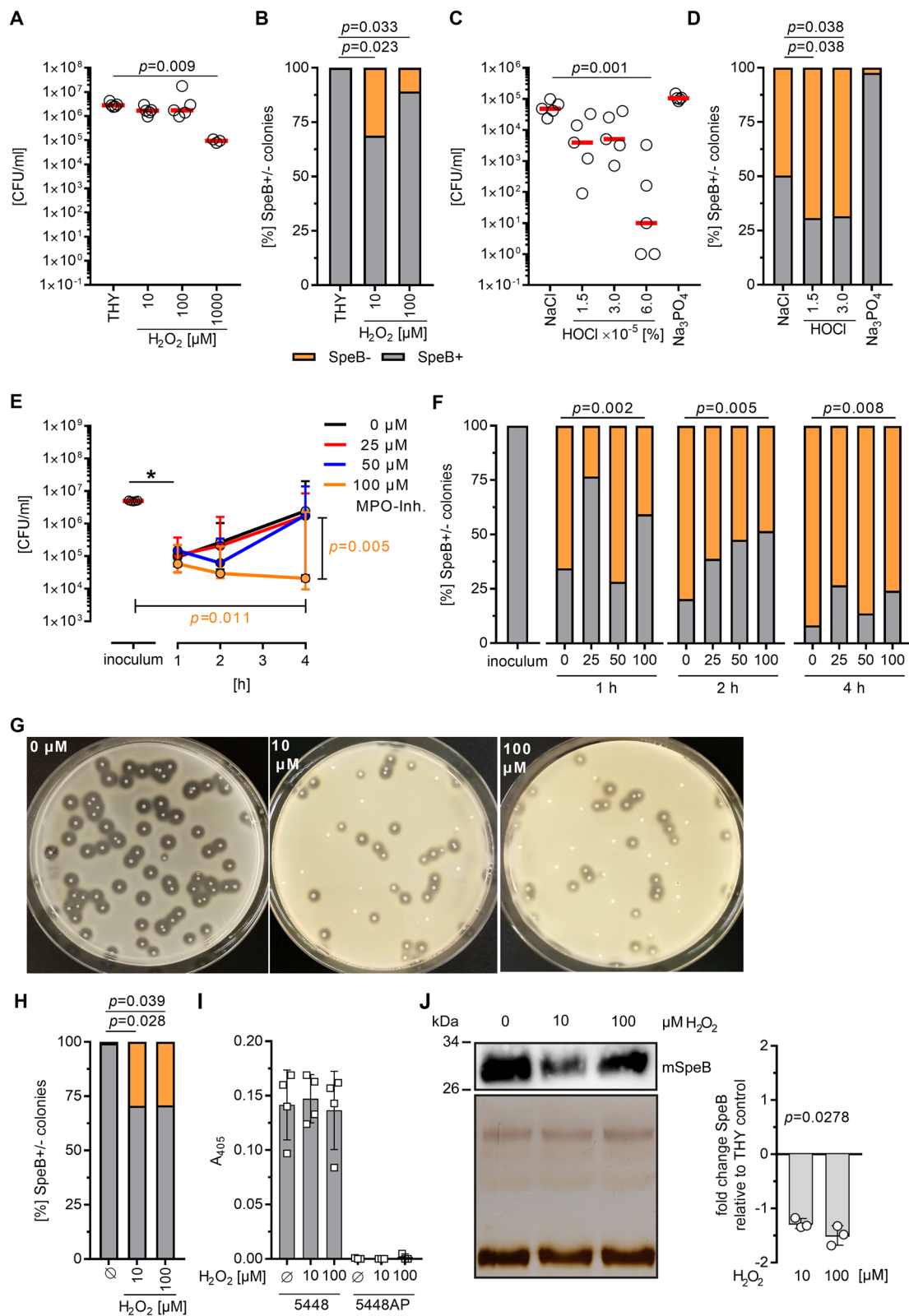


**Fig. 4** (See legend on previous page.)

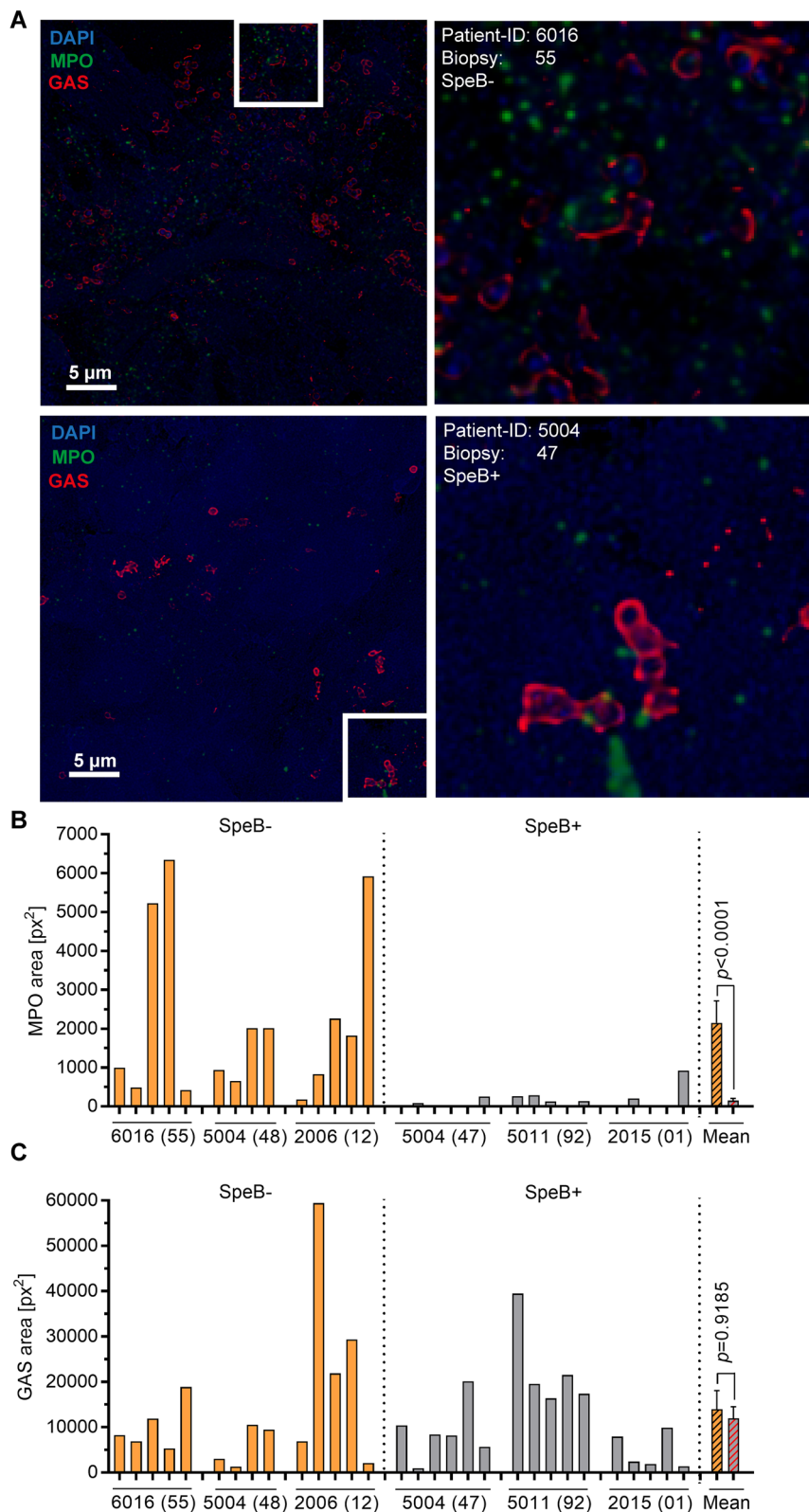


**Fig. 5** Increased levels of MPO in patient tissue biopsies associated with SpeB<sup>-</sup> GAS. **A** Representative immunofluorescence micrographs of the distribution of MPO in patient biopsies are shown. **B** Image analyses of MPO and **C** GAS stainings. Calculation of the stained area (px<sup>2</sup>) per analyzed micrograph is presented. Each bar within diagrams denotes analysis of one image from indicated tissue biopsies. Bars on the right of each diagram denote mean values  $\pm$  SD. The level of significance between the groups was determined using 2-tailed Mann–Whitney *U* test



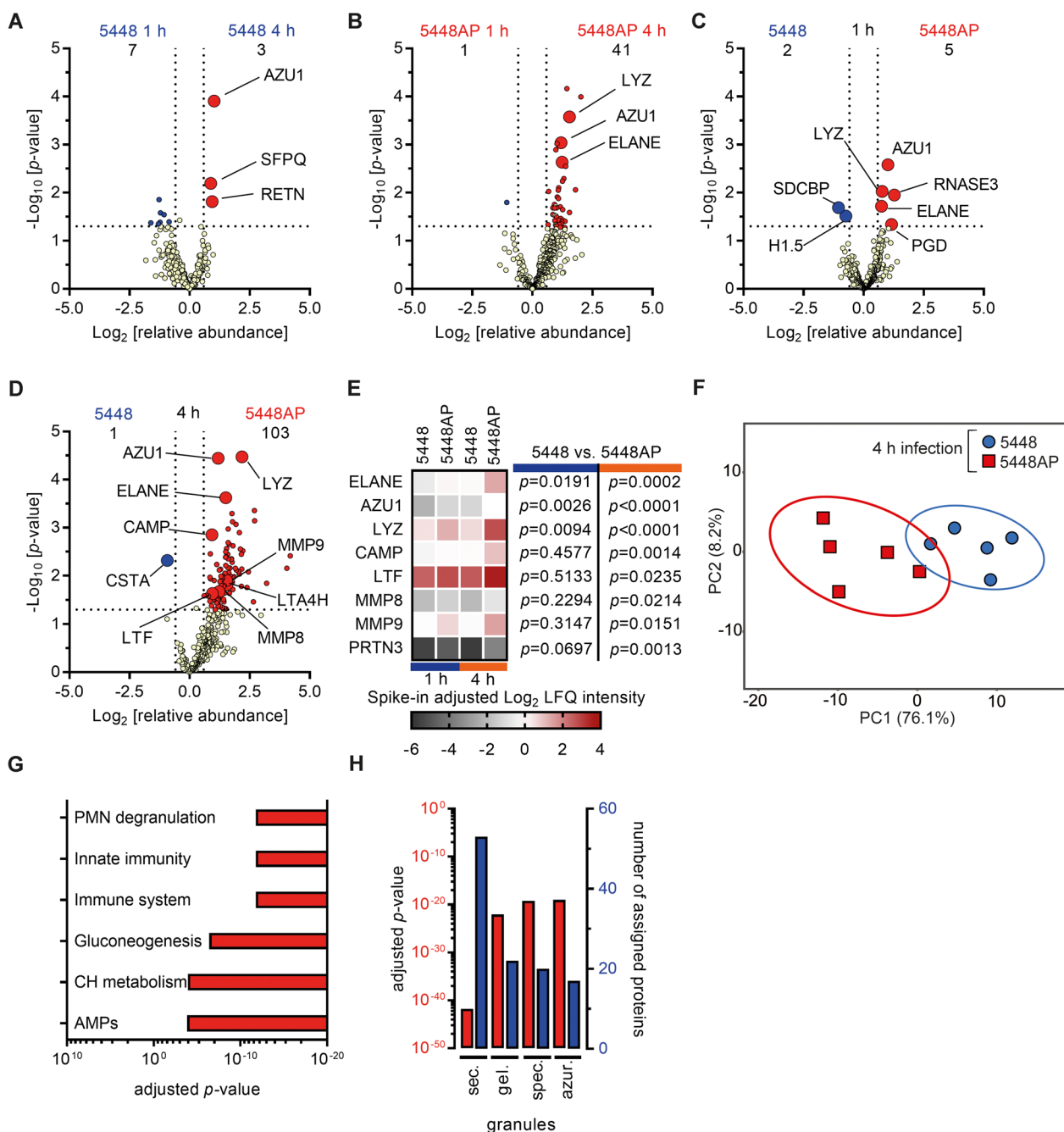


**Fig. 6** Hyper-responsiveness of human neutrophils induced by SpeB-negative GAS. **A, B** Time-dependent and **C, D** strain-dependent comparison of secretome profiles of human neutrophils exposed to 5448 or 5448AP strains. Displayed are changes in relative abundance and  $p$ -values of the original analyses in Additional file 2: Table S5 ( $n=5$ ). **E** Heat map highlighting some of the significant differences of protein/peptide abundance in neutrophil secretomes from **(A–D)**. **F** Principal component analysis of secreted proteins post 4 h of infection of indicated strains. Each dot represents one donor ( $n=5$ ). The ellipses indicate the calculated 95% probability region for a bivariate normal distribution with an average center of groups. **G** Top six upregulated pathways in 5448AP infections of primary neutrophils as compared to 5448 infections. Displayed are adjusted  $p$ -values as determined by functional profiling in the *Reactome* database (CH, carbohydrate; AMPs, antimicrobial peptides). **H** Cellular compartment analyses of protein/peptides found in higher abundance in neutrophil secretomes of 5448AP infections as compared to 5448 infections. Displayed are adjusted  $p$ -values (left red axis, red bars) and number of proteins (right blue axis, blue bars). Functional profiling was performed using *Reactome* database (sec., secretory; gel., gelatinase; spec., specific; azur., azurophilic)

resulting in improved survival of the bacteria and subsequently in higher tissue inflammation and pathology in NSTI.

Bacteria are highly adaptable species. Their genetic information and other structures are capable of alterations. Some of them are reversible when a particular pressure is lifted, whereas other alterations are maintained [7]. GAS have adapted several strategies to survive within the hostile environment in NSTIs [18, 37, 48]. One of them is the enhanced mutational rate within the *covR/S* and *ropB* genes resulting in SpeB-negative clones. Studies on these two mutational hotspots are inconclusive with respect to impact on virulence. Some studies show that these variants are less virulent, while others demonstrated that natural *covR/S* mutants are hyper-virulent [6, 45]. In humans, it was shown that SpeB is readily detectable in sera and tissues of NSTI patients [10, 16, 33] and a mixture of SpeB<sup>+</sup> and SpeB<sup>-</sup> GAS clones is usually seen [16, 33]. Here, we demonstrate that in addition to the irreversible loss of SpeB, due to genetic mutations, a subpopulation of GAS reversibly abrogates SpeB secretion in the tissue setting. This phenomenon is more pronounced in *emm1* strains. Single colony proteomics showed that SpeB accumulates intracellularly and is not released. Once the tissue pressure is lifted, GAS regain the SpeB secreting function. Tissue necrosis, inflammation, neutrophil influx and degranulation are enhanced in patient biopsies associated with increased amount of SpeB<sup>-</sup> GAS clones. Our data further confirm previous observations that neutrophil activation and degranulation are the main hallmarks of GAS NSTIs [14–16, 38]. These pathologic processes seem to be further intensified in biopsies with higher frequencies of the SpeB<sup>-</sup> GAS. Notably, PGK, which has been demonstrated to be a potent activator of neutrophils, is highly susceptible to SpeB proteolysis and its activity can only be seen in SpeB<sup>-</sup> strains [43]. Also, Zhu et al. reported that loss of SpeB resulted in increased fitness of *emm1* GAS in a non-human primate model of necrotizing myositis [48]. Furthermore, it can be noted that in the non-human primate model neutrophil activation and degranulation was associated with tissue pathology [48].

It is widely accepted that *covR/S* mutations and the consequent total loss of SpeB result in upregulated expression of several virulence factors, which are susceptible to SpeB degradation, including Sda1, M protein, PGK, and streptolysin O. All of them facilitate pathogen's escape from neutrophils and other immune cell types [17, 45]. Notably, GAS single colony proteomics demonstrated that in comparison to SpeB<sup>+</sup>, SpeB<sup>-</sup> clones from the same neutrophil infections are characterized by enhanced accumulation of surface anchored M1 protein and C5a peptidase and the secreted virulence

factors DNaseB and Isp2. All of these factors are of crucial importance in immune system evasion and are implicated in hyper-inflammatory processes [32, 37]. In addition, Isp was recently reported to contribute to necrotizing myositis [18]. Therefore, we speculate that transient SpeB<sup>-</sup> clones might persist in the tissue for a longer period and subsequently contribute to excessive degranulation of neutrophils and hyper-inflammation. This fact is further supported by neutrophil secretome analyses. Increasing abundance of granule proteins was observed in 5448 infections over time. To rule out time-dependent effects, infections with stable hyper-virulent SpeB<sup>-</sup> 5448AP strain were performed. It should be emphasized that 5448AP harbors a global regulatory mutation which affects not only SpeB secretion. This strain is further characterized by an enhanced expression of antiphagocytic M1 protein and secretion of Sda1 and Streptokinase, among others [45]. In congruence with our data, it was shown that 5448AP strain limits production of ROS, thereby ensuring its survival [46]. In contrast to the report by Williams and colleagues [46], our analyses revealed that the SpeB<sup>-</sup> 5448AP strain activates neutrophils to a higher extent as compared to its parental SpeB<sup>+</sup> 5448 strain. In line with this, higher abundance of resistin and MPO was detected in biopsies associated with increased amounts of SpeB<sup>-</sup> GAS clones. This is in congruence with a previous report that in absence of SpeB, GAS trigger excessive neutrophil degranulation including the release of MPO [43]. MPO is associated with increased mortality in patients with sepsis [31] and a recent study demonstrated that GAS NSTIs patients had higher MPO levels in blood serum as compared to polymicrobial NSTIs. Moreover, patients presenting with STSS even significantly exceeded MPO levels of those who presented without shock [12].

Since our data suggested that neutrophils are the main cellular compartment responsible for SpeB-negativity, we subsequently analyzed the impact of neutrophil derived components on GAS phenotype. Among the tested effector molecules, H<sub>2</sub>O<sub>2</sub> and HOCl, and Cl<sup>-</sup> were responsible for the reversible loss of SpeB secretion by GAS. Neutrophils phagocytose and subsequently kill bacteria primarily through the activity of NADPH oxidase and MPO [2]. In addition, MPO can be found extracellularly through degranulation or NET formation. Both, extracellular as well as intracellular MPO converts H<sub>2</sub>O<sub>2</sub> to HOCl through oxidation of Cl<sup>-</sup> [2]. Moreover, increased survival of bacteria within neutrophils was associated with increasing percentage of SpeB<sup>-</sup> clones over time. Inhibition of MPO activity resulted in significantly reduced frequency of SpeB<sup>-</sup> GAS clones. However, there are certain limitations to this result: (i) NaCl, the source of Cl<sup>-</sup>, also impaired SpeB secretion by GAS and (ii) inhibition

of MPO in neutrophils only partially reversed the SpeB<sup>-</sup> phenotype. At this stage, we cannot rule out that Cl<sup>-</sup> itself can induce such bacterial phenotype. Nonetheless, HOCl is a less stable compound than H<sub>2</sub>O<sub>2</sub> and therefore, bacterial killing will only be effective in a short time. In this case, inhibition of MPO most likely resulted in H<sub>2</sub>O<sub>2</sub> accumulation within neutrophils and in the observed improved bacterial killing.

Production of fully active SpeB is a multistage process, which includes the involvement of trigger factor (RopA), the PPIase PrsA as well as cytoplasmic SpeB inhibitor Spi (reviewed in [5]). Furthermore, GAS encode highly conserved canonical Sec pathway [9], which components are enriched at the ExPortal microdomain [30]. It was shown that cationic antimicrobial peptides, including polymyxin B, preferentially target the ExPortal. Consequently, the anionic lipids and proteins are redistributed around the peripheral membrane, which is associated with the inhibition of toxin secretion, including SpeB [44]. Whether H<sub>2</sub>O<sub>2</sub>, HOCl or Cl<sup>-</sup> interfere with the above-mentioned processes remains to be elucidated.

To our knowledge, this study is the first to show that in addition to the genetically induced loss of SpeB expression, GAS transiently abrogate SpeB secretion in response to neutrophil-derived H<sub>2</sub>O<sub>2</sub> and HOCl. SpeB<sup>-</sup> clones resist phagocytic killing resulting in enhanced neutrophil degranulation, which is associated with pronounced tissue inflammation and pathology. This finding provides further insight how bacterial persistence arises in the tissue setting. Further experimental studies are warranted to determine the molecular mechanism responsible for transient loss of SpeB secretion in a subpopulation of GAS.

## Conclusions

Bacteria adapt their genetic information and phenotype to challenges they are facing during an infection. In severe GAS infections, hypervirulent SpeB-negative clones have been identified to arise due to *covR/S* and *ropB* mutations. Here we identify that such clones also arise through a transient phenotypic switch triggered by the neutrophil effector molecules hydrogen peroxide and hypochlorous acid. The resulting clones have abrogated SpeB secretion and trigger exacerbated neutrophil degranulation, which results in enhanced tissue pathology. Thus, this study identified a new virulence strategy by streptococci in severe tissue infections.

## Competing interests

The authors declare that they have no competing interests.

## Abbreviations

GAS	Group A streptococci
H <sub>2</sub> O <sub>2</sub>	Hydrogen peroxide
HOCl	Hypochlorous acid
MPO	Myeloperoxidase
NSTIs	Necrotizing soft tissue infections
SpeB	Streptococcal pyrogenic exotoxin B
STSS	Streptococcal toxic shock syndrome

## Supplementary Information

The online version contains supplementary material available at <https://doi.org/10.1186/s12929-023-00947-x>.

**Additional file 1.** Figures S1-S16 and methods section.

**Additional file 2.** Tables S1-S6.

## Acknowledgements

We thank all patients and their relatives. All volunteers are greatly acknowledged for blood donation. Thomas Thiele is acknowledged for organizing the blood donation. Dörte Becher is acknowledged for providing the platform for proteome measurements. We thank Karsta Barnekow for expert technical assistance.

INFECT Study Group:

Morten Hedetoft (Department of Anaesthesia, Head and Orthopedic Center, University Hospital Copenhagen, Rigshospitalet, Copenhagen, Denmark), Trond Bruun (Department of Medicine, Haukeland University Hospital, Bergen, Norway; Department of Clinical Science, University of Bergen, Bergen, Norway), Oddvar Oppegaard (Department of Medicine, Haukeland University Hospital, Bergen, Norway; Department of Clinical Science, University of Bergen, Bergen, Norway), Torbjørn Nedrebø (Department of Anaesthesia and Intensive care, Haukeland University Hospital, Bergen, Norway), Eivind Rath (Department of Medicine, Haukeland University Hospital, Bergen, Norway), Martin Bruun Madsen (Department of Intensive Care, Rigshospitalet, University of Copenhagen, Copenhagen, Denmark).

## Author contributions

Conceptualization: PS, ANT, NS; methodology: PS, TS, JH, KJH, OH, MN, PA, SS, ANT, NS; investigation: PS, TS, KM, BC, LAT, JH, KJH, OH, MN, MS, PA, SS, NS; visualization: PS, TS, KM, BC, LAT, JH, KJH, NS; funding acquisition: ANT, NS; project administration: ANT, NS; supervision: ANT, NS; writing—original draft: PS, TS, ANT, NS; writing—review & editing: PS, TS, BC, LAT, KM, JH, KJH, OH, MN, MS, PA, SS, ANT, NS.

## Funding

This research was supported by the German Research Foundation (DFG; Grants 407176682, 492903360, 503880638 to NS), the Center for Innovative Medicine (CIMED, to ANT) and Region Stockholm (20180058, to ANT), the Swedish Research Council (2018-02475, to ANT); the Swedish Governmental Agency for Innovation Systems (VINNOVA to ANT) under the frame of NordForsk (Project no. 90456, PerAID), and the Swedish Research Council (2018-02475; to ANT) under the frame of ERA PerMed (Project 2018-151, PerMIT).

## Availability of data and materials

All data associated with this study are presented in the paper and supplementary material. Whole genome sequencing data of GAS strains are available at the European Nucleotide Archive (ENA) under the reference number PRJNA 524111. The mass spectrometry proteomics data have been deposited to the ProteomeXchange Consortium via the PRIDE [29] partner repository with the dataset identifier PXD040160.

## Declarations

### Ethics approval and consent to participate

All studies were conducted in accordance with the Helsinki Declaration. Patient samples were retrieved from the INFECT patient cohort consisting of patients with NSTI (INFECT study; ClinicalTrials.gov, NCT01790698). The patient biopsies were obtained at surgical interventions and GAS infections were



primarily identified by routine diagnostics. Patient enrolment and sample analyses were approved by the regional Ethical Review Board at the National Committee on Health Research Ethics in Copenhagen (Ref. No. 1211709), the regional ethics committee in Gothenburg (Ref. No. 930-12), the regional ethics committee Vest, Norway (REK, Ref. No. 325786), and the regional Ethics Committee in Stockholm (Ref. No. 2012/2110-31/2). Blood samples from healthy volunteers or buffy coats of blood provided by the blood bank at the University Medicine Greifswald were used. The buffy coats were provided anonymously. In case of healthy volunteers, donors were individuals well acquainted with the research conducted and written informed consent was obtained. The ethical research committee at the University Medicine Greifswald approved the study (Ref. No. BB 014/14 and Ref. No. BB 006/18). All experiments were carried out in accordance with the approved guidelines.

#### Consent for publication

Not applicable.

#### Author details

<sup>1</sup>Department of Molecular Genetics and Infection Biology, University of Greifswald, Greifswald, Germany. <sup>2</sup>Department of Microbial Proteomics, Institute of Microbiology, University of Greifswald, Greifswald, Germany. <sup>3</sup>Center for Infectious Medicine, Karolinska Institutet, Karolinska University Hospital, Huddinge, Stockholm, Sweden. <sup>4</sup>Helmholtz Center for Infection Research, Brunswick, Germany. <sup>5</sup>Institute of Mathematics and Computer Science, University of Greifswald, Greifswald, Germany. <sup>6</sup>Department of Anaesthesia, Head and Orthopedic Center, University Hospital Copenhagen, Rigshospitalet, Copenhagen, Denmark. <sup>7</sup>Institute of Clinical Medicine, University of Copenhagen, Copenhagen, Denmark. <sup>8</sup>Department of Anaesthesia, Surgical Services and Intensive Care, Karolinska Institute, Karolinska University Hospital, Stockholm, Sweden. <sup>9</sup>Department of Anaesthesiology and Intensive Care Medicine, Sahlgrenska University Hospital, Gothenburg, Sweden. <sup>10</sup>Department of Medicine, Haukeland University Hospital, Bergen, Norway. <sup>11</sup>Department of Clinical Science, University of Bergen, Bergen, Norway.

Received: 24 February 2023 Accepted: 3 July 2023

Published online: 10 July 2023

#### References

- Anaya DA, McMahon K, Nathens AB, Sullivan SR, Foy H, Bulger E. Predictors of mortality and limb loss in necrotizing soft tissue infections. *Arch Surg*. 2005;140(2):151–7.
- Beavers WN, Skaar EP. Neutrophil-generated oxidative stress and protein damage in *Staphylococcus aureus*. *Pathog Dis*. 2016;74(6).
- Bruun T, Kittang BR, de Hoog BJ, Aardal S, Flaatten HK, Langeland N, Mylvaganam H, Vindenes HA, Skrede S. Necrotizing soft tissue infections caused by *Streptococcus pyogenes* and *Streptococcus dysgalactiae* subsp. *equisimilis* of groups C and G in western Norway. *Clin Microbiol Infect*. 2013;19(12):E545–550.
- Bruun T, Rath E, Bruun Madsen M, Oppeggaard O, Nekludov M, Arnell P, Karlsson Y, Babbar A, Bergøy F, Itzek A, Hyldegaard O, Norrby-Teglund A, Skrede S. Risk factors and predictors of mortality in streptococcal necrotizing soft-tissue infections: a multicenter prospective study. *Clin Infect Dis*. 2020;72:293.
- Carroll RK, Musser JM. From transcription to activation: how group A streptococcus, the flesh-eating pathogen, regulates SpeB cysteine protease production. *Mol Microbiol*. 2011;81(3):588–601.
- Cole JN, McArthur JD, McKay FC, Sanderson-Smith ML, Cork AJ, Ranson M, Rohde M, Itzek A, Sun H, Ginsburg D, Kotb M, Nizet V, Chhatwal GS, Walker MJ. Trigger for group A streptococcal M1T1 invasive disease. *FASEB J*. 2006;20(10):1745–7.
- Culyba MJ, Van Tyne D. Bacterial evolution during human infection: adapt and live or adapt and die. *PLoS Pathog*. 2021;17(9): e1009872.
- Cuyper F, Klabunde B, Gesell Salazar M, Surabhi S, Skorka SB, Burchhardt G, Michalik S, Thiele T, Rohde M, Volker U, Hammerschmidt S, Siemens N. Adenosine Triphosphate neutralizes pneumolysin-induced neutrophil activation. *J Infect Dis*. 2020;222(10):1702–12.
- Ferretti JJ, McShan WM, Ajdic D, Savic DJ, Savic G, Lyon K, Primeaux C, Sezate S, Suvorov AN, Kenton S, Lai HS, Lin SP, Qian Y, Jia HG, Najjar FZ, Ren Q, Zhu H, Song L, White J, Yuan X, Clifton SW, Roe BA, McLaughlin R. Complete genome sequence of an M1 strain of *Streptococcus pyogenes*. *Proc Natl Acad Sci U S A*. 2001;98(8):4658–63.
- Gubba S, Low DE, Musser JM. Expression and characterization of group A *Streptococcus* extracellular cysteine protease recombinant mutant proteins and documentation of seroconversion during human invasive disease episodes. *Infect Immun*. 1998;66(2):765–70.
- Hecht A, Glasgow J, Jaschke PR, Bawazer LA, Munson MS, Cochran JR, Endy D, Salit M. Measurements of translation initiation from all 64 codons in *E. coli*. *Nucleic Acids Res*. 2017;45(7):3615–26.
- Hedetoft M, Bennett MH, Hyldegaard O. Adjunctive hyperbaric oxygen treatment for necrotising soft-tissue infections: a systematic review and meta-analysis. *Diving Hyperb Med*. 2021;51(1):34–43.
- Hollands A, Aziz RK, Kansal R, Kotb M, Nizet V, Walker MJ. A naturally occurring mutation in *ropB* suppresses SpeB expression and reduces M1T1 group A streptococcal systemic virulence. *PLoS ONE*. 2008;3(12): e4102.
- Johansson L, Linner A, Sunden-Cullberg J, Haggar A, Herwald H, Lore K, Treutiger CJ, Norrby-Teglund A. Neutrophil-derived hyper-resistinemia in severe acute streptococcal infections. *J Immunol*. 2009;183(6):4047–54.
- Johansson L, Snall J, Sendi P, Linner A, Thulin P, Linder A, Treutiger CJ, Norrby-Teglund A. HMGB1 in severe soft tissue infections caused by *Streptococcus pyogenes*. *Front Cell Infect Mi* 2014;4.
- Johansson L, Thulin P, Sendi P, Hertzén E, Linder A, Akesson P, Low DE, Agerberth B, Norrby-Teglund A. Cathelicidin LL-37 in severe *Streptococcus pyogenes* soft tissue infections in humans. *Infect Immun*. 2008;76(8):3399–404.
- Kachroo P, Eraso JM, Beres SB, Olsen RJ, Zhu L, Nasser W, Bernard PE, Cantu CC, Saavedra MO, Arredondo MJ, Strobe B, Do H, Kumaraswami M, Vuopio J, Grondahl-Yli-Hannuksela K, Kristinsson KG, Gottfredsson M, Pesonen M, Pensar J, Davenport ER, Clark AG, Corander J, Caugant DA, Gaini S, Magnussen MD, Kubiak SL, Nguyen HAT, Long SW, Porter AR, DeLeo FR, Musser JM. Integrated analysis of population genomics, transcriptomics and virulence provides novel insights into *Streptococcus pyogenes* pathogenesis. *Nat Genet*. 2019;51(3):548–59.
- Kachroo P, Eraso JM, Olsen RJ, Zhu L, Kubiak SL, Pruitt L, Yerramilli P, Cantu CC, Ojeda Saavedra M, Pensar J, Corander J, Jenkins L, Kao L, Granillo A, Porter AR, DeLeo FR, Musser JM. New pathogenesis mechanisms and translational leads identified by multidimensional analysis of necrotizing myositis in primates. *mBio* 2020;11(1).
- Kaul R, McGeer A, Low DE, Green K, Schwartz B. Population-based surveillance for group A streptococcal necrotizing fasciitis: clinical features, prognostic indicators, and microbiologic analysis of seventy-seven cases. Ontario Group A Streptococcal Study. *Am J Med*. 1997;103(1):18–24.
- Kubica M, Guzik K, Koziel J, Zarebski M, Richter W, Gajkowska B, Golda A, Maciak-Gudowska A, Brix K, Shaw L, Foster T, Potempa J. A potential new pathway for *Staphylococcus aureus* dissemination: the silent survival of *S. aureus* phagocytosed by human monocyte-derived macrophages. *PLoS ONE*. 2008;3:e1409.
- Ly AT, Noto JP, Walwyn OL, Tanz RR, Shulman ST, Kabat W, Bessen DE. Differences in SpeB protease activity among group A streptococci associated with superficial, invasive, and autoimmune disease. *PLoS ONE*. 2017;12(5): e0177784.
- Madsen MB, Skrede S, Perner A, Arnell P, Nekludov M, Bruun T, Karlsson Y, Hansen MB, Polzik P, Hedetoft M, Rosen A, Saccanti E, Bergøy F, Martins-Dos Santos VAP, Norrby-Teglund A, Hyldegaard O. Patient's characteristics and outcomes in necrotising soft-tissue infections: results from a Scandinavian, multicentre, prospective cohort study. *Intensive Care Med*. 2019;45(9):1241–51.
- Mairpady SS, Siemens N, Monk IR, Mohan DB, Mukundan S, Krishnan KC, Prabhakara S, Snall J, Kearns A, Vandenesch F, Svensson M, Kotb M, Gopal B, Arakere G, Norrby-Teglund A. A point mutation in *AgrC* determines cytotoxic or colonizing properties associated with phenotypic variants of ST22 MRSA strains. *Sci Rep*. 2016;6:31360.
- Nauseef WM. Myeloperoxidase in human neutrophil host defence. *Cell Microbiol*. 2014;16(8):1146–55.
- Nelson DC, Garbe J, Collin M. Cysteine proteinase SpeB from *Streptococcus pyogenes*—a potent modifier of immunologically important host and bacterial proteins. *Biol Chem*. 2011;392(12):1077–88.

26. Norrby-Teglund A, Thulin P, Gan BS, Kotb M, McGeer A, Andersson J, Low DE. Evidence for superantigen involvement in severe group A streptococcal tissue infections. *J Infect Dis*. 2001;184(7):853–60.
27. Palma Medina LM, Rath E, Jahagirdar S, Bruun T, Madsen MB, Stralin K, Unge C, Hansen MB, Arnell P, Nekludov M, Hyldegaard O, Lourda M, Santos V, Saccenti E, Skrede S, Svensson M, Norrby-Teglund A. Discriminatory plasma biomarkers predict specific clinical phenotypes of necrotizing soft-tissue infections. *J Clin Invest*. 2021;131(14).
28. Papayannopoulos V, Metzler KD, Hakkim A, Zychlinsky A. Neutrophil elastase and myeloperoxidase regulate the formation of neutrophil extracellular traps. *J Cell Biol*. 2010;191(3):677–91.
29. Perez-Riverol Y, Bai J, Bandla C, Garcia-Seisdedos D, Hewapathirana S, Kamatchinathan S, Kundu DJ, Prakash A, Frericks-Zipper A, Eisenacher M, Walzer M, Wang S, Brazma A, Vizcaino JA. The PRIDE database resources in 2022: a hub for mass spectrometry-based proteomics evidences. *Nucleic Acids Res*. 2022;50(D1):D543–52.
30. Rosch JW, Caparon MG. The ExPortal: an organelle dedicated to the biogenesis of secreted proteins in *Streptococcus pyogenes*. *Mol Microbiol*. 2005;58(4):959–68.
31. Schrijver IT, Kemperman H, Roest M, Kesecioglu J, de Lange DW. Myeloperoxidase can differentiate between sepsis and non-infectious SIRS and predicts mortality in intensive care patients with SIRS. *Intensive Care Med*. 2017;52(1):43.
32. Shumba P, Mairpady Shambat S, Siemens N. The role of streptococcal and staphylococcal exotoxins and proteases in human necrotizing soft tissue infections. *Toxins (Basel)*. 2019;11(6):332.
33. Siemens N, Chakrakodi B, Shambat SM, Morgan M, Bergsten H, Hyldegaard O, Skrede S, Arnell P, Madsen MB, Johansson L, Juarez J, Bosnjak L, Morgelin M, Svensson M, Norrby-Teglund A. Biofilm in group A streptococcal necrotizing soft tissue infections. *JCI Insight*. 2016;1(10):e87882.
34. Siemens N, Fiedler T, Normann J, Klein J, Munch R, Patenge N, Kreikemeyer B. Effects of the ERES pathogenicity region regulator Ralp3 on *Streptococcus pyogenes* serotype M49 virulence factor expression. *J Bacteriol*. 2012;194(14):3618–26.
35. Siemens N, Kittang BR, Chakrakodi B, Oppegaard O, Johansson L, Bruun T, Mylvaganam H, Svensson M, Skrede S, Norrby-Teglund A. Increased cytotoxicity and streptolysin O activity in group G streptococcal strains causing invasive tissue infections. *Sci Rep*. 2015;5:16945.
36. Siemens N, Oehmcke-Hecht S, Hossmann J, Skorka SB, Nijhuis RHT, Ruppen C, Skrede S, Rohde M, Schultz D, Lalk M, Itzek A, Pieper DH, van den Bout CJ, Claas ECJ, Kuijper EJ, Mauritz R, Sendi P, Wunderink HF, Norrby-Teglund A. Prothrombotic and proinflammatory activities of the beta-hemolytic group b streptococcal pigment. *J Innate Immun*. 2019;12:291.
37. Siemens N, Snall J, Svensson M, Norrby-Teglund A. Pathogenic mechanisms of streptococcal necrotizing soft tissue infections. *Adv Exp Med Biol*. 2020;1294:127–50.
38. Snall J, Linner A, Uhlmann J, Siemens N, Ibold H, Janos M, Linder A, Kreikemeyer B, Herwald H, Johansson L, Norrby-Teglund A. Differential neutrophil responses to bacterial stimuli: streptococcal strains are potent inducers of heparin-binding protein and resistin-release. *Sci Rep*. 2016;6:21288.
39. Stevens DL, Bryant AE. Necrotizing soft-tissue infections. *N Engl J Med*. 2017;377(23):2253–65.
40. Sumbly P, Whitney AR, Graviss EA, DeLeo FR, Musser JM. Genome-wide analysis of group A streptococci reveals a mutation that modulates global phenotype and disease specificity. *PLoS Pathog*. 2006;2(1): e5.
41. Thanert R, Itzek A, Hossmann J, Hamisch D, Madsen MB, Hyldegaard O, Skrede S, Bruun T, Norrby-Teglund A, Medina E, Pieper DH. Molecular profiling of tissue biopsies reveals unique signatures associated with streptococcal necrotizing soft tissue infections. *Nat Commun*. 2019;10(1):3846.
42. Thulin P, Johansson L, Low DE, Gan BS, Kotb M, McGeer A, Norrby-Teglund A. Viable group A streptococci in macrophages during acute soft tissue infection. *PLoS Med*. 2006;3(3): e53.
43. Uhlmann J, Siemens N, Kai-Larsen Y, Fiedler T, Bergman P, Johansson L, Norrby-Teglund A. Phosphoglycerate kinase-a novel streptococcal factor involved in neutrophil activation and degranulation. *J Infect Dis*. 2016;214(12):1876–83.
44. Vega LA, Caparon MG. Cationic antimicrobial peptides disrupt the *Streptococcus pyogenes* ExPortal. *Mol Microbiol*. 2012;85(6):1119–32.
45. Walker MJ, Hollands A, Sanderson-Smith ML, Cole JN, Kirk JK, Henningham A, McArthur JD, Dinkla K, Aziz RK, Kansal RG, Simpson AJ, Buchanan JT, Chhatwal GS, Kotb M, Nizet V. DNase Sda1 provides selection pressure for a switch to invasive group A streptococcal infection. *Nat Med*. 2007;13(8):981–5.
46. Williams JG, Ly D, Geraghty NJ, McArthur JD, Vyas HKN, Gorman J, Tsatsaronis JA, Sluyter R, Sanderson-Smith ML. *Streptococcus pyogenes* M1T1 variants induce an inflammatory neutrophil phenotype including activation of inflammatory caspases. *Front Cell Infect Microbiol*. 2020;10:596023.
47. Witko-Sarsat V, Rieu P, Descamps-Latscha B, Lesavre P, Halbwachs-Mecarelli L. Neutrophils: molecules, functions and pathophysiological aspects. *Lab Invest*. 2000;80(5):617–53.
48. Zhu L, Olsen RJ, Beres SB, Eraso JM, Saavedra MO, Kubiak SL, Cantu CC, Jenkins L, Charbonneau ARL, Waller AS, Musser JM. Gene fitness landscape of group A streptococcus during necrotizing myositis. *J Clin Invest*. 2019;129(2):887–901.

## Publisher's Note

Springer Nature remains neutral with regard to jurisdictional claims in published maps and institutional affiliations.

Ready to submit your research? Choose BMC and benefit from:

- fast, convenient online submission
- thorough peer review by experienced researchers in your field
- rapid publication on acceptance
- support for research data, including large and complex data types
- gold Open Access which fosters wider collaboration and increased citations
- maximum visibility for your research: over 100M website views per year

At BMC, research is always in progress.

Learn more [biomedcentral.com/submissions](https://biomedcentral.com/submissions)



## Supplemental Material

### Neutrophil-derived reactive agents induce a transient SpeB negative phenotype in *Streptococcus pyogenes*

Patience Shumba<sup>1</sup>, Thomas Sura<sup>2</sup>, Kirsten Moll<sup>3</sup>, Bhavya Chakrakodi<sup>3</sup>, Lea A. Tölken<sup>1</sup>, Jörn Hoßmann<sup>4</sup>, Katharina J. Hoff<sup>5</sup>, Ole Hyldegaard<sup>6,7</sup>, Michael Nekludov<sup>8</sup>, Mattias Svensson<sup>3</sup>, Per Arnell<sup>9</sup>, Steinar Skrede<sup>10,11</sup>, INFECT Study Group<sup>12</sup>, Anna Norrby-Teglund<sup>3#</sup>, and Nikolai Siemens<sup>1#\*</sup>

<sup>1</sup>Department of Molecular Genetics and Infection Biology, University of Greifswald, Greifswald, Germany

<sup>2</sup>Department of Microbial Proteomics, Institute of Microbiology, University of Greifswald, Greifswald, Germany

<sup>3</sup>Center for Infectious Medicine, Karolinska Institutet, Karolinska University Hospital, Huddinge, Stockholm, Sweden

<sup>4</sup>Helmholtz Center for Infection Research, Braunschweig, Germany

<sup>5</sup>Institute of Mathematics and Computer Science, University of Greifswald, Greifswald, Germany

<sup>6</sup>Department of Anaesthesia, Head and Orthopedic Center, University Hospital Copenhagen, Rigshospitalet, Copenhagen, Denmark

<sup>7</sup>Institute of Clinical Medicine, University of Copenhagen, Copenhagen, Denmark

<sup>8</sup>Department of Anaesthesia, Surgical Services and Intensive Care, Karolinska Institute, Karolinska University Hospital, Stockholm, Sweden

<sup>9</sup>Department of Anaesthesiology and Intensive Care Medicine, Sahlgrenska University Hospital, Gothenburg, Sweden

<sup>10</sup>Department of Medicine, Haukeland University Hospital, Bergen, Norway

<sup>11</sup>Department of Clinical Science, University of Bergen, Bergen, Norway

<sup>12</sup>INFECT Study Group (Morten Hedetoft<sup>6</sup>, Trond Bruun, Oddvar Oppegaard<sup>10,11</sup>, Torbjørn Nedrebø<sup>13</sup>, Eivind Rath<sup>10</sup>, Martin Bruun Madsen<sup>14</sup>)

<sup>13</sup>Department of Anaesthesia and Intensive care, Haukeland University Hospital, Bergen, Norway

<sup>14</sup>Department of Intensive Care, Rigshospitalet, University of Copenhagen, Copenhagen, Denmark

#ANT and NS contributed equally to this work

\*Correspondance: Nikolai Siemens; Email: nikolai.siemens@uni-greifswald.de

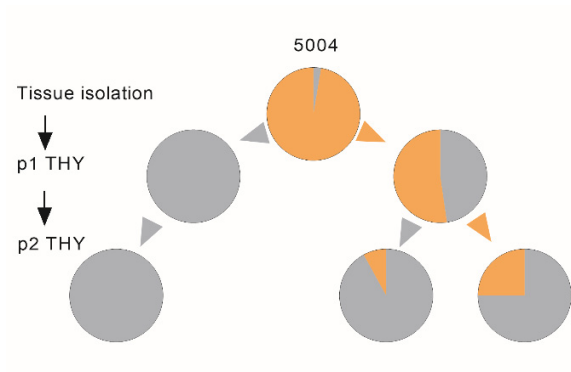


**Fig. S1. Reversible loss of SpeB secretion after tissue recovery.** Sections of the tissue biopsy of patient 5004 were cultured on casein agar plates. SpeB+ and SpeB- colonies were recovered and passaged in THY media over night. SpeB-positivity/-negativity were assessed via casein agar assay (SpeB+ [grey]; SpeB- [orange]).

10 20 30 40 50 60 70 80 90 1  
WP\_002991036.1  
SPY2001\_covS  
SPY2002\_covS  
SPY2006\_covS  
SPY2015\_covS  
SPY2028\_covS  
SPY5006A\_covS  
SPY5004\_covS  
SPY5006B\_covS  
SPY5006C\_covS  
SPY5011\_covS  
SPY6013\_covS  
SPY6016\_covS  
SPY6018\_covS  
SPY6025\_covS  
SPY6026\_covS  
SPY6028\_covS

100 110 120 130 140 150 160 170 180 190 200  
WP\_002991036.1  
SPY2001\_covS  
SPY2002\_covS  
SPY2006\_covS  
SPY2015\_covS  
SPY2028\_covS  
SPY5006A\_covS  
SPY5004\_covS  
SPY5006B\_covS  
SPY5006C\_covS  
SPY5011\_covS  
SPY6013\_covS  
SPY6016\_covS  
SPY6018\_covS  
SPY6025\_covS  
SPY6026\_covS  
SPY6028\_covS

210 220 230 240 250 260 270 280 290 300  
WP\_002991036.1  
SPY2001\_covS  
SPY2002\_covS  
SPY2006\_covS  
SPY2015\_covS  
SPY2028\_covS  
SPY5006A\_covS  
SPY5004\_covS  
SPY5006B\_covS  
SPY5006C\_covS  
SPY5011\_covS  
SPY6013\_covS  
SPY6016\_covS  
SPY6018\_covS  
SPY6025\_covS  
SPY6026\_covS  
SPY6028\_covS

310 320 330 340 350 360 370 380 390 400  
WP\_002991036.1  
SPY2001\_covS  
SPY2002\_covS  
SPY2006\_covS  
SPY2015\_covS  
SPY2028\_covS  
SPY5006A\_covS  
SPY5004\_covS  
SPY5006B\_covS  
SPY5006C\_covS  
SPY5011\_covS  
SPY6013\_covS  
SPY6016\_covS  
SPY6018\_covS  
SPY6025\_covS  
SPY6026\_covS  
SPY6028\_covS

410 420 430 440 450 460 470 480 490 500  
WP\_002991036.1  
SPY2001\_covS  
SPY2002\_covS  
SPY2006\_covS  
SPY2015\_covS  
SPY2028\_covS  
SPY5006A\_covS  
SPY5004\_covS  
SPY5006B\_covS  
SPY5006C\_covS  
SPY5011\_covS  
SPY6013\_covS  
SPY6016\_covS  
SPY6018\_covS  
SPY6025\_covS  
SPY6026\_covS  
SPY6028\_covS

510 520 530 540 550 560 570 580 590 600  
WP\_002991036.1  
SPY2001\_covS  
SPY2002\_covS  
SPY2006\_covS  
SPY2015\_covS  
SPY2028\_covS  
SPY5006A\_covS  
SPY5004\_covS  
SPY5006B\_covS  
SPY5006C\_covS  
SPY5011\_covS  
SPY6013\_covS  
SPY6016\_covS  
SPY6018\_covS  
SPY6025\_covS  
SPY6026\_covS  
SPY6028\_covS



610 620 630 640 650 660 670 680 690 700  
WP\_002991036.1  
SPY2001\_covS  
SPY2002\_covS  
SPY2006\_covS  
SPY2015\_covS  
SPY2028\_covS  
SPY5006A\_covS  
SPY5004\_covS  
SPY5006B\_covS  
SPY5006C\_covS  
SPY5011\_covS  
SPY6013\_covS  
SPY6016\_covS  
SPY6018\_covS  
SPY6025\_covS  
SPY6026\_covS  
SPY6028\_covS

710 720 730 740 750 760 770 780 790 800  
WP\_002991036.1  
SPY2001\_covS  
SPY2002\_covS  
SPY2006\_covS  
SPY2015\_covS  
SPY2028\_covS  
SPY5006A\_covS  
SPY5004\_covS  
SPY5006B\_covS  
SPY5006C\_covS  
SPY5011\_covS  
SPY6013\_covS  
SPY6016\_covS  
SPY6018\_covS  
SPY6025\_covS  
SPY6026\_covS  
SPY6028\_covS

810 820 830 840 850 860 870 880 890 900  
WP\_002991036.1  
SPY2001\_covS  
SPY2002\_covS  
SPY2006\_covS  
SPY2015\_covS  
SPY2028\_covS  
SPY5006A\_covS  
SPY5004\_covS  
SPY5006B\_covS  
SPY5006C\_covS  
SPY5011\_covS  
SPY6013\_covS  
SPY6016\_covS  
SPY6018\_covS  
SPY6025\_covS  
SPY6026\_covS  
SPY6028\_covS

910 920 930 940 950 960 970 980 990 1000  
WP\_002991036.1  
SPY2001\_covS  
SPY2002\_covS  
SPY2006\_covS  
SPY2015\_covS  
SPY2028\_covS  
SPY5006A\_covS  
SPY5004\_covS  
SPY5006B\_covS  
SPY5006C\_covS  
SPY5011\_covS  
SPY6013\_covS  
SPY6016\_covS  
SPY6018\_covS  
SPY6025\_covS  
SPY6026\_covS  
SPY6028\_covS

1010 1020 1030 1040 1050 1060 1070 1080 1090 1100  
WP\_002991036.1  
SPY2001\_covS  
SPY2002\_covS  
SPY2006\_covS  
SPY2015\_covS  
SPY2028\_covS  
SPY5006A\_covS  
SPY5004\_covS  
SPY5006B\_covS  
SPY5006C\_covS  
SPY5011\_covS  
SPY6013\_covS  
SPY6016\_covS  
SPY6018\_covS  
SPY6025\_covS  
SPY6026\_covS  
SPY6028\_covS

1110 1120 1130 1140 1150 1160 1170 1180 1190 1200  
WP\_002991036.1  
SPY2001\_covS  
SPY2002\_covS  
SPY2006\_covS  
SPY2015\_covS  
SPY2028\_covS  
SPY5006A\_covS  
SPY5004\_covS  
SPY5006B\_covS  
SPY5006C\_covS  
SPY5011\_covS  
SPY6013\_covS  
SPY6016\_covS  
SPY6018\_covS  
SPY6025\_covS  
SPY6026\_covS  
SPY6028\_covS

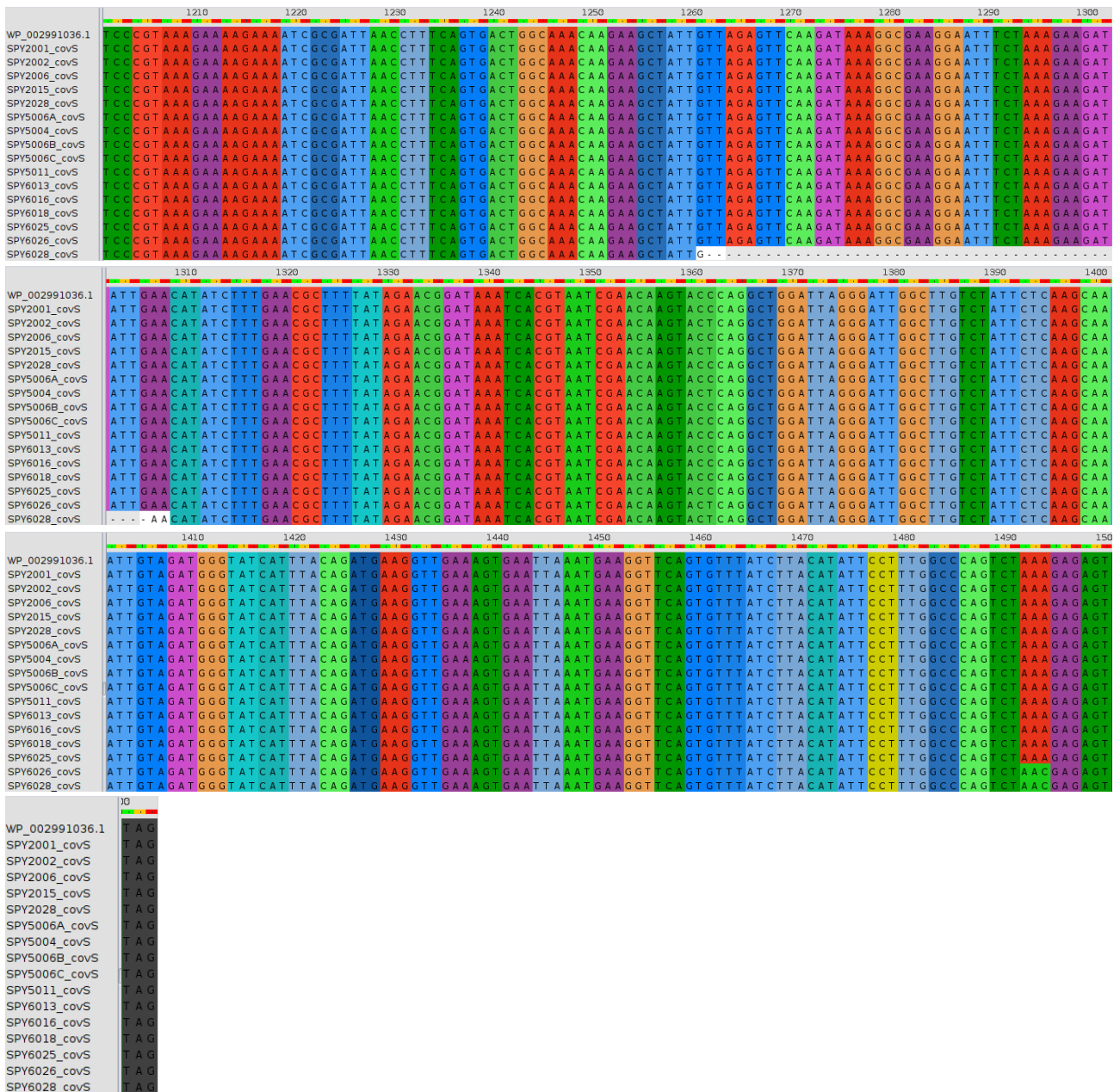


**Fig. S2. CovS gene sequence alignment of indicated strains isolated from NSTI patient's biopsies (Figure 1A).**

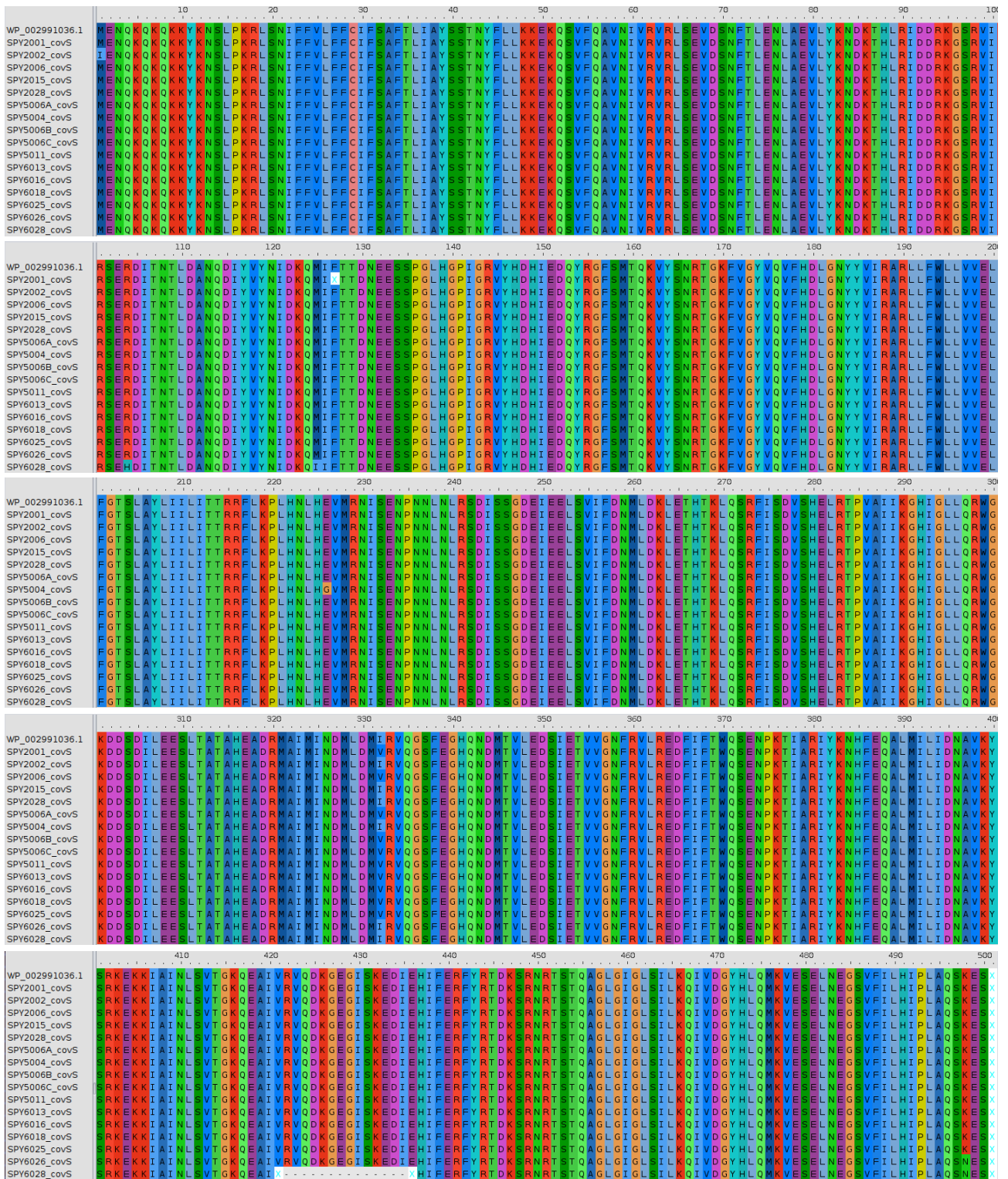


**Fig. S3. CovS amino acid sequence alignment of indicated strains isolated from NSTI patient's biopsies (Figure 1A).**



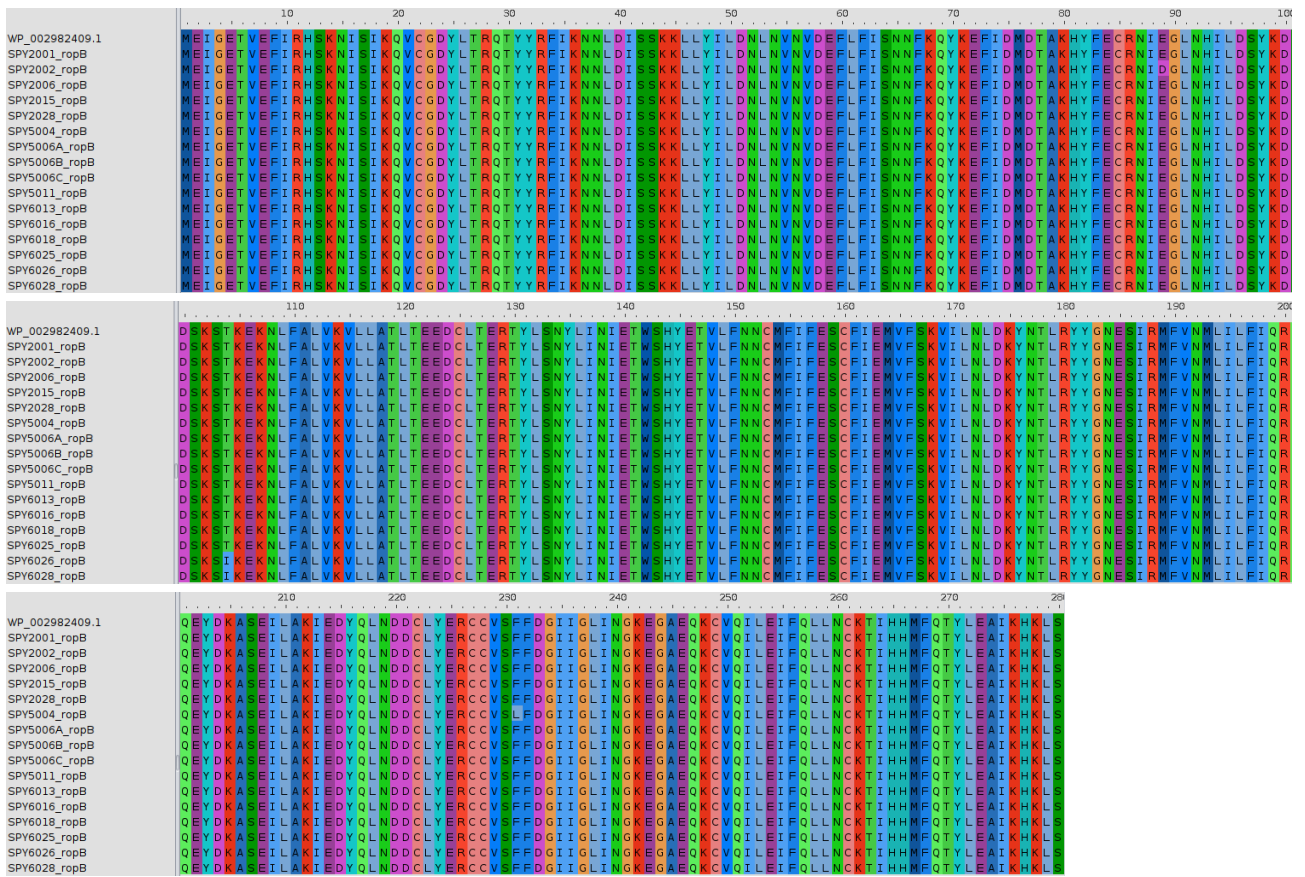


**Fig. S4. RopB amino acid sequence alignment of indicated strains isolated from NSTI patient's biopsies (Figure 1A).**

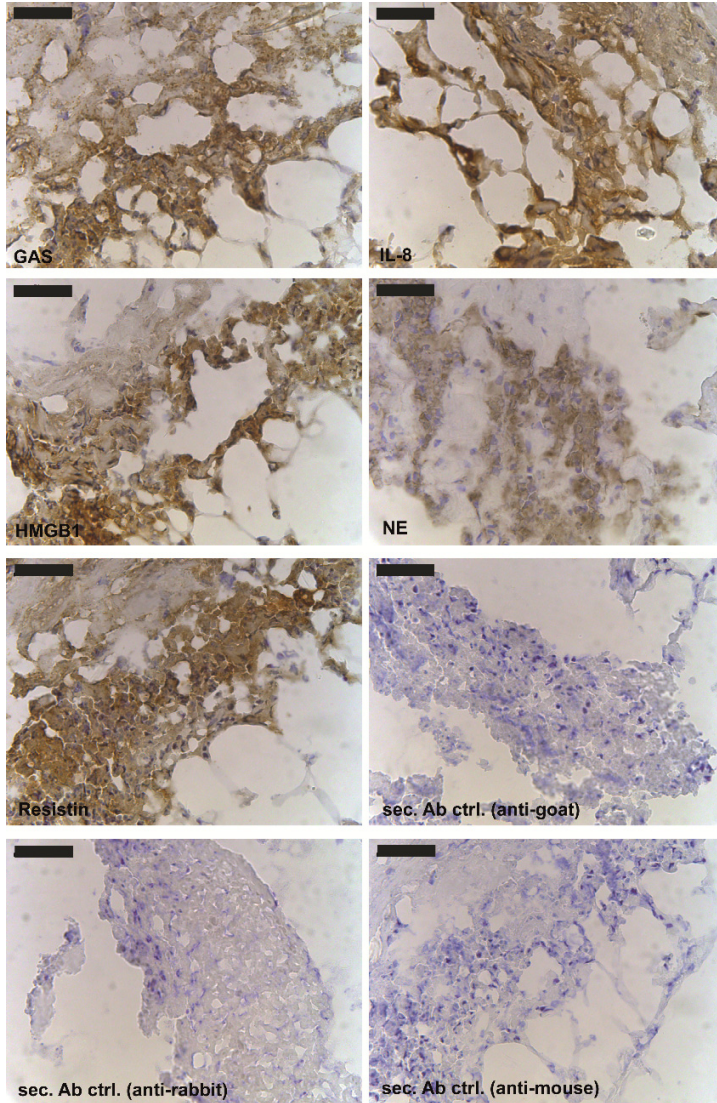


**Fig. S5. Inflammation and phagocytic infiltration at the local site of infection.** Representative immunohistochemically stained tissue biopsies from GAS NSTI patients. (GAS, group A streptococcus; HMGB1, High-mobility group protein B1; NE, neutrophil elastase; black bars: 50  $\mu$ m).

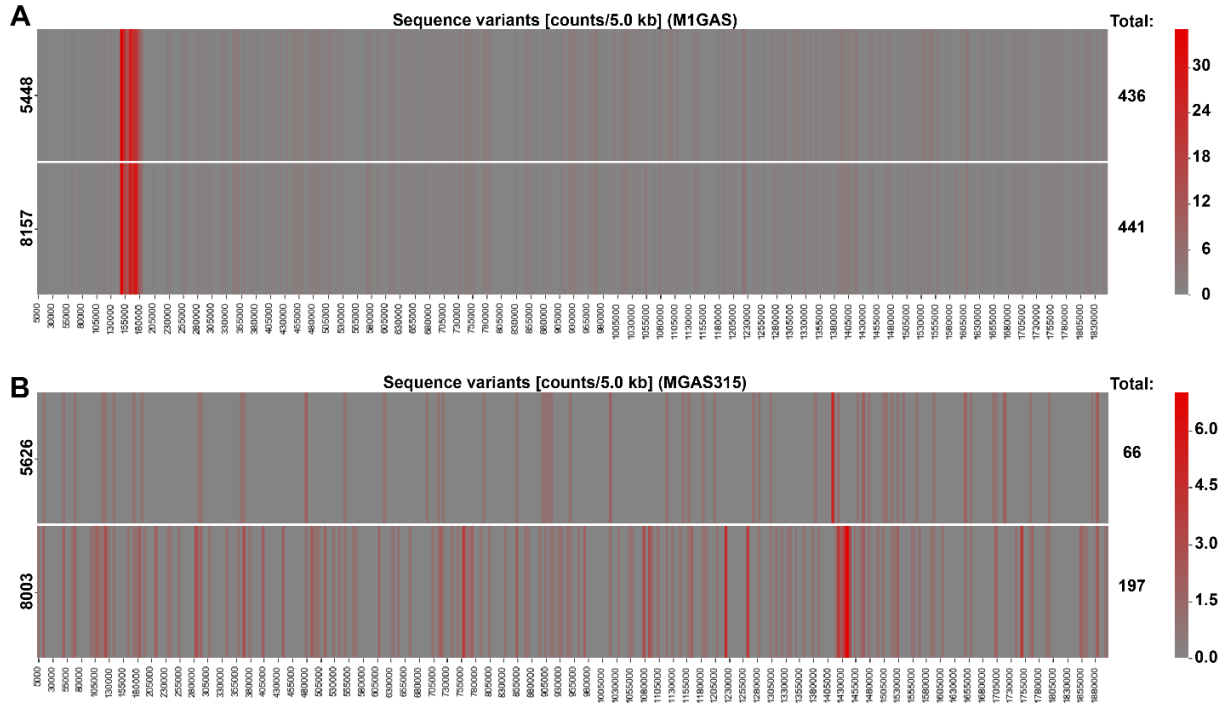


**Figure S6. Whole genome sequencing analyses.** Base differences per 5.0 kb based on the comparison of the whole genomes of the indicated strains with the annotated genomes of **(A)** M1GAS (*emm1* strains) and **(B)** MGAS315 (*emm3* strains).

```

Spy_0336      MENQKQKQKKYKNSLPKRLSNIPFVLFCCI FSAFTLIAYSSSTNYFLKKEKQSVFQAVNI
SpyM3_0245    MENQKQKQKKYKNSLPKRLSNIPFVLFCCI FSAFTLIAYSSSTNYFLKKEKQSVFQAVNI
CNGIITCF_01748 MENQKQKQKKYKNSLPKRLSNIPFVLFCCI FSAFTLIAYSSSTNYFLKKEKQSVFQAVNI
IKGFMBIA_01747 MENQKQKQKKYKNSLPKRLSNIPFVLFCCI FSAFTLIAYSSSTNYFLKKEKQSVFQAVNI
DNELCKEF_00023 MENQKQKQKKYKNSLPKRLSNIPFVLFCCI FSAFTLIAYSSSTNYFLKKEKQSVFQAVNI
LCNJLPCO_00752 MENQKQKQKKYKNSLPKRLSNIPFVLFCCI FSAFTLIAYSSSTNYFLKKEKQSVFQAVNI
*****

Spy_0336      VRVRLSEVDSNFTLENLAEVLYKNDKTHLRIDDRKGSRVIRSERDITNTLDANQDIYVYN
SpyM3_0245    VRVRLSEVDSNFTLENLAEVLYKNDKTHLRIDDRKGSRVIRSERDITNTLDANQDIYVYN
CNGIITCF_01748 VRVRLSEVDSNFTLENLAEVLYKNDKTHLRIDDRKGSRVIRSERDITNTLDANQDIYVYN
IKGFMBIA_01747 VRVRLSEVDSNFTLENLAEVLYKNDKTHLRIDDRKGSRVIRSERDITNTLDANQDIYVYN
DNELCKEF_00023 VRVRLSEVDSNFTLENLAEVLYKNDKTHLRIDDRKGSRVIRSERDITNTLDANQDIYVYN
LCNJLPCO_00752 VRVRLSEVDSNFTLENLAEVLYKNDKTHLRIDDRKGSRVIRSERDITNTLDANQDIYVYN
*****

Spy_0336      IDKQMIFTTNEESSPGLHGPIGRVYHDHIEDQYRGSMTQKVYSNRTGKFGVYVQVFHD
SpyM3_0245    IDKQMIFTTNEESSPGLHGPIGRVYHDHIEDQYRGSMTQKVYSNRTGKFGVYVQVFHD
CNGIITCF_01748 IDKQMIFTTNEESSPGLHGPIGRVYHDHIEDQYRGSMTQKVYSNRTGKFGVYVQVFHD
IKGFMBIA_01747 IDKQMIFTTNEESSPGLHGPIGRVYHDHIEDQYRGSMTQKVYSNRTGKFGVYVQVFHD
DNELCKEF_00023 IDKQMIFTTNEESSPGLHGPIGRVYHDHIEDQYRGSMTQKVYSNRTGKFGVYVQVFHD
LCNJLPCO_00752 IDKQMIFTTNEESSPGLHGPIGRVYHDHIEDQYRGSMTQKVYSNRTGKFGVYVQVFHD
*****

Spy_0336      LGNYVIRARLLFWLLVVELFGTSLAYLIILITRRFLKPLHNLHEVMRNISENPNLNL
SpyM3_0245    LGNYVIRARLLFWLLVVELFGTSLAYLIILITRRFLKPLHNLHEVMRNISENPNLNL
CNGIITCF_01748 LGNYVIRARLLFWLLVVELFGTSLAYLIILITRRFLKPLHNLHEVMRNISENPNLNL
IKGFMBIA_01747 LGNYVIRARLLFWLLVVELFGTSLAYLIILITRRFLKPLHNLHEVMRNISENPNLNL
DNELCKEF_00023 LGNYVIRARLLFWLLVVELFGTSLAYLIILITRRFLKPLHNLHEVMRNISENPNLNL
LCNJLPCO_00752 LGNYVIRARLLFWLLVVELFGTSLAYLIILITRRFLKPLHNLHEVMRNISENPNLNL
*****

Spy_0336      RSDISSGDEIEELSVIFDNMLDKLETHTKLQSRFISDVSHLRTFVAIIKGHIGLLQRWG
SpyM3_0245    RSDISSGDEIEELSVIFDNMLDKLETHTKLQSRFISDVSHLRTFVAIIKGHIGLLQRWG
CNGIITCF_01748 RSDISSGDEIEELSVIFDNMLDKLETHTKLQSRFISDVSHLRTFVAIIKGHIGLLQRWG
IKGFMBIA_01747 RSDISSGDEIEELSVIFDNMLDKLETHTKLQSRFISDVSHLRTFVAIIKGHIGLLQRWG
DNELCKEF_00023 RSDISSGDEIEELSVIFDNMLDKLETHTKLQSRFISDVSHLRTFVAIIKGHIGLLQRWG
LCNJLPCO_00752 RSDISSGDEIEELSVIFDNMLDKLETHTKLQSRFISDVSHLRTFVAIIKGHIGLLQRWG
*****

Spy_0336      KDDSDILEESLTATAHEADRMAIMINDMLDMIRVQGSFEGHQNDMTVLEDSIETVVGNER
SpyM3_0245    KDDSDILEESLTATAHEADRMAIMINDMLDMIRVQGSFEGHQNDMTVLEDSIETVVGNER
CNGIITCF_01748 KDDSDILEESLTATAHEADRMAIMINDMLDMIRVQGSFEGHQNDMTVLEDSIETVVGNER
IKGFMBIA_01747 KDDSDILEESLTATAHEADRMAIMINDMLDMIRVQGSFEGHQNDMTVLEDSIETVVGNER
DNELCKEF_00023 KDDSDILEESLTATAHEADRMAIMINDMLDMIRVQGSFEGHQNDMTVLEDSIETVVGNER
LCNJLPCO_00752 KDDSDILEESLTATAHEADRMAIMINDMLDMIRVQGSFEGHQNDMTVLEDSIETVVGNER
*****

Spy_0336      VLREDFIFTWQSENPKTIARIYKNHFEQALMILIDNAVYSRKEKKIAINLSVTGKQEA
SpyM3_0245    VLREDFIFTWQSENPKTIARIYKNHFEQALMILIDNAVYSRKEKKIAINLSVTGKQEA
CNGIITCF_01748 VLREDFIFTWQSENPKTIARIYKNHFEQALMILIDNAVYSRKEKKIAINLSVTGKQEA
IKGFMBIA_01747 VLREDFIFTWQSENPKTIARIYKNHFEQALMILIDNAVYSRKEKKIAINLSVTGKQEA
DNELCKEF_00023 VLREDFIFTWQSENPKTIARIYKNHFEQALMILIDNAVYSRKEKKIAINLSVTGKQEA
LCNJLPCO_00752 VLREDFIFTWQSENPKTIARIYKNHFEQALMILIDNAVYSRKEKKIAINLSVTGKQEA
*****

Spy_0336      VRVQDKGEGISKEDIEHIFERFYRTDKSRNRTSTQAGLGIGLSILKQIVDGYHLQMKVES
SpyM3_0245    VRVQDKGEGISKEDIEHIFERFYRTDKSRNRTSTQAGLGIGLSILKQIVDGYHLQMKVES
CNGIITCF_01748 VRVQDKGEGISKEDIEHIFERFYRTDKSRNRTSTQAGLGIGLSILKQIVDGYHLQMKVES
IKGFMBIA_01747 VRVQDKGEGISKEDIEHIFERFYRTDKSRNRTSTQAGLGIGLSILKQIVDGYHLQMKVES
DNELCKEF_00023 VRVQDKGEGISKEDIEHIFERFYRTDKSRNRTSTQAGLGIGLSILKQIVDGYHLQMKVES
LCNJLPCO_00752 VRVQDKGEGISKEDIEHIFERFYRTDKSRNRTSTQAGLGIGLSILKQIVDGYHLQMKVES
*****

Spy_0336      ELNEGSVFILHIPLAQSKE      MIGAS      (SPyxxxx)
SpyM3_0245    ELNEGSVFILHIPLAQSKE      MGAS315    (SPyM3_xxxx)
CNGIITCF_01748 ELNEGSVFILHIPLAQSKE      5448      (CNGIITCF_xxxxx)
IKGFMBIA_01747 ELNEGSVFILHIPLAQSKE      8157      (IKGFMBIA_xxxxx)
DNELCKEF_00023 ELNEGSVFILHIPLAQSKE      5626      (DNELCKEF_xxxxx)
LCNJLPCO_00752 ELNEGSVFILHIPLAQSKE      8003      (LCNJLPCO_xxxxx)
*****

```

**Fig. S7. Mutation within *covS* gene in 8003 strain results in T<sub>214</sub>P substitution.** Amino acid alignment of the indicated four GAS strains used in this study.

5448            8157 5626 8003

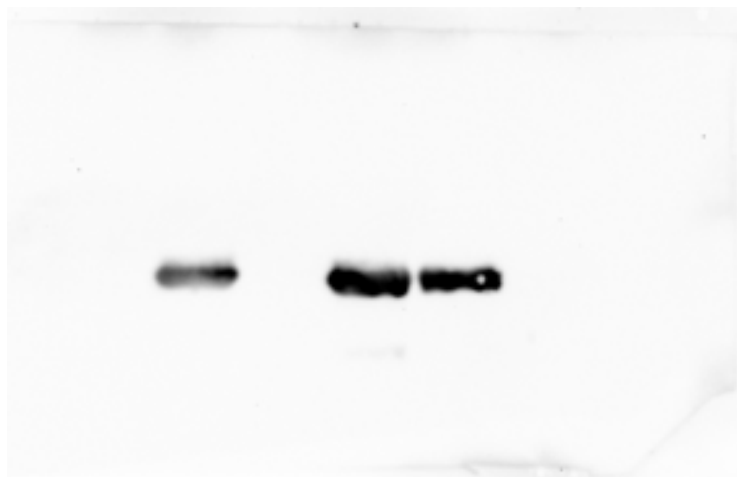


**Fig. S8. Original SpeB blot as displayed in Fig. 2**

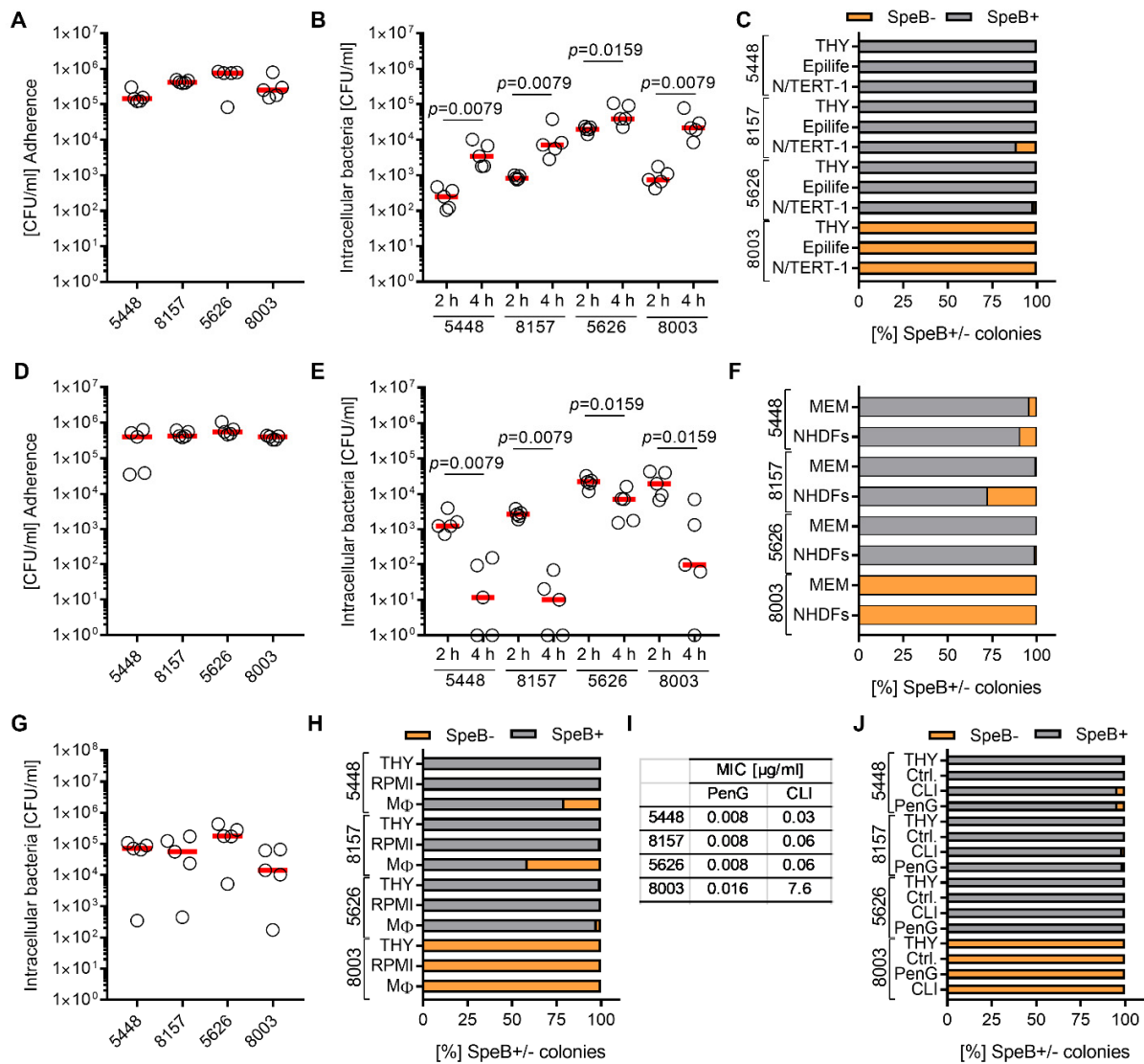


**Fig. S9. SpeB phenotype in GAS co-culture with keratinocytes, fibroblasts, and macrophages.** Extracellular (A) and intracellular (B) bacterial numbers recovered from keratinocytes after indicated time points of infection. Each dot represents one independent experiment. The horizontal lines denote median values (n=5). (C) Assessment of SpeB positivity/negativity of indicated strains via casein agar assay recovered after 4 h of intracellular passage in keratinocytes. Mean percentage from five independent experiments is shown (n=5). Extracellular (D) and intracellular (E) bacterial numbers recovered from human primary fibroblasts after indicated time points of infection. Each dot represents one independent experiment. The horizontal lines denote median values (n=5). (F) Assessment of SpeB positivity/negativity of indicated strains via casein agar assay recovered after 2 h of intracellular passage in fibroblasts. Mean percentage from five independent experiments is shown (n=5). (G) Intracellular bacterial counts after 2 h of macrophage infection. Each dot represents an experiment with macrophages from one donor. The horizontal lines denote median values (n=5). (H) Assessment of SpeB positivity/negativity of indicated strains recovered from primary human macrophages shown in (G). Mean percentage of SpeB+ and SpeB- clones from five independent experiments are shown (n=5). Bacteria incubated in EpiLife, RPMI, and THY media served as controls. (I) Penicillin G (PenG) and clindamycin (CLI) minimal inhibitory concentrations (MICs) of indicated

GAS strains (n=4). (K) Distribution of SpeB<sup>+</sup> and SpeB<sup>-</sup> clones post antibiotic treatment. Displayed are mean [%] of four independent experiments (n=4). The level of significance was determined using Kruskal-Wallis test with Dunn's multiple comparison post-test.



**A**

1 MNKKKLGVRLLSLLALGGFVLANPVFADQN FARNEKEAK **DSAITFIQK** SAAIKAGAR **SAE**  
 61 **DIKLDK** VNLGGELSGSNMYVYNI STGGFVIVSGDKR **SPEILGYSTSGSFDANGKENIASF**  
 121 **MESYVEQIKENKLDTTYAGTAEIK** QPVVKSLLDSK **GIHYNQGNPYNLLTPVIEK** VKPGE  
 181 QSFVQHAATGCVATATAQIMKY **YHNYPNK** GLK **DYTYTLSSNNPYFNHPKNLFAAISTRQY**  
 241 **NWNNILPTYSGR** ESNVQKMAISELMADVGISVDMDYGPSSGSAGSSRVQR **ALKENFGYNQ**  
 301 **SVHQINR** GDFSK **QDWEAQIDKELSONQPVYYQGVGKVGGHAFVIDGADGR** NFYHVNWGWG  
 361 GVSDGFFR **LDALNPSALGTGGGAGGFNGYQSAVVGIKP**

**B**

SEQUENCE	START POSITION	END POSITION	LENGTH
<b>DSAITFIQK</b>	40	48	9
<b>SAEDIKLDK</b>	58	66	9
<b>SPEILGYSTSGSFDANGK</b>	97	114	18
<b>ENIASFMESYVEQIK</b>	115	129	15
<b>ENIASFMESYVEQIKENK</b>	115	132	18
<b>KLDTTYAGTAEIK</b>	133	145	13
<b>LDTTYAGTAEIK</b>	134	145	12
GIHYNQGNPYNLLTPVIEK	157	175	19
YHNYPNK	203	209	7
DYTYTLSSNNPYFNHPK	213	229	17
NLFAAISTR	230	238	9
QYNWNNILPTYSGR	239	252	14
ALKENFGYNQSVHQINR	291	307	17
ENFGYNQSVHQINR	294	307	14
QDWEAQIDK	313	321	9
QDWEAQIDKELSONQPVYYQGVGK	313	336	24
ELSONQPVYYQGVGK	322	336	15
VGGHAFVIDGADGR	337	350	14
LDALNPSALGTGGGAGGFNGYQSAVVGIKP	369	398	30

**Fig. S10. SpeB single colony analysis. (A)** Fasta sequence of SpeB-zymogene with SpeB tryptic peptides (green), detected by mass spectrometry in the single colony analysis. **(B)** SpeB tryptic peptides detected by mass spectrometry in the single colony analysis. The pro-domain is depicted in red whereas the sequence for mature SpeB is indicated in black.



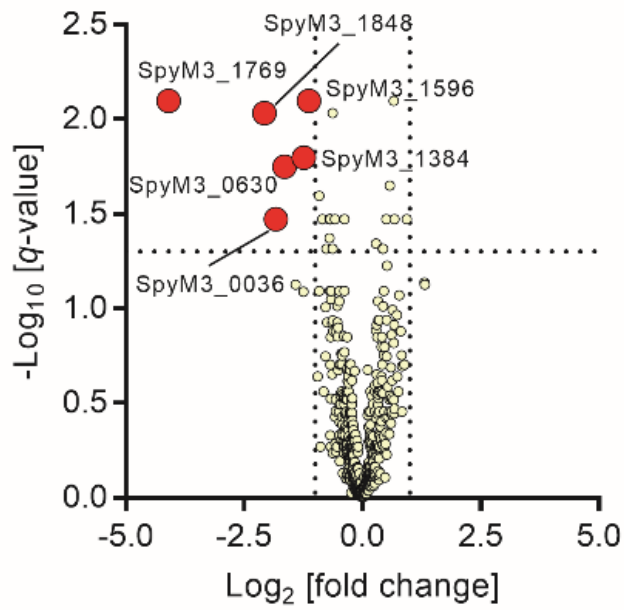


**Fig. S11. Single colony proteome analysis of GAS 8003.** Volcano plot displaying significant differences of single colony proteome post neutrophils infection compared to the THY control. Original data is displayed in Supplemental Table 3.

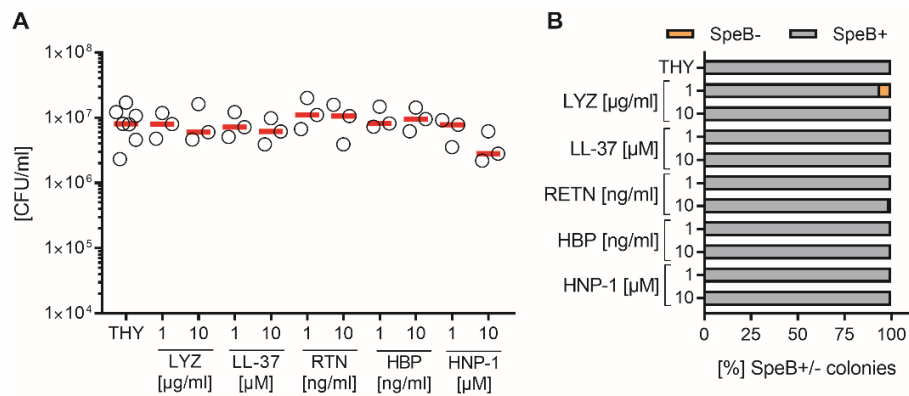


**Fig. S12. The impact of neutrophil derived peptides/proteins on group A streptococcal SpeB secretion.** 5448 GAS strain was exposed to indicated concentrations of proteins/peptides for 3 h and bacterial viability (**A**) and SpeB secretion (**B**) were assessed. (**A**) Each dot represents one independent experiment. The horizontal lines denote median values ( $n \geq 3$ ). (**B**) Mean percentage from three independent experiments (shown in A) is displayed (LYZ, lysozyme; RTN, resistin; HBP, heparin binding protein; HNP-1, human neutrophil peptide 1).

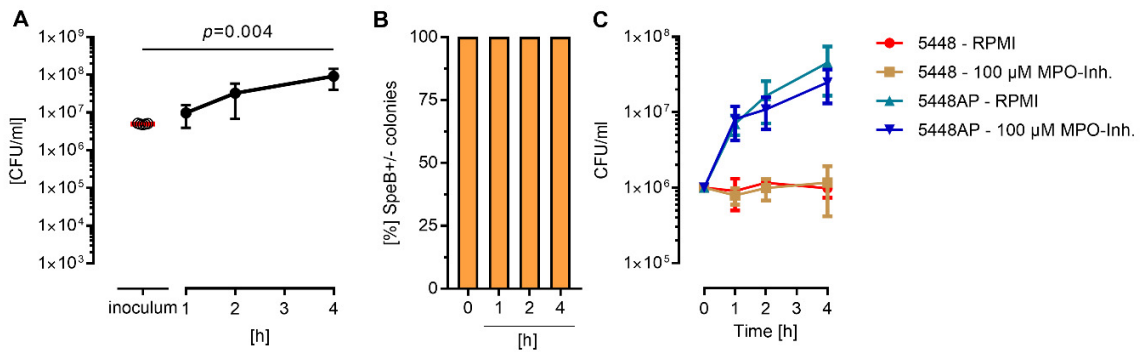


**Fig. S13. 5448AP survives intracellular neutrophil passage.** (A) Human primary neutrophils were infected GAS strain 5448AP and intracellular bacteria were determined by plating serial dilution of neutrophil lysates on casein agar plates post indicated time points. Dots represent the median value  $\pm$  range of independent experiments with five donors (n=5). (B) Assessment of SpeB positivity/negativity of 5448AP strain recovered from primary human neutrophils shown in (A) (n=5). All 5448AP clones remained negative (orange). The level of significance between the groups of all experiments was determined using Kruskal Wallis test with Dunn's posttest. (C) Control experiment confirming that 100  $\mu$ M MPO-inhibitor had no effect on bacterial growth (n=3).

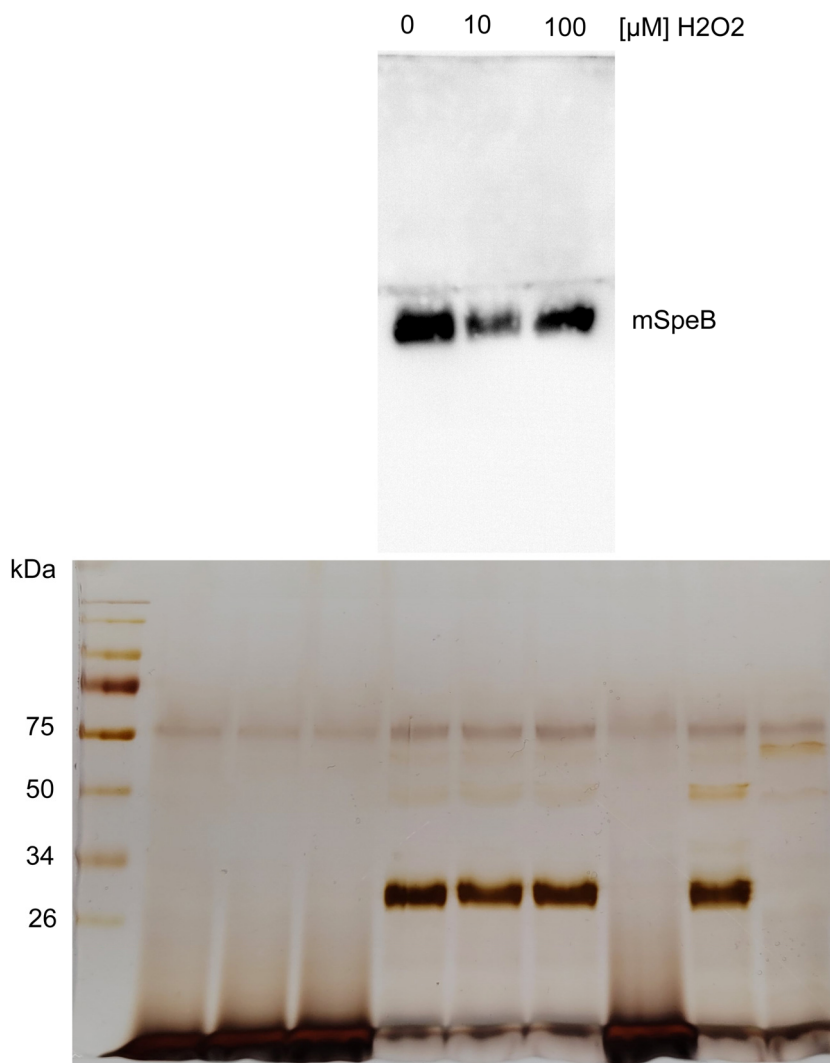


**Fig. S14.** Original Western blot (upper panel) and silver staining of the loading control (lower panel) of GAS 5448 supernatants post exposure to indicated concentrations of H<sub>2</sub>O<sub>2</sub>.

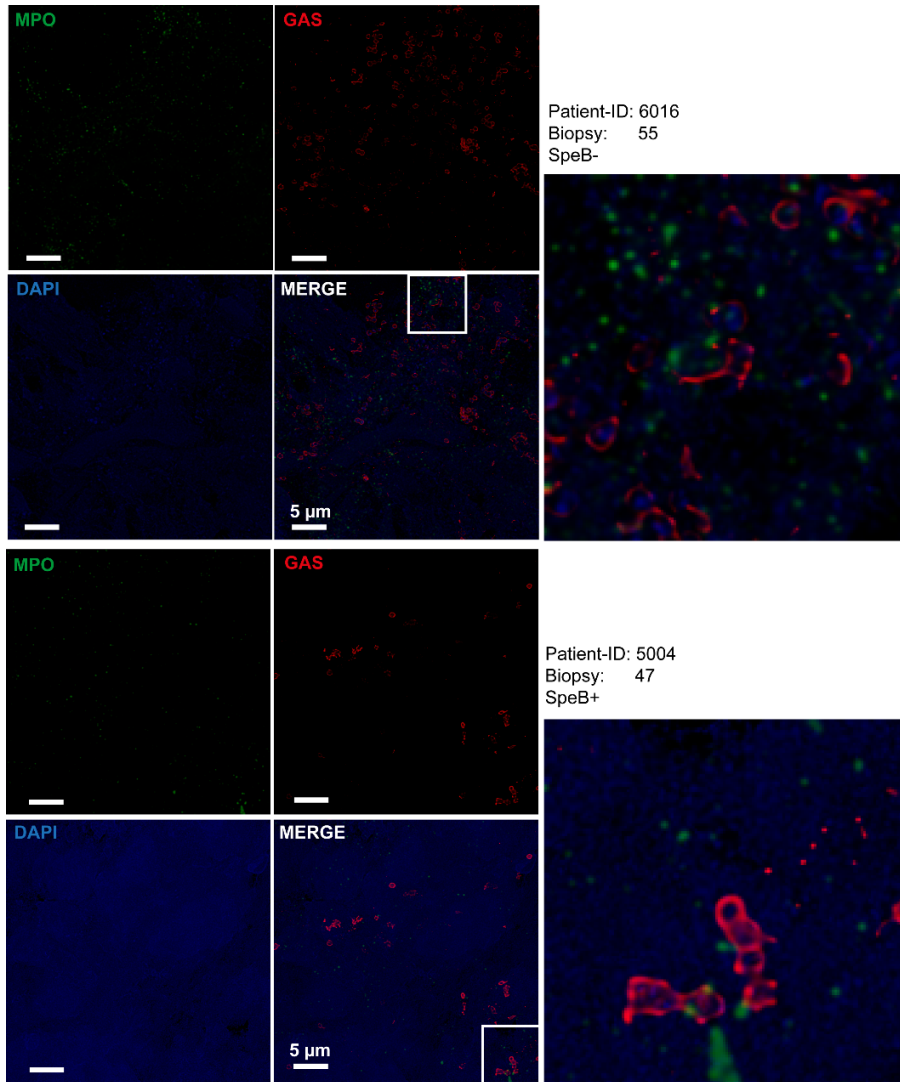


**Fig. S15. Increased levels of MPO in patient tissue biopsies associated with SpeB<sup>-</sup> GAS.** Representative immunofluorescence micrographs of the distribution of MPO in patient biopsies.

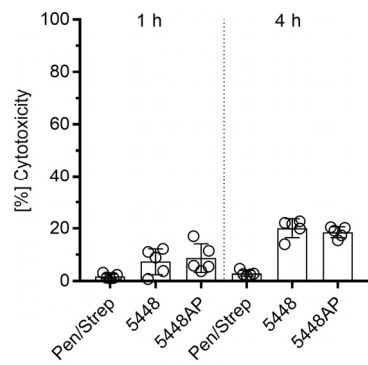


**Fig. S16.** Cytotoxicity induced by bacterial infections towards human primary neutrophils. Mean values  $\pm$  s.d. from five donors (n=5) are shown. Each dot represents one donor.

## Materials and Methods

**Whole genome sequencing and data processing.** DNA extraction from GAS strains 5448, 5626, 8003, and 8157, whole genome sequencing, and analyses were performed as previously described [14]. Briefly, Bacterial DNA was purified utilizing the DNeasy Blood & Tissue kit (Qiagen). Sequencing libraries were prepared using the NEBNext Ultra II DNA Library Prep Kit (NEB). Genomes were sequenced using Illumina MiSeq (2x300 bp). Sequencing data are deposited in the European Nucleotide Archive (ENA database) under the BioProject PRJNA524111 [3]. Raw reads were processed in paired-end mode by fastq-mcf version 1.05. Processed reads were assembled using SPAdes (version 3.11.1) de novo genome assembler software [2] in careful mode. Contigs with a length less than 200 bp or average coverage lower than 15 were discarded. Average contig coverage was determined by first mapping processed reads to the assembled contigs utilizing Bowtie2 (version 2.3.2) determining the per base coverage using the SAMtools (version 1.8) [11] and calculating the mean coverage for each contig. All assemblies were annotated utilizing Prokka genome annotation software (version 1.4) [13]. Gene comparisons are based on orthologous genes identified by the Proteinortho software (version 5.16b) [8]. Processed reads of 5448 and 8157 strains were mapped to the *S. pyogenes* M1GAS (*emm1*) reference genome and of 5626 and 8003 strains to MGAS315 (*emm3*) genome using Bowtie2 [6]. Variants were called using mpileup part of BCFtools (version 1.8) [10]. Variants were filtered out by a minimum SNP and INDEL distance of 10 bp, variant quality of 30, coverage of 50, mapping quality of 40 and a Z-score of 1.96 [5].

The genomes of GAS strains (Figure 1) were retrieved from the European Nucleotide Archive in FASTA format [9]. As reference strain, assembly GCF\_000006785.2\_ASM678v2 from the National Center for Biotechnology was used. The gene that encodes *covS* corresponds to the protein WP\_002991036.1, *covR* corresponds to protein WP\_002991052.1, and *ropB* corresponds to WP\_002982409.1 in the reference strain. The reference protein sequences for CovS, CovR and RopB were searched in the genomes of strains using NCBI-BLAST version 2.9.0+ [1,4]. In case of CovR and RopB, the protein sequence in reference strains was extracted from the first BLAST hit, respectively. For CovS, the BLAST output showed that SPY2001 has a frame-shift causing deletion. Thus, cdbfasta tools version 0.99 (<https://github.com/gperteacdbfasta>, last accessed on February 18th 2021) were used to excise the corresponding coding sequence of BLAST hits from the strain genomes. For CovS, we performed a multiple

protein sequence alignment with CLUSTAL version 2.1 [15]. Subsequently, a translation of the aligned sequences was performed with AliView version 1.26 [7].

**Protein extraction, LC-MS/MS analyses, and data processing of single GAS colonies and neutrophil secretome.** Single SpeB<sup>+</sup> and/or SpeB<sup>-</sup> colonies, as assessed by casein agar assay, were transferred into tubes containing 200 µl 50 mM triethylammonium bicarbonate (TEAB) lysis buffer and 100 µl Lysing matrix B (MP Biomedicals). Bacteria were disrupted by bead beating (6 m/s, 5×20 s; 60 s ice incubation between the cycles) via FastPrep-24 5G (MP Biomedicals). Protein-containing supernatant was separated from bacterial debris via centrifugation (10 min, 10,000×g, 4°C). Protein concentrations were determined using BCA-assay (Thermo Fisher Scientific). 2.5 µg of total protein was reduced (5 mM Tris(2-carboxyethyl)phosphine [TCEP]; 45 min; 65°C), alkylated (10 mM iodoacetamide [IAA]; 15 min; room temperature; dark), and an in-solution digest with 250 ng of trypsin was performed (18 h; 37°C). Samples were concentrated and desalted via ZipTips (C18; Millipore), dried, and stored at -80°C until further use.

Samples were measured on a QExactive mass spectrometer coupled to an EASY nLC-1000 liquid chromatography system. Samples were loaded on an in-house packed column (ReproSil-Pur 120 C18-AQ, 3 µm) of 20 cm length and 100 µm inner diameter. Peptides were eluted by a non-linear 86 min gradient from 2% to 99% solvent B (acetonitrile with 0.1% acetic acid). The overview scans (MS<sup>1</sup>) covered a mass range of 300–1650 m/z at a resolution of 70,000 (at 200 m/z). The 12 most abundant precursors were selected for HCD fragmentation at NCE 27.5 with an AGC target of 1e5 and an under-fill ratio of 5%. Dynamic exclusion was set to 30 s, lock mass correction was enabled, and ions with unknown charge of one or higher than six were excluded from fragmentation.

MaxQuant version 1.6.10.43 and ncbi genome assembly data base id=233599 (M1GAS) and id=299846 (MGAS315) were used for protein identification. The minimal number of unique peptides per protein group was set to 2 to be considered as identified. Oxidation (M) was considered as a variable and carbamidomethyl (C) as a fixed modification. Data were analyzed using Perseus version 1.6.10.43. Quantitative values were log<sub>2</sub> transformed and the resulting values were filtered based on the following criteria: only identified by site, reverse, potential contamination, quantified in at least 75% of biological



replicates per group. Differential expression of bacterial proteins was determined via Student's *t* test with Benjamini-Hochberg FDR correction. Proteins were considered to be significantly differentially expressed if *q*-value was <0.01 and log<sub>2</sub> fold change was ≥1. The principle component analysis (PCA) of the scaled data was carried out using the ClustVis web tool [12].

Neutrophil secretome profiling: 500 µl neutrophil supernatant was reduced with TCEP (5 mM, 45 min, 65°C) and alkylated with IAA (10 mM, 20 min, room temperature, dark). Five microliters of SP3 beads (hydrophobic: Sera-Mag Speedbeads carboxylate-modified particles [GE Healthcare]; hydrophilic: Speedbead magnetic carboxylate-modified particles [GE Healthcare]) were added to the sample and acetonitrile added to a final concentration of 70% (v/v) and incubated in a thermomixer (5 min, 24 °C, 900 rpm). Tubes were placed in a magnetic rack to collect the beads and the supernatant was removed. Beads were washed with 80% (v/v) ethanol twice and air dried. Proteins were digested by adding 25 µl digestion buffer (50 mM TEAB) containing 100 ng of trypsin followed by 30 s sonication in a water bath to disaggregate the beads and an incubation at 37°C for 18 h. Beads were removed by centrifugation (20,000 g, 1 min) and by placing the tubes in a magnetic rack to transfer the supernatant to a glass vial. The supernatants were dried by vacuum centrifugation and peptides were reconstituted in 12 µl 0.1% acetic acid in water containing iRT peptides.

Generated tryptic peptides were analyzed by LC-MS/MS. Therefore, an EASY nLC 1000 (Thermo Fischer) was coupled to an QExactive mass spectrometer (Thermo Fisher). Peptides were loaded onto in house packed fused silica columns of 20 cm length and an inner diameter of 75 µm, filled with Dr. Maisch ReproSil Pur 120 C18-AQ 1.9 µm (Dr. Maisch). Peptides were eluted using a non-linear binary gradient of 86 min from 2% to 99% solvent B (0.1% acetic acid in acetonitrile) in solvent A (0.1% acetic acid). The overview scans (MS1) covered a mass range of 300–1650 *m/z* at a resolution of 70,000 (at 200 *m/z*). The 10 most abundant precursors were selected for HCD fragmentation at NCE 27.5 with an AGC target of 1e5 and an under-fill ratio of 10%. Dynamic exclusion was set to 30 s, lock mass correction was enabled, and ions with unknown charge, charge of one or higher than six were excluded from fragmentation.

MaxQuant version 1.6.17.0 and ncbi genome assembly data base id=233599 (M1GAS) and UniProt human reference proteome (downloaded 20190715) were used for protein identification. The minimal number of

unique peptides per protein group was set to 2 to be considered as identified. Oxidation (M) was considered as a variable and carbamidomethyl (C) as a fixed modification. Data were analyzed using Perseus version 1.6.14.0. Quantitative values were  $\log_2$  transformed and the resulting values were filtered based on the following criteria: only identified by site, reverse, potential contamination, quantified in at least 4 of 5 biological replicates per group. LFQ intensities were normalized to the intensity of the spiked iRT. Differential expression of bacterial proteins was determined via Student's *t* test with Benjamini-Hochberg FDR correction. Proteins were considered to be significantly differentially expressed if *p*-value was  $<0.05$  and  $\log_2$  fold change was  $\geq 1$ .

**Cytotoxicity LDH release assay.** Cytotoxicity was determined by measurement of the LDH activity via CytoTox 96 Non-Radio Kit (Promega) according to manufacturer's guidelines.

## References

1. Altschul S.F., Gish W., Miller W., Myers E.W. and Lipman D.J. Basic local alignment search tool. *J Mol Biol* 215(3):403-410, 1990.
2. Bankevich A., Nurk S., Antipov D., Gurevich A.A., Dvorkin M., Kulikov A.S., Lesin V.M., Nikolenko S.I., Pham S., Prjibelski A.D., Pyshkin A.V., Sirotkin A.V., Vyahhi N., Tesler G., Alekseyev M.A. and Pevzner P.A. SPAdes: a new genome assembly algorithm and its applications to single-cell sequencing. *J Comput Biol* 19(5):455-477, 2012.
3. Bruun T., Rath E., Bruun Madsen M., Oppegaard O., Nekludov M., Arnell P., Karlsson Y., Babbar A., Bergey F., Itzek A., Hyldegaard O., Norrby-Teglund A., Skrede S. and Group I.S. Risk factors and Predictors of Mortality in Streptococcal Necrotizing Soft-Tissue Infections: A Multicenter Prospective Study. *Clin Infect Dis*, 2020.
4. Camacho C., Coulouris G., Avagyan V., Ma N., Papadopoulos J., Bealer K. and Madden T.L. BLAST+: architecture and applications. *BMC Bioinformatics* 10:421, 2009.
5. Kaas R.S., Leekitcharoenphon P., Aarestrup F.M. and Lund O. Solving the problem of comparing whole bacterial genomes across different sequencing platforms. *PLoS One* 9(8):e104984, 2014.
6. Langmead B. and Salzberg S.L. Fast gapped-read alignment with Bowtie 2. *Nat Methods* 9(4):357-359, 2012.
7. Larsson A. AliView: a fast and lightweight alignment viewer and editor for large datasets. *Bioinformatics* 30(22):3276-3278, 2014.
8. Lechner M., Findeiss S., Steiner L., Marz M., Stadler P.F. and Prohaska S.J. Proteinortho: detection of (co-)orthologs in large-scale analysis. *BMC Bioinformatics* 12:124, 2011.
9. Leinonen R., Akhtar R., Birney E., Bower L., Cerdeno-Tarraga A., Cheng Y., Cleland I., Faruque N., Goodgame N., Gibson R., Hoad G., Jang M., Pakseresht N., Plaister S., Radhakrishnan R., Reddy K., Sobhany S., Ten Hoopen P., Vaughan R., Zalunin V. and Cochrane G. The European Nucleotide Archive. *Nucleic Acids Res* 39(Database issue):D28-31, 2011.
10. Li H. A statistical framework for SNP calling, mutation discovery, association mapping and population genetical parameter estimation from sequencing data. *Bioinformatics* 27(21):2987-2993, 2011.
11. Li H., Handsaker B., Wysoker A., Fennell T., Ruan J., Homer N., Marth G., Abecasis G., Durbin R. and Genome Project Data Processing S. The Sequence Alignment/Map format and SAMtools. *Bioinformatics* 25(16):2078-2079, 2009.
12. Metsalu T. and Vilo J. ClustVis: a web tool for visualizing clustering of multivariate data using Principal Component Analysis and heatmap. *Nucleic Acids Res* 43(W1):W566-570, 2015.
13. Seemann T. Prokka: rapid prokaryotic genome annotation. *Bioinformatics* 30(14):2068-2069, 2014.
14. Siemens N., Oehmcke-Hecht S., Hossmann J., Skorka S.B., Nijhuis R.H.T., Ruppen C., Skrede S., Rohde M., Schultz D., Lalk M., Itzek A., Pieper D.H., van den Bout C.J., Claas E.C.J., Kuijper E.J., Mauritz R., Sendi P., Wunderink H.F. and Norrby-Teglund A. Prothrombotic and Proinflammatory Activities of the beta-Hemolytic Group B Streptococcal Pigment. *J Innate Immun*:1-13, 2019.
15. Thompson J.D., Higgins D.G. and Gibson T.J. CLUSTAL W: improving the sensitivity of progressive multiple sequence alignment through sequence weighting, position-specific gap penalties and weight matrix choice. *Nucleic Acids Res* 22(22):4673-4680, 1994.